ORGANOBORANES AS ^{18}F FLUORIDE ANION CAPTORS

A Dissertation

by

KANTAPAT CHANSAENPAK

Submitted to the Office of Graduate and Professional Studies of
Texas A&M University
in partial fulfillment of the requirements for the degree of

DOCTOR OF PHILOSOPHY

Chair of Committee,	François P. Gabbaï
Committee Members,	Donald J. Darensbourg
	Hongcai Zhou
	Jean-Philippe Pellois
Head of Department,	François P. Gabbaï

August 2015

Major Subject: Chemistry

ABSTRACT

Fluorine-18 (^{18}F) is the most frequently used radionuclide in positron emission tomography (PET). This is, in part, due to the fact that fluorine is the element that is prevalent in organic molecules as well as easy to introduce directly into a molecule of interest. In addition, the labelling of biomolecules; such as, oligonucleotide, peptides, and proteins with radioisotopes for use in PET imaging is an increasingly important research aspect due to the use of these biomolecules in medical diagnostic or therapeutic applications. Unfortunately, the direct fluorination of peptides and proteins is difficult since harsh reaction conditions (high temperatures, acidic or basic conditions) that are required to get high radiochemical yields may destroy those biomolecules. To solve this problem, peptides and proteins are generally radiolabelled through a suitable prosthetic group under mild conditions.

This dissertation focuses on the synthesis and properties of novel organoboranes designed for ^{18}F fluoride anion capture for PET application. With the goal of developing new boron-based radiotracer, a series of *ortho*-phenylene phosphino-boranes and carbene-borane adducts were synthesized and studied. This general strategy of attaching cationic moiety close to trifluoroborates leads to a B-F bond stabilization in aqueous environment. Gratifyingly, these compounds can be radiolabeled *via* direct ^{18}F-^{19}F isotopic exchange reactions. With these results in hands, the radiolabeled organoborane/biomolecule conjugates have been synthesized and evaluated *in vivo* to use as potential PET probes. In addition to trifluoroborate species, we have also prepared

a new class of fluorescent dyes called triazaborolopyridiniums and investigated their capability as PET/fluorescence dual modality probes.

In a more fundamental aspect of the some of the ideas presented above, we have also decided to explore the synthesis and properties of ambiphilic molecules featuring adjacent phosphine and methylium groups. The structures and isomerization processes of these compounds are also described in this dissertation.

DEDICATION

For My Parents

ACKNOWLEDGEMENTS

First of all, I would like to thank my research advisor, Prof. François P. Gabbaï, for his guidance, patience and encouragement throughout my Ph. D study. Without his support, I could never have come this far and had several opportunities in my career. I would also like to acknowledge Prof. Donald Darensbourg, Prof. Hongcai Zhou, and Prof. Jean-Philippe Pellois for sitting on my committee.

I am extremely appreciative to the members of the Gabbaï's group who have been both friends and wonderful coworkers: Dr. Casey Wade, Dr. Haiyan Zhao, Dr. Tzu-Pin Lin, Dr. Iou-Sheng Ke, Dr. Baofei Pan, Dr. Sikun Cheng, Dr. Kewei Huang, Dr. Boris Vabre, Dr. Daniel Tofan, Dr. Mitsukimi Tsunoda, Masato Hirai, James (Stuart) Jones, Lauren Leamer, Haifeng Yang, Adriana Hampton, Ahmed Ali, Anna-Marie DeLaRosa, Srobona Sen, Chang-Hong Chen, Moncy Yang, Elham Tabei, Di You, Ying-Hao Lo, and Junsang Cho. I would especially like to thank Casey Wade for training me on the air-sensitive techniques which become the most important skills in my Ph. D work. I would like to acknowledge the staff members: Dr. K.P. Sarathy, Dr. Steven Silber, Dr. Vladimir Bakhmoutov, Dr. Gregory Wylie, Dr. Nattamai Bhuvanesh, Dr. Joseph H. Reibenspies, Dr. Lisa Perez, Dr. Yohannes Rezenom, Vanessa Santiago, Angie Wilson, and Sandy Manning as well as my research collaborators: Dr. Zibo Li, Dr. Shuanglong Liu, and Mengzhe Wang for their useful advice and assistance, especially, Dr. Zibo Li who also offers me a postdoc job.

I also would like thank the former/current Thai graduate students in chemistry program at TAMU: Dr. Osit Karroonnirun, Dr. Supakarn Chamni, and Dr. Sakunchai Khumsubdee, Jaru Taechalertpaisan as well as the AF members: Anyanee Kamkaew, Termpan Pitakbunkate, Jakkrit Suriboot, Peerada Samunual, Veerachai Pongkittiphan and Moji for their friendship and supports throughout the past five years. Special thanks go to Anyanee Kamkaew for generous advices during my hard times in Ph. D study.

Furthermore, I would like to express my sincere gratitude to my parents, Siripen and Watsawat Chansaenpak for their love, support, and encouragement over the past twenty-eight years and to Suthasinee Bampentham for her love and patience while I finished my Ph. D.

Last but not least, I would like to acknowledge the National Science Foundation (NSF), the Welch Foundation, and the Cancer Prevention Research Institute of Texas (CPRIT) for research funding, the Department of Chemistry, the Office of Graduate Studies, and the World Molecular Imaging Congress 2013 for travel grants, and the National Science and Technology Development Agency of Thailand (NSTDA) for financial support to attend the 63rd Lindau Nobel Laureate Meeting. Special acknowledgement goes to the Development and Promotion of Science and Technology Talent project (DPST) for the prestigious scholarship which has supported me from high school to Ph. D and believed that I could be a good scientist.

TABLE OF CONTENTS

Page

ABSTRACT ii

DEDICATION iv

ACKNOWLEDGEMENTS v

TABLE OF CONTENTS vii

LIST OF FIGURES x

LIST OF TABLES xviii

CHAPTER I INTRODUCTION TO BORON-BASED RADIOTRACERS FOR POSITRON EMISSION TOMOGRAPHY 1

1.1 Introduction 1
1.2 Boron-based radiotracers featuring electron-withdrawing groups 3
1.3 Boron-based dyes for PET/fluorescence dual modality imaging 8
1.4 Influence of the cationic moiety on the Lewis acidity of the boron atom and its application for the construction of boron-based radiotracers. 17
1.5 Objectives 24

CHAPTER II *ORTHO*-PHENYLENE PHOSPHINO-BORANES FOR [^{18}F]-FLUORIDE ANION CAPTURE AND *IN VIVO* STABILITY STUDIES 26

2.1 Introduction 26
2.2 Synthesis and characterizations 29
2.3 Kinetic studies 34
2.4 Zwitterionic stibonium aryltrifluoroborate and its stabilization against hydrolysis 36
2.5 Radiofluorination 38
2.6 *In vivo* stability studies 42
2.7 Conclusion 44
2.8 Experimental 45

CHAPTER III SYNTHESIS AND *IN VIVO* EVALUATION OF [^{18}F]-ZWITTERIONIC ARYLTRIFLUOROBORATE/INDOMETHACIN CONJUGATES AS POTENTIAL PET PROBES 64

3.1 Introduction 64

3.2 Synthesis and characterizations....67
3.3 Kinetic studies....70
3.4 Radiochemistry....72
3.5 *In vivo* imaging studies....74
3.6 Conclusion....77
3.7 Experimental....77

CHAPTER IV CARBENE-BORANE ADDUCTS FOR ^{18}F FLUORIDE ANION CAPTURE AND *IN VIVO* STABILITY STUDIES....104

4.1 Introduction....104
4.2 Synthesis and characterization....106
4.3 Kinetic studies....114
4.4 Radiofluorination and *in vivo* imaging studies....115
4.5 Conclusion....121
4.6 Experimental....122

CHAPTER V TRIAZABOROLOPYRIDINIUMS FOR POSITRON EMISSION TOMOGRAPHY/ FLUORESCENCE DUAL MODALITY IMAGING....148

5.1 Introduction....148
5.2 Synthesis and characterizations....151
5.3 Fluorination and aqueous stability of the dyes....159
5.4 Conclusion....163
5.5 Experimental....163

CHAPTER VI SYNTHESIS, STRUCTURE, AND ISOMERIZATION OF PHOSPHINO-METHYLIUM COMPOUNDS....192

6.1 Introduction....192
6.2 Synthesis and characterizations....194
6.3 Conclusion....203
6.4 Experimental....203

CHAPTER VII SUMMARY....220

7.1 Zwitterionic arytrifluoroborate for ^{18}F fluoride anion capture....220
7.2 [^{18}F]-Zwitterionic aryltrifluoroborate/indomethacin conjugates for potential PET probes....221
7.3 [^{18}F]-Carbene-borane adducts as a novel radio-prosthetic group for PET imaging....222
7.4 Triazaborolopyridinium dyes for PET/Fluorescence dual modality imaging agents....223
7.5 Synthesis, structure, and isomerization of phosphino-methylium compounds....224
7.6 Conclusion....225

REFERENCES...226

LIST OF FIGURES

Page

Figure 1. Kinetic scheme for $ArBF_3$ hydrolysis. 2

Figure 2. Scheme showing the synthesis of **5** and **6**. 4

Figure 3. Scheme showing the fluorination reaction of **7** and **9**. 5

Figure 4. Scheme showing the radiosynthesis of [^{18}F]-**13**. 6

Figure 5. Scheme showing biomolecule conjugation of **14** *via* click chemistry. 8

Figure 6. Illustration of PET/fluorescence dual modality imaging agent **16**. 9

Figure 7. Illustration of activated BODIPY **17** and **18**. 10

Figure 8. Scheme showing the radiosynthesis of **19** and *in vivo* images of [^{18}F]-**20**. 11

Figure 9. Scheme showing the radiosynthesis of **21**. 13

Figure 10. Scheme showing the radiosynthesis of **23**. 14

Figure 11. Scheme showing the radiosynthesis of [^{18}F]-BODIPY®FL-RGD. 15

Figure 12. Scheme showing the radiosynthesis of BODIPY dyes using in situ generated TfOH as a catalyst. 16

Figure 13. Scheme showing the fluorination reaction of **24** and **25**. 17

Figure 14. Scheme showing the fluorination reaction of **26** and **27**. 18

Figure 15. Illustration of sulfonium boranes **28** and **29**. 19

Figure 16. Illustration of zwitterionic aryltrifluoroborate **30**, **31**, and **32**, and their hydrolytic rate constants. 20

Figure 17. Scheme showing the synthesis of **33**. 21

Figure 18. Illustration of peptide conjugated $AMBF_3$ A) ^{18}F-$AMBF_3$-TATE, B) ^{18}F-$AMBF_3$-B9858, and C) ^{18}F-$AMBF_3$-B9958. 23

Figure 19. Illustration of carbene-BF_3 adduct **34**. 25

Figure 20. Illustration of the *ortho*-phenylene phosphine-boranes **30**, **35**, **36**, and **37**.....28

Figure 21. Scheme showing the synthesis of **35**, **36**, and **37**.....30

Figure 22. Crystal structure of **35**. Displacement ellipsoids are scaled to the 50% probability level and hydrogen atoms have been omitted for clarity. Selected bond lengths (Å) and angles (deg) for **35**: P1-B1 3.386, B1-F1 1.414(2), B1-F2 1.403(2), B1-F3 1.404(2); P1-C1-C6 123.05(13), C1-C6-B1 127.21(16).....31

Figure 23. Crystal structure of **36**. Displacement ellipsoids are scaled to the 50% probability level and hydrogen atoms have been omitted for clarity. Selected bond lengths (Å) and angles (deg) for **36**: P1-B1 3.491, B1-F1 1.368(10), B1-F2 1.391(11), B1-F3 1.367(10), C21-O1 1.305(8), C21-O2 1.202(8); P1-C1-C6 122.3(5), C1-C6-B1 132.2(6). 32

Figure 24. Crystal structure of **37**. Displacement ellipsoids are scaled to the 50% probability level and hydrogen atoms have been omitted for clarity. Selected bond lengths (Å) and angles (deg) for **37**: P1-B1 3.429, B1-F1 1.395(3), B1-F2 1.425(3), B1-F3 1.400(3), C11-O1 1.336(3), C11-O2 1.195(3); P1-C1-C6 122.28(16), C1-C6-B1 129.4(2). 33

Figure 25. Kinetic plots for the hydrolysis of **30**, **35**, **36**, and **37**.The data were obtained at room temperature in D_2O/CD_3CN (8/2 vol.) at pH 7.5. The data shown for **30** has been previously reported[5] and is provided for the sake of comparison. 35

Figure 26. Scheme showing the synthesis of **38**. 36

Figure 27. Optimized structure of **38**. 37

Figure 28. HPLC profiles obtained in the radiofluorination of **30**. (A) Radio signal. (B) UV signal.....39

Figure 29. Direct ^{18}F-^{19}F isotopic exchange reaction employed for the radiolabeling of **30**, **35**, and **36** in aqueous solutions. 40

Figure 30. Decay-corrected whole-body microPET Sagittal images of athymic female nude mice from a static scan at 0.5, and 2 h after injection of [$^{18/19}F$]**30** and [$^{18/19}F$]**35**. The images are corrected based on the injected activity. The signal intensity is reported in % of the injected dose per gram (%ID/g). Preparations from entries 7 and 9 were used for these imaging experiments.....43

Figure 31. Calibration curves of compound **30** and **35** used for specific activity measurements. The standard injection volume is 200 µL. The first data point is obtained by diluting 10 µL of the standard solution to a total volume of 200 µL. The second data point is obtained by diluting 20 µL of the standard solution to a total volume of 200 µL. The third data point is obtained by injecting 200 µL of the stock solution. 60

Figure 32. Four representative independent ^{18}F-fluorination of compound **30** using condition mentioned at Table 1, entry 7. HPLC was performed on a phenomenex Luna 5µ C18 column (250 × 4.6 mm). The flow was 1 mL/min, with the mobile phase starting from 95% solvent A (0.1% TFA in water) and 5% solvent B (0.1% TFA in MeCN) (0–2 min) to 5% solvent A and 95% solvent B at 22 min. 61

Figure 33. Chemical structure of the indomethacin compound. 65

Figure 34. Chemical structure of the carboxy-X- rhodamine conjugated indomethacin.....66

Figure 35. Chemical structures of the zwitterionic phosphonium trifluoroborates.....66

Figure 36. Scheme showing the synthesis of the indomethacin containing ammonium group with various chain lengths.....68

Figure 37. Scheme showing the synthesis of *ortho*-phenylene phosphine-boranes connecting indomethacin compound. 69

Figure 38. Kinetic plots for the hydrolysis of **37** and **45** in aqueous conditions.....72

Figure 39. Reaction scheme showing direct ^{18}F-^{19}F isotopic exchange reaction proceeded for the radiolabeling of **45** and **46** in aqueous solution. 73

Figure 40. Crude radio-signal HPLC profiles obtained in the radiofluorination of [$^{18/19}$F]**46** (A) and [$^{18/19}$F]**45** (B).....74

Figure 41. (Above) Decay-corrected whole-body microPET Sagittal images of nude mice bearing U87MG tumor from a static scan at 15, 40, and 90 min after injection of [$^{18/19}$F]**45** and [$^{18/19}$F]**46**. The images are corrected based on the injected activity. The signal intensity is reported in % of the injected dose per gram (%ID/g). (Below) MicroPET quantifications for U87MG tumor and bone uptake for [$^{18/19}$F]**45** and [$^{18/19}$F]**46**. 76

Figure 42. 2-Dimentional NMR spectrum of **39**. 79

Figure 43. 2-Dimentional NMR spectrum of **40**. 81

Figure 44. 2-Dimentional NMR spectrum of **41**. 82

Figure 45. 2-Dimentional NMR spectrum of **42**. 84

Figure 46. 2-Dimentional NMR spectrum of **43**. 85

Figure 47. 2-Dimentional NMR spectrum of **44**. 87

Figure 48**.** 2-Dimentional NMR spectrum of **45**. 89

Figure 49. 2-Dimentional NMR spectrum of **46**. 91

Figure 50. 2-Dimentional NMR spectrum of **47**. 93

Figure 51. 2-Dimentional NMR spectrum of **48**. 95

Figure 52. MicroPET images of nude mice bearing U87MG tumor after injection of [$^{18/19}$F]**45** at 15, 40, and 90 min. 102

Figure 53. MicroPET images of nude mice bearing U87MG tumor after injection of [$^{18/19}$F]**46** at 15, 40, and 90 min. 103

Figure 54. Chemical structure of organoboranes used for ^{18}F fluoride captor in Positron Emission Tomography (PET) application and their hydrolysis rate constant (k_{Obs}). 105

Figure 55. Scheme showing the synthesis of **49**. 107

Figure 56. Scheme showing the synthesis of Arduengo carbene borane adducts tethered nitro (**51**), amine (**52**), succinimide (**53**), succinic acid (**54**), maleic acid (**55**), and maleimide (**56**) functional groups. 109

Figure 57. Crystal structure of **49**. Displacement ellipsoids are scaled to the 50% probability level and hydrogen atoms have been omitted for clarity. Selected bond lengths (Å) and angles (deg) for **49**: B1-C1 1.637(3), B1-F1 1.389(4), B1-F2 1.398(3), B1-F3 1.398(3); N1-C1-N2 105.8(3). 110

Figure 58. Crystal structure of **51**. Displacement ellipsoids are scaled to the 50% probability level and hydrogen atoms have been omitted for clarity. Selected bond lengths (Å) and angles (deg) for **51**: B1-C1 1.6575(18), B1-F1 1.3928(16), B1-F2 1.3948(16), B1-F3 1.3933(15); N1-C1-N2 106.50(10). 111

Figure 59. Crystal structure of **56**. Displacement ellipsoids are scaled to the 50% probability level and hydrogen atoms have been omitted for clarity.

Selected bond lengths (Å) and angles (deg) for **56**: B1-C1 1.656(9), B1-F1 1.347(9), B1-F2 1.395(9), B1-F3 1.390(10); N1-C1-N2 106.8(5).....112

Figure 60. Scheme showing the synthesis of **58** and **61**.....114

Figure 61. Scheme showing the radiolabeling of **49** employed by $SnCl_4$ assisted isotopic ^{18}F-^{19}F exchange. 116

Figure 62. Scheme showing the preparation of [^{18}F]-**56**/ H-Cys-Phe-OH conjugate. ..118

Figure 63. Left: UV trace of **56** as the standard reference. Right: Crude radio-HPLC profile for the ^{18}F-labeling of **56**.....118

Figure 64. Left: UV traces of BF_3-carbene-Cys-Phe as the standard reference. Right: Crude radio-HPLC profile for the ^{18}F-labeling of BF_3-carbene-Cys-Phe. 119

Figure 65. A: [^{18}F]**56**-peptide standard Radio-HPLC profile. B,C,D: [^{18}F]**56**-peptide in 1x PBS for 0.5h, 1h and 2h with purity of 96.6%, 93.9%, and 92.5%, respectively. 120

Figure 66. Decay-corrected whole-body microPET-CT sagittal images of nude mice from a static scan at 1, 2 h and 4 h after injection of [^{18}F]**56**/ H-Cys-Phe-OH conjugate. 121

Figure 67. Scheme showing the synthesis of **61**. 128

Figure 68. ^{1}H, ^{13}C, ^{11}B, and ^{19}F NMR spectra of **49** in CD_3CN.....134

Figure 69. ^{1}H, ^{13}C, ^{11}B, and ^{19}F NMR spectra of **51** in CD_3CN.....135

Figure 70. ^{1}H, ^{13}C, ^{11}B, and ^{19}F NMR spectra of **52** in CD_3CN.....136

Figure 71. ^{1}H, ^{13}C, ^{11}B, and ^{19}F NMR spectra of **53** in CD_3CN.....137

Figure 72. ^{1}H, ^{13}C, ^{11}B, and ^{19}F NMR spectra of **54** in D_2O. 138

Figure 73. ^{1}H, ^{13}C, ^{11}B, and ^{19}F NMR spectra of **55** in D_2O. 139

Figure 74. ^{1}H, ^{13}C, ^{11}B, and ^{19}F NMR spectra of **56** in CD_3CN.....140

Figure 75. ^{1}H, ^{13}C, ^{11}B, and ^{19}F NMR spectra of **58** in CD_3CN.....141

Figure 76. Scheme showing the radiofluorination of a BODIPY dye through a) an activated BODIPY dye, b) a Lewis acid-assisted isotopic ^{18}F-^{19}F exchange. 149

Figure 77. Illustration of the triazaborolopyridinium dye invented by Arterburn's group. 150

Figure 78. Scheme showing the synthesis of hydrazone precursors with different substituents. 151

Figure 79. Scheme showing the synthesis of triazaborolopyridinium dyes **65**, **66**, **67**, and **68**. 152

Figure 80. Scheme showing the synthesis of compound **69**. 154

Figure 81. Crystal structure of **69**. Displacement ellipsoids are scaled to the 50% probability level and hydrogen atoms have been omitted for clarity. Selected bond lengths (Å) and angles (deg) for **69**: B1-F1 1.371(3), B1-F2 1.367(3), B1-N1 1.596(3), B1-N3 1.561(3), N1-N2 1.402(2), N2-C1 1.350(3), N3-C1 1.354(3), N2-C6 1.450(3); F1-B1-F2 111.9(2), N1-B1-N3 96.45(17), B1-N1-N2 108.89(17), B1-N3-C1 111.65(18), N1-N2-C1 110.71(18), N2-C1-N3 111.90(19). 155

Figure 82. Scheme showing the synthesis of compound **70**. 156

Figure 83. Crystal structure of **70**. Displacement ellipsoids are scaled to the 50% probability level and hydrogen atoms have been omitted for clarity. Selected bond lengths (Å) and angles (deg) for **70**: B1-F1 1.377(3), B1-N4 1.560(3), B1-N1 1.531(3), B1-N3 1.557(3), N1-N2 1.401(3), N2-C1 1.333(3), N3-C1 1.374(3); F1-B1-N4 108.6(2), N1-B1-N3 97.08(19), B1-N1-N2 112.81(19), B1-N3-C1 108.4(2), N1-N2-C1 105.13(19), N2-C1-N3 116.5(2). 157

Figure 84. Scheme showing the synthesis of HPY dye **71**. 158

Figure 85. Scheme showing the fluorination of compound **70**. 160

Figure 86. ^{11}B NMR spectra of the fluorination reaction of **70** at different reaction times. 160

Figure 87. Scheme showing the fluorination of compound **71**. 161

Figure 88. Kinetic plots for the hydrolysis of **65**, **66**, **67**, and **68**. The data were obtained at room temperature in 10% w/v triton X-100 in H_2O/ DMSO (7/3 vol) at pH = 7.5. 162

Figure 89. ^{1}H, ^{13}C, ^{11}B, and ^{19}F NMR spectra of **65** in $CDCl_3$. 174

Figure 90. ^{1}H, ^{13}C, ^{11}B, and ^{19}F NMR spectra of **66** in $CDCl_3$. 175

Figure 91. ^{1}H, ^{13}C, ^{11}B, and ^{19}F NMR spectra of **67** in $CDCl_3$. 176

Figure 92**.** ^{1}H, ^{13}C, ^{11}B, and ^{19}F NMR spectra of **68** in $CDCl_3$. 177

Figure 93. ^{1}H, ^{13}C, ^{11}B, and ^{19}F NMR spectra of **69** in CD_3CN.....178

Figure 94. ^{1}H, ^{13}C, ^{11}B, and ^{19}F NMR spectra of **70** in $CDCl_3$. 179

Figure 95. ^{1}H, ^{13}C, and ^{11}B NMR spectra of **71** in $CDCl_3$. 180

Figure 96. ^{1}H, ^{13}C, ^{11}B, and ^{19}F NMR spectra of **72** in $CDCl_3$. 181

Figure 97. Absorption (blue) and emission (red) spectra of **65** in CH_2Cl_2. 188

Figure 98. Absorption (blue) and emission (red) spectra of **66** in CH_2Cl_2. 189

Figure 99. Absorption (blue) and emission (red) spectra of **67** in CH_2Cl_2. 189

Figure 100. Absorption (blue) and emission (red) spectra of **68** in CH_2Cl_2. 190

Figure 101. Absorption (blue) and emission (red) spectra of **71** in CH_2Cl_2. 190

Figure 102. Absorption (blue) and emission (red) spectra of **72** in CH_2Cl_2. 191

Figure 103. Illustration of intramolecular frustrated Lewis pair systems. 193

Figure 104. Illustration of the intramolecular P/C^{+} frustrated Lewis pairs synthesized in this work.....194

Figure 105. Scheme depicting the synthesis of phosphino-methylium **73** and **74**.....195

Figure 106. Crystal structure of **73**. Displacement ellipsoids are scaled to the 50% probability level. Tetrafluoroborate counter anion and hydrogen atoms were omitted for clarity. Selected bond lengths (Å) and angles (deg) for **73**: P1-C1 1.871(4), C1-C2 1.597(5), C2-C3 1.401(5), P1-C3 1.735(4); C1-P1-C3 80.33(18), P1-C1-C2 83.4(2), C1-C2-C3 101.7(3), C2-C3-P1 94.6(3). 196

Figure 107. Crystal structure of **74**. Displacement ellipsoids are scaled to the 50% probability level. Tetrafluoroborate counter anion and hydrogen atoms were omitted for clarity. Selected bond lengths (Å) and angles (deg) for **74**: P1-C1 1.9129(18), C1-C2 1.542(2), C2-C3 1.395(3), P1-C3 1.7727(19); C1-P1-C3 74.28(8), P1-C1-C2 83.63(10), C1-C2-C3 104.74(15), C2-C3-P1 93.39(12). 197

Figure 108. Scheme depicting the isomerization of phosphino-methylium **73** and **74**.....199

Figure 109. Crystal structure of **75**. Displacement ellipsoids are scaled to the 50% probability level. Tetrafluoroborate counter anion and hydrogen atoms were omitted for clarity. Selected bond lengths (Å) and angles (deg) for **75**: P1-C1 1.7848(18), C1-C2 1.400(2), C2-C3 1.517(2), C3-C4 1.524(2), C4-C5 1.399(2), P1-C5 1.7838; C1-P1-C5 109.54(8), P1-C1-C2 118.56(12), C1-C2-C3 123.38(14), C2-C3-C4 114.87(13), C3-C4-C5 122.25(14), C4-C5-P1 119.09(12). 200

Figure 110. Crystal structure of **76**. Displacement ellipsoids are scaled to the 50% probability level. Tetrafluoroborate counter anion and hydrogen atoms were omitted for clarity. Selected bond lengths (Å) and angles (deg) for **76**: P1-C1 1.773(5), C1-C2 1.405(5), C2-C3 1.513(5), C3-C4 1.529(5), C4-C5 1.406(5), P1-C5 1.779(5); C1-P1-C5 106.65(18), P1-C1-C2 121.8(3), C1-C2-C3 125.5(3), C2-C3-C4 118.8(3), C3-C4-C5 125.1(4), C4-C5-P1 121.8(3).....201

Figure 111. Kinetic plot of the isomerization process of **73**. 202

Figure 112. ^{1}H, ^{13}C, and ^{31}P NMR spectra of **73**.....209

Figure 113. ^{1}H, ^{13}C, and ^{31}P NMR spectra of **74**.....210

Figure 114. ^{1}H, ^{13}C, and ^{31}P NMR spectra of **75**.....211

Figure 115. ^{1}H, ^{13}C, and ^{31}P NMR spectra of **76**.....212

Figure 116. Illustration of zwitterionic aryltrifluoroborate **30**, **35**, **36**, and **37**. 221

Figure 117. Illustration of zwitterionic aryltrifluoroborate/indomethacin conjugates **45** and **46**. 222

Figure 118. Illustration of carbene-borane adducts **34** and **56**/H-Cys-Phe-OH conjugate.....223

Figure 119. Illustration of Triazaborolopyridinium dyes **71**.....224

Figure 120. Illustration of phosphino-methylium compounds **73** and **74**. 225

LIST OF TABLES

Page

Table 1. Radiosynthetic results. 41

Table 2. Crystal data, data collections, and structure refinements of **35**. 51

Table 3. Crystal data, data collections, and structure refinements of **36**. 52

Table 4. Crystal data, data collections, and structure refinements of **37**. 53

Table 5. Kinetic data for the hydrolysis of **35**. The values provided for F^- and $ArBF_3$ correspond to the integration of the corresponding NMR signal. 55

Table 6. Kinetic data for the hydrolysis of **36**. The values provided for F^- and $ArBF_3$ correspond to the integration of the corresponding NMR signal. 56

Table 7. Kinetic data for the hydrolysis of **37**. The values provided for F^- and $ArBF_3$ correspond to the integration of the corresponding NMR signal. 57

Table 8. Kinetic data for the hydrolysis of **37** in D_2O–CD_3CN (8/2 vol) at pH 7.5 ([phosphate buffer] = 500 mM). The values provided for F^- and $ArBF_3$ correspond to the integration of the corresponding NMR signal. 97

Table 9. Kinetic data for the hydrolysis of **37** in 10% w/v triton X-100 in H_2O/ DMSO (7/3 vol) at pH = 7.5 ([phosphate buffer] = 500 mM). The values provided for F^- and $ArBF_3$ correspond to the integration of the corresponding NMR signal. 98

Table 10. Kinetic data for the hydrolysis of **45** in 10% w/v triton X-100 in H_2O/ DMSO (7/3 vol) at pH = 7.5 ([phosphate buffer] = 500 mM). The values provided for F^- and $ArBF_3$ correspond to the integration of the corresponding NMR signal. 99

Table 11. Radiosynthetic results. 117

Table 12. Crystal data, data collections, and structure refinements of **49**. 131

Table 13. Crystal data, data collections, and structure refinements of **51**. 132

Table 14. Crystal data, data collections, and structure refinements of **56**. 133

Table 15. Kinetic data for the hydrolysis of **49**. The values provided for F^- and $ArBF_3$ correspond to the integration of the corresponding NMR signal. 143

Table 16. Kinetic data for the hydrolysis of **52**. The values provided for F^- and $ArBF_3$ correspond to the integration of the corresponding NMR signal. 144

Table 17. Kinetic data for the hydrolysis of **54**. The values provided for F^- and $ArBF_3$ correspond to the integration of the corresponding NMR signal. 145

Table 18. Crystal data, data collections, and structure refinements of **69**. 183

Table 19. Crystal data, data collections, and structure refinements of **70**. 184

Table 20. Kinetic data for the hydrolysis of **65** in 10% w/v triton X-100 in H_2O/ DMSO (7/3 vol) at pH = 7.5 ([phosphate buffer] = 500 mM). The values provided for F^- and $ArBF_3$ correspond to the integration of the corresponding NMR signal. 186

Table 21. Kinetic data for the hydrolysis of **66** in 10% w/v triton X-100 in H_2O/ DMSO (7/3 vol) at pH = 7.5 ([phosphate buffer] = 500 mM). The values provided for F^- and $ArBF_3$ correspond to the integration of the corresponding NMR signal. 186

Table 22. Kinetic data for the hydrolysis of **67** in 10% w/v triton X-100 in H_2O/ DMSO (7/3 vol) at pH = 7.5 ([phosphate buffer] = 500 mM). The values provided for F^- and $ArBF_3$ correspond to the integration of the corresponding NMR signal. 187

Table 23. Kinetic data for the hydrolysis of **68** in 10% w/v triton X-100 in H_2O/ DMSO (7/3 vol) at pH = 7.5 ([phosphate buffer] = 500 mM). The values provided for F^- and $ArBF_3$ correspond to the integration of the corresponding NMR signal. 187

Table 24. Crystal data, data collections, and structure refinements of **73**. 214

Table 25. Crystal data, data collections, and structure refinements of **74**. 215

Table 26. Crystal data, data collections, and structure refinements of **75**. 216

Table 27. Crystal data, data collections, and structure refinements of **76**. 217

Table 28. Kinetic data for the isomerization of **73**. 219

CHAPTER I

INTRODUCTION TO BORON-BASED RADIOTRACERS FOR POSITRON EMISSION TOMOGRAPHY

1.1 Introduction

Positron emission tomography (PET) has become a popular imaging technique that provides *in vivo* information on the distribution of radiolabeled biomolecules. This technique, which relies on the coincident detection of two 180° high-energy photons that are released simultaneously upon positron-electron annihilation, requires the incorporation of a positron-emitting atom into the biomolecule under study.[1,2] Fluorine-18 has become one of the most popular radionuclides used in PET because of the characteristics of its nuclear decay and its relative ease of preparation by irradiation of [^{18}O]-water.[3] However, with a half-life of 110 minutes, the incorporation of [^{18}F]-fluorine into biomolecules needs to be carried out in a swift and efficient manner to minimize any loss of activity. As an added complication, the irradiation of [^{18}O]-water produces aqueous solutions of [^{18}F]-fluoride ions whose reactivity is dampened by hydration. Because of these obstacles, further growth in the field of ^{18}F PET imaging hinges on the development of fast and reliable radiofluorination protocols that can be implemented in aqueous solutions.

An approach that is gaining increasing visibility is based on the use of trifluoroborate derivatives, highly fluorophilic boron compounds that are referred to as fluoride captors. The hydrolysis of aryltrifluoroborates has been previously

investigated.[4] Although the mechanism of fluoride dissociation involves multiple steps (Figure 1), it has been demonstrated that dissociation of the first fluoride anion is a rate-determining step. In turn, the kinetics of such reactions can be properly treated by a simple first-order rate law (rate = k_{obs}[$ArBF_3$]).

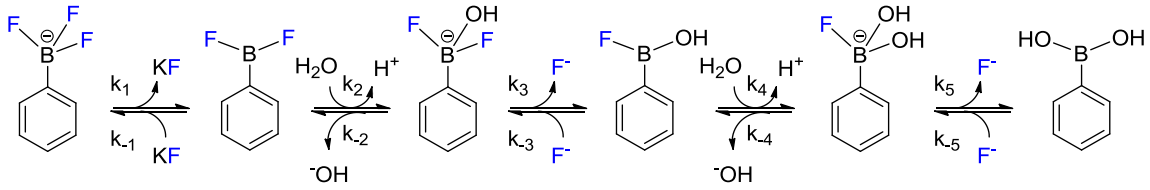

Figure 1. Kinetic scheme for $ArBF_3$ hydrolysis.

In this chapter, I will provide the relevant background information regarding boron-based radiotracers. Three different topics will be presented, including 1) boron-based radiotracers featuring electron-withdrawing groups, 2) boron-based dyes for PET/fluorescence dual modality imaging, and 3) the influence of the cationic moiety on the Lewis acid of the boron atom and its application in the construction of boron-based radiotracers.

1.2 Boron-based radiotracers featuring electron-withdrawing groups

The effects of substituents on the stability of aryltrifluoroborate in aqueous solution were first studied by Perrin and coworkers.[4] In their work, they found that electron-donating substituents, e.g., methoxy groups, accelerate the rate of aryltrifluoroborate hydrolysis, whereas electron-withdrawing substituents, e.g., fluoro groups, slow it down. With this concept in hand, the Perrin group used 2,4,6-trifluoro-3-carboxy phenyl boronic ester (**1**) and 2,6-difluoro-4-carboxy phenyl boronic ester (**2**) as prosthetic groups to capture [^{18}F]-fluoride anions in aqueous solution. Compound **1** was conjugated with fluorescent boron-dipyrromethene (BODIPY) dye[5], which would allow for the visualization of sub-nanomole quantities of radiolabeled aryltrifluoroborate on a TLC plate, whereas compound **2** was connected to amino-linked biotin[6] to for potential streptavidine labeling (Figure 2). Both conjugated compounds (**3** and **4**) can be transformed into aryltrifluoroborate derivatives (**5** and **6**) by treatment with KHF_2 in acidic conditions. The radioactive species **5** and **6** can be prepared by the reaction of [^{18}F]-fluoride anion with arylboronate ester derivatives **3** and **4** using [^{19}F]-KHF_2 as a carrier. The kinetic stability of [^{18}F]-**5** and [^{18}F]-**6** was investigated by their relative autoradiographic density on the TLC plate. The rate constants (k_{obs}) for the defluorination of [^{18}F]-**5** and [^{18}F]-**6** calculated from the first-order rate equation are 1.2 ± 0.4 x 10^{-4} min^{-1} and 2.8 ± 0.9 x 10^{-4} min^{-1}, respectively (k_{obs} of K[$PhBF_3$] = 0.0245 min^{-1}). These results indicate that the electron-withdrawing nature of the fluorine atoms on the benzene ring in **5** and **6** may help stabilize the trifluoroborate moiety in aqueous solution.

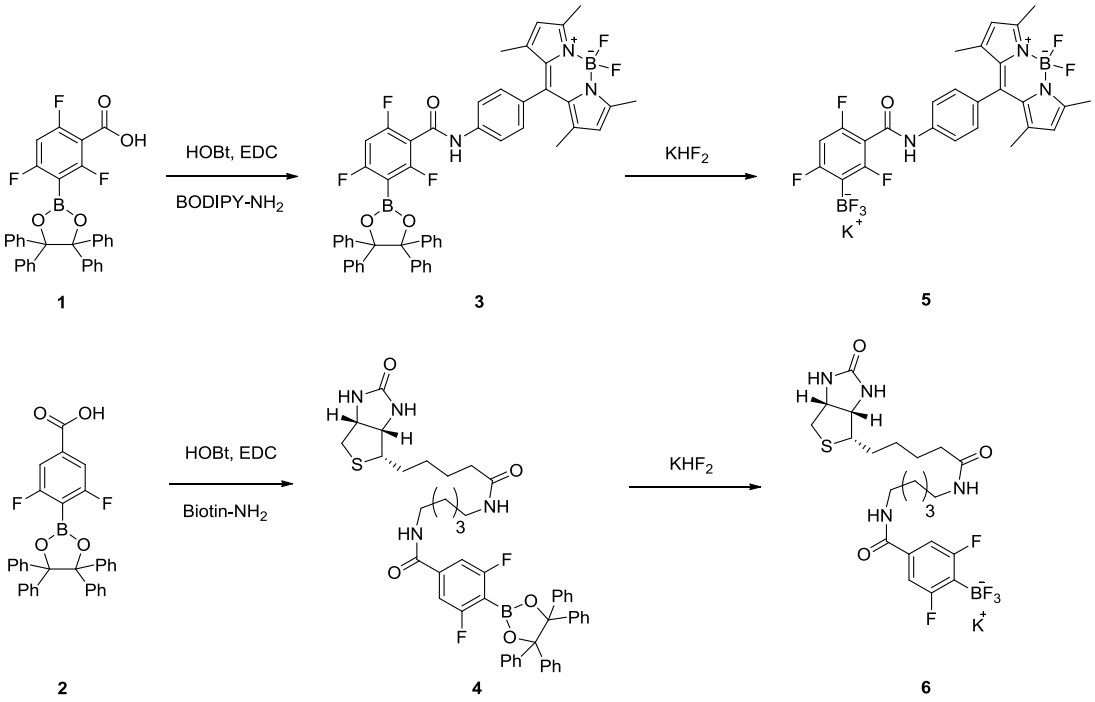

Figure 2. Scheme showing the synthesis of **5** and **6**.

To prove that fluoro-substituted phenyl boronic ester can be used as a prosthetic group for PET imaging and that its corresponding aryltrifluoroborate is stable *in vivo*, Perrin and coworkers prepared a new biotinylated arylboronic ester (**7**) *via* an amide coupling reaction between **1** and biotinylated piperazine to test its *in vivo* stability.[7] The [^{18}F]-biotinylated aryltrifluoroborate **8** can be prepared by the reaction of **7** with [^{18}F]-KHF_2 in aqueous solution at pH 4.5 (Figure 3). After silica column purification, [^{18}F]-**8** was injected into the tail vein of a 16-week-old female mouse. PET images showed that the [^{18}F]-**8** accumulated in the bladder, liver, and salivary glands. Surprisingly, no radio-signal accumulation in bones was observed. This result is noteworthy because it is the

first demonstration that a [^{18}F]-labeled trifluoroborate is stable *in vivo*. To further validate the use of phenyl boronate ester for ^{18}F fluoride anion capture, **1** was conjugated to marimastat, a noncovalent matrix metalloproteinase (MMP) inhibitor (Figure 3).[8,9] Matrix metalloproteinases are zinc-dependent endopeptidases that are strongly associated with pathogenic markers of cancer. The marimastat-arylboronic ester conjugate (**9**) was used as a captor for aqueous ^{18}F fluoride anion in a rapid one-step reaction at ambient temperature.[9] In an *in vivo* imaging study, [^{18}F]-marimastat aryltrifluoroborate (**10**) demonstrated detectable and specific uptake in the primary tumor of tumor-bearing mice at 60 min post injection.[8] Moreover, in a control experiment, no tumor localization was observed after the injection of the [^{18}F]-**1** into tumor-bearing nude mice. These results illustrate that [^{18}F]-**10** is a good candidate for clinical applications.

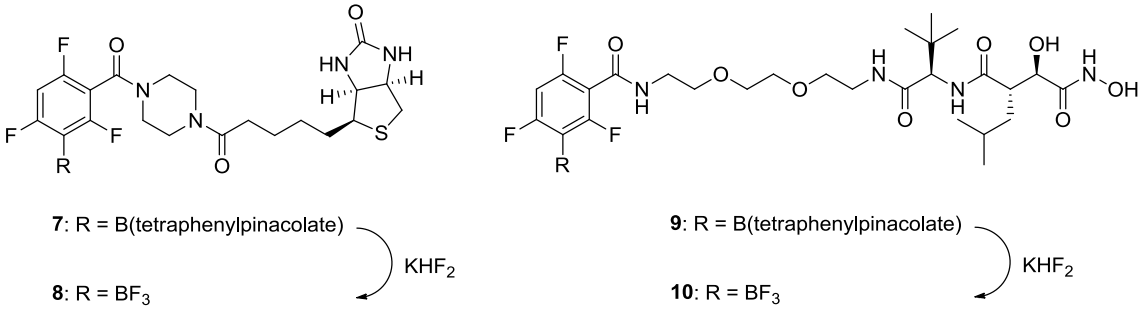

Figure 3. Scheme showing the fluorination reaction of **7** and **9**.

The copper(I)-catalyzed alkyne-azide cycloaddition (CuAAC or "click") reaction is an appealing approach for prosthetic group conjugation in PET radiopharmaceutical

research. Although the click chemistry of aryltrifluoroborate was first studied by Molado and co-worker[10], Perrin and his colleague developed this reaction for radiochemical research. In Perrin's work, a B(dan)-protected radiosynthon connected with an alkyne functional group (**11**) was used as a precursor to generate [^{18}F]-aryltrifluoroborate **12** by treatment with [^{18}F]-KF at acidic pH (pH 2) (Figure 4).[11] To obtain an accurate specific activity (SA), [^{18}F]-**12** was clicked to rhodamine-N_3 in the presence of copper(II) sulfate and sodium ascorbate. This method produced the [^{18}F]-rhodamine conjugated aryltrifluoroborate (**13**) with high specific activity (15 Ciμmol^{-1}). They also confirmed that the specific activity of the conjugated radiotracer can be reliably calculated by tripling the specific activity of the [^{18}F]-fluoride anion.[11] This one-pot two-step labeling protocol is mild, fast (30 min), and efficient (high specific activity), and it can be applied to the radiosynthesis of biomolecules.[11-13]

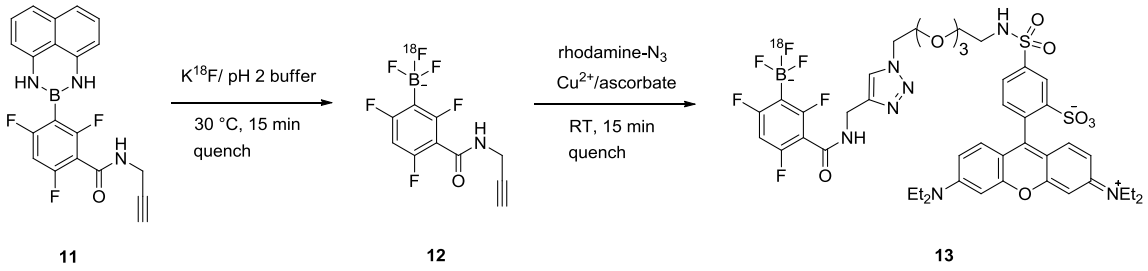

Figure 4. Scheme showing the radiosynthesis of [^{18}F]-**13**.

To broaden the collection of potential aryltrifluoroborate prosthetics, Perrin and coworkers reported a new route to the synthesis of a new heteroaryl-BF_3^- featuring

bromine substituents (**14**).[14] The B-F bonds in this compound are stabilized by the inductive electron withdrawing effects derived from the bromo substituents, the amide functional group, and the pyridyl nitrogen atom. Compound **14** was conjugated to azide containing RGD peptide *via* a copper catalyzed cycloaddition reaction (Figure 5). Prior to testing the stability of the RGD conjugated heteroaryltrifluoroborate (**15**), the authors decided to examine the solvolytic stability of the parent 2-amino-3,5-dibromopyridyl-4-trifluoroborate ($hArBF_3$) by nuclear magnetic resonance (NMR) of fluorine nuclei. The ^{19}F NMR spectroscopy revealed that the rate of $hArBF_3$ hydrolysis is extremely slow. The solvolysis decomposition data were fitted to a first-order rate equation, with a rate constant of 4.2×10^{-5} min^{-1} and a half-life of 16500 min. This half-life is 10-fold longer than that of the previous trifluoro-substituted aryltrifluoroborate. Then, compound **15** was radiofluorinated by an ^{18}F-^{19}F isotopic exchange reaction with mild heating (45 °C) under acidic conditions (pH = 2). [^{18}F]-**15** was obtained with good radiochemical yield (20 % decay corrected) and high specific activity (3 Ci μmol^{-1}). This [^{18}F]-radiotracer also showed good stability *in vitro* in mouse plasma incubated at 37 °C with <1% degradation observed after 150 min. The stability was also confirmed by *in vivo* imaging showing that minimal bone uptake was observed (~0.5%) after 60 min.

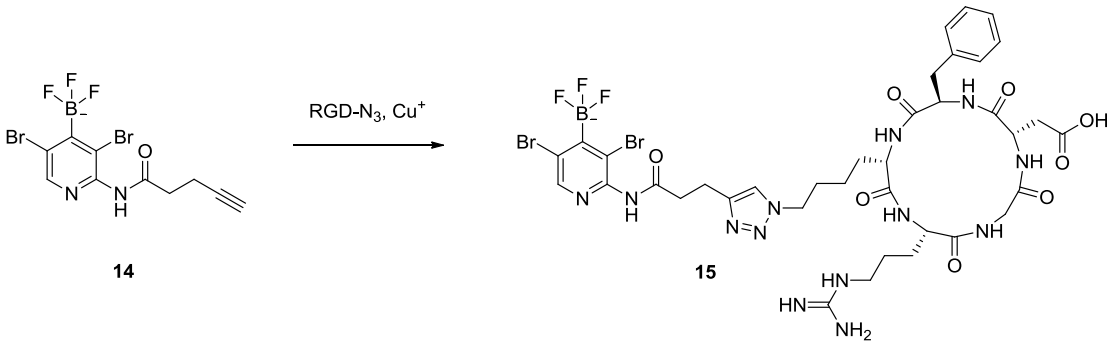

Figure 5. Scheme showing biomolecule conjugation of **14** *via* click chemistry.

1.3 Boron-based dyes for PET/fluorescence dual modality imaging

[^{18}F]-positron emission tomography is a powerful imaging technique used to monitor metabolic pathways *in vivo*. However, because of the relatively low spatial resolution (1–2 mm) provided by this technique, combining PET imaging with a second imaging technique such as fluorescence gives much higher spatial and temporal resolution. This approach necessitates the incorporation of a fluorophore into a radiolabeled component. In 2010, Tsien and coworkers combined a novel organoboronate ester for [^{18}F]-fluoride anion trapping with a near-infrared fluorophore, a cyanine derivative, into a single molecule (**16**) (Figure 6).[15] This molecule was tagged with Lymphoseek, a mannosylated 16 kDa dextran conjugate that was developed for sentinel lymph node mapping through an amide coupling reaction at the N-hydroxysuccinimide (NHS) ester functional group. The sentinel lymph node is the target organ primarily reached by cancer cells from a tumor. Therefore, detection of the sentinel lymph node prior to cancerous dissemination is highly significant for medical diagnosis. A Lymphoseek-conjugated radioactive species was successfully prepared by

treatment with [^{18}F]-KHF_2 in 0.25 M HCl/25% MeOH/75% H_2O solution at 40 °C. Gratifyingly, it can target mouse sentinel lymph nodes (SLNs) within 1 h, which is superior to the current SLN mapping agents.

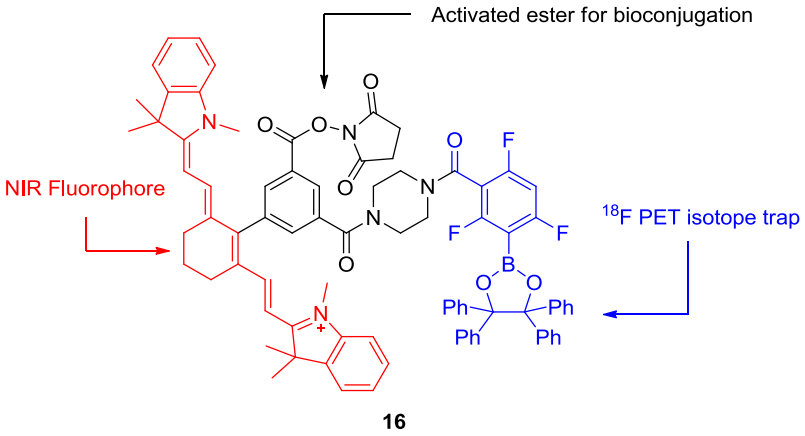

Figure 6. Illustration of PET/fluorescence dual modality imaging agent **16**.

In 2008, Gabbai and coworkers were the first group to investigate the late stage B-F bond formation of the BODIPY dye. The BODIPY boronium cation **17** was prepared from a reaction of the corresponding difluoro BODIPY dye with trimethylsilyltriflate (TMSOTf) followed by the addition of 4-dimethylaminopyridine (DMAP).[16] This compound, which can react with tetrabutylammonium fluoride (TBAF) to afford the difluoro dye BODIPY, was developed for use as a fluoride anion sensor. To quench the fluorescent signal of **17**, 10 equivalents of tetrabutylammonium iodide (TBAI) were added to a solution of **17** in chloroform. The addition of 1 equivalent of TBAF to the solution mixture of **17** and 10 equiv. of TBAI increased the fluorescence intensity by a factor f = 500%. This turn-on response, which could be detected with the

naked eye, suggested that this approach can be used for fluoride anion sensing applications. Two years later, our group reported a method for synthesizing a new B-OH containing BODIPY dye, **18**.[17] This hydroxide derivative (**18**) was prepared from the corresponding BODIPY-phenylboron chloride by simply passing a solution of the chloride derivative through silica gel. Although the B-Cl BODIPY precursor is sensitive to moisture, the B-OH BODIPY derivative (**18**) is air and water stable. Gratifyingly, compound **18** can be easily transformed to the BODIPY-phenylboron fluoride species by the reaction of **18** with potassium hydrogen bifluoride (KHF_2) in THF. These results are significant because they suggest that both **17** and **18** can be used as precursors for the preparation of ^{18}F-labeled BODIPY dyes.

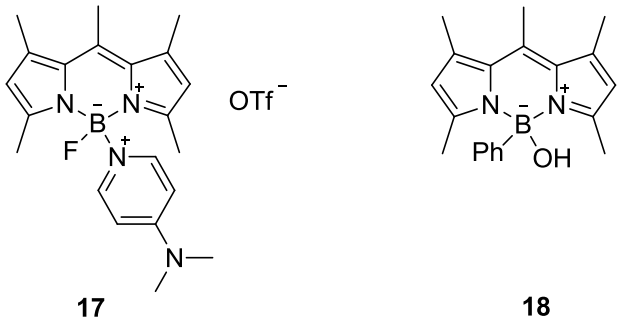

17 **18**

Figure 7. Illustration of activated BODIPY **17** and **18**.

With these preliminary results in hand, our group decided to develop a new ^{18}F incorporation reaction that would proceed in aqueous conditions from the stable BODIPY precursor.[18,19] To reach this goal, we synthesized a new ammonium BODIPY-phenylboron hydroxide (**19**) and attempted its fluorination. Delightfully, conversion into

the fluoro derivative (**20**) can be achieved by the addition of KHF_2 to an acidic mixed MeOH/water (1/1 vol.) solution of **19** (Figure 8). This approach was applied to the ^{18}F radiofluorination of **19,** affording [^{18}F]-**20** in 22 ± 3 % radiochemical yield (decay corrected) with a specific activity of 25 ± 4 mCi/μmol. *In vitro* stability studies of [^{18}F]-**20** in phosphate buffer solution pH 7.5 showed only 5% decomposition after 6 h, suggesting that this compound has high stability in aqueous solution. To further confirm its potential for *in vivo* PET imaging, [^{18}F]-**20** was injected into normal nude mice. Splendidly, the PET images showed no bone uptake signals even at 4 h post injection. (Figure 8)

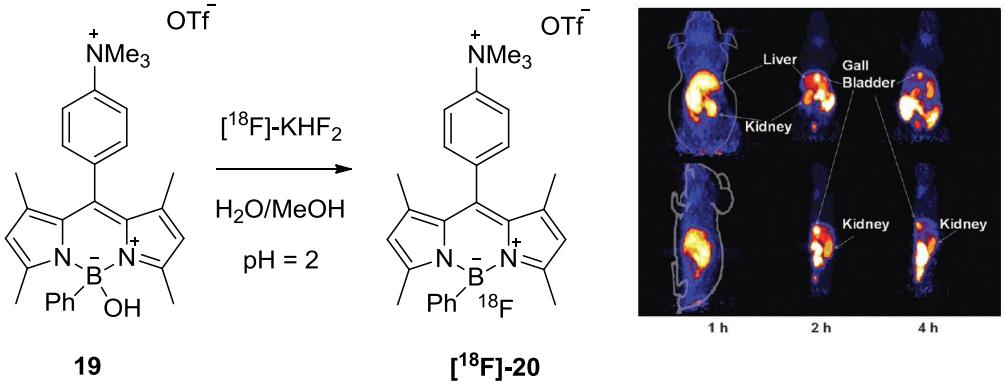

Figure 8. Scheme showing the radiosynthesis of **19** and *in vivo* images of [^{18}F]-**20**.

Subsequently, Mazitschek and coworkers investigated the ^{18}F-incorporation reaction of our reported DMAP-activated BODIPY dye (**17**).[19] They found that efficient conversion into [^{18}F]-1,3,5,7,8-pentamethyl BODIPY difluoroborate ([^{18}F]-**21**) can only be done at high temperature (100 °C) in DMF (Figure 9, Scheme A). This fluorination

condition and the prolonged heating required to synthesize the DMAP intermediate tend to be incompatible with certain sensitive functional groups typically present in complex biologically active small molecules such as N-hydroxysuccinimide (NHS) ester. To avoid this problem, the Mazitschek group has developed a mild fluorination condition for this protocol. They discovered that TMSOTf can be used to abstract one fluoride from the BODIPY core in a quantitative yield at 0 °C in less than 5 minutes. The activated BODIPY triflate (**22**) can be easily transformed into its starting material (**21**) upon the addition of fluoride anion into organic medium. In addition, to avoid the formation of TMSF species, *tert*-butyl alcohol was added to the reaction to quench any excess TMSOTf. Mazitschek and coworkers also proved that this approach can be applied to the fluorination of more sensitive derivatives such as BODIPY *N*-hydroxysuccinimide ester. With these results in hand, the construction of [^{18}F]-**21** can be done within 2 minutes (Figure 9, Scheme B) with 67% radiochemical yield and a specific activity of 0.96 Ci/μmol. Moreover, [^{18}F]-BODIPY NHS ester, which can be prepared by the same condition with 73% radiochemical yield, was successfully conjugated to Trastuzumab, the monoclonal antibody that is normally used to treat HER-2 positive breast cancer. These results are significant because they manifest the viability of this approach for the labeling of biological macromolecules.

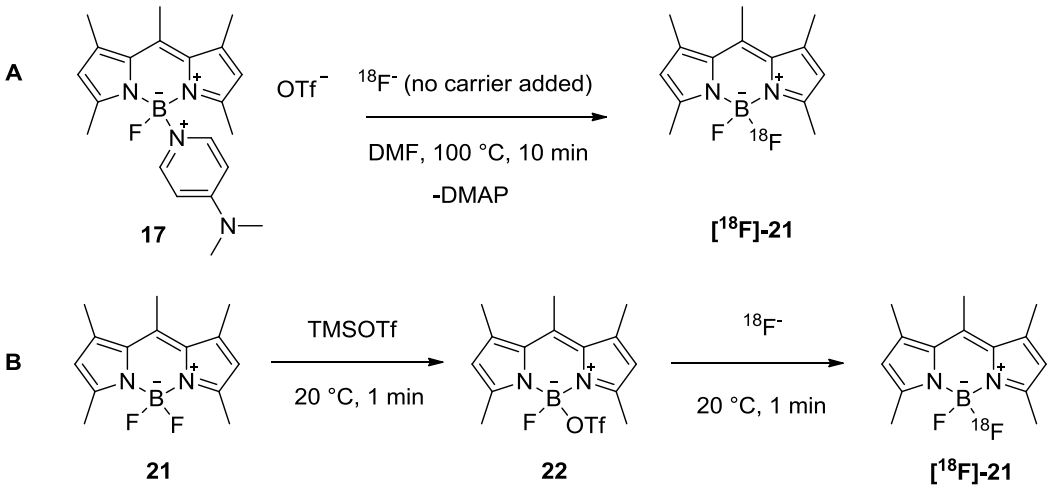

Figure 9. Scheme showing the radiosynthesis of **21**.

A new strategy to use the $–BF_2$ unit as a specific site for isotopic exchange with [^{18}F]-fluoride anion to form [^{18}F]-BODIPY was developed by Li and coworkers.[20] This protocol is promising because the time-consuming process of preparing an activated hydroxide, triflate, or DMAP BODIPY derivative is not necessary. In this study, Lewis acidic reagents were used to promote the fluoride exchange process. Initially, the ^{18}F-^{19}F isotopic exchange of **23** was performed in aqueous medium under acidic conditions. Regrettably, the radiochemical yield of this process was extremely low (<2 %). Then, they directed their attention to the radiofluorination process of **23** in organic medium. They found that the Lewis acid $SnCl_4$ noticeably promoted the ^{18}F-^{19}F isotopic exchange of **23** at ambient temperature (25 °C) in acetonitrile with excellent radiochemical yield (> 95%) (Figure 10). They also proved that the starting radioactivity (50 vs 10 mCi) did not significantly affect the yield. However, the use of a more polar solvent such as DMSO lowered the radiochemical yield due to a high solvent-Lewis acid interaction.

Favorably, Li and coworkers also discovered that [^{18}F]-**23** can be selectively accumulated in cardiac muscle based on a cellular uptake assay and the biodistribution signal in microPET images.[21] The biodistribution data showed a high level of [^{18}F]-**23** accumulation in heart tissue as well as good heart-to-blood and heart-to-lung contrast. With these results in hand, they concluded that [^{18}F]-**23** is a good candidate to use in myocardial perfusion imaging applications. This approach is also applicable for the ^{18}F labeling of BODIPY *N*-succinimide ester, a more sensitive derivative that can be used to construct a radiolabeled BODIPY-peptide conjugate (Figure 11 A).

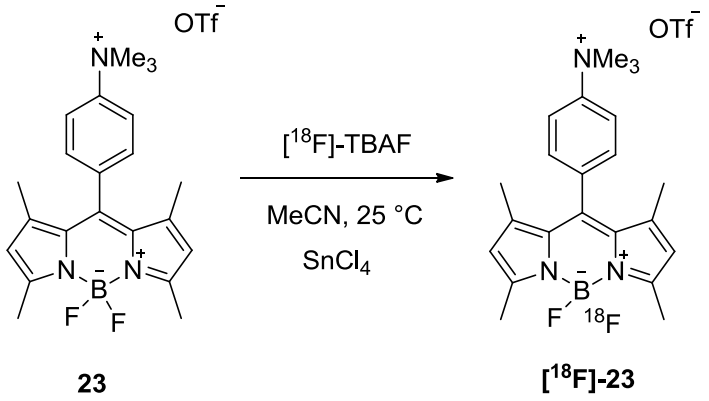

Figure 10. Scheme showing the radiosynthesis of **23**.

Although most approaches to synthesize [^{18}F]-BODIPY conjugates tend to incorporate ^{18}F into the BODIPY dye before its conjugation to a biomolecule[19,20], Li and coworkers recently reported a new protocol that addresses this limitation.[22] In this report, they showed that ^{18}F-^{19}F isotopic exchange can be performed directly on a BODIPY®FL-RGD conjugate in the presence of a Lewis acid (Figure 11 B). In this

case, they found that the $SnCl_4$ was not a good activator for this radio-fluoride exchange reaction as a relatively low yield of the [^{18}F]-BODIPY-peptide conjugate was acquired in this condition due to the decomposition of BODIPY®FL-RGD. Therefore, milder Lewis acids such as $ZnCl_2$ and $SnCl_2$ were selected for use in this application. Interestingly, $SnCl_2$ can efficiently transform BODIPY®FL-RGD into [^{18}F]-BODIPY®FL-RGD at room temperature with high radiochemical yield (82.8%). This new method is significant because the two-step synthesis of [^{18}F]-BODIPY®FL-RGD conjugate was simplified into a one-step process, thereby shortening the radio-synthetic time. Moreover, this protocol can also be applied to the radiolabeling of the near-infrared (NIR) dye BODIPY®R6G. Radioactive NIR fluorescent dyes are important for *in vivo* imaging applications because they can efficiently penetrate into targeted tissue.

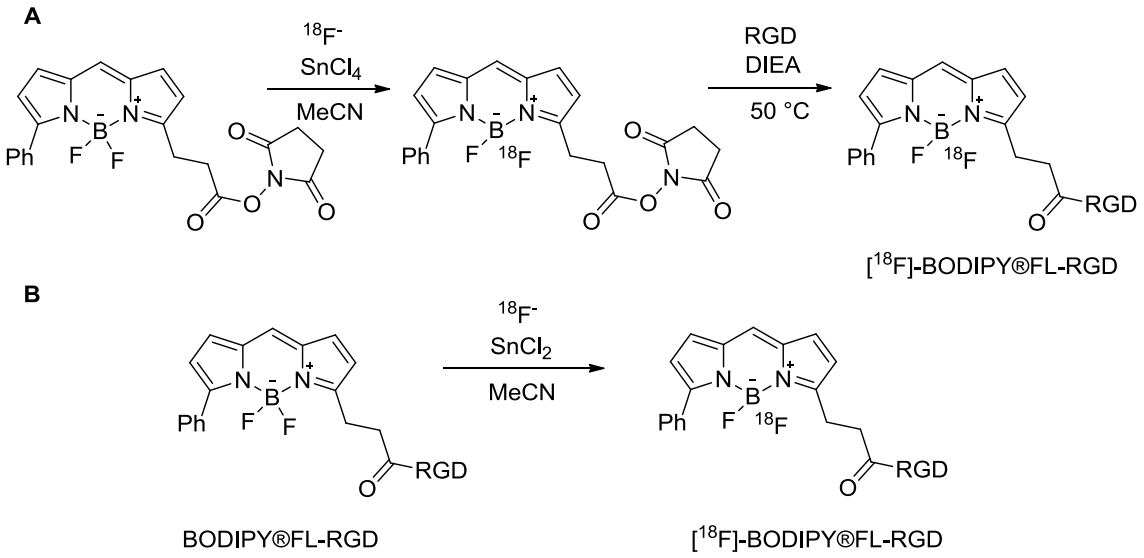

Figure 11. Scheme showing the radiosynthesis of [^{18}F]-BODIPY®FL-RGD.

This acid-catalyzed protocol was further studied by Weissleder and coworkers.[23] In this case, trifluormethanesulfonic acid (TfOH) was generated in situ by the addition of trifluormethanesulfonic anhydride (Tf_2O) and *tert*-butyl alcohol (*t*-BuOH) into a solution of BODIPY dye in the presence of azeotropically dried ^{18}F source at 50 °C to promote the ^{18}F-^{19}F isotopic exchange process (Figure 12). It is important to note that the addition of commercial TfOH to the reaction mixture led to the rapid decomposition of the BODIPY precursor. Based on their kinetic study, they found that the rate of this isotopic exchange reaction is dependent on both the Tf_2O/*t*-BuOH ratio and the amount of BODIPY dye in the solution. This approach is promising because it can be applied to the radio-labeling of several commercially bioconjugable BODIPY molecules and BODIPY-conjugated biomolecules.

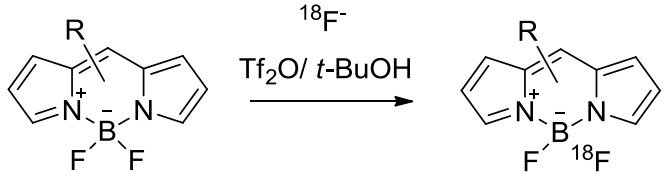

Figure 12. Scheme showing the radiosynthesis of BODIPY dyes using in situ generated TfOH as a catalyst.

1.4 Influence of the cationic moiety on the Lewis acidity of the boron atom and its application for the construction of boron-based radiotracers

Gabbai and coworkers have been developing novel cationic organoboranes to use as anion receptors for the past decade. In this approach, a cationic moiety is used to increase the Lewis acidity of the boron atom *via* Coulombic effects. They discovered that Coulombic stabilization increases when the cationic substituent is conjugated close to the boron center, as shown in reports on ammonium[24], phosphonium[25,26], stibonium[27], sulfonium[28], and telluronium[29] boranes. In the case of ammonium boranes, they showed that *ortho*-ammonium borane (**24**) can capture fluoride anions in aqueous solution with a fluoride binding constant of 910 (±50) M^{-1}, whereas the para-derivative (**25**) cannot take fluoride anion under the same condition (Figure 13).[24] The increased Lewis acidity of the boron atom in **24** may also be facilitated by the formation of stabilizing hydrogen bonds between the C-H in the trimethyl ammonium group and the B-F moiety.

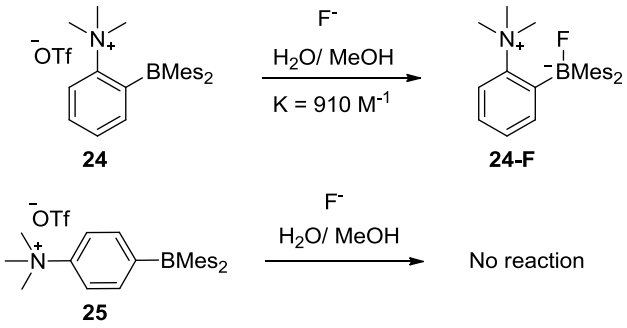

Figure 13. Scheme showing the fluorination reaction of **24** and **25**.

In addition, *ortho*-phosphonium borane (**26**) also shows excellent fluoride affinity in methanol with an extremely high fluoride binding constant ($K > 10^6$ M^{-1}), which is at least four orders of magnitude higher than the measured binding constant of *para*-isomer (**27**) ($K = 400 (\pm 50)$ M^{-1}) (Figure 14).[25] The high fluoride affinity of **26** is also supplemented by the formation of a B-F→P donor-acceptor interaction between the fluorine lone-pair electron and the σ* orbital of the P-C bond. These results support the concept that the anionic affinity of such complexes can be enhanced by closer positioning of the cationic group.

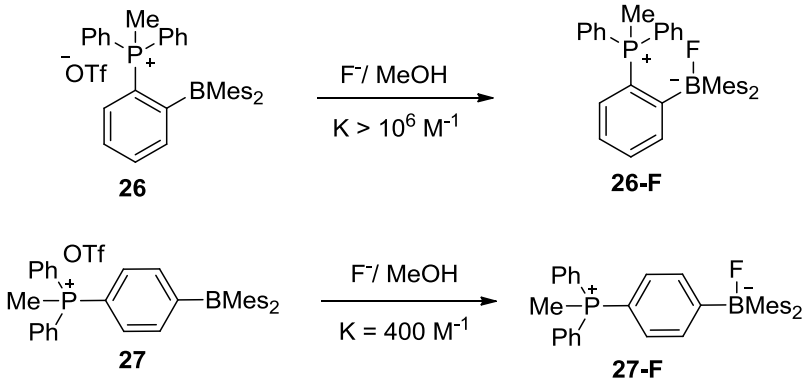

Figure 14. Scheme showing the fluorination reaction of **26** and **27**.

Similar effects are observed with sulfonium boranes (Figure 15) as the Lewis acidity of the boron center is enhanced by the proximal sulfonium group. Based on a spectrophotometric tritration experiment, **28** starts to bind hydroxide at pH ≥ 7, whereas **29** is stable up to pH 9.5, which suggests that **28** is more acidic than **29**.[28] This unusual difference can be explained by the presence of an lp(S)→p(B) donor-acceptor interaction

that partially quenches the Lewis acidity of the boron center. The more convergent orientation of the sulfonium and boron moiety in **29** leads to a strong lp(S)→p(B) donor-acceptor interaction, thus lowering the Lewis acidity. Surprisingly, the more Lewis acidic **28** can be used as a selective cyanide sensor in pure water *via* a fluorescence turn-off response.

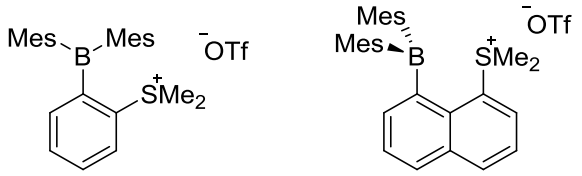

28 **29**

Figure 15. Illustration of sulfonium boranes **28** and **29**.

Once Gabbai and coworkers had established the concept that the fluoride affinity of organoboranes can be noticeably increased by introduction of a proximal cationic moiety as shown in **24**, **26**, and **28**, they decided to investigate whether a similar protocol could be used to stabilize aryltrifluoroborates against hydrolysis. With this in mind, they synthesized the zwitterionic aryltrifluoroborates **30**, **31**, and **32** (Figure 16) and examined the stability of these compounds in aqueous solution (pH = 7.5). The fluoride dissociation reaction of aryltrifluoroborate can be treated properly by a simple first order rate equation (rate = $k_{obs}[ArBF_3]$). Based on the kinetic data, **30** is the most stable species as the lowest rate constant (k_{obs}) was obtained. It is more stable than either **31** or **32**. The lower stability of **32** may derive from the lone-pair electron of sulfur, which may

destabilize the BF_3 unit through electron repulsions. Fortunately, such repulsions do not exist in the case of **30** and **31**, thereby retarding the rate of fluoride dissociation. The stability of **30** and **31** may also be supplemented by the accepting ability of the phosphonium center and hydrogen bond interactions, respectively. These results are noteworthy as they indicate that both phosphonium and ammonium trifluoroborates are appealing candidates to use as radiotracers in PET imaging.

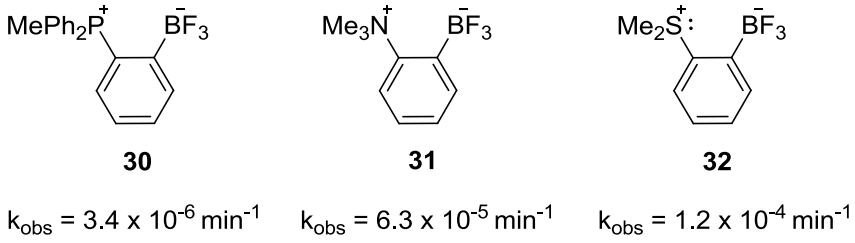

Figure 16. Illustration of zwitterionic aryltrifluoroborate **30**, **31**, and **32**, and their hydrolytic rate constants.

Recently, Perrin and coworkers reported a new zwitterionic alkylammoniomethyltrifluoroborate ($AMBF_3$) (**33**) (Figure 17) to use as a potential ^{18}F-radioprosthetic group.[30] This compound is noteworthy as it has greatly improved qualities for radiotracer development. These qualities consist of 1) *in vitro* and *in vivo* stability, 2) simple labeling by ^{18}F-^{19}F isotopic exchange, 3) HPLC-free purification, 4) synthetic simplicity, and 5) *in vivo* imaging of several tumor targets. $AMBF_3$ is easily synthesized by the akylation of a tertiary amine followed by treatment with KHF_2 in aqueous solution. This synthetic approach is also applicable for preparing an azidoethyl-

$AMBF_3$ and a tris–propargylether $AMBF_3$, which can provide considerable synthetic simplicity for bioconjugation

.

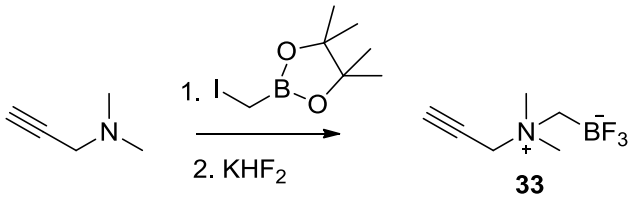

Figure 17. Scheme showing the synthesis of **33**.

To test the efficacy of $AMBF_3$ labeling, **33** was conjugated to octreotate and B9858/B9958 peptides for use as radiotracers for imaging somatostatin receptor subtype 2 and the bradykinin B1 receptor, respectively. Somatostatin receptor subtype 2 (sstr2) is overexpressed in many neuroendocrine tumors, whereas the bradykinin B1 receptor (B1R) is upregulated in inflamed and cancer tissues. Because sstr2 and B1R are not normally expressed in healthy tissues, they are attractive targets for the development of therapeutic agents for cancer treatment. In the case of the octreotate-based imaging agent, the [^{18}F]-alkyltrifluoroborate-octreotate conjugate (^{18}F-$AMBF_3$-TATE) (Figure 18) was efficiently prepared in a one-step ^{18}F-^{19}F exchange reaction with high radiochemical yield (20-25 %, non-decay-corrected) and high specific activity (3 Ci/ μmol). Gratifyingly, ^{18}F-$AMBF_3$-TATE displayed more than 5-fold higher sstr2 binding affinity than did a gallium –DOTATATE radiotracer under the same conditions. In addition, ^{18}F-$AMBF_3$-TATE is highly stable *in vitro* and *in vivo* because only negligible decomposition products of ^{18}F-$AMBF_3$-TATE were observed in a plasma stability assay

(37 °C) and minimal bone uptake signal was noted in the PET/CT images. In the case of the B1R imaging agent, $AMBF_3$ was conjugated to two potent peptides, B9858 and B9958, which have different amino acid sequence and units, to compare their binding affinity toward B1R. Following the previous method, ^{18}F-$AMBF_3$- B9858/ B9958 (Figure 18) were prepared in one step by isotopic exchange at 80 °C under acidic conditions (pH 2) within 30 min. Biodistribution and imaging studies proved that both ^{18}F-$AMBF_3$-B9858 and ^{18}F-$AMBF_3$-B9958 selectively bound to B1R tumors. However, ^{18}F-$AMBF_3$-B9958 is a promising candidate for clinical translation because it provided better tumor-to-background contrast. Overall, these tumor-imaging results are significant because they support the concept that $AMBF_3$ can be used broadly for peptide-based radiotracer development.

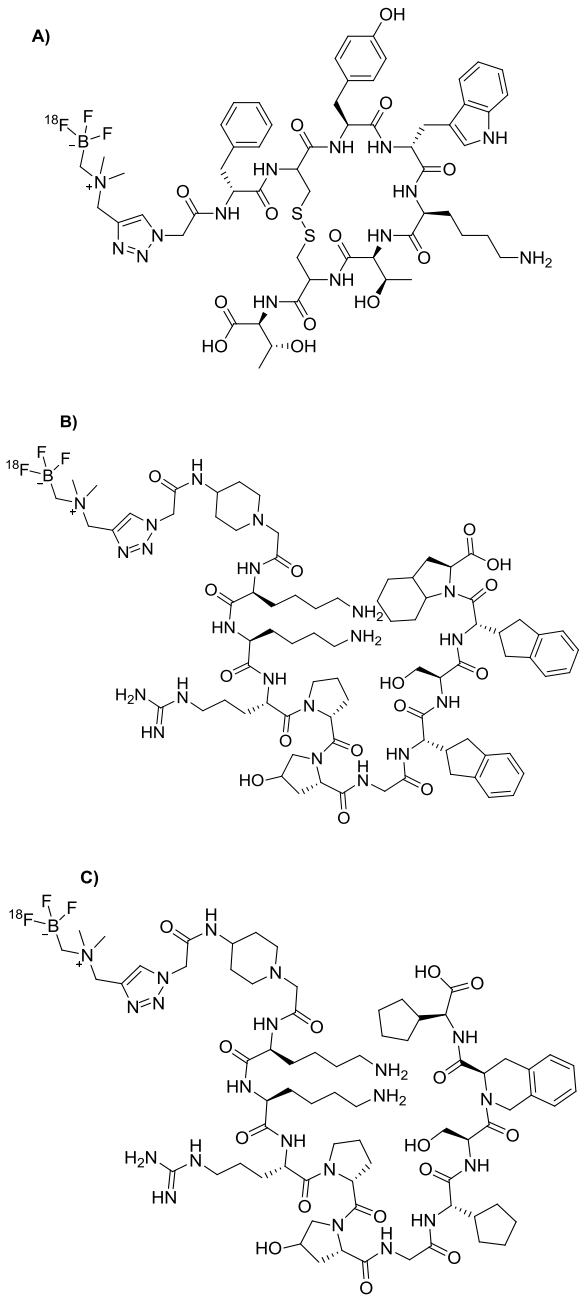

Figure 18. Illustration of peptide conjugated $AMBF_3$ A) ^{18}F-$AMBF_3$-TATE, B) ^{18}F-$AMBF_3$-B9858, and C) ^{18}F-$AMBF_3$-B9958.

1.5 Objectives

As shown in our previous study, the zwitterionic aryltrifluoroborate with an *ortho*-phosphonium group (**30**) is the most stable species in aqueous solution compared to the ammonium and sulfonium aryltrifluoroborates (**31** and **32**). Thus, the phosphonium derivative is expected be a good candidate for use as an ^{18}F-radiotracer as it would be stable *in vivo*. With this result in mind, we have decided to investigate the use of *ortho*-phosphonium aryltrifluoroborates as [^{18}F]-fluoride anion receptors. As part of this objective, we will study how the nature of the phosphine substituent affects the stability of the zwitterionic aryltrifluoroborate. Another aspect of this project is related to the conjugation of our synthesized phosphonium aryltrifluoroborates with potential biomolecules, which will be used as targeted radiotracers.

In addition to phosphonium aryltrifluoroborates, we were attracted by the remarkable stability of imidazolium trifluoroborates (**34**) (Figure 19). This compound, which can also be described as a carbene-BF_3 adduct, can be recrystallized from boiling water, which suggests that it is highly resistant to hydrolysis.[31] Therefore, we decided to investigate the applicability of this compound for use as a radioprosthetic group in radiopharmaceutical products. The objective of this experiment is to 1) synthesize novel carbene-BF3 adducts with a conjugable functional group and 2) examine their stability *in vitro* and *in vivo*.

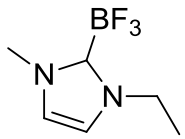

34

Figure 19. Illustration of carbene-BF_3 adduct **34**.

As mentioned above, BODIPY dyes have been extensively developed for use as PET/fluorescent dual modality imaging agents. The major studies have focused on the methodology used to radiofluorinate BODIPY dyes. With these results in mind, we wondered whether such methods could be applied to other boron-containing dyes. To satisfy our curiosity, we decided to synthesize a new fluorescent dye class called triazaborolopyridinium, which was recently developed by Arterburn and coworkers.[32] The objective for this experiment is to 1) prepare and characterize novel triazaborolopyridinium dyes with different functionalities; and 2) examine whether these dyes are resistant to hydrolysis.

CHAPTER II

ORTHO-PHENYLENE PHOSPHINO-BORANES FOR [^{18}F]-FLUORIDE ANION CAPTURE AND *IN VIVO* STABILITY STUDIES*

2.1 Introduction

Positron emission tomography (PET) has become a popular imaging technique widely used for diagnostic purposes. This technique necessitates the incorporation of a positron emitting atom in the biomolecule under study.[1] To date, much attention has been devoted to ^{18}F-fluoride because of the characteristic of its nuclear decay, as well as its relative ease of preparation from [^{18}O]water.[33,34] However, with a half-life of 110 minutes, the incorporation of ^{18}F-fluorine into biomolecules needs to be carried out in a swift and efficient manner to minimize any loss of activity. These synthetic and kinetic considerations constitute one of the critical barriers to progress in the field of ^{18}F-PET imaging. In turn, the discovery of general and reliable protocols for the rapid incorporation of ^{18}F-fluorine atoms into biomolecules would be highly beneficial, especially if these protocols can be carried out directly in the irradiated [^{18}O]water.

An approach that has gained interest in the past few years involves the use of a

---

*Reprinted in part permission from, "Harvesting ^{18}F-fluoride ions in water *via* direct ^{18}F–^{19}F isotopic exchange: radiofluorination of zwitterionic aryltrifluoroborates and *in vivo* stability studies"; Li, Z.; Chansaenpak, K.; Liu, S.; Wade, C.R.; Conti, P.S.; Gabbai, F. P. *Med. Chem. Commun*., **2012**, 3, 1305. Copyright 2012 by the Royal Society of Chemistry.

fluoride binding agent (referred to as a fluoride captor) that is appended to a biomolecule and treated with ^{18}F-fluoride just prior to injection.[35-39] Such an approach is appealing because time-consuming synthetic steps can be carried out before introduction of the relatively short-lived ^{18}F radionuclide. In turn, this method can be used to optimize the specific activity of radiolabeled biomolecules thus facilitating their *in vivo* imaging. However, this field of research remains relatively underdeveloped with only a few types of captors investigated thus far. In one of the most elegant approaches, Perrin and coworkers has shown that arylboronic acids or esters featuring electron-withdrawing substituents quickly react with fluoride ions to form the corresponding arylfluoroborates.[40,41] This approach has been employed for the radiolabeling of different biomolecules which have been imaged *in vivo*.[35,42-46] In passing, we will note that similar concepts have been used by us[47] and subsequently others[48,49] for the radiosynthesis of [^{18}F]BODIPY dyes as dual modality PET/fluorescence imaging agents.

One of the key aspects in the chemistry of [^{18}F]arylfluoroborates lies in the use of an electron-withdrawing substituent. The latter slows down the hydrolytic release of free fluoride ions making it essentially negligible on the time scale of the ^{18}F nuclear decay.[40] Such electron-withdrawing substituents effectively prevent the release of ^{18}F-fluoride ions that would otherwise bind to the bones giving unwanted and interfering background signals. Despite the elegance of this approach, some problems remain. In particular, these syntheses are usually implemented with a carrier-added fluoride source such as KHF_2. Although the use of KHF_2 does not necessarily invalidate this elegant approach as documented by recent successes,[35,42-46] it occurred to us that boron-based fluoride

captors with enhanced fluoride affinity could become amenable to direct radiofluorination reactions.

As part of our investigations in the chemistry of cationic boranes as fluoride anion receptors,[50] we have discovered that fluoroborate moieties are efficiently stabilized by neighboring onium ions.[51-55] These effects are illustrated by the kinetic stability of the phosphoniumtrifluoroborate **30** which is hydrolyzed in water/MeCN at a rate (k_{obs} = 3.4 × 10^{-6} min^{-1}) 7200 times lower than that of $K[C_6H_5BF_3]$ (k_{obs} = 24.5 × 10^{-3} min^{-1}).[56] Encouraged by these results we have now decided to investigate the radiofluorination and *in vivo* stability of such zwitterions. In this paper, we report the results that we have obtained with the known zwitterion **30** as well as **35**, **36**, and **37**, three new phopshosphiumtrifluoroborate species that we synthesized to assess substituents effects.

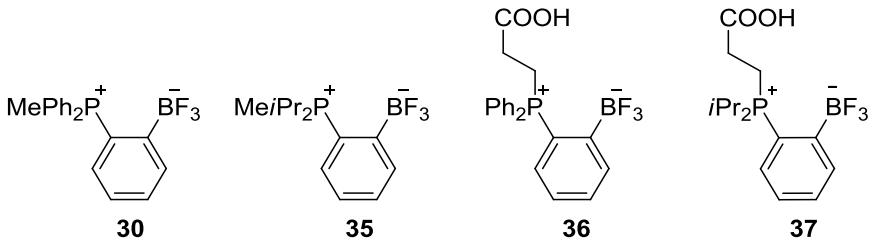

30 **35** **36** **37**

Figure 20. Illustration of the *ortho*-phenylene phosphine-boranes **30**, **35**, **36**, and **37**.

2.2 Synthesis and characterizations

Inspired by a recent report from Bourissou and coworkers,[57] we synthesized **35** in a 67% overall yield by reaction of the known *ortho*-(*i*-$Pr_2P)C_6H_4(BMes_2)$[57] with methyliodide, followed by treatment of the resulting phosphonium salt with pyridine-HF (Figure 21). The carboxylic acid functionalized diphenylphosphonium derivative **36** was prepared by reaction of *ortho*-$(Ph_2P)C_6H_4(Bpin)$[58] (Bpin = pinacolboryl) with 3-iodoproprionic acid followed by treatment of the resulting phosphonium salt with KHF_2. Finally, the carboxylic acid functionalized di-*iso*-propylphosphonium derivative **37** was prepared by the deprotonation of the known [*ortho*-(*i*$Pr_2PH)C_6H_4(Bpin)][BF_4]$[59] followed by treatment of 3-iodoproprionic acid at elevated temperature and KHF_2 at room temperature, respectively. These new derivatives have been fully characterized. The presence of the phosphonium moiety is confirmed by the detection of a ^{31}P NMR resonance at 41.10 ppm for **35**, 30.60 for **36**, and 42.9 for **37**. The trifluoroborate moiety gives rise to a ^{11}B NMR resonance at 2.4 ppm for **35**, 2.8 for **36**, and 3.1 for **37** as well as a ^{19}F NMR resonance at -136.3 ppm for **35**, -133.6 for **36** and -134.4 for **37**.

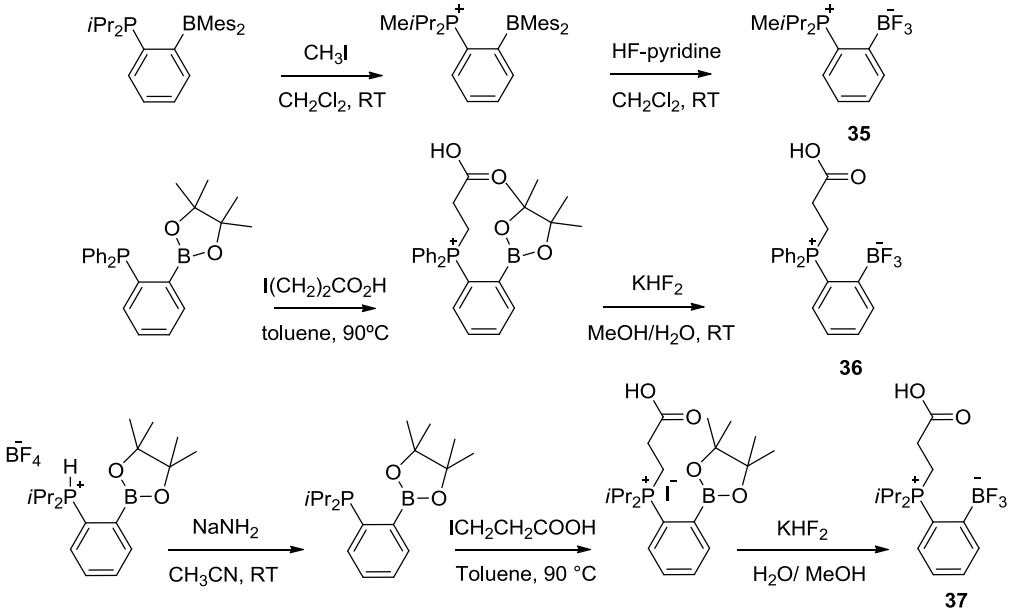

Figure 21. Scheme showing the synthesis of **35**, **36**, and **37**.

The structure of these compounds has also been confirmed by single crystal X-ray diffraction as shown in Figure 22, 23, and 24. As in the structure of **30**,[56] the short B(1)-P(1) separation of 3.386 Å in **35**, 3.491 Å in **36** and 3.429 Å in **37** suggests that these zwitterions benefits from a strong Coulombic stabilization. These strong Coulombic effects may be supplemented by a F(lone pair) → P–C(σ*) donor acceptor interaction as suggested by the F(1)-P(1) separation of 3.013 Å for **35**, 3.064 Å for **36**, and 3.048 Å for **37**. In the case of **35** and **37**, hydrogen bonding interactions between the CH group of the *i*-Pr ligands and one of the fluorine atoms may also play a stabilizing role.[51,57,60]

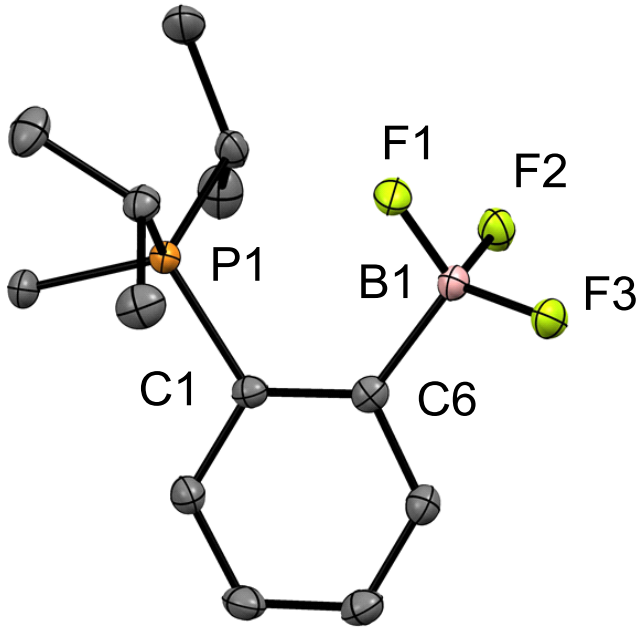

Figure 22. Crystal structure of **35**. Displacement ellipsoids are scaled to the 50% probability level and hydrogen atoms have been omitted for clarity. Selected bond lengths (Å) and angles (deg) for **35**: P1-B1 3.386, B1-F1 1.414(2), B1-F2 1.403(2), B1-F3 1.404(2); P1-C1-C6 123.05(13), C1-C6-B1 127.21(16).

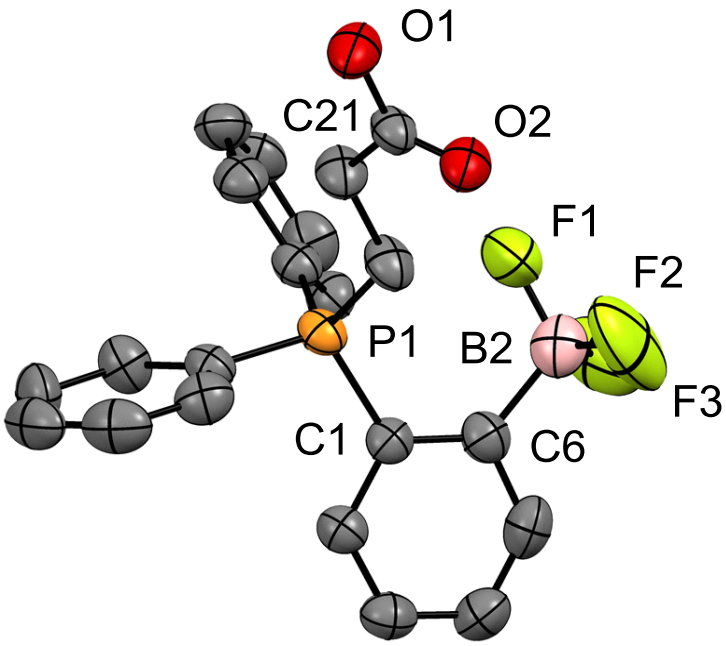

Figure 23. Crystal structure of **36**. Displacement ellipsoids are scaled to the 50% probability level and hydrogen atoms have been omitted for clarity. Selected bond lengths (Å) and angles (deg) for **36**: P1-B1 3.491, B1-F1 1.368(10), B1-F2 1.391(11), B1-F3 1.367(10), C21-O1 1.305(8), C21-O2 1.202(8); P1-C1-C6 122.3(5), C1-C6-B1 132.2(6).

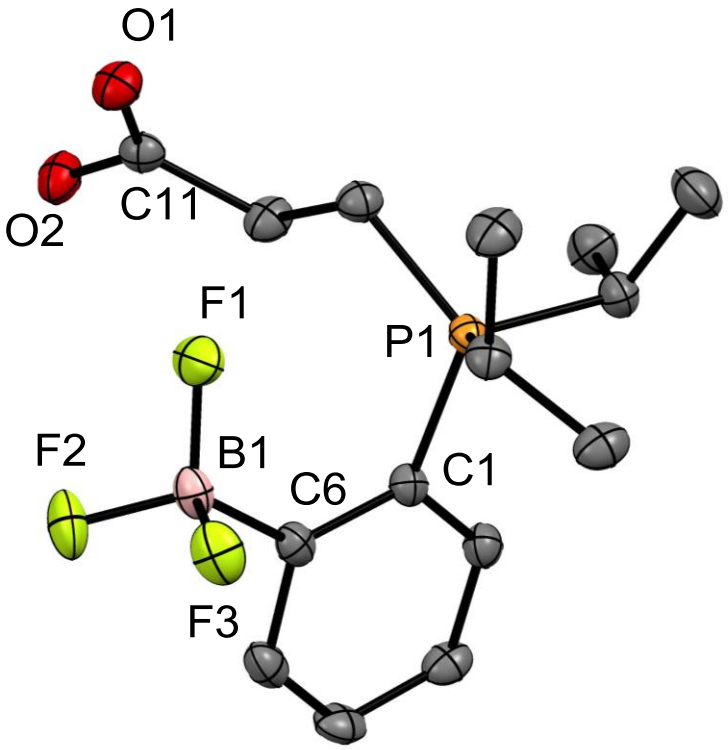

Figure 24. Crystal structure of **37**. Displacement ellipsoids are scaled to the 50% probability level and hydrogen atoms have been omitted for clarity. Selected bond lengths (Å) and angles (deg) for **37**: P1-B1 3.429, B1-F1 1.395(3), B1-F2 1.425(3), B1-F3 1.400(3), C11-O1 1.336(3), C11-O2 1.195(3); P1-C1-C6 122.28(16), C1-C6-B1 129.4(2).

2.3 Kinetic studies

Next, we decided to compare the rate of hydrolysis of these new compounds with those of **30** which has been previously investigated. This hydrolysis reaction, which converts the trifluoroborate moiety into the corresponding boronic acid according to a first order rate process ($v = k_{obs}[ArBF_3]$), was monitored by ^{19}F NMR spectroscopy in D_2O/CD_3CN (8/2 vol.) at pH 7.5 ([phosphate buffer] = 500 mM, $[ArBF_3]$ = 20 mM with $ArBF_3$ = zwitterionic trifluoroborate). Surprisingly, we observed that the first order hydrolysis rate constant of **35**, **36**, and **37** (k_{obs} (**35**) = 3.9×10^{-5} min^{-1}, k_{obs} (**36**) = 1.5×10^{-5} min^{-1}, k_{obs} (**37**) = 5.2×10^{-5} min^{-1}) are significantly higher than that of **1** (k_{obs} (**1**) = 3.4×10^{-6} min^{-1}). The kinetic plots for the hydrolysis of **35**, **36**, and **37** were shown in F igure 25. While it is difficult to rationalize the difference observed in the hydrolytic sensitivity of **35**, **36** and **37**, these experiments show us that subtle substituent changes have an impact on the stability of the complexes.

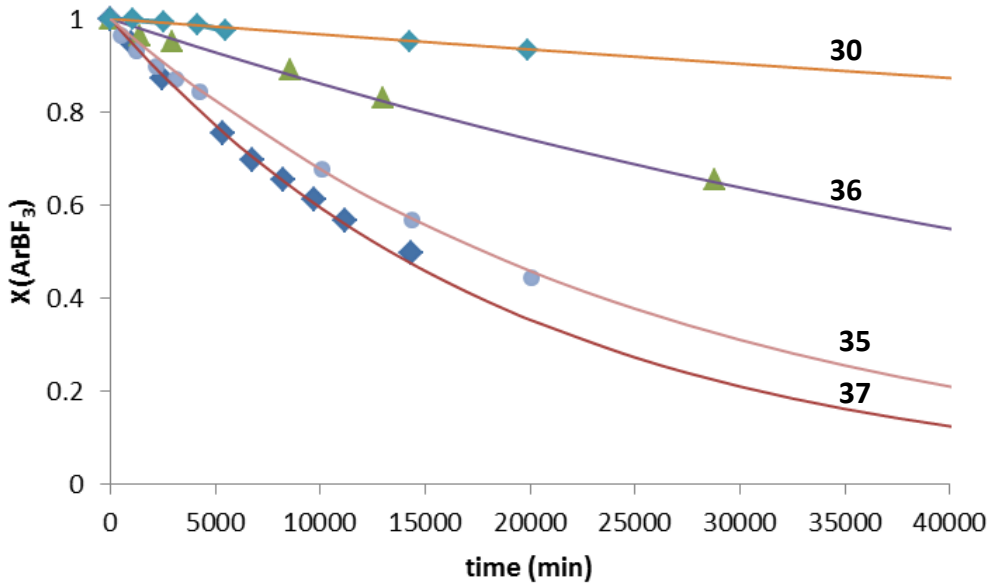

Figure 25. Kinetic plots for the hydrolysis of **30**, **35**, **36**, and **37**.The data were obtained at room temperature in D_2O/CD_3CN (8/2 vol.) at pH 7.5. The data shown for **30** has been previously reported[5] and is provided for the sake of comparison.

2.4 Zwitterionic stibonium aryltrifluoroborate and its stabilization against hydrolysis

Because of the increased size, polarizability, and electropositivity of the heavier pnictogen elements, stibonium moeities display stronger Lewis acidity than their corresponding phosphonium congeners.[61] With this in mind, we prepared a new zwitterionic stibonium aryltrifluoroborate by the reaction of the reported *ortho*-$(Ph_2MeSb)C_6H_4(BMes_2)$[61] with HF-pyridine (Figure 26). The product was obtained in 42% yield. This new compound has been characterized by NMR spectroscopy. The presence of a trifluoroborate moiety was confirmed by the ^{11}B NMR and ^{19}F NMR signals at 2.7 ppm and -135.8 ppm, respectively. The ^{1}H NMR of the methyl group displayed a quartet at 2.30 ppm ($J_{H\text{-}F}$ = 1.53 Hz) indicating coupling of the three fluorine nuclei.

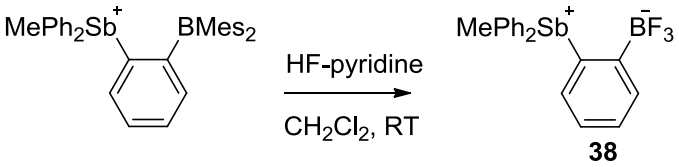

Figure 26. Scheme showing the synthesis of **38**.

Next, we determined the rate of hydrolysis of this compound. Unfortunately, the first order rate constant of **38** (k_{obs} = 4.0 × 10^{-4} min^{-1}) is close to that of the sulfonium derivative (**32**) and much higher than that of the phosphonium derivatives (**30**, **35**, **36**, and **37**). The poor stability of **38** towards hydrolysis may result from the exceptionally strong Lewis acidity of stibonium moiety. To understand the effect of the stibonium

group, we chose to perform DFT calculations (Optimized structure shown in Figure 27). In the optimized structure, the Sb(1)-F(1) separation was found to be 2.424 Å, which is considerably shorter than sum of the Sb-F Van der Waals radii (3.70 Å).[62] This suggests a strong donor-acceptor interaction between the stibonium center and one of the trifluoroborate fluorine atoms. This result was also supplemented by natural bond orbital (NBO) analysis, which revealed the presence of a strong F(lone pair) → Sb-C(σ*) interaction, as suggested by deletion energy of 31.04 kcal mol^{-1}. In addition, the B(1)-F(1) separation of 1.516 Å in the optimized structure is longer than a typical B-F covalent bond (1.410 Å).[63] Based on these computational results, the stibonium center tends to abstract a fluorine atom from trifluoroborate moiety suggested by B(1)-F(1) bond elongation. This process may lower the activation energy of fluoride dissociation pathway yielding rapid rate of trifluoroborate hydrolysis.

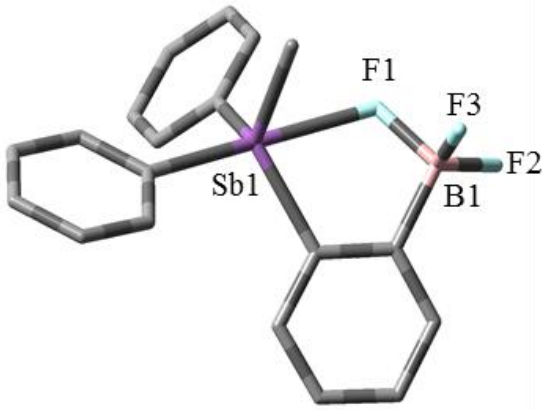

Figure 27. Optimized structure of **38**.

2.5 Radiofluorination[1]

Because of its greater resistance to hydrolysis, compound **30** was chosen as the first candidate for radiofluorination. Emulating the elegant approach developed by Perrin for the preparation of related [^{18}F]-radiolabeled trifluoroborate derivatives,[35,42-46] we investigated the reaction of the pinacolboryl precursor [*o*-MePh$_2$P(C$_6$H$_4$)Bpin]OTf[56] (250 μg, 0.45μmol in 100 μL, MeOH) with a solution of [^{19}F]-KHF$_2$ (8.0μL, 0.1 mol L^{-1}) and [^{18}F]-fluoride ions (30 ± 3 mCi in 100 μL unfixed target [^{18}O]-water). The resulting solution was heated to 60ºC for 10 minutes. After dilution with 800 μL of water, the crude mixture was loaded onto a reverse phase HPLC which indicated the formation of [$^{18/19}$F]**1** with a % conversion of 76 ± 3 % (based on HPLC, n = 4). The specific activity of the final product was calculated to be 47 ± 15 mCi/μmol by comparing its UV absorption with the standard titration curve. The identity of [$^{18/19}$F]**30** was confirmed by the comparison of its elution time with that of its non-radioactive analog **30** (Figure 28). This experiment has been repeated four times and the results are consistent. The use of MeOH/H$_2$O as a stationary phase led to analogous results, thus helping us to confirm the identity of [$^{18/19}$F]**30**.

[1] This experiment was carried out by our collaborator, Dr. Zibo Li, at department of Radiology, University of Southern California, Los Angeles, CA.

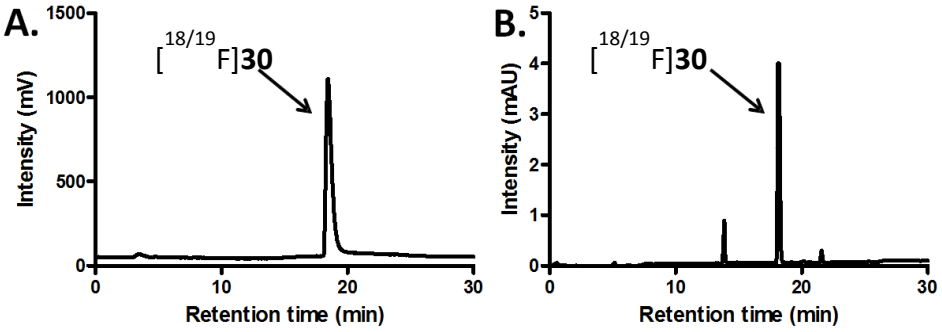

Figure 28. HPLC profiles obtained in the radiofluorination of **30**. (A) Radio signal. (B) UV signal.

While we were very pleased to establish a quick and robust radiofluorination protocol that can be implemented in water/methanol mixtures, in the matter of minutes, it occurred to us that higher specific activity could be obtained in the absence of KHF_2. With this in mind, we decided to attempt the generation of [$^{18/19}$F]**30** by direct ^{18}F-^{19}F isotopic exchange, a strategy that has proven successful for the radiofluorination of main group molecules, including BF_4^-[64,65] as well as fluorosilane derivatives.[36,37] Inspired by the acidic conditions used for the preparation of [^{18}F]BF_4^-,[64,65] we found that simple stirring of a [^{18}O]water solution (100 ± 10 μl) containing 30 ± 3 mCi ^{18}F, **30** (2.5×10^{-3} mol L^{-1}, dissolved in MeCN first) and HCl (pH = 1.5) at room temperature for 20 minutes afforded [$^{18/19}$F]**30** with a % conversion of 87.0 ± 4.5% (Table 1, entry 1). This radiosynthetic result is noteworthy for the following two reasons: i), we demonstrate for the first time that ^{18}F-^{19}F isotopic exchange is a very efficient strategy for the synthesis of trifluoroborates with elevated specific activities; ii) we demonstrate that such ^{18}F-^{19}F isotopic exchange reaction can be implemented directly in the irradiated [^{18}O]water

solution, thus alleviating the need for any time consuming drying steps.

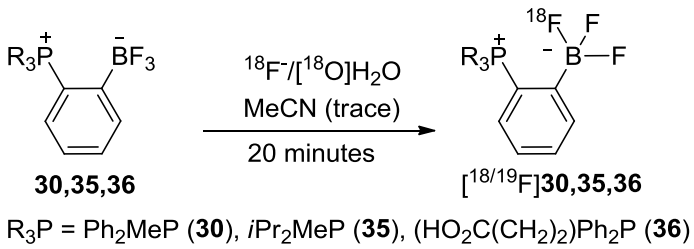

Figure 29. Direct ^{18}F-^{19}F isotopic exchange reaction employed for the radiolabeling of **30**, **35**, and **36** in aqueous solutions.

As illustrated by entries 1-4 (Table 1), **30** undergoes efficient fluoride exchange but only at low pH. When a lower quantity of **30** is employed as in entries 5 and 6, a net decrease in the extent of conversion is observed, a trend that underscores the effect of dilution on reaction kinetics. Fortunately, the same effects can be used to achieve high levels of conversion and specific activities that are comparatively higher. Indeed, when the reaction is carried out under much more concentrated conditions as in entry 7, the % conversion exceeds 90%, affording [$^{18/19}$F]**30** with a specific activity of 520 ± 174 (mCi/μmol). Gratifyingly, the fluoride exchange reaction can also be applied to **35** and **36**, which are efficiently radiofluorinated, albeit under acidic conditions (entries 8-12). When the reaction is carried out at a higher ^{18}F-fluoride/**35** ratios (entry 11), a comparatively high specific activity can be obtained. The carboxylate functionalized borane **36** behaves similarly to **30** and is also amenable to facile radiofluorination by isotopic exchange. A comparison of the measured and estimated specific activities

indicates that the former are typically lower than the latter. This difference is assigned to decomposition of part of the starting material that does not participate in the reaction. It is also possible that experimental factors inherent to the handling of small sample sizes play a role in the noted deviations.

Table 1. Radiosynthetic results.

Entry[a]	Cpd	Amount (μmol)	pH	Conversion (%)[c]	Measured SA[e] (mCi/μmol)	Estimated SA[e,f] (mCi/μmol)[e]
1[a,d]	**30**	0.73	1.5	87 ± 4.5	38 ± 7	27.8 ± 2.8
2[a]	**30**	0.73	6.5	< 5	N/D	1.60 ± 0.2
3[a]	**30**	0.73	5.3	< 8	N/D	3.3 ± 0.4
4[a]	**30**	0.73	3.0	85	35.4	35 ± 4
5[a]	**30**	0.036	1.5	23	N/D	149 ± 15
6[a]	**30**	0.0073	1.5	11	N/D	351 ± 35
7[b,d]	**30**	0.036	1.5	>90	520 ± 174	514 ± 52
8[a,d]	**35**	1.4	1.5	>90	20 ± 4	15.0 ± 1.5
9[a]	**35**	0.14	1.5	87	185.2	145 ± 15
10[a]	**35**	0.14	6.5	0	-	-
11[a]	**35**	0.029	1.5	51	421	410.0 ± 41
12[a]	**36**	0.73	1.5	>90	N/D	28.7 ± 2.9

For all reactions, the isotopic exchange reaction was allowed to proceed for 20 min with an initial ^{18}F activity of 30 ± 3 mCi. Reactions at acidic pH (pH 3 or 1.5) are carried out in 0.001 and 0.032 M HCl. Reactions at elevated pH are carried out using 0.1 M NH_4OAc (pH = 5.3) and 0.1 M phosphate (pH = 6.5) buffer. [a]The reactions are performed in 100 ± 10 μL of [^{18}O]-water solution containing 15 ± 5μL of MeCN used for solubilization of the phosphonium trifluoroborate. The reaction was performed at room temperature for 20 min. [b]The irradiated [^{18}O]-water solution containing 30 ± 3 mCi

activity was dried under a nitrogen flow and the activity was taken up with a solution of **30** in MeCN and water (1:3 v/v, 5 µL, pH = 1.5). [c]The percentages of conversion have been determined by HPLC and are relative to the starting ^{18}F activity. [d]The reactions have been repeated four times with the SA representing the average of these four measurements (n = 4). [e]SA: specific activity. [f]Estimated SA based on the percentage of conversion, the starting activity and the amount of precursor; the values are decay-corrected with an overall processing time of 40 min for entries 1-6, 8-12 and 60 min for entry 7. N/D: not determined.

2.6 *In vivo* stability studies[2]

To conclude this study, we injected 100 ± 10 µCi of [$^{18/19}$F]**30** and [$^{18/19}$F]**35** in female nude mice. At 0.5, and 2 h post injection, static microPET scans were achieved and the sagittal images for each compound are shown in Figure 30. [$^{18/19}$F]**30** shows a clear localization of activity in the liver of the animal, in accordance with the lipophilic nature of this molecule.[47] The absence of any signal from the skeleton of the animal indicates that the [^{18}F]-fluoride ions are not released during the time frame of the imaging experiments. At 0.5 h post injection, [$^{18/19}$F]**35** also showed relatively good *in vivo* stability. This compound appears to have better clearance properties, possibly because of their increased hydrophilicity, and are quickly cleared through the urinary track as indicated by the quick disappearance of the signal from the liver as well as a

[2] This experiment was carried out by our collaborator, Dr. Zibo Li, at department of Radiology, University of Southern California, Los Angeles, CA.

strong signal from the bladder of the animal. We also note that [$^{18/19}$F]**35** also resulted in gallbladder and intestine uptake. At 2 h post injection, [$^{18/19}$F]**35** did show some defluorination *in vivo* as we observed certain level of bone uptake. This fluoride release reaction can be correlated to the higher hydrolysis rate constant measured for this compound. Based on the hydrolysis rate constant measured for **35**, ~1.5 mol% of F^- should be liberated after 2 hours, an amount that may suffice to explain the observed bone signal. We also note that, *in vivo,* fluoride release may be accelerated by a variety of processes including pH variations and enzymatic and/or oxidative decompositions.

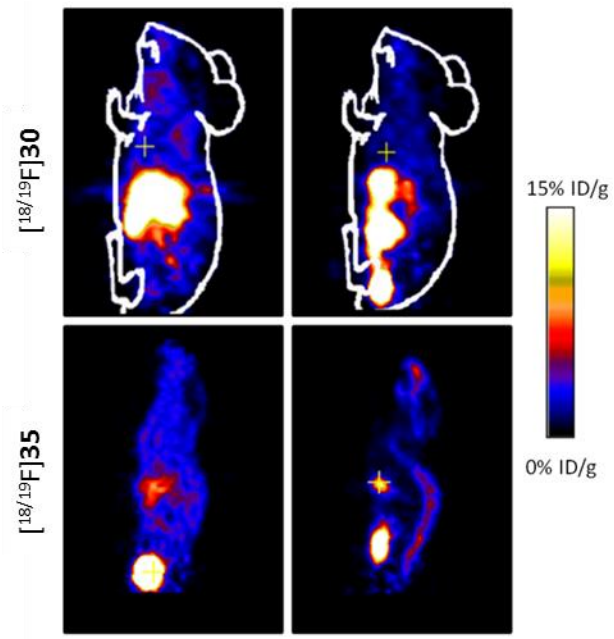

Figure 30. Decay-corrected whole-body microPET Sagittal images of athymic female nude mice from a static scan at 0.5, and 2 h after injection of [$^{18/19}$F]**30** and [$^{18/19}$F]**35**. The images are corrected based on the injected activity. The signal intensity is reported

in % of the injected dose per gram (%ID/g). Preparations from entries 7 and 9 were used for these imaging experiments.

2.7 Conclusion

First, the results presented in this paper allow us to firmly establish that *ortho*-phosphonium groups can be used to enhance the *in vivo* stability of radiofluorinated aryltrifluoroborates, allowing for extended imaging times. Our results also demonstrate that the stability of these compounds is very sensitive to the nature of the phosphorus atom substituents, with the diphenylmethylphosphonium derivative **30** being significantly more stable than the di-(*iso*-propyl)methylphosphonium derivative **35**. A second outcome of this work is the demonstration that ^{18}F-^{19}F isotopic exchange reactions can be used to radiolabel aryltrifluoroborates directly in the irradiated [^{18}O]water. Because of short reaction times and limited isotopic dilution, this simple method affords radiolabeled compounds with good reasonable activities. Finally, we will note that the carboxylic acid functionalized derivative **36** and **37** should be amenable to simple bioconjugation protocols, opening new horizons for the radiolabeling of amine terminated biomolecules.

2.8 Experimental

General Consideration

Ortho-(*i*-$Pr_2P)C_6H_4(BMes_2)$[66], *ortho*-$(Ph_2P)C_6H_4(Bpin)$[2] and [*ortho*-($iPr_2PH)C_6H_4(Bpin)][BF_4]$[59] were prepared according to the published procedure. CH_3I was purchased from Alfa Aesar. HF-pyridine was purchased from Sigma-Aldrich and 3-iodoproprionic acid was bought from Oakwood Product, Inc. Solvents were dried by passing through an alumina column (CH_2Cl_2) or refluxing under N_2 over Na/K (Et_2O). Air sensitive compounds were handled under a N_2 atmosphere using standard Schlenk and glovebox techniques. Electrospray mass spectra were acquired from a MDS Sciex API QStar Pulsar. The spray voltage was 4.5 kV. Elemental analyses were performed at Atlantic Microlab (Norcross, GA). NMR spectra were recorded on a Varian Unity Inova 300 NMR and an Inova 400 NMR spectrometer at ambient temperature. Chemical shifts are given in ppm, and are referenced to residual ^1H and ^{13}C solvent signals as well as external BF_3-Et_2O (^{11}B), $CFCl_3$ (^{19}F) and H_3PO_4 (^{31}P).

*Preparation of ortho-($iPr_2MeP)C_6H_4(BF_3)$ (**35**)*

Methyl iodide (0.06 mL, 0.984 mmol) was added to a solution of *ortho*-(*i*-$Pr_2P)C_6H_4(BMes_2)$ (0.145 g, 0.328 mmol) in dichloromethane (7 mL) at room temperature. After being stirred overnight, the solution was concentrated in *vacuo* to a volume of 1 mL. To the concentrated solution, was added Et_2O (10 mL) which resulted in the precipitation of a pale yellow solid (0.145g, 96% yield).^1H NMR (299.9 MHz, $CDCl_3$): δ 1.10 (dd, 6H, isopropyl-C*H*$_3$, $^3J_{H\text{-}P}$ = 17.99 Hz, $^3J_{H\text{-}H}$ = 7.20 Hz), 1.16 – 1.29

(m, 6H, isopropyl-C*H*$_3$), 1.34 (s, 3H, Mes-C*H*$_3$), 1.84 (d, 3H, P-C*H*$_3$, $^2J_{H\text{-}P}$ = 53.98), 1.87 (s, 3H, Mes-C*H*$_3$), 1.98 (s, 3H, Mes-C*H*$_3$), 2.08 (s, 3H, Mes-C*H*$_3$), 2.22 (s, 3H, Mes-C*H*$_3$), 2.26 (s, 3H, Mes-C*H*$_3$), 2.56 – 2.70 (m, 1H, isopropyl-C*H*), 3.38 – 3.52 (m, 1H, isopropyl-C*H*), 6.68 – 6.84 (m, 4H, Mes-C*H*), 7.48 – 7.62 (m, 2H, phenyl-C*H*), 7.78 (t, 1H, phenyl-C*H*, $^3J_{H\text{-}H}$ = 7.50 Hz), 8.33 (dd, 1H, phenyl-C*H*, $^3J_{H\text{-}P}$ = 11.0 Hz, $^3J_{H\text{-}H}$ = 7.50 Hz). ^{13}C NMR (125.6 MHz, $CDCl_3$): δ 2.01, 2.41, 16.59, 17.28, 21.39 (d, $J_{C\text{-}P}$ = 6.28 Hz), 23.21, 23.59, 23.85,24.87, 25.08, 25.56, 25.92, 105.16,121.75, 122.36, 129.20, 129.50,129.77, 129.96, 131.59 (d, $J_{C\text{-}P}$ = 12.43 Hz), 133.58 (d, $J_{C\text{-}P}$ = 3.14 Hz), 136.25, 136.35, 136.66, 136.76, 140.40, 141.26, 141.44, 141.95, 142.12, 142.45. ^{11}B NMR (128.2 MHz, $CDCl_3$): not observed. ^{31}P NMR (121.4 MHz, $CDCl_3$): 40.95. Anal. Calcd for $C_{31}H_{43}PBI$: C, 62.72; H, 7.42. Found: C, 62.22; H, 7.12. Without further purification, the pale yellow solid was treated with excess hydrogen fluoride pyridine in dichloromethane (2 mL) at room temperature. After being stirred for 18 h, the mixture was quenched by water (2 mL). The dichloromethane layer was separated from the mixture, dried with $MgSO_4$, and filtered to remove $MgSO_4$, respectively. The solvent was removed under reduced pressure. The residue was washed with Et_2O (3 × 2 mL) yielding **35** as yellow solid (63.1 mg, 70% yield). ^{1}H NMR (299.9 MHz, $CDCl_3$): δ 1.07 (dd, 6H, isopropyl-C*H*$_3$, $^3J_{H\text{-}P}$ = 20.99 Hz, $^3J_{H\text{-}H}$ = 7.20 Hz), 1.37 (dd, 6H, isopropyl-C*H*$_3$, $^3J_{H\text{-}P}$ = 17.99 Hz, $^3J_{H\text{-}H}$ = 7.50 Hz), 1.89 (d, 3H, P-C*H*$_3$, $^2J_{H\text{-}P}$ = 11.70 Hz), 3.56 (m, 2H, isopropyl-C*H*), 7.41 – 7.46 (m, 2H, phenyl-C*H*), 7.59 (t, 1H, $^3J_{H\text{-}H}$ = 6.30 Hz), 8.13 (dd, 1H, $^3J_{H\text{-}P}$ = 6.60 Hz, $^3J_{H\text{-}H}$ = 4.80 Hz). ^{13}C NMR (75.4 MHz, $CDCl_3$): δ -1.83 (d, $^1J_{C\text{-}P}$ = 54.06 Hz), 17.16 (d, $^2J_{C\text{-}P}$ = 2.26 Hz), 17.66 (d, $^2J_{C\text{-}P}$ = 2.19 Hz), 23.27 (d, $^1J_{C\text{-}P}$ = 4.98

Hz), 23.88 (d, $^{1}J_{C\text{-}P}$ = 4.45 Hz), 126.65 (d, $J_{C\text{-}P}$ = 12.14 Hz), 130.20 (d, $J_{C\text{-}P}$ = 11.00 Hz), 132.83 (d, $J_{C\text{-}P}$ = 3.09 Hz), 136.41 (dd, $^{1}J_{C\text{-}P}$ = 15.98 Hz, $^{3}J_{C\text{-}F}$ = 3.32 Hz). ^{11}B NMR (128.2 MHz, $CDCl_3$): δ 2.37 (q, $^{1}J_{B\text{-}F}$ = 46.28 Hz). ^{31}P NMR (121.4 MHz, $CDCl_3$): δ 41.10. ^{19}F NMR (282.2 MHz; $CDCl_3$): -136.3. Anal. Calcd for $C_{13}H_{21}PBF_3$: C, 54.97; H, 7.67. Found: C, 54.56; H, 7.38.

*Preparation of ortho-((HO$_2$C(CH$_2$)$_2$)Ph$_2$P)C$_6$H$_4$(BF$_3$) (**36**)*

A solution of the *ortho*-(Ph_2P)C_6H_4(Bpin) (0.428 g, 1.102 mmol) and 3-iodoproprionic acid (0.225 g, 1.125 mmol) in toluene (5 mL) was heated to 90 °C for 18 h. After 18 h, the mixture was concentrated in *vacuo* to a volume of 1 mL. Addition of Et_2O (10 mL) to the resulting solution resulted in the precipitation of a pale yellow solid (0.578 g). Without further purification, the precipitate was dissolved in methanol (4 mL) and treated with a solution of KHF_2 (0.307 g, 3.931 mmol) in water (4 mL). The resulting solution was sonicated for 15 minutes and stirred for 1 h. The mixture was extracted by dichloromethane (3 x 15 mL) and the organic layer was dried with $MgSO_4$. After filtration, the solution was concentrated to 1 mL and treated with Et_2O (15 mL), leading to the precipitation of **36** as a pale yellow solid (0.421g, 72 % yield). ^{1}H NMR (399.5 MHz, CD_3CN): δ 2.66 (dt, 2H, -C*H*$_2$COOH, $^{3}J_{H\text{-}P}$ = 6.79 Hz, $^{3}J_{H\text{-}H}$ = 8.79 Hz), 3.62 (dt, 2H, -PC*H*$_2$CH$_2$COOH, $^{2}J_{H\text{-}P}$ = 13.18 Hz, $^{3}J_{H\text{-}H}$ = 8.79 Hz), 7.13 (dd, 1H, phenyl-C*H*, $^{3}J_{H\text{-}P}$ = 14.38 Hz, $^{3}J_{H\text{-}H}$ = 7.19 Hz), 7.32 (tdd, 1H, phenyl-C*H*, *J* = 7.59, 3.16, 1.24 Hz), 7.51 – 7.68 (m, 9H, phenyl-C*H*), 7.75 (td, 2H, phenyl-C*H*, *J* = 7.59, 1.20 Hz), 7.95 (dd, 1H, phenyl-C*H*, *J* = 7.59, 5.19 Hz). ^{13}C NMR (125.6 MHz, CD_3CN): δ 20.38

(d, -P<u>C</u>H$_2$CH$_2$COOH, $^1J_{C\text{-}P}$ = 55.26 Hz), 28.62 (d, -PCH$_2$<u>C</u>H$_2$COOH, $^2J_{C\text{-}P}$ = 2.39 Hz), 122.96, 123.65, 127.95 (d, $J_{C\text{-}P}$ = 13.82 Hz), 130.45 (d, $J_{C\text{-}P}$ = 11.93 Hz), 131.18 (d, $J_{C\text{-}P}$ = 12.43 Hz), 134.06, 134.09, 134.13, 134.28 (d, $J_{C\text{-}P}$ = 9.17 Hz), 134.73 (d, $J_{C\text{-}P}$ = 3.01 Hz), 136.06 (d, $J_{C\text{-}P}$ = 15.07 Hz), 136.24 (dq, $J_{C\text{-}P}$ = 17.58 Hz, $J_{C\text{-}F}$ = 3.26 Hz), 172.42 (d, $J_{C\text{-}P}$ = 15.07 Hz). ^{11}B NMR (128.2 MHz, CD_3CN): δ 2.83. ^{31}P NMR (161.7 MHz, CD_3CN): δ 30.6. ^{19}F NMR (375.9 MHz; CD_3CN): δ -133.6. MS (ESI$^-$) calcd for **3** $(C_{21}H_{18}BF_3O_2P)^-$: 400.8211, found: 401.1122.

*Preparation of ortho-((HO$_2$C(CH$_2$)$_2$)iPr$_2$P)C$_6$H$_4$(BF$_3$) (**37**)*

To a stirred solution of the [*ortho*-(*i*Pr$_2$PH)C$_6$H$_4$(Bpin)][BF$_4$] (0.838 g, 2.07 mmol) in CH_3CN (15 mL) was added $NaNH_2$ (0.081 g, 2.07 mmol) at room temperature. The mixture was stirred for 1 h. Then, the mixture was filtered through celite to remove a sodium salt. The solvent was removed in *vacuo* affording a pale yellow powder. Without further purification, the powder was dissolved in toluene (15 mL) and 3-iodoproprionic acid (0.415 g, 2.07 mmol) was added to the solution. The reaction mixture was heated to 90 °C for 18 h. After 18 h, toluene was removed under vacuum yielding a pale yellow solid. Then, the solid was dissolved in methanol (6 mL) and treated with a solution of KHF_2 (0.485 g, 6.21 mmol) in water (6 mL). The resulting solution was sonicated for 15 minutes and stirred for 1 h. The mixture was extracted by dichloromethane (3 x 15 mL) and the organic layer was dried with MgSO$_4$. After filtration, the solution was concentrated to 1 mL and treated with Et$_2$O (15 mL), leading to the precipitation of **37** as a pale yellow solid (0.456 g, 66.2 % yield). **^{1}H NMR** (399.5

MHz, CD_3CN): δ 1.25 (dd, 6H, isopropyl-C*H*$_3$, $^3J_{H\text{-}P}$ = 16.78 Hz, $^3J_{H\text{-}H}$ = 7.59 Hz), 1.37 (dd, 6H, isopropyl-C*H*$_3$, $^3J_{H\text{-}P}$ = 16.78 Hz, $^3J_{H\text{-}H}$ = 7.19 Hz), 2.62 (m, 2H, -PCH$_2$C*H*$_2$COOH), 2.90 (m, 2H, -PC*H*$_2$CH$_2$COOH), 3.37 (m, 2H, isopropyl-C*H*), 7.43 (m, 1H, phenyl-C*H*), 7.52 – 7.64 (m, 2H, phenyl-C*H*), 7.97 (dd, 1H, $J_{H\text{-}H}$ = 7.19, 4.39Hz). **^{13}C NMR** (100.5 MHz, CD_3CN): δ 11.39 (d, $J_{C\text{-}P}$ = 3.52 Hz), 11.89 (d, $J_{C\text{-}P}$ = 3.02 Hz), 16.35 (d, $J_{C\text{-}P}$ = 3.12 Hz), 17.25 (d, $J_{C\text{-}P}$ = 3.12 Hz), 23.69 (d, $J_{C\text{-}P}$ = 3.72 Hz), 24.14 (d, $J_{C\text{-}P}$ = 3.72 Hz), 27.58, 127.04 (d, $J_{C\text{-}P}$ = 12.26 Hz), 132.53, 132.76 (d, $J_{C\text{-}P}$ = 10.75 Hz), 136.19 (d, $J_{C\text{-}P}$ = 3.82 Hz), 136.35 (d, $J_{C\text{-}P}$ = 3.82 Hz). **^{11}B NMR** (128.2 MHz, CD_3CN): δ 3.05 (q, $J_{B\text{-}F}$ = 47.56 Hz). **^{19}F NMR** (375.9 MHz, CD_3CN): δ -134.36. **^{31}P NMR** (161.7 MHz, CD_3CN): δ 42.92. Mass (ESI$^-$): calcd for $C_{15}H_{23}BF_3O_2P$ $(M\text{-}H)^-$, 333.14; found 332.83.

*Preparation of ortho-(Ph$_2$MeSb)C$_6$H$_4$(BF$_3$) (**38**)*

Ortho-(Ph_2MeSb)C_6H_4($BMes_2$) (0.112 g, 0.182 mmol) was treated with excess hydrogen fluoride pyridine in dichloromethane (2 mL) at room temperature. After being stirred for 18 h, the mixture was quenched by water (2 mL). The dichloromethane layer was separated from the mixture, dried with $MgSO_4$, and filtered to remove $MgSO_4$, respectively. The solvent was removed under reduced pressure. The residue was washed with Et_2O (3 × 2 mL) yielding **38** as yellow solid (33.2 mg, 42 % yield). **^{1}H NMR** (399.5 MHz, $CDCl_3$): δ 2.30 (q, 3H, $J_{H\text{-}F}$ = 1.53 Hz -C*H*$_3$), 7.01 (d, 1H, $J_{H\text{-}H}$ = 7.99 Hz, phenyl-C*H*) 7.46 – 7.63 (m, 10H, phenyl-C*H*), 7.96 (m, 2H, phenyl-C*H*) 8.77 (d, 1H, $J_{H\text{-}H}$ = 7.99 Hz, phenyl-C*H*). **^{13}C NMR** (100.5 MHz, $CDCl_3$): δ 29.67, 128.29, 130.24,

132.28, 132.48, 132.85, 133.29, 134.38, 134.84, 134.98. **^{11}B NMR** (128.2 MHz, $CDCl_3$): δ 2.73. **^{19}F NMR** (375.9 MHz, $CDCl_3$): δ -135.81.

Crystallographic Measurements

Single crystals of **35** were obtained by slow diffusion of Et_2O into a CH_2Cl_2 solution of **35**. In addition, single crystals of **36** were obtained by slow diffusion of pentane into a THF solution of **36**. Finally, single crystals of **37** were obtained by slow diffusion of CH_2Cl_2 from a 4:2 CH_2Cl_2/toluene solution of **37**. The crystallographic measurement of **35**, **36**, and **37** were performed using a Bruker APEX-II CCD area detector diffractometer, with graphite-monochromated Mo-K_α radiation (λ = 0.71069 Å). A specimen of suitable size and quality was selected and mounted onto a nylon loop. The semi-empirical method SADABS was applied for absorption correction.[3] The structure was solved by direct methods, and refined by the full-matrix least-square method against F^2 with the anisotropic temperature parameters for all non-hydrogen atoms. All H atoms were geometrically placed and refined using the riding model approximations.[4] Data reduction and further calculations were performed using the Bruker SAINT+ and SHELXTL NT program packages. The crystal data are included in Table 2-4.

Table 2. Crystal data, data collections, and structure refinements of **35**.

Crystal data	**35**	
Empirical formula	$C_{13}H_{21}BF_3P$	
Formula weight	276.08	
Crystal size/mm	0.25 x 0.2 x 0.2	
Temperature	110(2) K	
Wavelength	0.71073 Å	
Crystal system	Orthorhombic	
Space group	Pna2(1)	
Unit cell dimensions	a = 11.372(4) Å	α = 90°
	b = 11.428(5) Å	β = 90°
	c = 11.129(4) Å	γ = 90°
Volume	1446.3(10) $Å^3$	
Z	4	
Density (calculated)	1.268 g cm^{-3}	
μ	0.203 mm^{-1}	
F(000)	584.0	
Scan mode	ω, φ	
hkl ranges	-14 → +14	
	-14 → +15	
	-14 → +15	
Reflections collected	16834	
Unique reflections [Rint]	3484 [0.0393]	
Reflection used for refinement	3484	
Refined parameters	163	
GooF	0.776	
R1,[a] *w*R2[b] (all data)	0.0317, 0.0991	
Largest diff. peak and hole	0.293, -0.183 e.$Å^{-3}$	

[a]$R1 = \Sigma||F_o| - |F_c||/ \Sigma|F_o|$. [b]$wR2\ ([w(F_o^2 - F_c^2)^2]/[\Sigma w(F_o^2)^2])^{1/2}$; $w = 1/[\sigma^2(F_o^2) + (ap)^2 + bp]$; $p = (F_o^2 + 2F_c^2)/3$ with $a = 0.0382$ and $b = 0.2933$.

Table 3. Crystal data, data collections, and structure refinements of **36**.

Crystal data	**36**	
Empirical formula	$C_{21}H_{19}BF_3O_2P$	
Formula weight	382.99	
Crystal size/mm	0.33 x 0.07 x 0.02	
Temperature	110(2) K	
Wavelength	0.71073 Å	
Crystal system	Monoclinic	
Space group	P21/c	
Unit cell dimensions	a = 9.163(1) Å	α = 90°
	b = 12.426(14) Å	β = 100.483(2)°
	c = 17.335(2) Å	γ = 90°
Volume	1941(4) $Å^3$	
Z	4	
Density (calculated)	1.376 g cm^{-3}	
μ	0.181 mm^{-1}	
F(000)	756.0	
Scan mode	ω, φ	
hkl ranges	-9 → +10	
	-14 → +14	
	-20 → +19	
Reflections collected	11319	
Unique reflections [Rint]	3212 [0.0675]	
Reflection used for refinement	3212	
Refined parameters	253	
GooF	1.032	
R1,[a] *w*R2[b] (all data)	0.0895, 0.2884	
Largest diff. peak and hole	1.001, -0.405 e.$Å^{-3}$	

[a]$R1 = \Sigma||F_o| - |F_c||/ \Sigma|F_o|$. [b]$wR2 = ([w(F_o^2 - F_c^2)^2]/[\Sigma w(F_o^2)^2])^{1/2}$; $w = 1/[\sigma^2(F_o^2) + (ap)^2 + bp]$; $p = (F_o^2 + 2F_c^2)/3$ with $a = 0.1533$ and $b = 2.95$.

Table 4. Crystal data, data collections, and structure refinements of **37**.

Crystal data	**37**	
Empirical formula	$C_{15}H_{23}BF_3O_2P$	
Formula weight	334.11	
Crystal size/mm	0.17 x 0.17 x 0.06	
Temperature	110(2) K	
Wavelength	0.71073 Å	
Crystal system	Monoclinic	
Space group	P21/n	
Unit cell dimensions	a = 8.174(8) Å	α = 90°
	b = 14.54(1) Å	β = 92.57(1)°
	c = 13.76(1) Å	γ = 90°
Volume	1634(3) $Å^3$	
Z	4	
Density (calculated)	1.358 g cm^{-3}	
μ	0.202 mm^{-1}	
F(000)	704	
Scan mode	ω, φ	
hkl ranges	-10 → +10	
	-19 → +18	
	-16 → +17	
Reflections collected	14358	
Unique reflections [Rint]	3926 [0.0576]	
Reflection used for refinement	3926	
Refined parameters	199	
GooF	1.046	
R1,[a] *w*R2[b] (all data)	0.0483, 0.1230	
Largest diff. peak and hole	0.36, -0.39 e.$Å^{-3}$	

[a]$R1 = \Sigma||F_o| - |F_c||/ \Sigma|F_o|$. [b]$wR2 = ([w(F_o^2 - F_c^2)^2]/[\Sigma w(F_o^2)^2])^{1/2}$; $w = 1/[\sigma^2(F_o^2) + (ap)^2 + bp]$; $p = (F_o^2 + 2F_c^2)/3$ with $a = 0.0522$ and $b = 0.4268$.

Kinetic studies of the hydrolysis reactions

As previously reported for **30**,[5] a sample of **35**, **36**, and **37** (5 mg) was dissolved in 0.2 mL CD_3CN and 1.0 mL D_2O phosphate buffer (pH 7.5, 500 mM). The ^{19}F NMR spectra of **35**, **36**, and **37** were collected periodically. The decomposition of aryltrifluoroborate species were monitored by integration of the decreasing aryltrifluoroborate signal in conjunction with the increasing signal corresponding to free F^-. All spectra were processed using the VNMRJ Version 2.2 NMR software. The rate constant, k_{obs}, was calculated using a well-established NMR method reported in the literature.[6] This method is based on the fact that the concentration in $ArBF_3$ species is proportional to the ^{19}F NMR integration of $ArBF_3$ signal divided by the sum of the integration of $ArBF_3$ signal and the free fluoride signal. For convenience, the value of the $ArBF_3$ integration is arbitrarily set at 100 and the free fluoride integration determined. The resulting data is provided in Table 5-7.

Table 5. Kinetic data for the hydrolysis of **35**. The values provided for F^- and $ArBF_3$ correspond to the integration of the corresponding NMR signal.

		Data for **35**		
				k_{obs} = 3.90E-05
			exp. ratio	calc. ratio
Time (min)	F^-	$ArBF_3$	$ArBF_3$/ ($ArBF_3$+F^-)	$ArBF_3$/ ($ArBF_3$+F^-)
0	0	100	1.000	1.000
520	3.8	100	0.96	0.98
1280	7.7	100	0.93	0.95
2210	11.6	100	0.90	0.92
3160	15.1	100	0.87	0.88
4280	18.8	100	0.84	0.85
10100	48.3	100	0.67	0.67
14420	76.2	100	0.57	0.57
20110	126.2	100	0.44	0.46
25000				0.38
30000				0.31
35000				0.25
40000				0.21
45000				0.17
50000				0.14

Table 6. Kinetic data for the hydrolysis of **36**. The values provided for F^- and $ArBF_3$ correspond to the integration of the corresponding NMR signal.

		Data for **36**		
				k_{obs} = 1.50E-05
			exp. ratio	calc. ratio
Time (min)	F^-	$ArBF_3$	$ArBF_3$/ ($ArBF_3$+F^-)	$ArBF_3$/ ($ArBF_3$+F^-)
0	0	100	1.000	1.000
1440	3.9	100	0.96	0.98
2940	5.3	100	0.95	0.96
8610	12.4	100	0.89	0.88
12990	20.7	100	0.83	0.82
28800	53.1	100	0.65	0.65
35000				0.59
40000				0.55
45000				0.51
50000				0.47

Table 7. Kinetic data for the hydrolysis of **37**. The values provided for F^- and $ArBF_3$ correspond to the integration of the corresponding NMR signal.

Data for **37**				
				K_{obs} = 5.2E-5
			exp. Ratio	calc. ratio
Time (min)	[F^-]	[BF3]	[BF3]/([BF3]+[F^-]	[BF3]/([BF3]+[F^-]
0	0	100	1.000	1.000
1030	5.4	100	0.95	0.95
2491	14.86	100	0.87	0.88
5367	32.58	100	0.75	0.77
6800	43.52	100	0.70	0.70
8240	52.59	100	0.66	0.65
9689	63.75	100	0.61	0.60
11189	76.21	100	0.57	0.56
20000				0.35
30000				0.21
40000				0.13
50000				0.07
60000				0.04

Radiochemistry Experiments

All chemicals obtained commercially were of analytic grade and used without further purification. The syringe filter and polyethersulfone membranes (pore size, 0.22 μm; diameter, 13 mm) were obtained from Nalge Nunc International (Rochester, NY). Analytical reversed-phase high-performance liquid chromatography (HPLC) was accomplished on a Waters 515 chromatography system with a Waters 2487 dual λ absorbance detector (218 and 254 nm) and model 2200 scaler ratemeter radiation detector from Ludlum Measurements, Inc. (Sweetwater, TX). Empower 2 software from Waters Corporation (Milford, MA) was used to record chromatograms. HPLC was performed on a phenomenex Luna 5μ C18 column (250 × 4.6 mm). The flow was 1 mL/min, with the mobile phase starting from 95% solvent A (0.1% TFA in water) and 5% solvent B (0.1% TFA in acetonitrile) (0–2 min) to 5% solvent A and 95% solvent B at 22 min.

Radiochemistry

Unless otherwise noted, the reactions were performed using the following protocol. 18F-Fluoride was produced with an in-house cyclotron. Zwitterions **30**, **35**, or **36** (dissolved in MeCN, 15 ± 5μL) was added to 30 ± 3 mCi ^{18}F-fluoride in 100 ± 10 μL [^{18}O]water (The activity/volume ratio was adjusted by dilution when necessary). The reaction mixture stayed at room temperature for 20 min. The final % conversion of each reaction was measured by loading approximately 30 μCi reaction mixture onto a reverse phase analytical HPLC equipped with radio detector. The retention time of [$^{18/19}$F]**30**,

[$^{18/19}$F]**35** and [$^{18/19}$F]**36** is 18.1, 11.6, and 17.4 min, respectively. The identities of the compounds were confirmed by comparison of the retention times with those of the starting (non-radioactive) compounds as well as by co-injection of the starting and radiofluorinated derivatives.

Specific activity

In order to determine the specific activity of the product after labeling, a standard solution was made at a concentration 0.1 mg/mL. This solution was used to establish a UV-HPLC calibration curve, which could be easily done by correlating the volume of the injection with the resulting UV peak area. To determine the specific activity of the product at the time of analysis, a portion of crude reaction mixture (4µL) was taken out. The total amount of radio-activity of the portion was measured using a dosimeter. The % of activity incorporated in the captor compound was then determined by radio-HPLC, which was then converted to the absolute amount of activity by multiplying the % of activity conversion with the total amount of activity (mCi). The specific activity of the product was calculated by dividing the total amount of product activity by the amount of product (µmol, based on the integration of the UV-HPLC-UV and determined with the calibration curve (Figure 31). For entry 1, 7 and 8, the experiments were repeated four times and the average values reported. The radio traces obtained for the four independent syntheses in entry 7 are shown in Figure 32 for illustrative purposes.

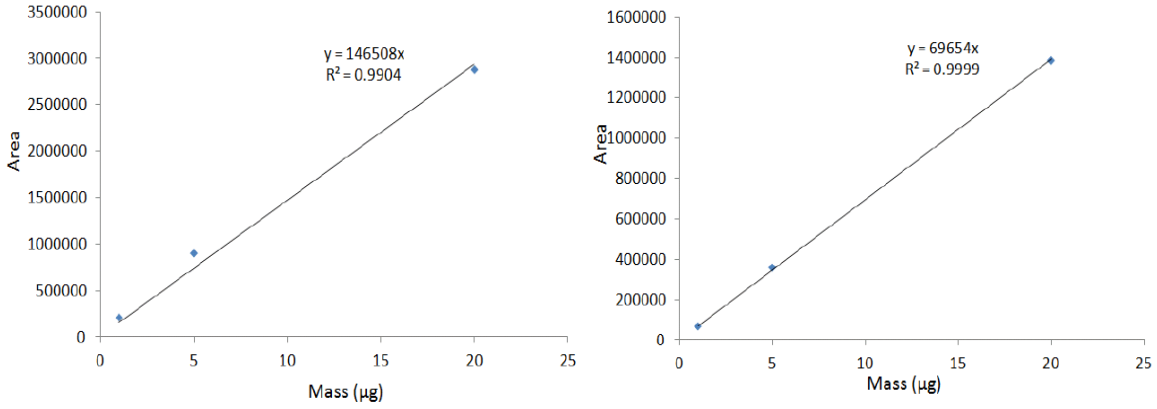

Figure 31. Calibration curves of compound **30** and **35** used for specific activity measurements. The standard injection volume is 200 µL. The first data point is obtained by diluting 10 µL of the standard solution to a total volume of 200 µL. The second data point is obtained by diluting 20 µL of the standard solution to a total volume of 200 µL. The third data point is obtained by injecting 200 µL of the stock solution.

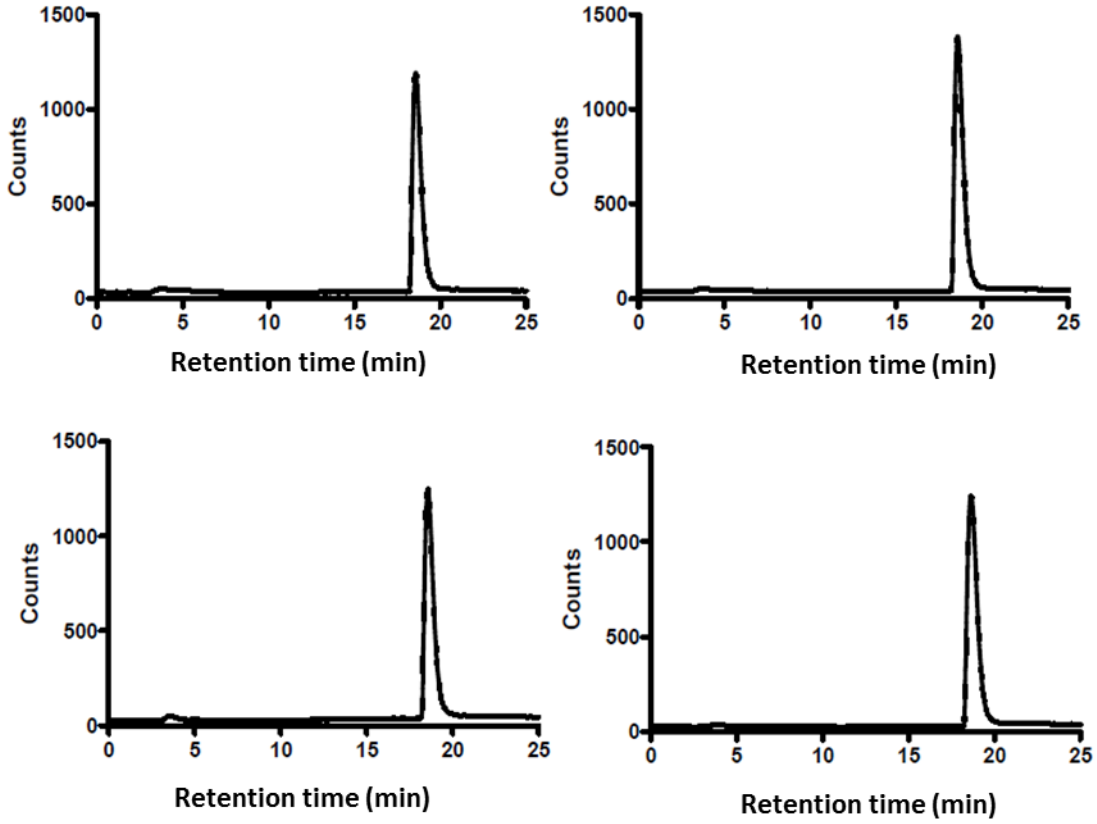

Figure 32. Four representative independent ^{18}F-fluorination of compound **30** using condition mentioned at Table 1, entry 7. HPLC was performed on a phenomenex Luna 5µ C18 column (250 × 4.6 mm). The flow was 1 mL/min, with the mobile phase starting from 95% solvent A (0.1% TFA in water) and 5% solvent B (0.1% TFA in MeCN) (0–2 min) to 5% solvent A and 95% solvent B at 22 min.

MicroPET Imaging

Animal procedures were performed according to a protocol approved by the University of Southern California Institutional Animal Care and Use Committee. The animal care and use program at USC meets the requirements of the Federal Law (89-544 and 91-570). The USC program is also accredited by the American Association for Accreditation of Laboratory Animals. MicroPET scans were performed on a microPET R4 rodent model scanner (Siemens Medical Solutions USA, Inc., Knoxville, TN). The scanner has a computer-controlled bed and 10.8-cm transaxial and 8-cm axial fields of view (FOVs). It has no septa and operates exclusively in the 3-dimensional (3D) list mode. Animals were placed near the center of the FOV of the scanner. For static microPET scans, normal nu/nu mice were injected with about 3.7 MBq (100 μCi) of radio products ([$^{18/19}$F]**30**, [$^{18/19}$F]**35**) *via* the tail vein. At 0.5 h, and 2 h post injection (p.i.), the mice were anesthetized with isoflurane (5% for induction and 2% for maintenance in 100% O2) using a knock-down box.

With the help of a laser beam attached to the scanner, the mice were placed in the prone position and near the center of the field of view of the scanner. The 3-min static scans were then obtained. Images were reconstructed by use of a 2-dimensional ordered-subsets expectation maximization (OSEM) algorithm. No background correction was performed. Regions of interest (ROIs; 5 pixels for coronal and transaxial slices) were drawn over the tumor on decay-corrected whole-body coronal images. The maximum counts per pixel per minute were obtained from the ROI and converted to counts per milliliter per minute by using a calibration constant. With the assumption of a tissue density of 1 g/ml, the ROIs were converted to counts per gram per min. Image ROI-derived %ID/g values were determined by dividing counts per gram per minute by injected dose. No attenuation correction was performed. Finally, the animals are awake between the scans, which can accelerate the rate of excretion.

CHAPTER III

SYNTHESIS AND *IN VIVO* EVALUATION OF [^{18}F]-ZWITTERIONIC ARYLTRIFLUOROBORATE/INDOMETHACIN CONJUGATES AS POTENTIAL PET PROBES

3.1 Introduction

Cyclooxygenase (COX) enzymes play a vital role in the biotransformation of arachidonic acid into a wide variety of prostaglandins, which are important mediators of inflammation.[67] They are also the pharmacological targets of nonsteroidal anti-inflammatory drugs. There are two types of COX enzymes which are COX-1 and COX-2.[68] Despite similarities in amino acid sequence and three-dimensional structures, COX-1 and COX-2 have different regulation, tissue localizations, and substrate specificity. The COX-1 enzyme is expressed in most tissues and plays an important role in the production of prostaglandins; however, the COX-2 enzyme is only expressed in a few normal tissues and is highly upregulated in inflamed tissues as well as in many premalignant and malignant tumours. Selective COX-2 inhibitors can be useful in the treatment of various cancers.[69,70] Therefore, the conjugation of COX-2 inhibitors with fluorescent or radioactive compounds can be used for the selective imaging of inflammation and tumours in living beings.

Indomethacin (Figure 33) is a powerful nonsteroidal anti-inflammatory drug that selectively binds and inhibits cyclooxygenase (COX) enzymes.[71-73] Moreover, indomethacin also shows anticancer activity, especially gastrointestinal cancer.[74]

According to these studies, indomethacin significantly extends the lifespan of a group of patients suffering from cancers. Unfortunately, indomethacin manifests an approximately 15-fold higher selectivity for COX-1 relative to COX-2.[71-73] The COX-1 inhibition causes gastrointestinal toxicity and obstruct platelet function leading to increased bleeding times.[75] Thus, a recent development of indomethacin based anti-inflammatory and anticancer drugs is focused on modifying new derivatives that shows low COX-1 inhibitory activity.

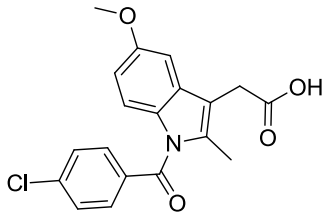

Figure 33. Chemical structure of the indomethacin compound.

Since the COX-2 active site is about 25% larger than the COX-1 active site, indomethacin derivatives of larger size have been targeted, [71-73] for example by increasing the length of the carboxylic side chain or enlarging the acyl group attached to the indole nitrogen. [76] Furthermore, many different amides and esters of indomethacin derivatives also showed a significant COX-2 selectivity.[77] This approach is noteworthy as it was applied to construct such as the carboxy-X-rhodamine conjugate (Figure 34) which can be used for COX-2-targeted fluorescent imaging agent.[78] Based on the imaging results shown in this work, this fluorescent compound highly accumulated in inflamed and tumour tissues providing an ample *in vivo* fluorescent signal.[78]

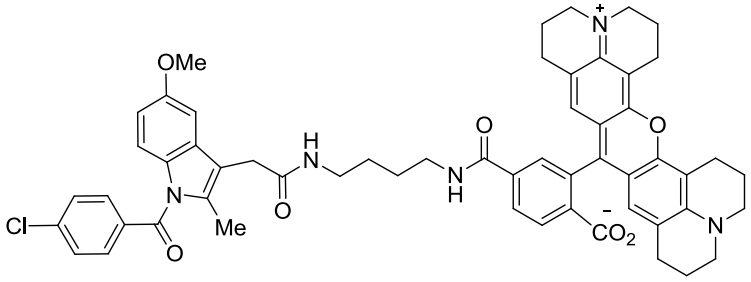

Figure 34. Chemical structure of the carboxy-X- rhodamine conjugated indomethacin.

These results suggested to us that a similar approach based on indomethacin as a targeting group could be extended to the design of Positron Emission Tomography (PET) probes for inflammation and cancer imaging. With this objective in mind, we have decided to conjugate indomethacin with zwitterionic phosphonium trifluoroborates (Figure 35),[79] a class of ^{18}F fluoride anions captors that we developed based on the pioneering work of Perrin on [^{18}F]-arylfluoroborates[7,11] as PET probes.[18-20,22,23] In this dissertation, we report the results of these efforts. We also describe the radiofluorination of the resulting conjugates and their evaluation as PET probes in a tumour bearing murine model.

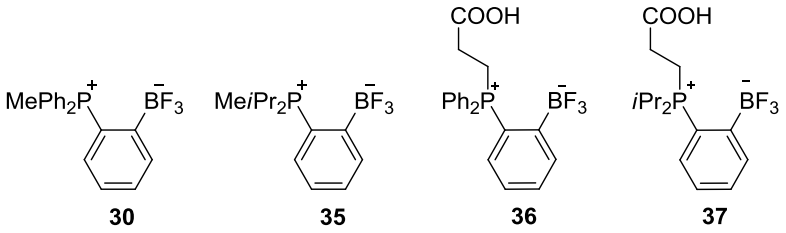

Figure 35. Chemical structures of the zwitterionic phosphonium trifluoroborates.

3.2 Synthesis and characterizations

In order to connect an amine functional group to cyclooxygenase targeting molecule, indomethacin was linked to *tert*-butyl (2-aminoethyl)carbamate through the amide coupling reaction. The reaction of indomethacin with EDC (1-ethyl-3-(3-dimethylaminopropyl) carbodiimide), HOBt (1-hydroxybenzotriazole), DIEA (di-*iso*-propylmethylamine) and *tert*-butyl (2-aminoethyl) carbamate in DMF yielded **39** as a white powder in 94% (Figure 36). Formation of **39** was first confirmed by ^{1}H NMR spectroscopy which shows two broad triplets at 6.75 ppm and 7.98 ppm corresponding to the amide functional groups. Since the COX-2 active site is larger than the COX-1 active site, indomethacin derivatives with longer carboxylic chains are also good candidates for selective COX-2 targeting. For this reason, we have prepared two analogs of **39** (namely compounds **40** and **41**) which feature longer diamine linkers. These analogs have been obtained by reaction of *tert*-butyl (2-aminobutyl)carbamate and *tert*-butyl (2-aminooctyl)carbamate with indomethacin compound using the amide coupling conditions used in the synthesis of **39** (Figure 36). Using this protocol, the indomethacin/butyl carbamate (**40**) and the indomethacin / octyl cabamate (**41**) have been obtained in 84 and 85 % yield, respectively. The ^{1}H NMR spectrum of these derivatives shows two triplets corresponding to the two amide groups. These signals are observed at 6.72 ppm and 7.97 ppm for **40** and 6.70 ppm and 7.96 ppm for **41**. With these new compounds in hand, we next focused on the deprotection of the the *tert*-butyl carbamate group which could be easily carried out by treatment of **39**, **40**, and **41** with 50% v/v trifluoroacetic acid (TFA) in CH_2Cl_2 at room temperature (Figure 36). These

reactions produce ethylammonium (**42**), butylammonium (**43**), and octylammonium (**44**) derivatives in high yields (97% yield for **42**, 95% yield for **43**, and 96% yield for **44**). The ^{1}H NMR spectra in DMSO shows a singlet broad peak corresponding to an ammonium ($-NH_3^+$) group at 7.88, 7.72, and 7.74 ppm for **42**, **43**, and, **44**, respectively. The singlet ^{19}F NMR signal at -74.3 ppm for **42** and -74.2 ppm for **43** and **44** indicates that the products were obtained as the trifluoroacetate salts. Treatment of **42**, **43**, and **44** with a strong base generates the indomethacin derivatives containing a carboxylic acid-reactive amine functionality which is suitable for an amide coupling reaction with a carboxylic functionalized fluoride captor.

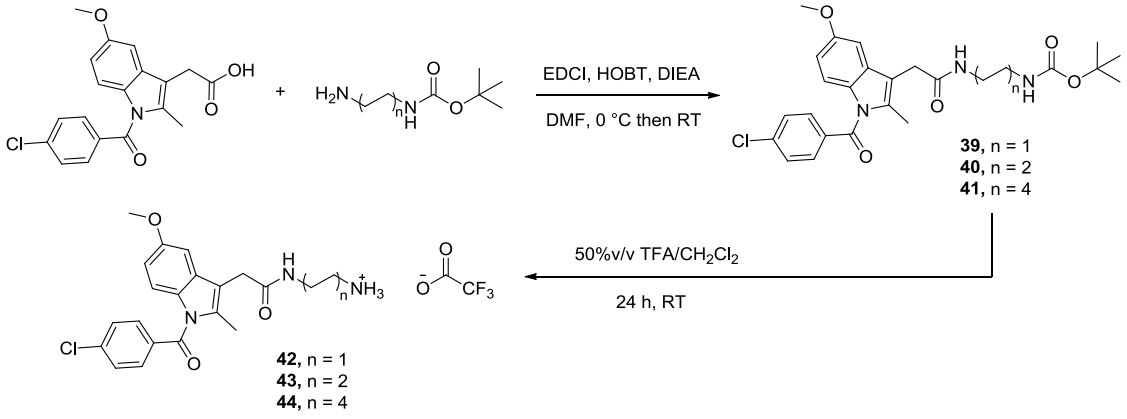

Figure 36. Scheme showing the synthesis of the indomethacin containing ammonium group with various chain lengths.

The fluoride captors/indomethacin conjugates were synthesized by reaction of **42**, **43**, or **44** with the *ortho*-phenylene phosphine-borane/ carboxylic acid derivatives **36** and **37** using EDCI, HOBT, and DIEA as coupling reagents (Figure 37). The di-*iso*-

propylphosphonium trifluoroborate/indomethacin conjugate **45** was obtained as a pale yellow powder in a 57 % yield. This compound has been fully characterized. The presence of the phosphonium moiety is confirmed by the detection of a ^{31}P NMR resonance at 44.2 ppm. The trifluoroborate moiety gives rise to a ^{11}B NMR resonance at 3.00 ppm and a ^{19}F NMR resonance at -133.9 ppm. The connection between the indomethacin unit and the phosphino-borane is indicated by the detection of two ^{1}H NMR signals at 6.67 and 6.75 ppm, corresponding to the two amide functional groups. Moreover, the ^{1}H NMR spectrum shows two doublets of doublets at 1.18 ppm and 1.35 ppm and a multiplet at 3.37 ppm which are the characteristic signals of the *iso*-propyl moiety.

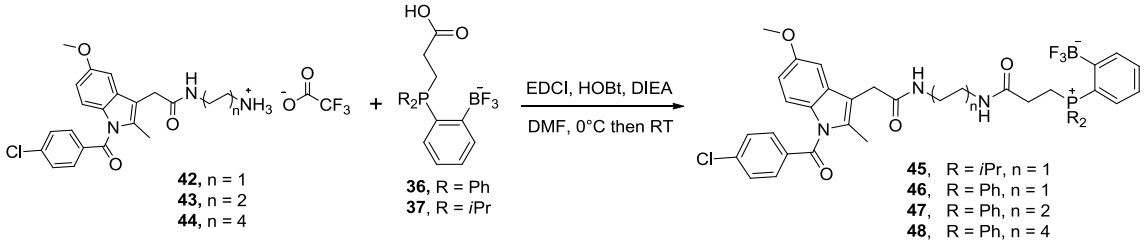

Figure 37. Scheme showing the synthesis of *ortho*-phenylene phosphine-boranes connecting indomethacin compound.

The diphenylphosphonium trifluoroborate derivatives **46**, **47**, and **48** were also obtained in moderate yield (62.8 % yield for **46**, 58.2 % yield for **47**, and 62.3 % yield for **48**). These compounds were characterized by multinuclear NMR spectroscopy. The ^{31}P NMR spectrum showed a singlet peak at 30.6 ppm for **46**, 30.9 ppm for **47**, and **48**

confirming the existence of phosphonium moiety. In addition, the trifluoroborate group of each compound was detected as a broad singlet signal by ^{11}B NMR spectroscopy at 2.9 ppm for **46**, at 3.0 ppm for **47**, and at 2.7 ppm for **48** as well as ^{19}F NMR spectroscopy at -133.4 ppm for **46**, at -131.3 ppm for **47**, and at -134.1 ppm for **48**. The ^{1}H NMR spectrum of each compound displays two triplets at 6.70 and 6.80 ppm for **46**, 7.82 and 7.98 ppm for **47**, and 7.72 and 7.96 ppm for **48** corresponding to the amide signals and thus confirming successful conjugation of the captors with the indomethacin unit.

3.3 Kinetic studies

As shown in various studies[5,79,80], aryltrifluoroborates undergo hydrolysis in aqueous media producing the corresponding boronic acids according to a first order rate reaction ($v = k_{obs}[ArBF_3]$).[4,81] To probe the possible influence of the phosphorus substituents, we first investigated the hydrolysis of the bis(*iso*-propyl) derivative **37** by ^{19}F NMR spectroscopy. As done for **30**, **35** and **36**, **37** was dissolved in D_2O–CD_3CN (8/2 vol) at pH 7.5 ([phosphate buffer] = 500 mM, [$ArBF_3$] = 20 mM with $ArBF_3$ = zwitterionic trifluoroborate) and monitored periodically. Based on the amount of $ArBF_3$ in solution determined by ^{19}F NMR *vs.* times, we found that the first order hydrolysis rate constant of **37** (k_{obs} = 5.2 x 10^{-5} min^{-1}) is slightly higher than **35** (k_{obs} = 3.9 x 10^{-5} min^{-1}) and **36** (k_{obs} = 1.5 x 10^{-5} min^{-1}) and noticeably higher than **30** (k_{obs} = 3.4 x 10^{-6} min^{-1}). These experiments confirm that the presence of *iso*-propyl substituents decreases the kinetic stability of the complexes. A comparison between the hydrolysis rate

constants of **35** and **37** also show that the pendent carboxylic acid functionality plays a labilizing role.

Next, we decided to examine the stability of our new indomethacin conjugates compounds **45**, **46**, **47**, and **48** in aqueous media. Unfortunately, all zwitterionic aryltrifluoroborate/indomethacin conjugates did not dissolved in D_2O–CD_3CN (8/2 vol) phosphate buffer solution. To address this solubility problem, we decided to use the neutral surfactant triton X-100. We found that all conjugates could be dissolved in 10% w/v triton X-100 in H_2O/ DMSO (7/3 vol) at pH = 7.5 ([phosphate buffer] = 500 mM, [$ArBF_3$] = 20 mM with $ArBF_3$ = zwitterionic trifluoroborate). In order to get a reference point in this new medium, we first evaluated the stability of **37** and obtained a hydrolysis rate constant (k_{obs}) of 1.2 x 10^{-5} min^{-1}. This hydrolysis rate constant is about five time lower than that measured in D_2O–CD_3CN (8/2 vol), which reflects the lower water content of the new H_2O/ DMSO (7/3 vol) medium. Using these new conditions, we observed that the hydrolysis reaction of the indomethacin conjugates is extremely slow. In the case of the diphenylphosphonium derivatives **46**, **47**, and **48**, we did not see any evidence of hydrolysis even after 7 days. In the case of the di-*iso*-propylphosphonium derivative **45**, we did notice a trace amount of free fluoride at the same period of time. By expanding this experiment to a longer timescale, we have been able to calculate k_{obs} = 4.0 x 10^{-7} for **45**. The kinetic plots for the hydrolysis of **37** and **45** were demonstrated in Figure 38. These results are consistent with the previous studies on the stability of the *ortho*-phosphonium aryltrifluoroborates that the rate of hydrolysis of the diphenylphosphonium derivatives **30** and **36** is slower than that of the di-*iso*-

propylphosphonium derivative **35** and **37**, respectively.[79,80] These results also show that the targeting group, in this case indomethacin, may have a drastic effect on the hydrolytic stability of the trifluoroborate.

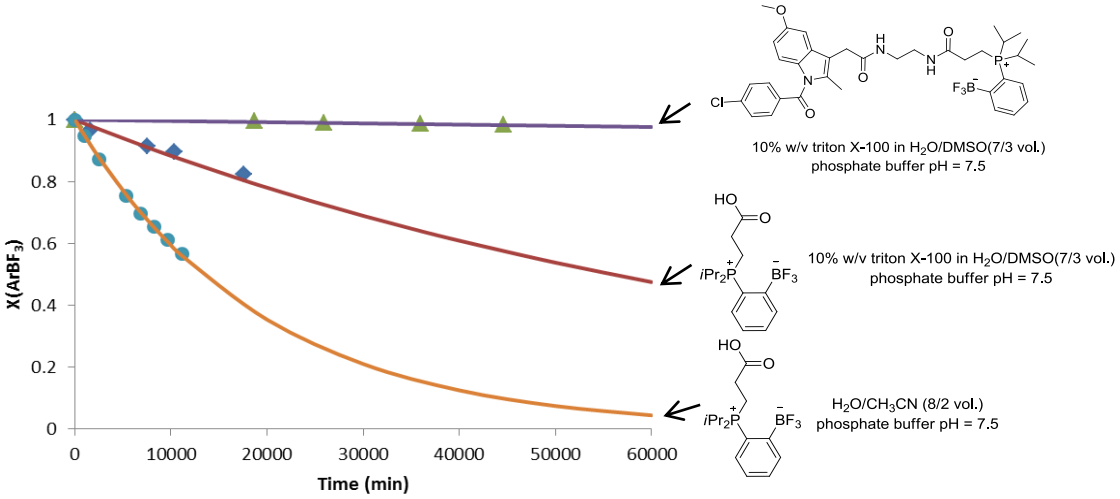

Figure 38. Kinetic plots for the hydrolysis of **37** and **45** in aqueous conditions.

3.4 Radiochemistry[3]

Using the conditions that we developed for the radiofluorination of zwitterionic aryltrifluoroborates,[79] we decided to radiolabel the novel indomethacin conjugates by ^{18}F-^{19}F isotopic exchange. This radiosynthetic approach, which is gaining interest, has also been used for the radiofluorination of main group molecules, for example, BF_4^-[82], organoboranes[14,30,83] and fluorosilane derivatives.[84,85] In a typical experiment, **46** (0.28

[3] This experiment was carried out by our collaborator, Dr. Zibo Li, at department of Radiology, University of Southern California, Los Angeles, CA.

μmol) was dissolved in DMSO (20 μL) and mixed with a solution of irradiated [^{18}O] water (100μL, pH 2) containing 45 mCi of ^{18}F at 75ºC for 10 minutes (Figure 39). The same approach was applied to the radiofluorination of conjugate **45**.

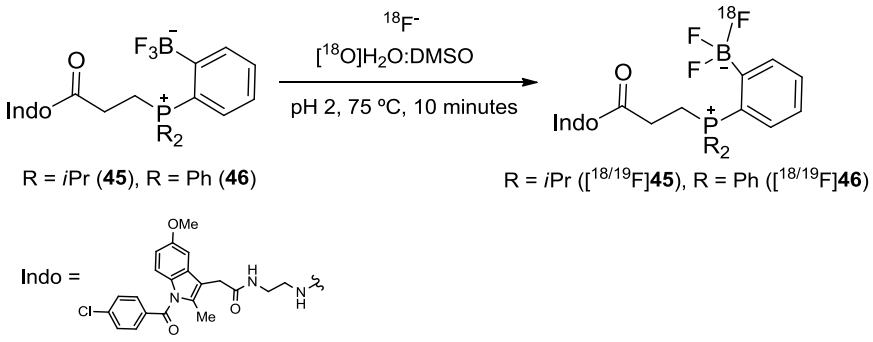

Figure 39. Reaction scheme showing direct ^{18}F-^{19}F isotopic exchange reaction proceeded for the radiolabeling of **45** and **46** in aqueous solution.

As shown in the crude radio-signal HPLC profile (Figure 40), [$^{18/19}$F]-**45** and [$^{18/19}$F]-**46** are cleanly obtained by the isotopic exchange process. The identity of [$^{18/19}$F]-**45** and [$^{18/19}$F]-**46** were confirmed by comparing the radio HPLC trace with the elution time of the non-labelled analogue. The radiochemical yields based on the radio-activity of isolated product and the starting radio-activity were calculated as 7% and 12% for [$^{18/19}$F]-**45** and [$^{18/19}$F]-**46**, respectively.

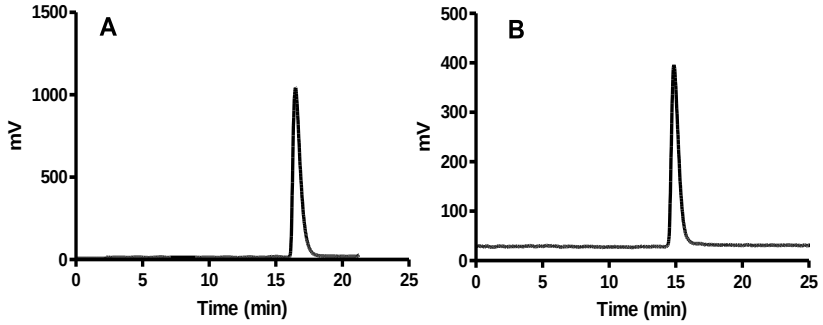

Figure 40. Crude radio-signal HPLC profiles obtained in the radiofluorination of [$^{18/19}$F]**46** (A) and [$^{18/19}$F]**45** (B).

3.5 *In vivo* imaging studies[4]

Next, we endeavoured to evaluate the *in vivo* imaging potential of these probes in a murine model bearing human gliobastoma (U87MG), a type of tumours known to overexpress COX-2[20]. We injected 0.02 mCi of [$^{18/19}$F]-**45** and [$^{18/19}$F]-**46** into female nude mice. At 15, 40, and 90 minutes post-injection, static microPET scans were obtained. The resulting sagittal images for [$^{18/19}$F]-**45** and [$^{18/19}$F]-**46** are shown in Figure 41 (above). At 15 min post injection, [$^{18/19}$F]-**46** showed a clear localization in the liver because of its lipophilic property while [$^{18/19}$F]-**45** was more quickly cleared through the urinary track as indicated by the appearance of a signal in the bladder of the animal. Surprisingly, [$^{18/19}$F]-**45** was the only tracer that accumulated into the tumour. In the

[4] This experiment was carried out by our collaborator, Dr. Zibo Li, at department of Radiology, University of Southern California, Los Angeles, CA.

microPET quantification analysis, the tumour uptake of [$^{18/19}$F]-**45** was determined to be 0.42, 0.47, and 0.55 %ID/g at 15, 40, and 90 min post-injection as shown in Figure 41 (below). This finding indicates that the indomethacin conjugate with more hydrophilic radio-prosthetic group ([$^{18/19}$F]-**45**) display better tumour binding properties than the more hydrophobic analogue ([$^{18/19}$F]-**46**). These results are important because that they show that changes in the structure of the radio-prosthetic group have an impact on the tumour binding property of the tracers. In addition, we also observed that the [$^{18/19}$F]-**45** undergoes a high degree of defluorination *in vivo* as confirmed by a distinct skeletal signal especially obvious in the sagittal images at 40 min and 90 min post-injection. MicroPET quantification analysis shows that the use of [$^{18/19}$F]-**45** leads to a bone uptake of 2.8, 3.1, and 4.7 %ID/g at 15, 40, and 90 min post-injection (Figure 41 (below)). These values, which are significantly higher than those measured for [$^{18/19}$F]-**46** (0.6, 0.8, and 1.2 %ID/g at 15, 40, and 90 min post-injection), can be correlated to the higher hydrolysis rate constants measured for the di-*iso*-propyl derivatives when compared to their diphenyl analogues.

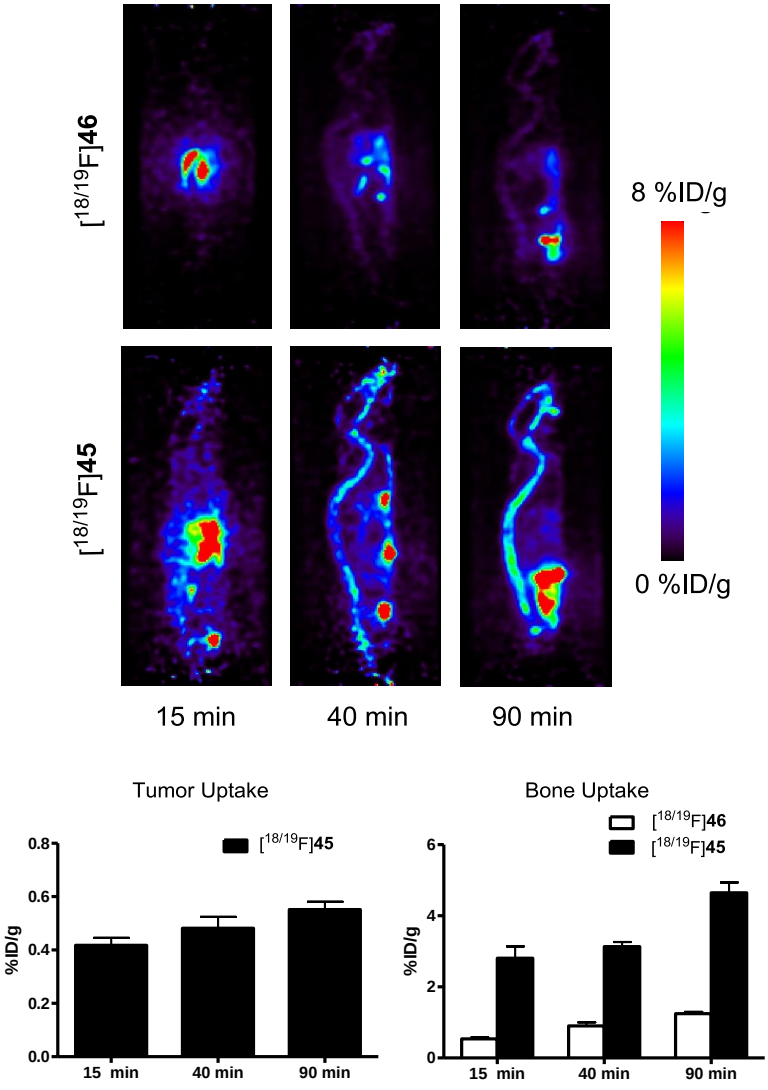

Figure 41. (Above) Decay-corrected whole-body microPET Sagittal images of nude mice bearing U87MG tumor from a static scan at 15, 40, and 90 min after injection of [$^{18/19}$F]**45** and [$^{18/19}$F]**46**. The images are corrected based on the injected activity. The signal intensity is reported in % of the injected dose per gram (%ID/g). (Below) MicroPET quantifications for U87MG tumor and bone uptake for [$^{18/19}$F]**45** and [$^{18/19}$F]**46**.

3.6 Conclusion

This report establishes that phosphonium aryltrifluoroborates can be conjugated with molecules of biological interest such as indomethacin using simple synthetic approaches. The resulting conjugates are amenable to late stage radiofluorination *via* simple isotopic ^{18}F-^{19}F exchange in aqueous solution. This approach affords PET probes which have been tested *in vivo* in a tumour bearing murine model. One of the key findings of these animal studies is the influence of the captor structure which largely governs the bio-distribution of the probe and its affinity for the tumour.

3.7 Experimental

General consideration

Tert-butyl (2-aminoethyl) carbamate[86], *tert*-butyl (4-aminobutyl) carbamate[86], *tert*-butyl (8-Aminooctyl) carbamate[86], *ortho*-($Ph_2(CH_2CH_2COOH)P$) $C_6H_4(BF_3)$[79], and [*ortho*-(iPr_2PH)C_6H_4(Bpin)][BF_4][59] were synthesized according to the published procedure. Indomethacin was purchased from Enzo life sciences; 1,2-diaminoethane was purchased from Mallinckrodt; 1,4-diaminobutane and 1,8-diaminooctane were purchased from Sigma Aldrich; hydroxylbenzotriazole (HOBT) was purchased from Advanced ChemTech; *tert*-butylcarbamate, 1-ethyl-3-(3-dimethylaminopropyl)carbodiimide (EDCI), N, N-di-*iso*-propylethylamine, and trifluoroacetic acid were purchased from Alfar Aesar. All chemicals were used without further purification. CH_2Cl_2 were dried by passing through an alumina column. Electrospray mass spectra were acquired from a MDS Sciex API QStar Pulsar. NMR spectra were recorded on a Varian Unity Inova 400

NMR and an Inova 500B spectrometer at ambient temperature. Chemical shifts are given in ppm, and are referenced to residual ^{1}H and ^{13}C solvent signals as well as external H_3PO_4 (^{31}P NMR) and BF_3-Et_2O (^{11}B NMR and ^{19}F NMR).

*Synthesis of tert-butyl (2-(2-(1-(4-chlorobenzoyl)-5-methoxy-2-methyl-1H-indol-3-yl)acetamido)ethyl)carbamate (**39**)*

To a stirred solution of indomethacin (0.870 g, 2.43 mmol) in DMF (25 mL) was added HOBt (0.558 g, 3.65 mmol) and EDCI (0.512 g, 2.67 mmol) at 0 °C. The solution was stirred at 0 °C for 15 min. After 15 min, *tert*-butyl (2-aminoethyl) carbamate (1.170 g, 7.32 mmol) and DIEA (1.30 mL, 7.36 mmol) were added to the mixture. The reaction mixture was stirred at room temperature for 16 h. Removal of solvent *in vacuo* afforded a residue, to which 30 mL water was added and extracted with EtOAc (3 x 25 mL). The organic layer was dried over $MgSO_4$, concentrated in *vacuo*, and precipitated from hexane affording **39** as a yellow powder (1.260 g, 93.8 % yield). **^{1}H NMR** (299.9 MHz, DMSO-d_6): δ 1.37 (s, 9H, CH_3), 2.22 (s, 3H, CH_3), 3.00 (m, 2H, -CH_2-), 3.09 (m, 2H, -CH_2-), 3.50 (s, 2H, CH_2CO), 3.77 (s, 3H, OCH_3), 6.72 (dd, $J_{H\text{-}H}$ = 9.00, 2.34 Hz, 1H, indolyl H-6), 6.79 (t, $J_{H\text{-}H}$ = 4.80 Hz, 1H, amide-H), 6.97 (d, $J_{H\text{-}H}$ = 9.00 Hz, 1H, indolyl H-7), 7.10 (d, $J_{H\text{-}H}$ = 2.40 Hz, indolyl H-4), 7.65 (d, $J_{H\text{-}H}$ = 8.10 Hz, 2H, *p*-chlorobenzoyl H-3, H-5), 7.71 (d, $J_{H\text{-}H}$ = 8.40 Hz, 2H, *p*-chlorobenzoyl H-2, H-6), 8.04 (t, $J_{H\text{-}H}$ = 5.40 Hz, 1H, amide-H). **^{13}C NMR** (125.58 MHz, DMSO-d_6): δ 13.81, 28.62, 31.58, 55.83, 78.10, 102.29, 111.71, 114.64, 115.05, 129.46, 130.71, 131.32, 131.57, 134.69, 135.57,

137.96, 155.98, 156.04, 168.27, 169.95. Mass (ESI^+): calcd for $C_{26}H_{30}ClN_3O_5Na$ $(M+Na)^+$, 522.98; found 522.16.

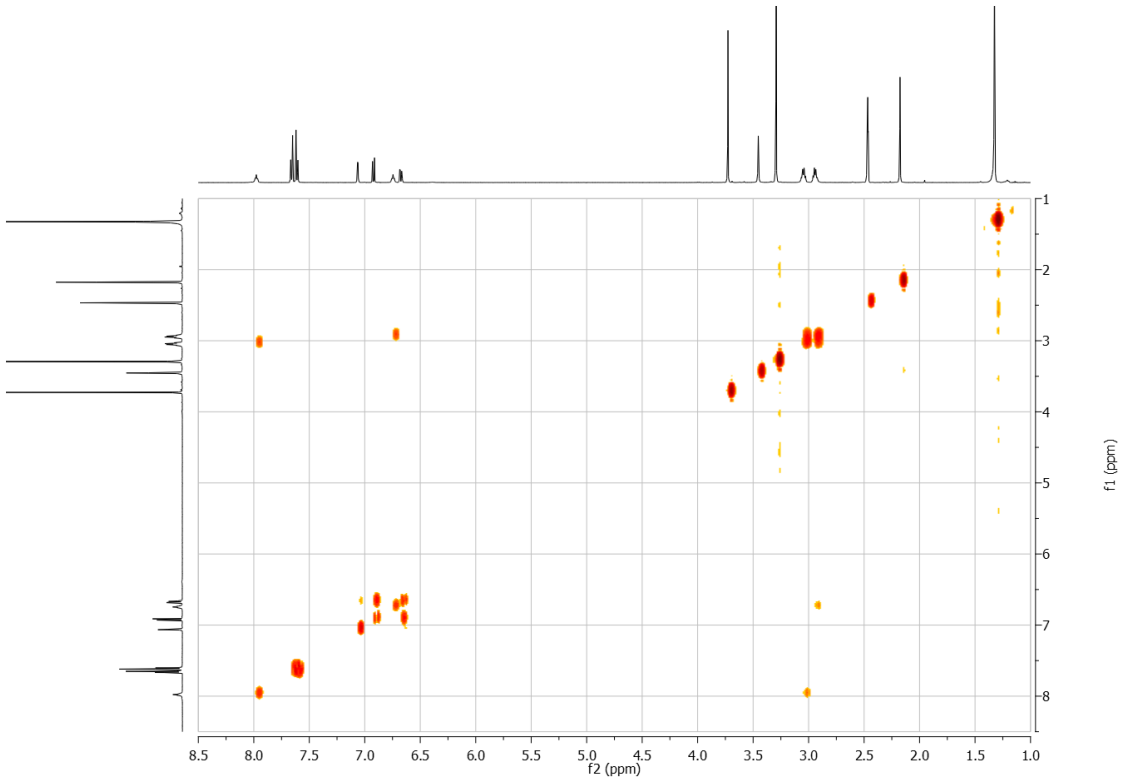

Figure 42. 2-Dimentional NMR spectrum of **39**.

*Synthesis of tert-butyl (4-(2-(1-(4-chlorobenzoyl)-5-methoxy-2-methyl-1H-indol-3-yl)acetamido)butyl)carbamate (**40**)*

To a stirred solution of indomethacin (0.870 g, 2.43 mmol) in DMF (25 mL) was added HOBt (0.558 g, 3.65 mmol) and EDCI (0.512 g, 2.67 mmol) at 0 °C. The solution was stirred at 0 °C for 15 min. After 15 min, *tert*-butyl (2-aminoethyl) carbamate (1.372 g, 7.29 mmol) and DIEA (1.30 mL, 7.36 mmol) were added to the mixture. The reaction mixture was stirred at room temperature for 16 h. Removal of solvent *in vacuo* afforded a residue, to which 50 mL water was added and extracted with EtOAc (3 x 50 mL). The organic layer was dried over $MgSO_4$, concentrated in *vacuo*, and precipitated from hexane affording **40** as a yellow powder (1.072 g, 83.6 % yield). **^{1}H NMR** (499.4 MHz, DMSO-d_6): δ 1.37 (s, br, 13H, CH_3 and -CH_2-), 2.23 (s, 3H, CH_3), 2.89 (m, 2H, -CH_2-), 3.04 (m, 2H, -CH_2-), 3.49 (s, 2H, CH_2CO), 3.77 (s, 3H, OCH_3), 6.71 (dd, $J_{H\text{-}H}$ = 9.49, 2.75 Hz, 1H, indolyl H-6), 6.77 (t, $J_{H\text{-}H}$ = 5.50 Hz, 1H, amide-H), 6.95 (d, $J_{H\text{-}H}$ = 8.49 Hz, 1H, indolyl H-7), 7.12 (d, $J_{H\text{-}H}$ = 2.35 Hz, indolyl H-4), 7.65 (d, $J_{H\text{-}H}$ = 8.49 Hz, 2H, *p*-chlorobenzoyl H-3, H-5), 7.70 (d, $J_{H\text{-}H}$ = 8.49 Hz, 2H, *p*-chlorobenzoyl H-2, H-6), 8.02 (t, $J_{H\text{-}H}$ = 5.49 Hz, 1H, amide-H). **^{13}C NMR** (125.59 MHz, DMSO-d_6): δ 13.85, 27.00, 27.46, 28.73, 31.64, 38.96, 55.89, 77.81, 102.31, 111.74, 114.93, 115.02, 129.51, 130.75, 131.40, 131.62, 134.76, 135.56, 138.01, 156.02, 156.05, 168.33, 169.67. Mass (ESI^+): calcd for $C_{28}H_{34}ClN_3O_5Li$ $(M+Li)^+$, 534.23; found 534.21.

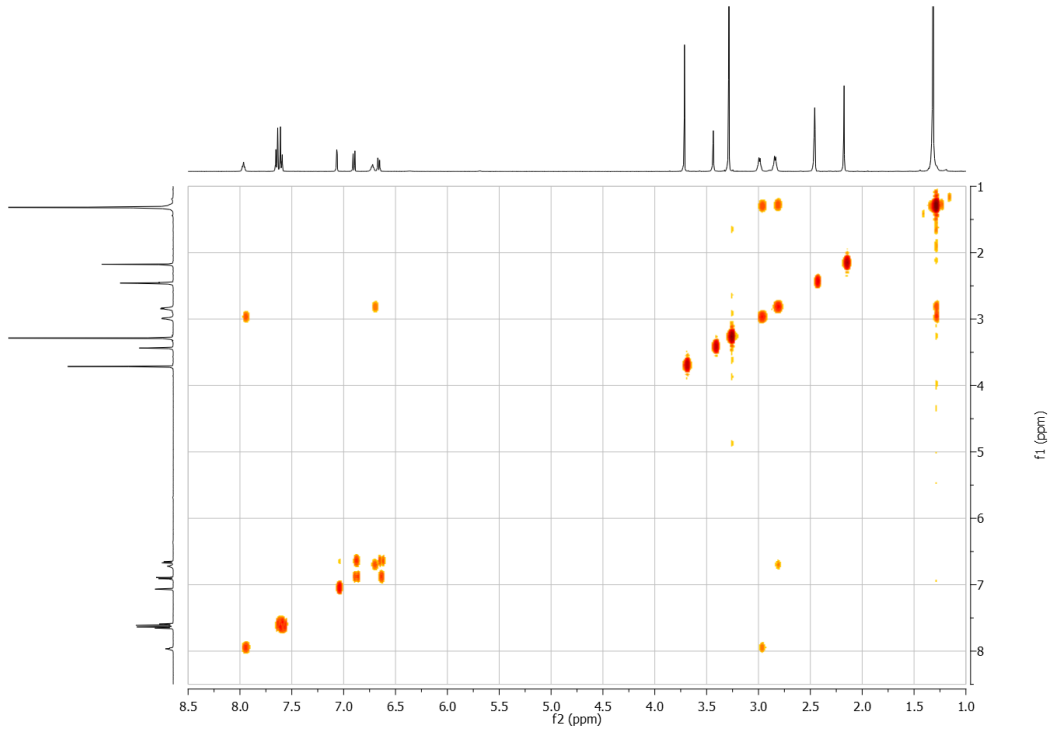

Figure 43. 2-Dimentional NMR spectrum of **40**.

*Synthesis of tert-butyl (8-(2-(1-(4-chlorobenzoyl)-5-methoxy-2-methyl-1H-indol-3-yl) acetamido)octyl)carbamate (**41**)*

To a stirred solution of indomethacin (0.870 g, 2.43 mmol) in DMF (25 mL) was added HOBt (0.558 g, 3.65 mmol) and EDCI (0.512 g, 2.67 mmol) at 0 °C. The solution was stirred at 0 °C for 15 min. After 15 min, *tert*-butyl (2-aminoethyl) carbamate (1.782 g, 7.29 mmol) and DIEA (1.30 mL, 7.36 mmol) were added to the mixture. The reaction mixture was stirred at room temperature for 16 h. Removal of solvent *in vacuo* afforded a residue, to which 50 mL water was added and extracted with EtOAc (3 x 50 mL). The organic layer was dried over $MgSO_4$, concentrated in *vacuo*, and precipitated from hexane affording **41** as a yellow powder (1.211 g, 85.3 % yield). **^{1}H NMR** (499.4 MHz,

DMSO-d_6): δ 1.20 (s, br, 8H, -CH_2-), 1.37 (s, br, 13H, CH_3 and -CH_2-), 2.23 (s, 3H, CH_3), 2.88 (m, 2H, -CH_2-), 3.05 (m, 2H, -CH_2-), 3.48 (s, 2H, CH_2CO), 3.76 (s, 3H, OCH_3), 6.71 (dd, $J_{H\text{-}H}$ = 8.99, 2.10 Hz, 1H, indolyl H-6), 6.75 (t, $J_{H\text{-}H}$ = 4.99 Hz, 1H, amide-H), 6.95 (d, $J_{H\text{-}H}$ = 9.49 Hz, 1H, indolyl H-7), 7.12 (d, $J_{H\text{-}H}$ = 2.10 Hz, indolyl H-4), 7.65 (d, $J_{H\text{-}H}$ = 8.99 Hz, 2H, *p*-chlorobenzoyl H-3, H-5), 7.69 (d, $J_{H\text{-}H}$ = 7.99 Hz, 2H, *p*-chlorobenzoyl H-2, H-6), 8.00 (t, $J_{H\text{-}H}$ = 5.99 Hz, 1H, amide-H). **^{13}C NMR** (125.59 MHz, DMSO-d_6): δ 13.85, 26.72, 26.83, 28.74, 29.17, 29.24, 29.61, 29.95, 31.71, 39.11, 55.85, 77.73, 102.35, 111.68, 114.99, 129.49, 130.75, 131.36, 131.61, 134.77, 135.53, 138.01, 156.01, 168.32, 169.62. Mass (ESI$^+$): calcd for $C_{32}H_{42}ClN_3O_5Li$ $(M+Li)^+$, 590.30; found 590.27.

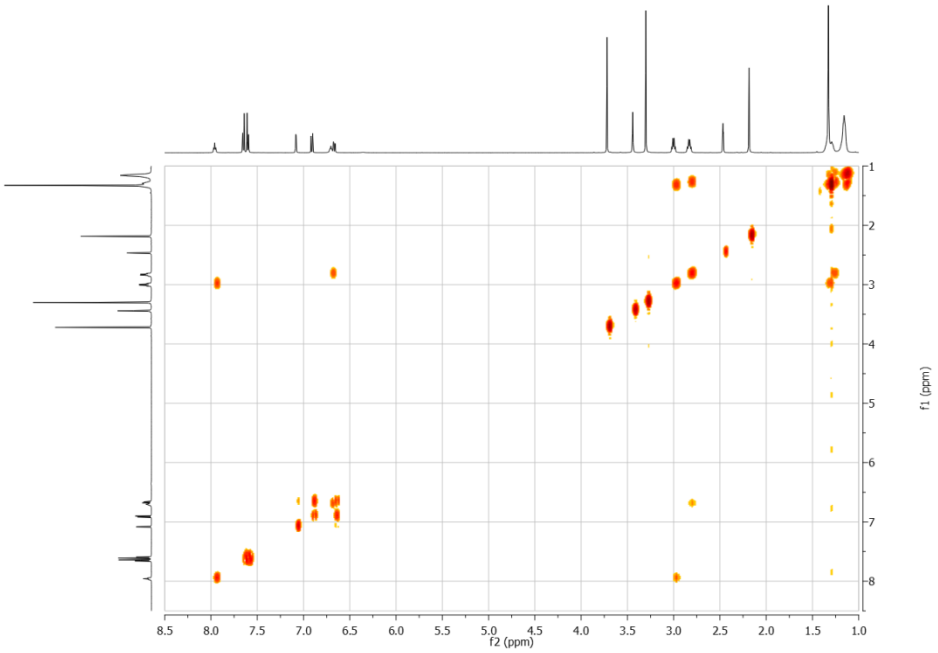

Figure 44. 2-Dimentional NMR spectrum of **41**.

*Synthesis of 2-(2-(1-(4-chlorobenzoyl)-5-methoxy-2-methyl-1H-indol-3-yl)acetamido) ethanaminium trifluoroacetate (**42**)*

Compound **39** (1.260 g, 2.521 mmol) was dissolved in 50%v/v solution of trifluorocarboxylic acid (TFA) in dichloromethane (20 mL). The reaction mixture was stirred at room temperature for 24 h. Then, the solution was concentrated in *vacuo* to a volume of 2 mL and hexane (20 mL) was added to precipitate **42** as a light brown solid (1.256 g, 96.9 % yield). **^{1}H NMR** (299.9 MHz, DMSO-d_6): δ 2.22 (s, 3H, CH_3), 2.86 (m, 2H, CH_2C), 3.29 (m, 2H, CCH_2), 3.53 (s, 2H, CH_2CO), 3.75 (s, 3H, OCH_3), 6.71 (dd, J_{H-H} = 9.00, 2.55 Hz, 1H, indolyl H-6), 6.94 (d, J_{H-H} = 9.30 Hz, 1H, indolyl H-7), 7.08 (d, J_{H-H} = 2.43 Hz, indolyl H-4), 7.64 (d, J_{H-H} = 8.70 Hz, 2H, *p*-chlorobenzoyl H-3, H-5), 7.69 (d, J_{H-H} = 8.70 Hz, 2H, *p*-chlorobenzoyl H-2, H-6), 7.82 (s, br, 3H, NH_3^+), 8.23 (m, 1H, N*H*$COCH_2$). **^{13}C NMR** (125.58 MHz, DMSO-d_6): δ 13.36 31.07 36.66 38.66 55.42 101.93 111.21 113.90 114.57 129.06 130.31 130.33 131.16 134.21 135.34 137.65 155.59 158.47 (q, J_{C-F} = 36.42 Hz) 167.87 170.38. **^{19}F NMR** (469.92 MHz, DMSO-d_6): δ -74.32. Mass (ESI^+): calcd for $C_{21}H_{23}ClN_3O_3$ $(M+H)^+$, 400.50; found 400.12.

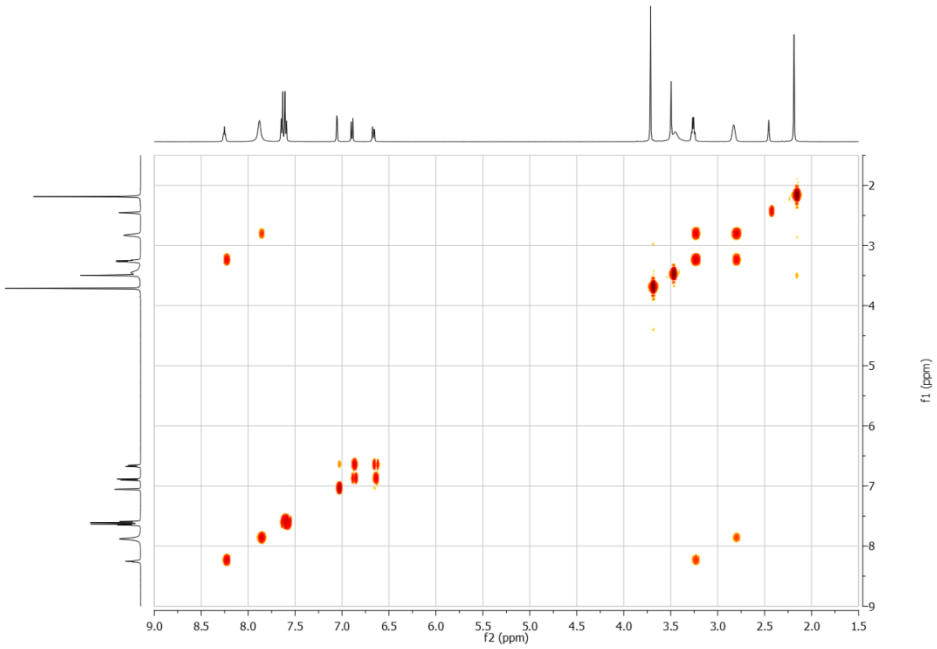

Figure 45. 2-Dimentional NMR spectrum of **42**.

*Synthesis of 4-(2-(1-(4-chlorobenzoyl)-5-methoxy-2-methyl-1H-indol-3-yl)acetamido) butan-1-aminium trifluoroacetate (**43**)*

Compound **40** (1.072 g, 2.030 mmol) was dissolved in 50%v/v solution of trifluorocarboxylic acid (TFA) in dichloromethane (20 mL). The reaction mixture was stirred at room temperature for 24 h. Then, the solution was concentrated in *vacuo* to a volume of 2 mL and hexane (20 mL) was added to precipitate **43** as a light brown solid (1.047 g, 95.2 % yield). **^{1}H NMR** (499.4 MHz, DMSO-d_6): δ 1.43 – 1.56 (m, 4H, -CH_2-), 2.24 (s, 3H, CH_3), 2.79 (m, 2H, -CH_2-), 3.07 (m, 2H, -CH_2-), 3.51 (s, 2H, CH_2CO), 3.77 (s, 3H, OCH_3), 6.72 (dd, $J_{H\text{-}H}$ = 9.49, 2.00 Hz, 1H, indolyl H-6), 6.94 (d, $J_{H\text{-}H}$ = 9.49 Hz, 1H, indolyl H-7), 7.12 (d, $J_{H\text{-}H}$ = 2.25 Hz, indolyl H-4), 7.65 (d, $J_{H\text{-}H}$ = 8.49 Hz, 2H,

p-chlorobenzoyl H-3, H-5), 7.69 (d, $J_{H\text{-}H}$ = 8.49 Hz, 2H, *p*-chlorobenzoyl H-2, H-6), 7.72 (s, br, 3H, NH_3^+), 8.11 (t, $J_{H\text{-}H}$ = 5.49 Hz, 1H, amide-H). **^{13}C NMR** (125.59 MHz, DMSO-d_6): δ 13.85, 24.98, 26.66, 31.61, 38.54, 39.00, 55.90, 102.41, 111.63, 114.80, 115.01, 129.52, 130.75, 131.38, 131.62, 134.71, 135.62, 138.07, 156.01, 158.81 (q, $J_{C\text{-}F}$ = 36.54 Hz), 168.32, 169.85. **^{19}F NMR** (469.92 MHz, DMSO-d_6): δ -74.19. Mass (ESI$^+$): calcd for $C_{23}H_{27}ClO_3N_3$ $(M+H)^+$, 428.17; found 428.14.

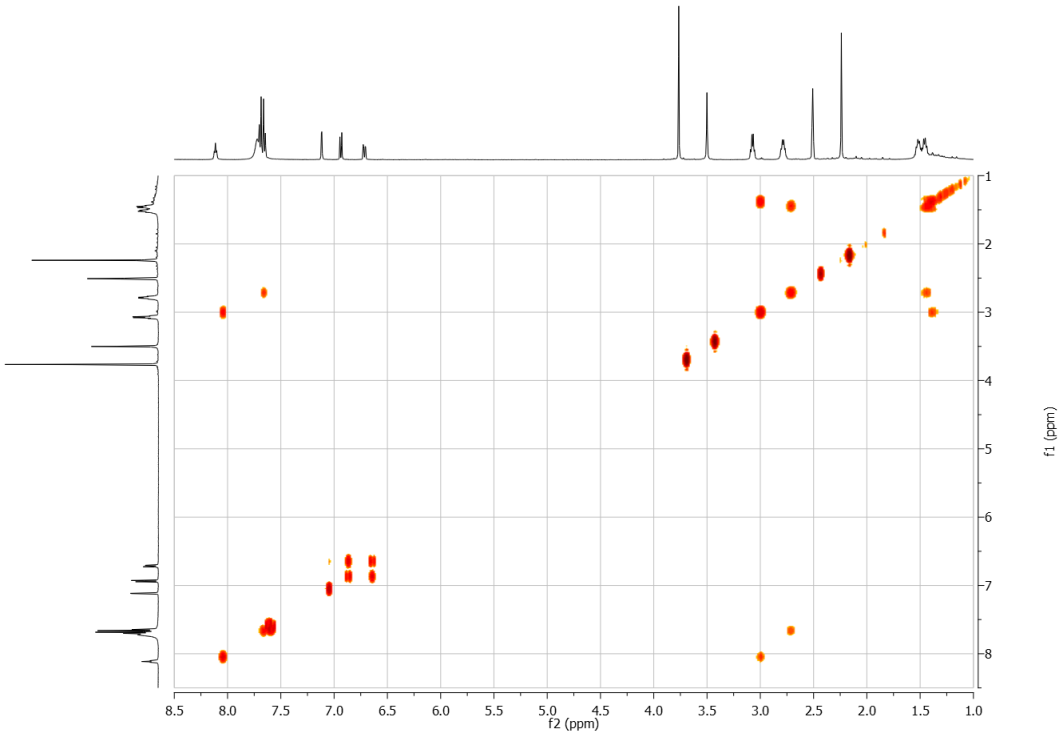

Figure 46. 2-Dimentional NMR spectrum of **43**.

*Synthesis of 8-(2-(1-(4-chlorobenzoyl)-5-methoxy-2-methyl-1H-indol-3-yl)acetamido) octan-1-aminium trifluoroacetate (**44**)*

Compound **41** (0.946 g, 1.620 mmol) was dissolved in 50%v/v solution of trifluorocarboxylic acid (TFA) in dichloromethane (20 mL). The reaction mixture was stirred at room temperature for 24 h. Then, the solution was concentrated in *vacuo* to a volume of 2 mL and hexane (20 mL) was added to precipitate **44** as a light brown solid (0.926 g, 95.7 % yield). **^{1}H NMR** (499.4 MHz, DMSO-d_6): δ 1.23 (s, br, 8H, -(C$\underline{H_2}$)$_4$-), 1.39 (m, 2H, -C$\underline{H_2}$-), 1.50 (m, 2H, -C$\underline{H_2}$-), 2.23 (s, 3H, CH_3), 2.76 (m, 2H, -CH_2-), 3.05 (m, 2H, -CH_2-), 3.49 (s, 2H, CH_2CO), 3.77 (s, 3H, OCH_3), 6.71 (dd, $J_{H\text{-}H}$ = 9.00, 2.15 Hz, 1H, indolyl H-6), 6.95 (d, $J_{H\text{-}H}$ = 9.00 Hz, 1H, indolyl H-7), 7.13 d, $J_{H\text{-}H}$ = 2.15 Hz, indolyl H-4), 7.65 (d, $J_{H\text{-}H}$ = 8.49 Hz, 2H, *p*-chlorobenzoyl H-3, H-5), 7.69 (d, $J_{H\text{-}H}$ = 8.49 Hz, 2H, *p*-chlorobenzoyl H-2, H-6), 7.72 (s, br, 3H, NH_3^+), 8.05 (t, $J_{H\text{-}H}$ = 5.49 Hz, 1H, amide-H). **^{13}C NMR** (125.59 MHz, DMSO-d_6): δ 13.77, 26.16, 26.68, 27.38, 28.88, 28.96, 29.53, 31.64, 39.03, 55.79, 55.81, 102.30, 111.62, 114.96, 116.27, 118.66, 129.44, 130.69, 131.30, 131.54, 134.69, 135.47, 137.94, 155.95, 158.63 (q, $J_{C\text{-}F}$ = 31.78 Hz), 168.26, 169.61. **^{19}F NMR** (469.92 MHz, DMSO-d_6): δ -73.18. Mass (ESI^+): calcd for $C_{27}H_{35}ClO_3N_3$ $(M+H)^+$, 484.24; found 484.18.

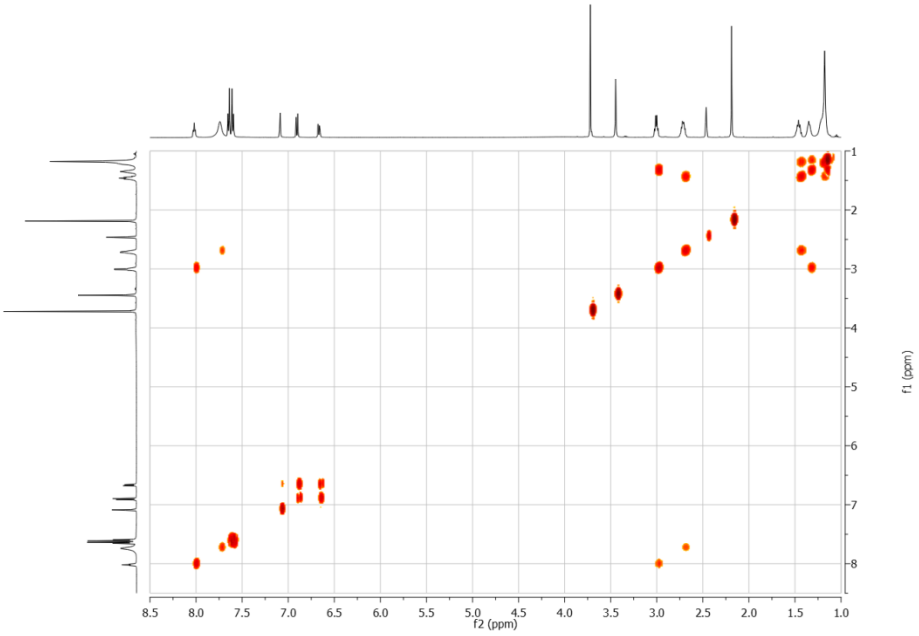

Figure 47. 2-Dimentional NMR spectrum of **44**.

*Synthesis of (2-((3-((2-(2-(1-(4-chlorobenzoyl)-5-methoxy-2-methyl-1H-indol-3-yl) acetamido)ethyl)amino)-3-oxopropyl)diisopropylphosphonio)phenyl) trifluoroborate (**45**)*

To a stirred solution of *ortho*-(*i*Pr_2(CH_2CH_2COOH)P)C_6H_4(BF_3) (0.288 g, 0.86 mmol) in DMF (25 mL) was added HOBt (0.198 g, 1.29 mmol) and EDCI (0.182 g, 0.95 mmol) at 0 °C. In the separated vial, DIEA (0.45 mL, 2.58 mmol) was added to a solution of compound **42** (0.575 g, 1.12 mmol) in DMF (5 mL). Then, the solution of compound **42** was transferred to the solution of *ortho*-(*i*Pr_2(CH_2CH_2COOH)P)C_6H_4(BF_3) at 0 °C. The reaction mixture was stirred at room temperature for 16 h. Removal of solvent *in vacuo* afforded a residue, to which 30 mL water was added and extracted with EtOAc (3 x 25 mL). Combined organic layer was washed by 2 M HCl (3 x 30 mL),

saturated $NaHCO_3$ (3 x 30 mL), and brine (1 x 30 mL), respectively. Finally, the washed organic layer was dried over $MgSO_4$, concentrated in *vacuo*, and precipitated from hexane affording **45** as a yellow powder (0.351 g, 57.03 % yield). **^{1}H NMR** (499.4 MHz, CD_3CN): δ 1.14 (dd, 6H, isopropyl-CH_3, $^3J_{H-P}$ = 16.48 Hz, $^3J_{H-H}$ = 7.49 Hz), 1.31 (dd, 6H, isopropyl-CH_3, $^3J_{H-P}$ = 16.48 Hz, $^3J_{H-H}$ = 7.49 Hz), 2.25 (s, 3H, CH_3), 2.35 (m, 2H, C$\underline{H_2}$$CH_2$P), 2.76 (m, 2H, CH_2C$\underline{H_2}$P), 3.18 (m, 4H, NHC$\underline{H_2}C\underline{H_2}$NH), 3.32 (m, 2H, isopropyl-CH), 3.53 (s, 2H, CH_2), 3.76 (s, 3H, OCH_3), 6.62 (s, br, 1H, amide-H), 6.64 (dd, 1H, J_{H-H} = 8.90, 2.40 Hz, indolyl H-6), 6.70 (s, br, 1H, amide-H), 6.94 (d, 1H, J_{H-H} = 9.00 Hz, indolyl H-7), 6.97 (d, 1H, J_{H-H} = 2.40 Hz, indolyl H-4), 7.37 (m, 1H), 7.46 – 7.58 (m, 4H), 7.68 (m, 2H), 7.93 (m, 1H). **^{13}C NMR** (125.59 MHz, CD_3CN): δ 13.01, 16.39 (d, $^2J_{C-P}$ = 2.14 Hz), 17.25 (d, $^2J_{C-P}$ = 2.14 Hz), 23.73 (d, $^1J_{C-P}$ = 4.40 Hz), 24.08 (d, $^1J_{C-P}$ = 4.40 Hz), 28.93 (d, $^1J_{C-P}$ = 4.02 Hz), 31.57, 39.33, 39.54, 55.43, 101.41, 111.61, 113.77, 115.19, 126.85, 126.93, 129.14, 129.18, 131.06, 131.18, 131.37, 132.34 (d, J_{C-P} = 3.39 Hz), 132.60, 132.68, 134.69, 136.11 (d, J_{C-P} = 3.89 Hz), 136.24 (d, J_{C-P} = 3.52 Hz), 136.34, 138.55, 156.22, 168.49, 170.39, 170.49, 170.60. **^{11}B NMR** (128.2 MHz, CD_3CN): δ 3.00. **^{19}F NMR** (375.9 MHz, CD_3CN): δ -133.9. **^{31}P NMR** (161.7 MHz, CD_3CN): δ 44.2. Mass (ESI^+): calcd for $C_{36}H_{43}ClN_3O_4PBF_3Li$ $(M+Li)^+$, 722.91; found 722.30.

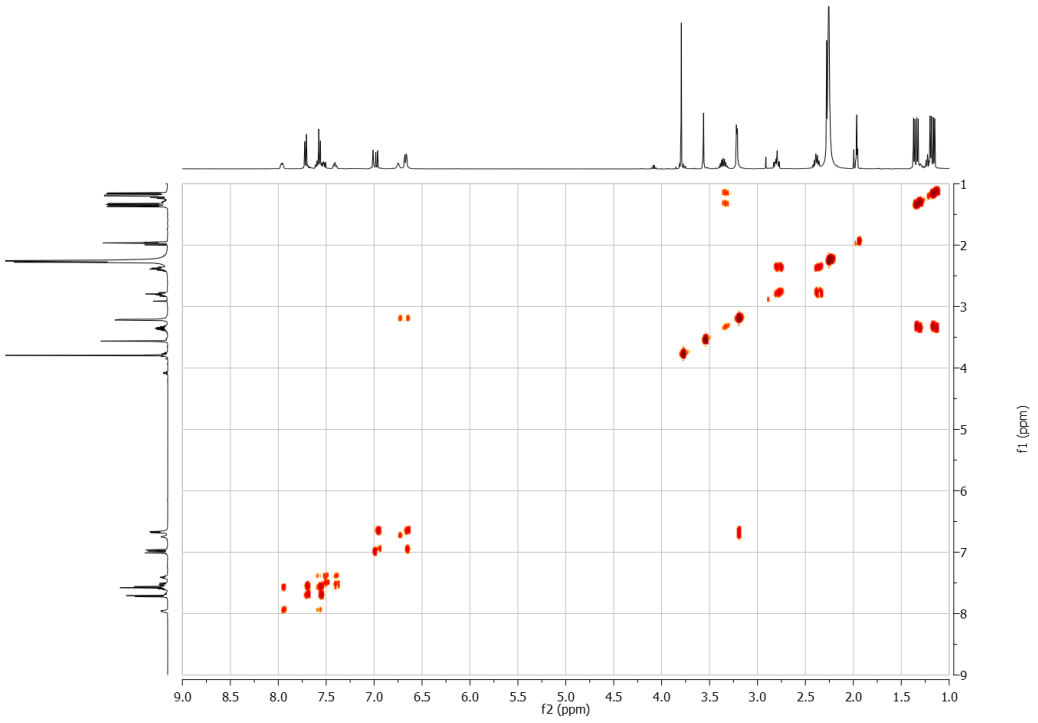

Figure 48. 2-Dimentional NMR spectrum of **45**.

*Synthesis of (2-((3-((2-(2-(1-(4-chlorobenzoyl)-5-methoxy-2-methyl-1H-indol-3-yl)acetamido)ethyl)amino)-3-oxopropyl)diphenylphosphonio)phenyl) trifluoroborate (**46**)*

To a stirred solution of *ortho*-($Ph_2(CH_2CH_2COOH)P)C_6H_4(BF_3)$ (0.280 g, 0.53 mmol) in DMF (25 mL) was added HOBt (0.122 g, 0.80 mmol) and EDCI (0.112 g, 0.58 mmol) at 0 °C. In the separated vial, DIEA (0.28 mL, 1.60 mmol) was added to a solution of compound **42** (0.409 g, 0.80 mmol) in DMF (5 mL). Then, the solution of compound **42** was transferred to the solution of *ortho*-($Ph_2(CH_2CH_2COOH)P)C_6H_4(BF_3)$ at 0 °C. The reaction mixture was stirred at room temperature for 16 h. Removal of solvent *in vacuo* afforded a residue, to which 30 mL water was added and extracted with

EtOAc (3 x 25 mL). Combined organic layer was washed by 2 M HCl (3 x 30 mL), saturated $NaHCO_3$ (3 x 30 mL), and brine (1 x 30 mL), respectively. Finally, the washed organic layer was dried over $MgSO_4$, concentrated in *vacuo*, and precipitated from hexane obtaining **46** as a yellow powder (0.261 g, 62.83 % yield) **^{1}H NMR** (499.4 MHz, CD_3CN): δ 2.27 (s, 3H, CH_3), 2.46 (m, 2H, C*H*$_2$CH_2P), 3.17 (s, br, 4H, NHC*H*$_2$C*H*$_2$NH), 3.56 (m, 2H, CH_2C*H*$_2$P), 3.56 (s, 2H, CH_2), 3.79 (s, 3H, OCH_3), 6.62 (dd, 1H, $J_{H\text{-}H}$ = 8.99, 2.35 Hz, indolyl H-6), 6.68 (s, br, 1H, amide-H), 6.78 (s, br, 1H, amide-H), 6.96 (d, 1H, $J_{H\text{-}H}$ = 8.49 Hz, indolyl H-7), 7.02 (d, 1H, $J_{H\text{-}H}$ = 1.70 Hz, indolyl H-4), 7.16 (dd, 1H, phenyl-C*H*, $^3J_{H\text{-}P}$ = 13.98 Hz, $^3J_{H\text{-}H}$ = 6.49 Hz), 7.36 (m, 1H, phenyl-C*H*), 7.53 – 7.81 (m, 11H, phenyl-C*H*), 7.99 (m, 1H, phenyl-C*H*). **^{13}C NMR** (125.59 MHz, CD_3CN): δ 12.98, 29.44, 31.56, 39.19, 39.57, 55.43, 101.43, 111.57, 113.82, 115.13, 122.39, 123.08, 127.06, 127.17, 129.12 (d, $J_{C\text{-}P}$ = 2.26 Hz), 129.16, 129.48, 129.59, 129.68, 131.05, 131.20, 131.35, 132.95, 133.02, 133.22 (d, $J_{C\text{-}P}$ = 3.77 Hz), 133.42, 133.49, 133.83 (d, $J_{C\text{-}P}$ = 3.01 Hz), 134.72, 135.17, 135.28, 135.41, 135.54, 136.31, 138.51, 156.17, 168.49, 170.34, 170.38, 170.51. **^{11}B NMR** (128.2 MHz, CD_3CN): δ 2.88. **^{19}F NMR** (375.9 MHz, CD_3CN): δ -133.4. **^{31}P NMR** (161.7 MHz, CD_3CN): δ 30.6. Mass (ESI^+): calcd for $C_{42}H_{39}ClN_3O_4PBF_3Li$ $(M+Li)^+$, 790.25; found 790.23.

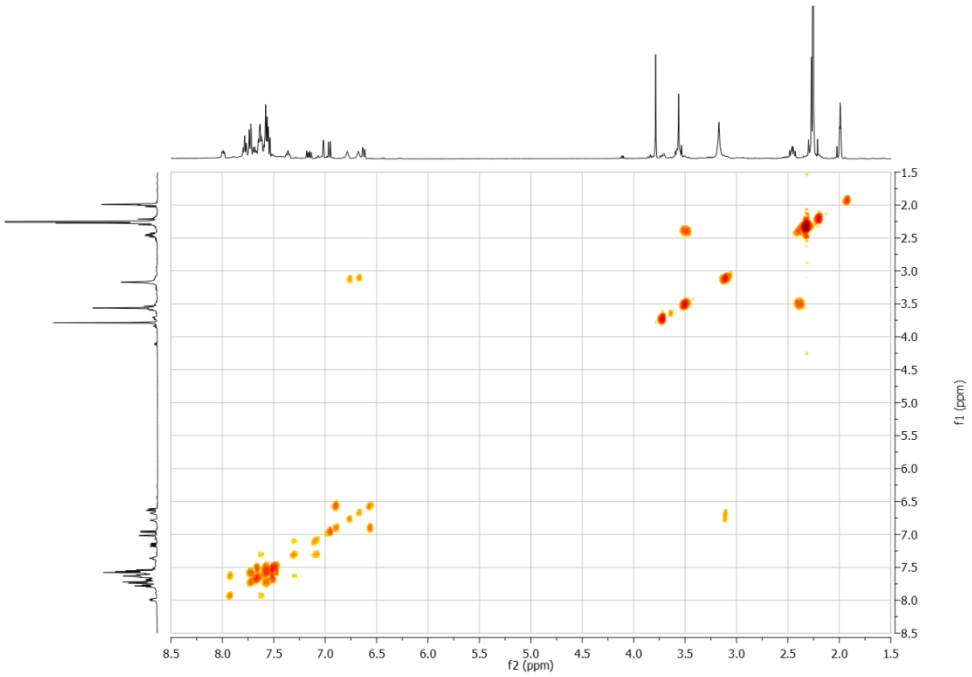

Figure 49. 2-Dimentional NMR spectrum of **46**.

*Synthesis of (2-((3-((4-(2-(1-(4-chlorobenzoyl)-5-methoxy-2-methyl-1H-indol-3-yl)acetamido)butyl)amino)-3-oxopropyl)diphenylphosphonio)phenyl) trifluoroborate (**47**)*

To a stirred solution of *ortho*-($Ph_2(CH_2CH_2COOH)P)C_6H_4(BF_3)$ (0.235 g, 0.445 mmol) in DMF (25 mL) was added HOBt (0.102 g, 0.670 mmol) and EDCI (0.094 g, 0.489 mmol) at 0 °C. I n the separated vial, DIEA (0.24 mL, 1.350 mmol) was added to a solution of compound **43** (0.362 g, 0.667 mmol) in DMF (5 mL). Then, the solution of compound **43** was transferred to the solution of *ortho*-($Ph_2(CH_2CH_2COOH)P)C_6H_4(BF_3)$ at 0 °C. The reaction mixture was stirred at room temperature for 16 h. Removal of solvent *in vacuo* afforded a residue, to which 30 mL water was added and extracted with

EtOAc (3 x 30 mL). Combined organic layer was washed by 2 M HCl (3 x 30 mL), saturated $NaHCO_3$ (3 x 30 mL), and brine (1 x 30 mL), respectively. Finally, the washed organic layer was dried over $MgSO_4$, concentrated in *vacuo*, and precipitated from hexane obtaining **47** as a yellow powder (0.210 g, 58.2 % yield). **^{1}H NMR** (499.4 MHz, DMSO-d_6): δ 1.35 (s, br, 4H, -C$\underline{H_2}$C$\underline{H_2}$-), 2.23 (s, 3H, CH_3), 2.45 (m, 2H, C$\underline{H_2}$$CH_2$P), 2.95 (dt, 2H, $J_{H\text{-}H}$ = 5.49, 6.49 Hz, NHC$\underline{H_2}$$(CH_2)_2CH_2$NH), 3.00 (dt, 2H, $J_{H\text{-}H}$ = 5.49, 6.49 Hz, $NHCH_2(CH_2)_2$C$\underline{H_2}$NH), 3.48 (s, 2H, -C$\underline{H_2}$-), 3.64 (m, 2H, CH_2C$\underline{H_2}$P), 3.74 (s, 3H, OC$\underline{H_3}$), 6.66 (dd, 1H, $J_{H\text{-}H}$ = 9.49, 2.05 Hz, indolyl H-6), 6.89 (d, 1H, $J_{H\text{-}H}$ = 8.99 Hz, indolyl H-7), 7.00 (dd, 1H, phenyl-C$\underline{H}$, $^3J_{H\text{-}P}$ = 14.48 Hz, $^3J_{H\text{-}H}$ = 7.49 Hz), 7.07 (d, 1H, $J_{H\text{-}H}$ = 2.75 Hz, indolyl H-4), 7.32 (m, 1H, phenyl-C$\underline{H}$), 7.53 – 7.67 (m, 11H, phenyl-C$\underline{H}$), 7.74 (m, 2H, phenyl-C$\underline{H}$), 7.82 (m, 2H, phenyl-C$\underline{H}$), 7.98 (m, 1H, phenyl-C$\underline{H}$). **^{13}C NMR** (125.59 MHz, DMSO-d_6): δ 13.85, 19.37, 19.83, 26.85, 27.04, 29.28, 31.64, 38.84, 38.95, 55.88, 102.33, 111.71, 114.93, 115.00, 119.11, 119.77, 122.28, 122.96, 127.36, 127.46, 129.51, 129.92, 130.02, 130.73, 131.38, 131.61, 133.20 (d, $J_{C\text{-}P}$ = 2.89 Hz), 133.64, 133.72, 134.04 (d, $J_{C\text{-}P}$ = 2.26 Hz), 134.74, 134.81, 134.93, 135.56, 138.02, 156.00, 168.32, 169.34, 169.47, 169.69. **^{11}B NMR** (128.2 MHz, DMSO-d_6): δ 3.01. **^{19}F NMR** (375.9 MHz, DMSO-d_6): δ -131.3. **^{31}P NMR** (161.7 MHz, DMSO-d_6): δ 30.9. Mass (MALDI$^+$): calcd for $C_{44}H_{43}O_4N_3ClPBF_3Li$ $(M+Li)^+$, 818.29; found 818.10.

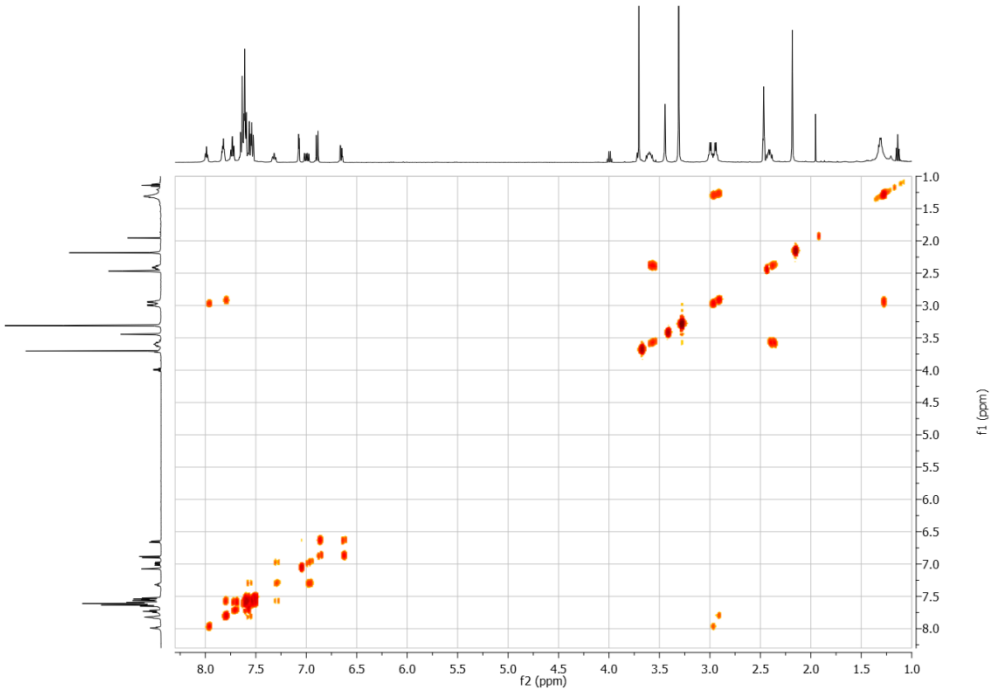

Figure 50. 2-Dimentional NMR spectrum of **47**.

*Synthesis of (2-((3-((8-(2-(1-(4-chlorobenzoyl)-5-methoxy-2-methyl-1H-indol-3-yl)acetamido)octyl)amino)-3-oxopropyl)diphenylphosphonio)phenyl) trifluoroborate (**48**)*

To a stirred solution of *ortho*-($Ph_2(CH_2CH_2COOH)P)C_6H_4(BF_3)$ (0.227 g, 0.429 mmol) in DMF (25 mL) was added HOBt (0.099 g, 0.646 mmol) and EDCI (0.090 g, 0.469 mmol) at 0 °C. In the separated vial, DIEA (0.22 mL, 1.292 mmol) was added to a solution of compound **44** (0.513 g, 0.858 mmol) in DMF (5 mL). Then, the solution of compound **44** was transferred to the solution of *ortho*-($Ph_2(CH_2CH_2COOH)P)C_6H_4(BF_3)$ at 0 °C. The reaction mixture was stirred at room temperature for 16 h. Removal of solvent *in vacuo* afforded a residue, to which 30 mL water was added and extracted with

EtOAc (3 x 30 mL). Combined organic layer was washed by 2 M HCl (3 x 30 mL), saturated $NaHCO_3$ (3 x 30 mL), and brine (1 x 30 mL), respectively. Finally, the washed organic layer was dried over $MgSO_4$, concentrated in *vacuo*, and precipitated from hexane obtaining **48** as a yellow powder (0.233 g, 62.3 % yield). **^{1}H NMR** (499.4 MHz, DMSO-d_6): δ 1.20 (m, 8H, -(C$\underline{H_2}$)$_4$-), 1.31 (s, br, 2H, -C$\underline{H_2}$-), 1.39 (s, br, 2H, -C$\underline{H_2}$-), 2.46 (m, 2H, C$\underline{H_2}$CH$_2$P), 2.97 (dt, 2H, $J_{H\text{-}H}$ = 6.49, 6.99 Hz, NHC$\underline{H_2}$(CH$_2$)$_6$CH$_2$NH), 3.04 (dt, 2H, $J_{H\text{-}H}$ = 5.99, 6.49 Hz, NHCH$_2$(CH$_2$)$_6$C$\underline{H_2}$NH), 3.49 (s, 2H, -C$\underline{H_2}$-), 3.64 (m, 2H, CH$_2$C$\underline{H_2}$P), 3.76 (s, 3H, OC$\underline{H_3}$), 6.71 (dd, 1H, $J_{H\text{-}H}$ = 8.99, 3.00 Hz, indolyl H-6), 6.95 (d, 1H, $J_{H\text{-}H}$ = 8.99 Hz, indolyl H-7), 7.04 (dd, 1H, phenyl-C$\underline{H}$, $^3J_{H\text{-}P}$ = 13.98 Hz, $^3J_{H\text{-}H}$ = 7.49 Hz), 7.13 (d, 1H, $J_{H\text{-}H}$ = 2.75 Hz, indolyl H-4), 7.36 (m, 1H, phenyl-C$\underline{H}$), 7.56 – 7.71 (m, 11H, phenyl-C$\underline{H}$), 7.78 (m, 2H, phenyl-C$\underline{H}$), 7.85 (m, 2H, phenyl-C$\underline{H}$), 8.02 (m, 1H, phenyl-C$\underline{H}$). **^{13}C NMR** (125.59 MHz, DMSO-d_6): δ 13.86, 26.81, 26.84, 29.13, 29.17, 29.19, 29.29, 29.39, 29.60, 31.70, 39.10, 39.25, 55.87, 102.36, 111.68, 115.00, 119.14, 119.81, 122.29, 122.97, 127.34, 127.45, 129.50, 129.91, 130.00, 130.75, 131.37, 131.61, 133.19 (d, $J_{C\text{-}P}$ = 3.14 Hz), 133.66, 133.74, 134.03 (d, $J_{C\text{-}P}$ = 3.01 Hz), 134.76, 135.53, 138.01, 156.01, 168.32, 169.28, 169.41, 169.64. **^{11}B NMR** (128.2 MHz, DMSO-d_6): δ 2.65. **^{19}F NMR** (375.9 MHz, DMSO-d_6): δ -134.1. **^{31}P NMR** (161.7 MHz, DMSO-d_6): δ 30.9. Mass (MALDI$^+$): calcd for $C_{44}H_{43}O_4N_3ClPBF_3Li$ $(M+Li)^+$, 875.11; found 875.34.

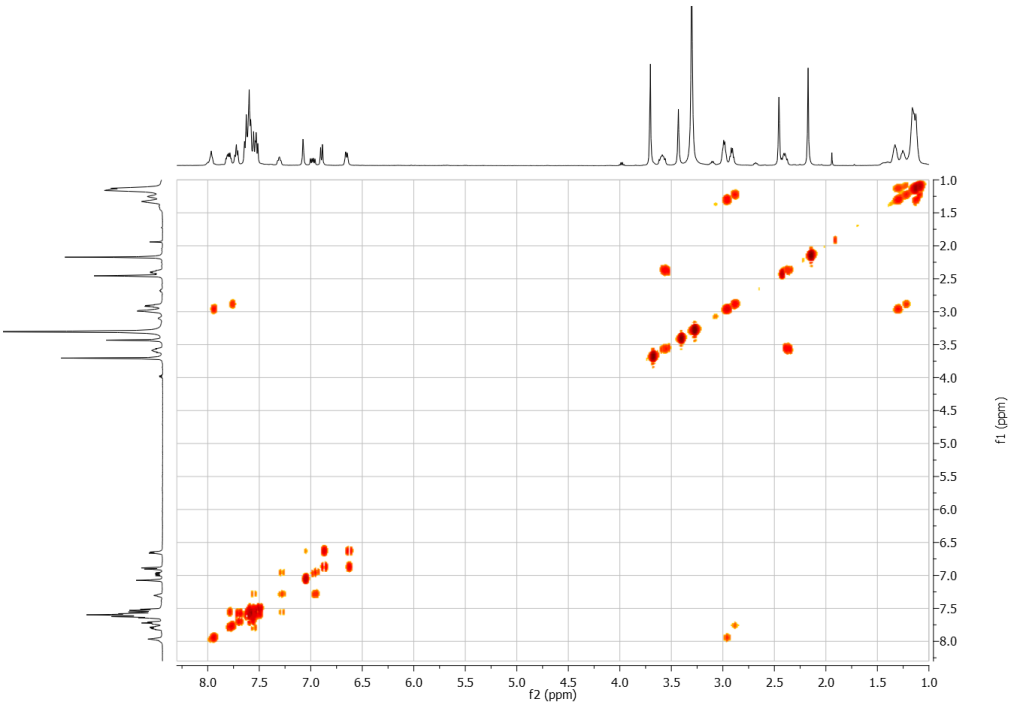

Figure 51. 2-Dimentional NMR spectrum of **48**.

Kinetic studies

A sample of **37** (5 mg) was dissolved in 0.2 mL CD_3CN and 0.8 mL D_2O phosphate buffer (pH 7.5, 500 mM). The ^{19}F NMR spectrum of **37** was collected periodically. The decomposition of aryltrifluoroborate species were monitored by integration of the decreasing aryltrifluoroborate signal in conjunction with the increasing signal corresponding to free F^-. In addition, a sample of **37**, **45**, **46**, **47**, and **48** was also dissolved in 0.3 mL DMSO and 0.7 mL of 10% w/v triton X-100 in H_2O phosphate buffer (pH 7.5, 500 mM) for the stability test. The rate of aryltrifluoroborate hydrolysis was monitored by ^{19}F NMR spectroscopy. All spectra were processed using the VNMRJ Version 2.2 NMR software. The rate constant, k_{obs}, was calculated using a well-established NMR method reported in the literature.[4] This method is based on the fact that the concentration in $ArBF_3$ species is proportional to the ^{19}F NMR integration of $ArBF_3$ signal divided by the sum of the integration of $ArBF_3$ signal and the free fluoride signal. For convenience, the value of the $ArBF_3$ integration is arbitrarily set at 100 and the free fluoride integration determined. The resulting data is provided in Table **8**, **9**, and **10**.

Table 8. Kinetic data for the hydrolysis of **37** in D_2O–CD_3CN (8/2 vol) at pH 7.5 ([phosphate buffer] = 500 mM). The values provided for F^- and $ArBF_3$ correspond to the integration of the corresponding NMR signal.

Data for **37** in D_2O–CD_3CN (8/2 vol) at pH 7.5				
				k_{obs} = 5.2E-5
			exp. Ratio	calc. ratio
Time (min)	[F^-]	[BF3]	[BF3]/([BF3]+[F^-]	[BF3]/([BF3]+[F^-]
0	0	100	1.0000	1.0000
1030	5.4	100	0.9488	0.9478
2491	14.86	100	0.8706	0.8785
5367	32.58	100	0.7543	0.7565
6800	43.52	100	0.6968	0.7022
8240	52.59	100	0.6554	0.6515
9689	63.75	100	0.6107	0.6042
11189	76.21	100	0.5675	0.5589
20000				0.3535
30000				0.2101
40000				0.1249
50000				0.0743
60000				0.0442

Table 9. Kinetic data for the hydrolysis of **37** in 10% w/v triton X-100 in H_2O/ DMSO (7/3 vol) at pH = 7.5 ([phosphate buffer] = 500 mM). The values provided for F^- and $ArBF_3$ correspond to the integration of the corresponding NMR signal.

Data for **37** in 10% w/v triton X-100 in H_2O/ DMSO (7/3 vol) at pH = 7.5				
				k_{obs}= 1.2E-5
			exp. Ratio	calc. ratio
Time (min)	[F]	[BF3]	[BF3]/([BF3]+[F]	[BF3]/([BF3]+[F]
0	0	100	1.0000	1.0000
1626	3.54	100	0.9658	0.9800
7512	9.38	100	0.9142	0.9111
10376	11.76	100	0.8948	0.8793
17576	21.44	100	0.8235	0.8042
20000				0.7804
25000				0.7334
30000				0.6894
35000				0.6479
40000				0.6090
50000				0.5379
60000				0.4752

Table 10. Kinetic data for the hydrolysis of **45** in 10% w/v triton X-100 in H_2O/ DMSO (7/3 vol) at pH = 7.5 ([phosphate buffer] = 500 mM). The values provided for F^- and $ArBF_3$ correspond to the integration of the corresponding NMR signal.

Data for **44** in 10% w/v triton X-100 in H_2O/ DMSO (7/3 vol) at pH = 7.5				
				k_{obs} = 4.0E-7
			exp. Ratio	calc. ratio
Time (min)	[F]	[BF3]	[BF3]/([BF3]+[F]	[BF3]/([BF3]+[F]
0	0	100	1.0000	1.0000
18720	0.49	100	0.9951	0.9926
25920	1.15	100	0.9886	0.9898
36012	1.26	100	0.9876	0.9859
44652	1.66	100	0.9837	0.9825
50000				0.9804
60000				0.9766

Radiochemistry Experiments

All chemicals are analytic grade and used without further purification. Analytical reversed-phase high-performance liquid chromatography (HPLC) was accomplished on a Waters 515 chromatography system. A Waters 2487 *dual* λ absorbance detector and model 2200 scaler ratemeter radiation detector were added to the HPLC. HPLC was performed on a phenomenex Luna 5μ C18 column with a flow of 1ml/min. The mobile phase was programmed to change from 95% solvent A and 5% solvent B (0~2min) to 5% solvent A and 95% solvent B at 22min, where solvent A is 0.1% TFA in water and solvent B is 0.1% TFA in acetonitrile.

Radiochemistry

The radio label reactions were carried out using the following protocol. Compound **45** and **46** (0.28 μmol) were dissolved in 20 μl DMSO. 45mCi of [^{18}F]-fluoride in 100 μl [^{18}O] water was added. pH was adjusted to 2 by adding 6N HCl. The reaction mixture was incubated at 75ºC for 10min. Then the reaction mixture was loaded onto the HPLC to measure the percentage of the reaction conversion. The labeled compounds were confirmed by comparison of the radio signal HPLC profile with the UV signal HPLC of the starting non-radioactive compounds.

MicroPET Imaging

MicroPET imaging were acquired using the Genesys^4 (Sofie Biosciences, Culver City, CA). The scanner has a 9.5cm axial and 4.4cm transaxial fields of view (FOV). For

PET image acquiring, each human gliobastoma (U87MG) tumor-bearing female nude mice was injected with 7.4MBq (0.02mCi) of [$^{18/19}$F]**45** and [$^{18/19}$F]**46** via the tail vein. At 15, 40 and 90min post injection, the mice were anesthetized using isoflurane (2% in oxygen), then placed into imaging chambers equipped with a heated coil to maintain body temperature and gas anesthesia as well. The static microPET acquisition were then achieved and reconstructed with the maximum likelihood and expectation maximization (MLEM) algorithm using the Sofie Biosciences software. Region of interest (ROIs) were drawn over the tumor and bone on decay-corrected whole body coronal sections. With the assumption of 1g/ml tissue density, ROIs were converted to counts per gram per min. Then dividing this by injected dose gave the image ROI derived %ID/g values.

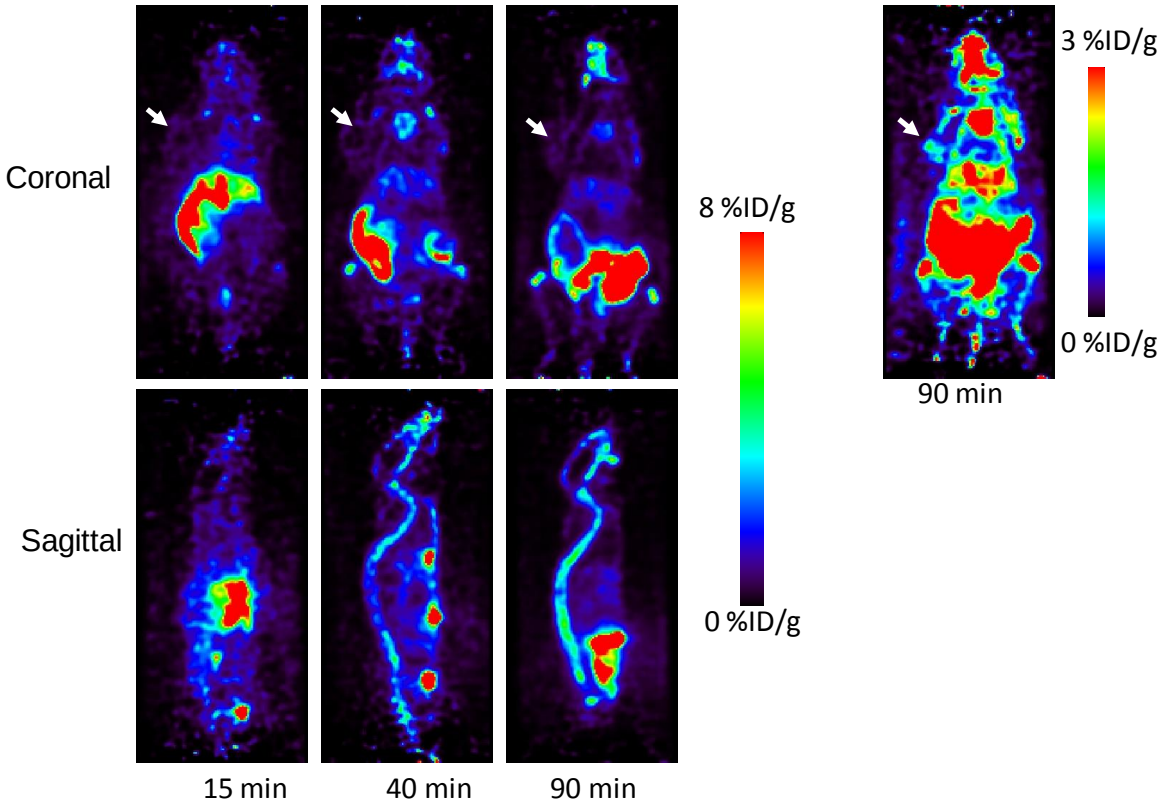

Figure 52. MicroPET images of nude mice bearing U87MG tumor after injection of [$^{18/19}$F]**45** at 15, 40, and 90 min.

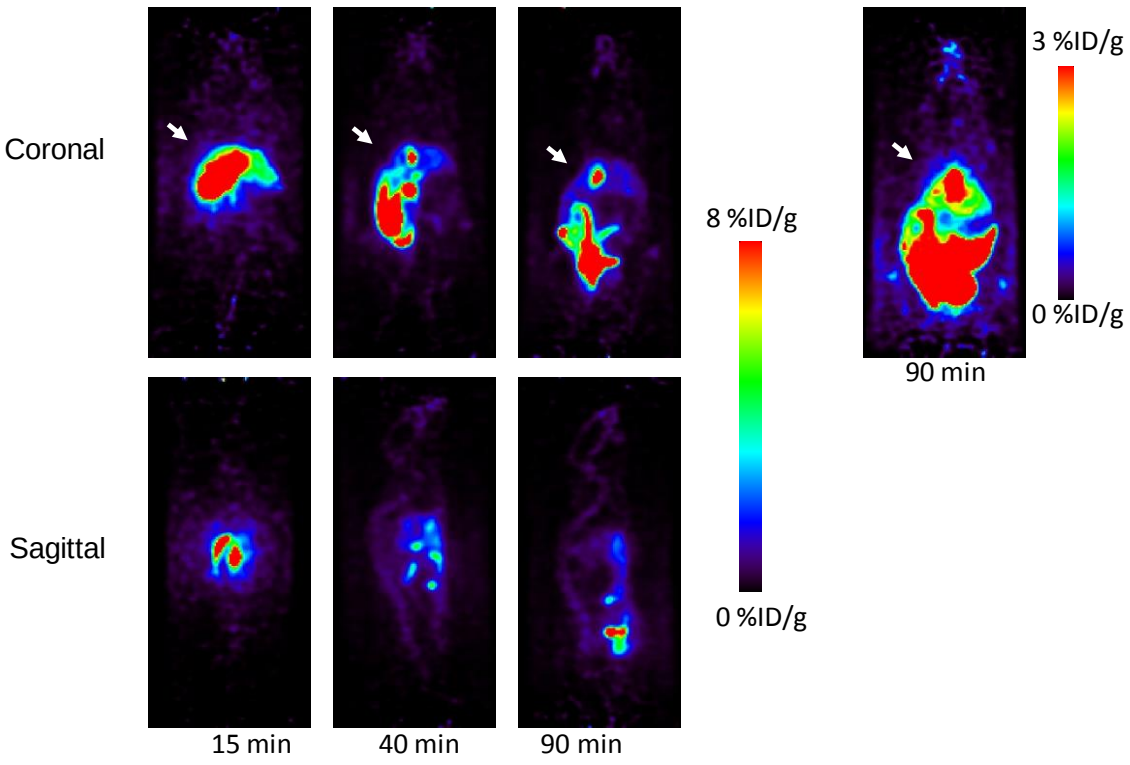

Figure 53. MicroPET images of nude mice bearing U87MG tumor after injection of [$^{18/19}$F]**46** at 15, 40, and 90 min.

CHAPTER IV

CARBENE-BORANE ADDUCTS FOR ^{18}F FLUORIDE ANION CAPTURE AND *IN VIVO* STABILITY STUDIES

4.1 Introduction

Positron Emission Tomography (PET) is a rapidly growing imaging technique that relies on the use molecular radiotracers containing a positron emitting isotope.[1] To date, a great deal of attention has been devoted to the use of fluorine-18 (^{18}F), a radionuclide that can be easily generated from [^{18}O]-water and whose nuclear decay characteristics are ideally suited for applications in PET imaging. One difficulty faced in the synthesis of ^{18}F-containing molecular radiotracers is the short half-life of the isotope (110 min). It follows that the best methods to access ^{18}F-containing molecular radiotracers should be fast and preferably carried out in the late stages of the synthesis of the radiopharmaceutical probe. An attractive approach that provides a possible solution to these challenges is based on molecules containing a boron atom as a fluoride binding site. This approach was pioneered by Perrin who showed that arylboronic acids or esters featuring electron-withdrawing groups quickly react with fluoride ions to form the corresponding aryltrifluoroborates.[4,7] Over the years, Perrin and other groups have investigated a number of backbones designed to stabilize the trifluoroborate unit and prevent its decomposition *in vivo* (Figure 54).[11,14,15,30,79] Although the rate of hydrolysis can be slowed down drastically, all fluoroborates investigated to date are unstable toward hydrolysis. This hydrolysis reaction is potentially problematic because the

fluoride ions liberated by hydrolysis of the radiotracer lead to unwanted background signal in particular from the skeleton.

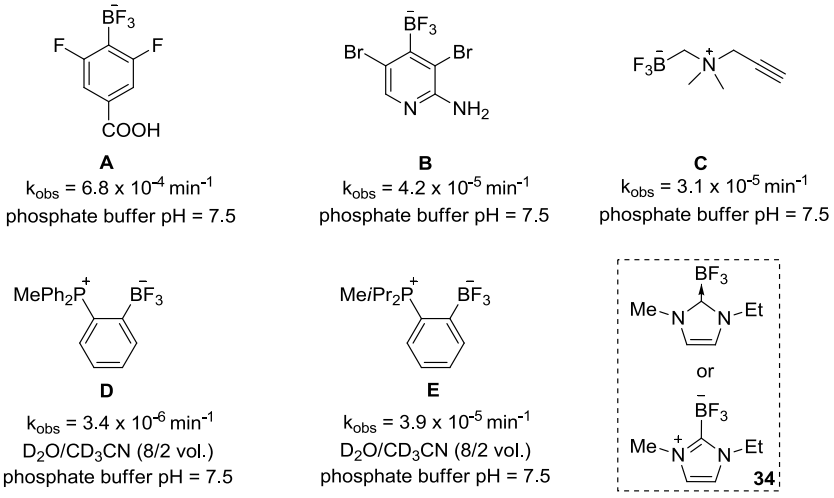

Figure 54. Chemical structure of organoboranes used for ^{18}F fluoride captor in Positron Emission Tomography (PET) application and their hydrolysis rate constant (k_{Obs}).

Recently we introduced a strategy based on the use of zwiterrionic trifluoroborates. In particular, we found that the trifluoroborate moiety can be significantly stabilized against hydrolysis by a proximal cationic functionality such as a phosphonium as in the case of **D** and **E**.[79,80] This approach is further validated by the recent work of Perrin who showed that ammonium trifluoroborate moieties of type **C** show sufficient stability for *in vivo* imaging.[30,83] As part of our continued interest in this chemistry, we were drawn by the remarkable stability of *N*-heterocyclic cabene (NHC) boron trifluoride adducts such as **34**.[31] This compound which can also be described as a

carbene-BF_3 adduct can be recrystallized from boiling water suggesting that it is highly resistant to hydrolysis. Encouraged by these properties, we questioned whether such carbene-BF_3 could be radiofluorinated and used as prosthetic groups for PET imaging. In this chapter, we describe the initial results that we have obtained while working toward this goal.

4.2 Synthesis and characterization

As a starting point for these studies, we synthesized the carbene-BF_3 adduct (**49**) as a model compounds. Using the method recently employed by Brozov for the monoethyl analog (**34**), compound **49** was obtained by thermolysis of 1, 3-dimethyl-1*H*-imidazolium tetrafluoroborate under reduced pressure in a 87% yield (Figure 55). The presence of the trifluoroborate moiety is confirmed by the detection of a quartet ^{11}B NMR resonance at 0.21 ppm ($J_{B\text{-}F}$ = 37.0 Hz) and a quartet ^{19}F NMR resonance at -139.2 ppm ($J_{B\text{-}F}$ = 37.0 Hz). The ^{1}H NMR spectrum shows two singlet peaks at 3.85 ppm and 7.11 ppm corresponding to the methyl and the methine groups, respectively. The structure of this compound has also been studied by single crystal X-ray diffraction (Figure 57). The B(1)-C(1) bond connecting the NHC ligand to the boron center (1.637(5) Å) is comparable to the boron-carbon bond of **34** (1.644(3) Å),[31] indicating a strong coordination of the NHC ligand to the boron atom.

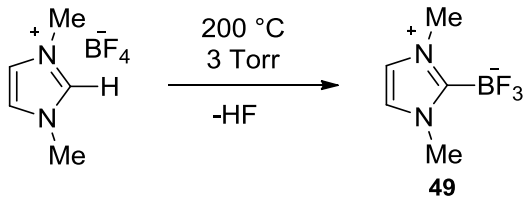

Figure 55. Scheme showing the synthesis of **49**.

Next, we turned our attention toward the synthesis of a NHC-BF_3 adduct that could be easily conjugated with biomolecules for targeted disease imaging. After reviewing different functionalization possibilities, we decided to synthesize the amino-substituted derivative **52**. We successfully accessed this new derivative by reaction of the known nitrocarbene-AgI complex **50** with BF_3-OEt_2. This reaction afforded the nitrocarbene-BF_3 adduct **51** as a white solid in 83 % yield (Figure 56). Hydrogenation of **51** over palladium afforded **52** in a 78% yield. The ^{1}H NMR spectrum of **51** and **52** display two singlets (3.94 ppm and 4.16 ppm for **51** and 3.61 and 3.73 ppm for **52**) corresponding to the methyl group and a singlet (8.21 ppm for **51** and 6.37 ppm for **52**) corresponding to the methine proton. The presence of an amino group in **52** is confirmed by the detection of a broad signal at 4.02 ppm. As in the case of **49**, quartets are observed in ^{11}B NMR and ^{19}F NMR of **51** and **52** are similar to those of **49** (^{11}B NMR signal at 0.13 ppm with $J_{B\text{-}F}$ = 33.6 Hz for **51** and 0.27 ppm with $J_{B\text{-}F}$ = 37.2 Hz for **52**; ^{19}F NMR signal at -137.9 ppm with $J_{B\text{-}F}$ = 33.6 Hz for **51** and -138.0 ppm with $J_{B\text{-}F}$ = 37.2 Hz for **52**). The crystal structure of **51** has also been determined. The carbene-BF_3 moiety is essentially analogous to that in **49**. The only notable difference is observed in the B(1)-C(1) separation (1.657(2) Å) which is slightly longer than in **49** (1.637(5) Å)

(Figure 58). This elongation is assigned to the electron withdrawing properties of the nitro group and the associated weaker donor properties of the carbene-carbon atom.

Compound **52** can be transformed into the succinimide derivative **53** by reaction with succinic anhydride in a presence of di-*iso*-propylethylamine (DIEA). Subsequent addition of NaOH to the solution of **53** in H_2O/THF mixture yielded the succinic acid derivative (**54**) in a 88% yield. The ^{1}H NMR spectrum of **53** showed a singlet peak at 2.89 ppm corresponding to the methylene group of the succinimide ring, while the ^{1}H NMR spectrum of **54** displayed two triplet peaks at 2.44 and 2.62 ppm indicating two different methylene groups in succinic acid functional group. The trifluoroborate moiety gives rise to a quartet ^{11}B NMR resonance at 0.29 ppm ($J_{B\text{-}F}$ = 35.4 Hz) for **53** and -0.33 ppm ($J_{B\text{-}F}$ = 38.4 Hz) for **54** as well as a quartet ^{19}F NMR resonance at -138.5 ppm ($J_{B\text{-}F}$ = 35.4 Hz) for **53** and -137.5 ppm ($J_{B\text{-}F}$ = 38.4 Hz) for **54**.

Compound **52** can also be easily converted into the maleimide derivative **56** by reaction with maleic anhydride and acetic anhydride/ sodium acetate. The spectroscopic properties of **56** are close to those of **52**. The methine signal is observed at 7.08 ppm. The trifluoroborate moiety gives rise to a quartet at 0.29 ppm in the ^{11}B NMR spectrum ($J_{B\text{-}F}$ = 35.6 Hz) as well as a quartet at -138.5 ppm in the ^{19}F NMR spectrum ($J_{B\text{-}F}$ = 35.6 Hz). The structure of this derivative has also been confirmed by X-ray diffraction (Figure 59) which shows a that the B(1)-C(1) separation (1.656(9) Å) is close to that in **51**, a characteristic consistent with the electron withdrawing effect of the maleimide functional group.

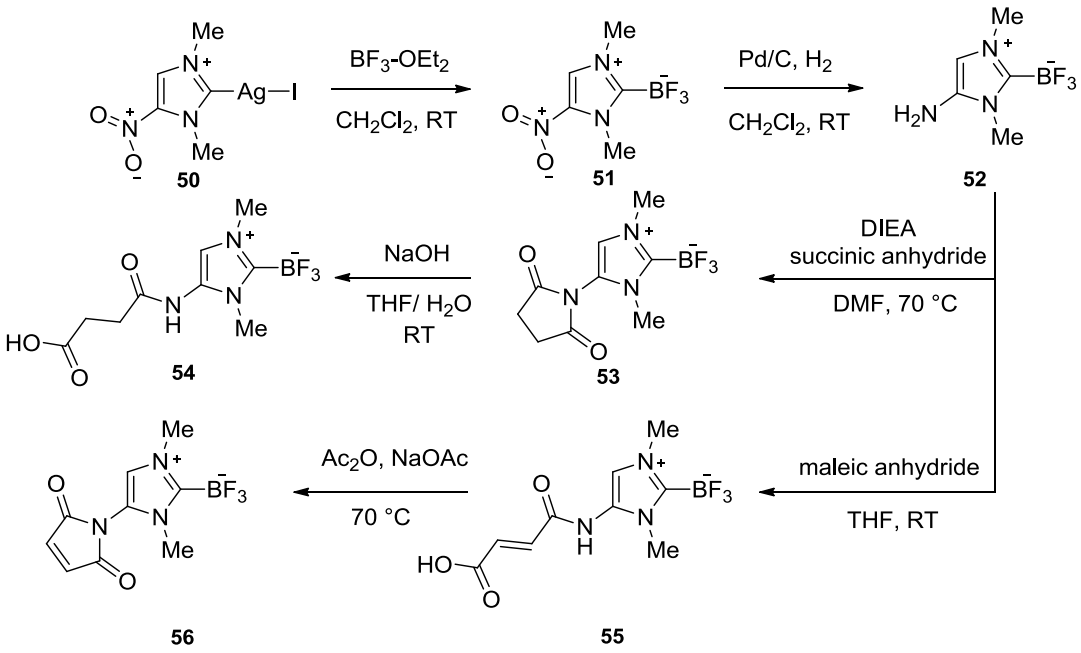

Figure 56. Scheme showing the synthesis of Arduengo carbene borane adducts tethered nitro (**51**), amine (**52**), succinimide (**53**), succinic acid (**54**), maleic acid (**55**), and maleimide (**56**) functional groups.

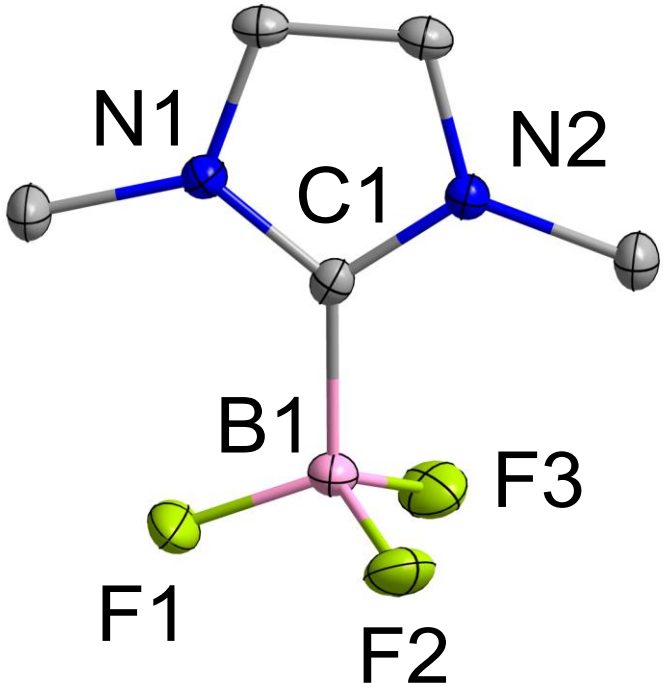

Figure 57. Crystal structure of **49**. Displacement ellipsoids are scaled to the 50% probability level and hydrogen atoms have been omitted for clarity. Selected bond lengths (Å) and angles (deg) for **49**: B1-C1 1.637(3), B1-F1 1.389(4), B1-F2 1.398(3), B1-F3 1.398(3); N1-C1-N2 105.8(3).

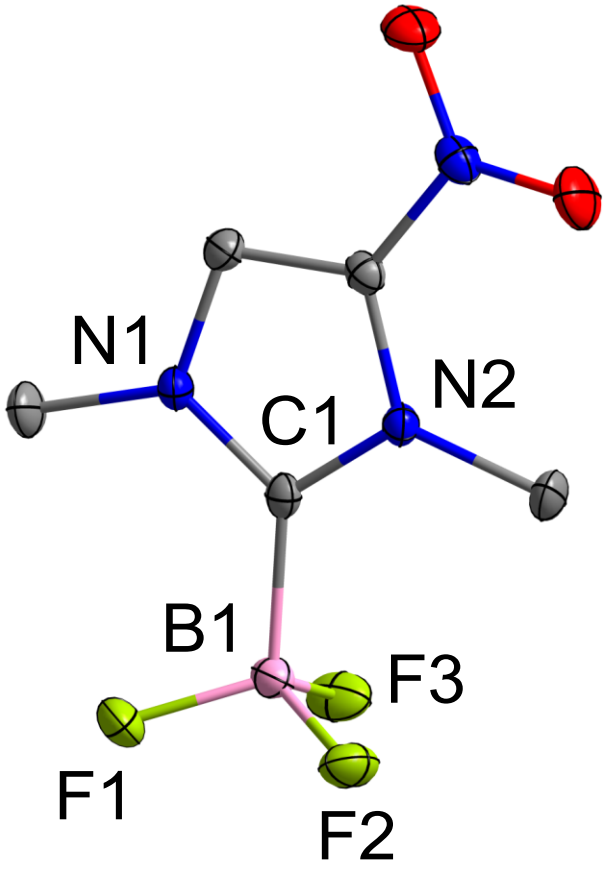

Figure 58. Crystal structure of **51**. Displacement ellipsoids are scaled to the 50% probability level and hydrogen atoms have been omitted for clarity. Selected bond lengths (Å) and angles (deg) for **51**: B1-C1 1.6575(18), B1-F1 1.3928(16), B1-F2 1.3948(16), B1-F3 1.3933(15); N1-C1-N2 106.50(10).

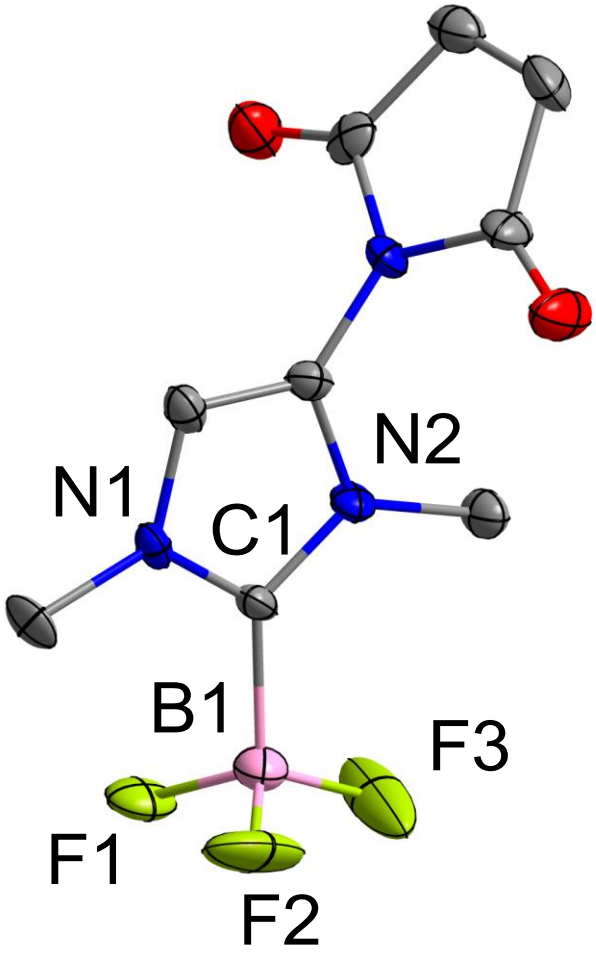

Figure 59. Crystal structure of **56**. Displacement ellipsoids are scaled to the 50% probability level and hydrogen atoms have been omitted for clarity. Selected bond lengths (Å) and angles (deg) for **56**: B1-C1 1.656(9), B1-F1 1.347(9), B1-F2 1.395(9), B1-F3 1.390(10); N1-C1-N2 106.8(5).

To expand our captors to the di-functional group derivatives, the di-cyano and the di-methylester BF_3-carbene adducts were synthesized by the reaction of the di-cyanocarbene-AgI and di-methylestercarbene-AgI complexes (**57** and **59**) with BF_3-OEt_2, respectively. These reactions afforded the di-cyanocarbene-BF_3 adduct **58** and the di-methylestercarbene-BF_3 **60** in a good yield (78 % yield for **58** and 72% for **60**) (Figure 60). Gratifyingly, the dicarboxylic acid carbene-BF_3 adduct can be successfully prepared by the treatment of **60** with NaOH in aqueous solution. These new di-functional group carbene-BF3 adducts were fully characterized by NMR spectroscopy. The presence of the trifluoroborate moiety is confirmed by the detection of a quartet ^{11}B NMR resonance at -0.20 ppm ($J_{B\text{-}F}$ = 31.7 Hz) for **58**, 0.17 ppm ($J_{B\text{-}F}$ = 34.3 Hz) for **60**, and 0.40 ppm ($J_{B\text{-}F}$ = 35.6 Hz) for **61**, as well as, a quartet ^{19}F NMR resonance at -138.9 ppm ($J_{B\text{-}F}$ = 31.7 Hz) for **58**, 137.5 ppm ($J_{B\text{-}F}$ = 34.3 Hz) for **60**, and -136.3 ppm ($J_{B\text{-}F}$ = 35.6 Hz) for **61**. The ^{1}H NMR spectra showed only one singlet peak at 3.99 ppm for **58** and 4.09 ppm for **61** corresponding to the *N*,*N* dimethyl groups on the imidazole ring. The ^{1}H NMR spectrum of **60** displayed the expected two singlet peaks at 3.92 and 3.95 ppm corresponding to the *N*,*N* dimethyl and the dimethylester groups, respectively.

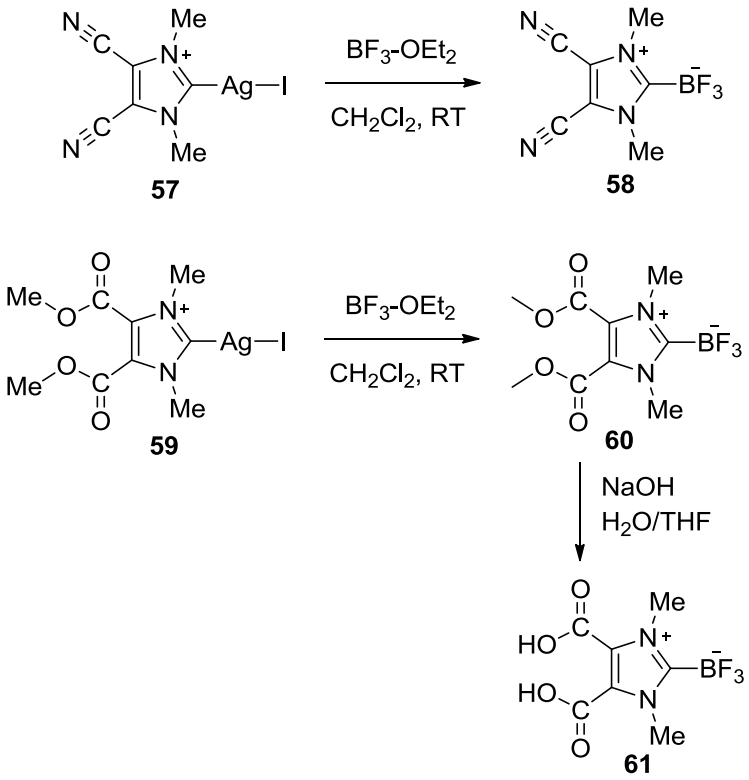

Figure 60. Scheme showing the synthesis of **58** and **61**.

4.3 Kinetic studies

Next, we decided to investigate the rates of hydrolysis reaction of these new NHC-BF_3 adducts (**49**, **51**, **52**, **56**). This hydrolysis reaction, which is expected to produce the corresponding boronic acid according to a first order rate process ($v = k_{obs}$[NHC-BF_3]), was monitored by ^{19}F NMR spectroscopy in D_2O/CD_3CN (8/2 vol) at pH 7.5 ([phosphate buffer] = 500 mM, [NHC-BF_3] = 20 mM). Surprisingly, we found that the hydrolysis of the adducts was extremely slow. After a week, we did not observe any free fluoride for **51** and **56** indicating that these two derivative are essentially immortal. Their stability is assigned to the electron withdrawing nature of the nitro or

maleimide functionality which increases the Lewis acidity of the boron center thereby preventing fluoride anion dissociation. Compounds **49** and **52** are also surprisingly stable and only show a trace amount of free fluoride after a week in D_2O/CD_3CN (8/2 vol) at pH 7.5. By extending this experiment to a longer timescale, we have been able to calculate the rate of hydrolysis for these two compounds. These rates, which are respectively equal to $k_{obs} = 1.2 \times 10^{-6}$ min^{-1} for **49** and 1.1×10^{-6} for **52** are lower than those measured under the same condition for the phosphonium borane **D**. Altogether, these results illustrate the remarkable resistance of NHC-BF_3 adducts to hydrolysis and suggest that they could be used as prosthetic groups for PET imaging.

4.4 Radiofluorination and *in vivo* imaging studies[5]

Employing the approach developed by our group for the preparation of [^{18}F]BODIPY dye, we decided to investigate the radiofluorination of these NHC-BF_3 adducts via ^{18}F-^{19}F isotopic exchange using $SnCl_4$ as a Lewis acid promoter.[87] We first tested this approach with the non-functionalized NHC-BF_3 adduct **49** which was mixed with $SnCl_4$ (5-15 eq) in MeCN and combined with a solution of [^{18}F]fluoride (as the tetra-*n*-butylammonium salt) in MeCN (Scheme 3, Table 1). The reaction mixture was then shaken for 10 min before being quenched by addition of water. The radiolabeled compound ([^{18}F]**49**) was immobilized on a Sep-Pak cartridge (Sep-Pak Plus tC18) and

[5] This experiment was carried out by our collaborator, Dr. Zibo Li, at department of Radiology, University of North Carolina, Chapel Hill, NC.

washed with water. [^{18}F]**49** was eluted off the cartridge with MeCN. An aliquot of the resulting MeCN solution was subjected to HPLC analysis.

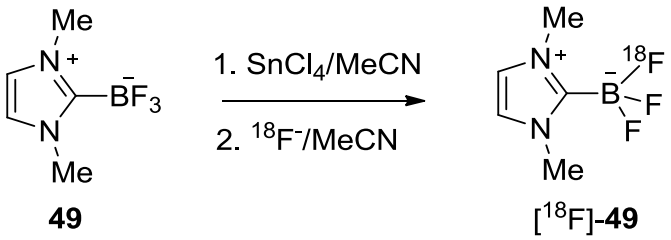

49 [^{18}F]-**49**

Figure 61. Scheme showing the radiolabeling of **49** employed by $SnCl_4$ assisted isotopic ^{18}F-^{19}F exchange.

Because we pre-processed the sample before HPLC analysis, we cannot calculate the radiochemical yield (RCY) based on HPLC integration. Therefore, we determined the RCY based on the radio-activity of isolated product and the starting radio-activity. As shown in Table 11, the RCY ranges from 35-56% for different reaction conditions. It was found that increasing the concentration of precursor leads to higher isolation yield (Entry 1-3). Interestingly, variation in the concentration of the Lewis acid promoter (Entry 3-5) or in the temperature (Entry 6-7) of the reaction had little impact on the RCY. When a long reaction time was employed as in entries 8 and 9, a decrease of isolation yield was observed due to product decomposition. The highest specific activity of the final product obtained in this experiment was calculated to be 53.5 mCi/μmol (Entry 8).

Table 11. Radiosynthetic results.

Entry	[**49**] (mM)	$SnCl_4$ (equiv.)	Temp. (°C)	Time (Min)	SA[a] (mCi/ μmol)	RCY[b] (%)
1	15	5	25	10	26.4	35.5
2	30	5	25	10	40.6	42.1
3	60	5	25	10	40.8	47.3
4	30	10	25	10	47.5	48.4
5	30	15	25	10	47.8	48.1
6	30	5	40	10	45.5	56.4
7	30	5	60	10	49.5	53.4
8	30	5	25	20	53.5	49.9
9	30	5	25	30	36.8	39.9

[a]Specific activity is determined by dividing the product activity by the amount of the product (based on the integration of UV-HPLC and compare with the UV chromatogram of the standard). [b]RCY = activity of the isolated product/starting ^{18}F activity. All yields are decay corrected.

Using condition from entry 7, we have also been able to prepare [^{18}F]**56** with specific activity of 51.3 mCi/μmol (RCY = 54%, Scheme 3). The identity of [^{18}F]**56** was confirmed by the co-injection with the non-radiolabeled standard (Figure 63). This radiofluorinated NHC-BF_3 adduct could be conveniently conjugated with the model peptide H-Cys-Phe-OH *via* a thiol-Michael addition reaction. This synthesis was carried out by mixing a solution of [^{18}F]**56** in MeCN with an aqueous solution of H-Cys-Phe-OH (400 μg, 1.5 μmol) (Figure 62). After shaking for 10 min at room temperature, a portion of the reaction mixture (0.01 mCi) was loaded onto the HPLC for purification

affording [^{18}F]**56**/H-Cys-Phe-OH with a 95.7% purity. The identity of [^{18}F]**56**/H-Cys-Phe-OH peptide was confirmed by its mass spectrum as well as by co-injection with the independently synthesized non-radiolabeled standard (Figure 64). The specific activity of [^{18}F]**56**/H-Cys-Phe-OH peptide was calculated as 40.8 mCi/μmol.

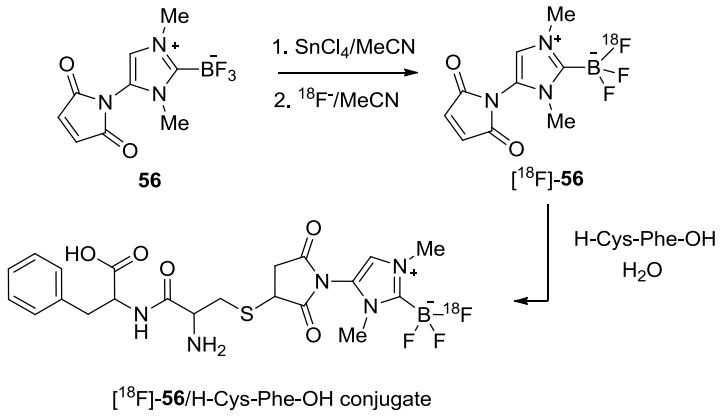

Figure 62. Scheme showing the preparation of [^{18}F]-**56**/ H-Cys-Phe-OH conjugate.

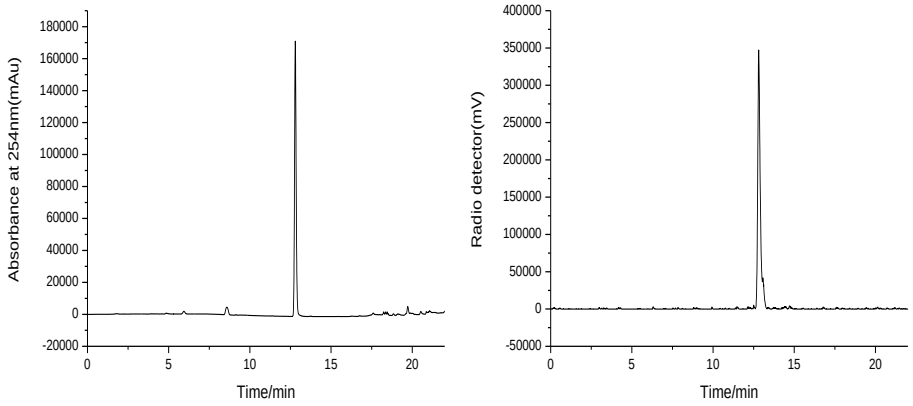

Figure 63. Left: UV trace of **56** as the standard reference. Right: Crude radio-HPLC profile for the ^{18}F-labeling of **56**.

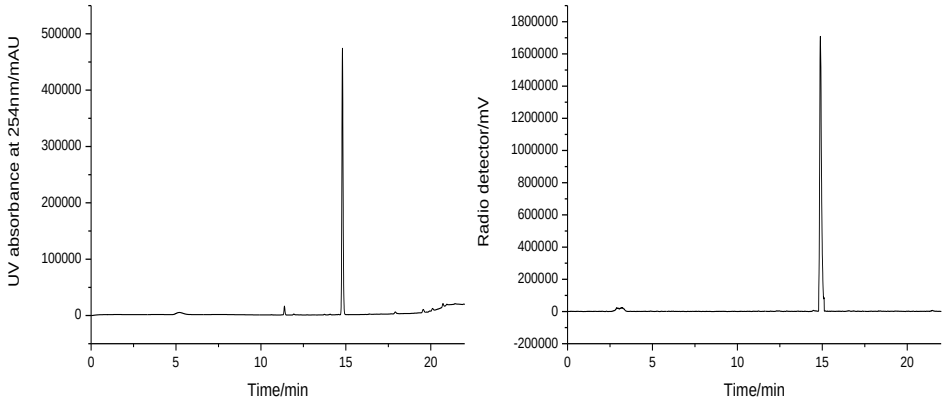

Figure 64. Left: UV traces of BF_3-carbene-Cys-Phe as the standard reference. Right: Crude radio-HPLC profile for the ^{18}F-labeling of BF_3-carbene-Cys-Phe.

After confirming these encouraging radiofluorination and conjugation results, the stability of [^{18}F]**56**/H-Cys-Phe-OH was investigated *in vivo*. As a prelude to these studies, we first tested the stability of the conjugate in a 1x PBS buffer at 37° (Figure 65). Even after 2 hours, the conjugate is not compromised as shown by the fact that its purity remains >90% pure. *In vivo* PET/CT imaging in a normal nude mouse afford consistent results. The microPET/CT images collected 1 h, 2 h, and 4 h post injection show liver and urinary track clearance of the conjugate. More importantly, no bone uptake is observed even 4 h post injections. Indicating that [^{18}F]-fluoride release by the radiofluorinated carbene unit is negligible (Figure 66)

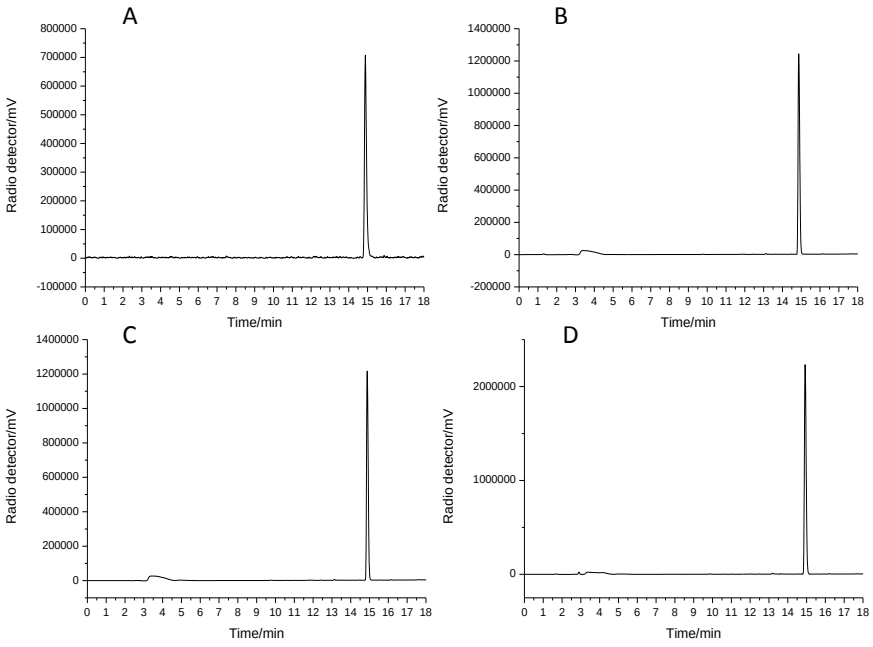

Figure 65. A: [^{18}F]**56**-peptide standard Radio-HPLC profile. B,C,D: [^{18}F]**56**-peptide in 1x PBS for 0.5h, 1h and 2h with purity of 96.6%, 93.9%, and 92.5%, respectively.

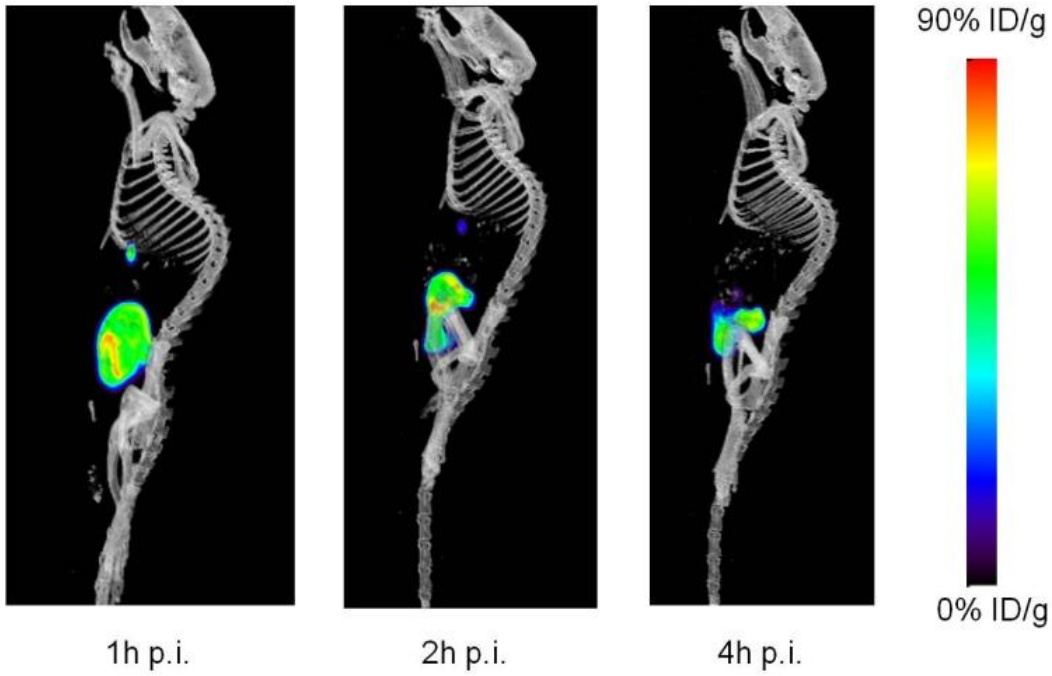

Figure 66. Decay-corrected whole-body microPET-CT sagittal images of nude mice from a static scan at 1, 2 h and 4 h after injection of [^{18}F]**56**/ H-Cys-Phe-OH conjugate.

4.5 Conclusion

In summary, we have identified a new boron-based fluoride captor with an unsurpassed resistance to hydrolytic fluoride release. The stability of this new probe is ascribed to its zwitterionic nature, with the cationic charge of the imidazolium unit acting as an electrostatic anchor for the boron-bound fluoride anions. These NHC-BF_3 fluoride captors are a new incarnation of the concepts underlying the stability of the phosphonium trifluoroborates of type **D** and **E** developed by us or ammonium trifluoroborates of type **C** recently reported by the Perrin group.

4.6 Experimental

General Consideration

1, 3-dimethyl-1*H*-imidazolium tetrafluoroborate[88], and 1, 3-dimethyl-4-nitroimidazolium silver complex[89] (**50**) were synthesized according to the reported procedure. 1-Methylimidazole, boron trifluoride diethyl etherate (BF_3-OEt_2), methyl iodide (CH_3I), 10% palladium supported carbon, and succinic anhydride were purchased from Alfar Aesar; 4-nitroimidazole was purchased from Tokyo Chemical Industry Co., Ltd; N, N-di-*iso*-propylethylamine (DIEA), and maleic anhydride were purchased from Sigma Aldrich; silver oxide was purchased from Strem chemicals; acetic anhydride was purchased from EM industries, Inc; sodium acetate was purchased from Mallinckrodt. All chemicals were used without further purification. Solvents were dried by passing through an alumina column (CH_2Cl_2), refluxing under N_2 over Na (Et_2O and THF), refluxing under N_2 over CaH_2 (CH_3CN). Electrospray mass spectra were acquired from a MDS Sciex API QStar Pulsar. NMR spectra were recorded on a Varian Unity Inova 400 NMR and an Inova 500B spectrometer at ambient temperature. Chemical shifts are given in ppm, and are referenced to residual ^1H and ^{13}C solvent signals as well as external BF_3-Et_2O (^{11}B NMR and ^{19}F NMR).

*Preparation of 1, 3-dimethylimidazolium-2-trifluoroborate (**49**)*

1, 3-Dimethyl-1*H*-imidazolium tetrafluoroborate (0.252 g, 1.37 mmol) was placed into a sublimation apparatus, connected *via* a liquid-N_2-cooled trap to a high-vacuum line. The powder was heated by a heating mantle under reduced pressure to 200 °C at which point compound **49** started condensing on the cold finger. The sublimation was continued for 15 min. Compound **49** (0.196 g, 1.19 mmol) was obtained in a 87 % yield. ^{1}H NMR (499.4 MHz, CD_3CN): δ 3.85 (s, 6H, -C*H*$_3$), 7.11 (s, 2H, =C*H*). ^{13}C NMR (125.6 MHz, CD_3CN): δ 35.93 (-*C*H$_3$), 122.64 (=*C*H). ^{11}B NMR (128.2 MHz, CD_3CN): δ 0.21 (q, $J_{B\text{-}F}$ = 37.0 Hz). ^{19}F NMR (282.2 MHz, CD_3CN): δ -139.2 (q, $J_{B\text{-}F}$ = 37.0 Hz). HRMS (ESI$^-$) calcd for $[M\text{-}F]^+$: 145.0748, found: 145.0758.

*Preparation of 1, 3-dimethyl-4-nitroimidazolium-2-trifluoroborate (**51**)*

BF_3-OEt_2 (0.34 mL, 2.75 mmol) was added to a suspension of **50** (0.691 g, 0.92 mmol) in CH_2Cl_2 (15 mL) at room temperature. The suspension was stirred for 4 h and filtered. The filtrate was purified by flash chromatography using silica gel as a stationary phase and CH_2Cl_2 as a mobile phase to remove an excess BF_3-OEt_2 and an imidazolium salt impurity. The purified solution was dried in *vacuo* resulting **51** as a white powder (0.160 g) in a 83 % yield. ^{1}H NMR (499.4 MHz, CD_3CN): δ 3.94 (s, 3H, -C*H*$_3$), 4.16 (s, 3H, -C*H*$_3$), 8.21 (s, 1H, =C*H*). ^{13}C NMR (125.6 MHz, CD_3CN): δ 35.84 (*C*H$_3$), 37.61 (*C*H$_3$), 126.04 (=*C*H), 138.55 (=*C*NO_2). ^{11}B NMR (128.2 MHz, CD_3CN): δ 0.13 (q, $J_{B\text{-}F}$ = 33.5 Hz). ^{19}F NMR (469.9 MHz, CD_3CN): δ -137.86 (q, $J_{B\text{-}F}$ = 33.5 Hz). HRMS (ESI$^-$) calcd for $[M\text{-}H]^-$: 208.0505, found: 208.0517.

*Preparation of 1, 3-dimethyl-4-amino-imidazolium-2-trifluoroborate (**52**)*

10% palladium on carbon (0.235 g, 0.221 mmol Pd) was added to a solution of **51** (0.461 g, 2.21 mmol) in CH_2Cl_2 (20 mL). Hydrogen gas was bubbled through the solution for 30 min. The mixture was stirred under a hydrogen atmosphere overnight at room temperature. The solution was then filtered over celite and the solvent was removed under vacuum yielding **52** as a white powder (0.307 g) in a 78 % yield. ^{1}H NMR (499.4 MHz, CD_3CN): δ 3.61 (s, 3H, -C*H*$_3$), 3.73 (s, 3H, -C*H*$_3$), 4.02 (s, 2H, -N*H*$_2$), 6.37 (s, 1H, =C*H*). ^{13}C NMR (125.6 MHz, CD_3CN): δ 30.67 (*C*H_3), 35.51 (*C*H_3), 104.57 (=*C*H), 138.20 (=*C*NH_2). ^{11}B NMR (128.2 MHz, CD_3CN): δ 0.27 (q, $J_{B\text{-}F}$ = 37.2 Hz). ^{19}F NMR (375.9 MHz, CD_3CN): δ -138.0 (q, $J_{B\text{-}F}$ = 37.2 Hz). HRMS (ESI$^-$) calcd for $[M\text{-}H]^-$: 178.0763, found: 178.0741.

*Preparation of 1, 3-dimethyl-4-succinimide-imidazolium-2-trifluoroborate (**53**)*

A solution of **52** (0.0587 g, 0.328 mmol), succinic anhydride (0.1650 g, 1.650 mmol) and diisopropylethylamine (DIEA) (0.23 mL, 1.320 mmol) in DMF (7 mL) was heated to 70 °C for 15 h. After 15 h, the solvent was removed in *vacuo*. The crude product was purified by flash chromatography using silica gel as a stationary phase and 99:1 CH_2Cl_2:MeOH solution as a mobile phase. The resulting solution was dried by rotary evaporator obtaining **53** (0.0568 g) as a pale yellow powder in a 66 %. ^{1}H NMR (399.5 MHz, CD_3CN): δ 2.89 (s, 4H, succinimide-C*H*$_2$), 3.63 (s, 3H, -C*H*$_3$), 3.89 (s, 3H, -C*H*$_3$), 7.23 (s, 1H, =C*H*). ^{13}C NMR (125.6 MHz, CD_3CN): δ 28.75 (succinimide-*C*H_2),

32.44 (*C*CH_3), 36.67 (*C*H_3), 120.65 (=*C*H), 122.81 (=*C*N(C(O)CH_2)$_2$) 176.19 (*C*=O). ^{11}B NMR (128.2 MHz, CD_3CN): δ 0.29 (q, $J_{B\text{-}F}$ = 35.4 Hz). ^{19}F NMR (375.9 MHz, CD_3CN): δ -138.5 (q, $J_{B\text{-}F}$ = 35.4 Hz). HRMS (ESI^-) calcd for $[M\text{-}H]^-$: 260.0818, found: 260.0855.

*Preparation of 1, 3-dimethyl-4-succinimic acid-imidazolium-2-trifluoroborate (**54**)*

0.70 mL of 0.5 M NaOH (0.350 mmol) was slowly added to a solution of **53** (0.0884 g, 0.339 mmol) in 1:1 water/THF mixture (6 mL) at room temperature. The reaction mixture was stirred for 3 h and then neutralized by addition of 0.5M HCl. The solvents were removed in vacuum and the resulting powder was re-dissolved in CH_3CN (10 mL). The suspension was filtered to remove NaCl salt. The filtrate was dried by rotary evaporator resulting **54** as a white powder (0.0835 g) in a 88 %. ^{1}H NMR (399.5 MHz, D_2O): δ 2.44 (t, 2H, C*H*$_2$, $J_{H\text{-}H}$ = 6.49 Hz), 2.62 (t, 2H, C*H*$_2$, $J_{H\text{-}H}$ = 6.49 Hz), 3.55 (s, 3H, -C*H*$_3$), 3.74 (s, 3H, -C*H*$_3$), 7.14 (s, 1H, =C*H*). ^{13}C NMR (125.6 MHz, CD_3CN): δ 32.93 (*C*H_3), 33.36 (-*C*H_2-), 33.74 (-*C*H_2-), 37.37 (*C*H_3), 118.45 (=*C*H), 128.83 (=*C*N(CO)$(CH_2)_2$COOH), 177.33 (*C*=O), 181.50 (*C*=O). ^{11}B NMR (128.2 MHz, D_2O): δ -0.33 (q, $J_{B\text{-}F}$ = 38.4 Hz). ^{19}F NMR (375.9 MHz, D_2O): δ -137.5 (q, $J_{B\text{-}F}$ = 38.4 Hz). HRMS (ESI^-) calcd for $[M\text{-}H]^-$: 278.0164, found: 278.0943.

*Preparation of 1, 3-dimethyl-4-maleic acid-imidazolium-2-trifluoroborate (**55**)*

Maleic anhydride (0.172 g, 1.76 mmol) was added to a solution of **52** (0.1572g, 0.88 mmol) in THF (8 mL). The reaction mixture was stirred for 20 h at room temperature resulting in a white precipitate. The powder was collected by filtration and then dried in *vacuo* yielding **55** (0.180 g) in a 74 % yield. ^{1}H NMR (399.5 MHz, D_2O): δ 3.46 (s, 3H, -C*H*$_3$), 3.61 (s, 3H, -C*H*$_3$), 6.22 (d, 1H, =C*H(*CO)), 6.39 (d, 1H, =C*H(*CO)), 7.08 (s, 1H, =C*H*) . ^{13}C NMR (125.6 MHz, CD_3CN): δ 31.64 (*C*H_3), 35.96 (*C*H_3), 116.92 (=*C*H), 126.56 (=*C*N(CO)(CH=CH)COOH), 129.99 (-H*C*=CH-), 131.67 (-HC=*C*H-), 167.35 (*C*=O), 168.71 (*C*=O). ^{11}B NMR (128.2 MHz, D_2O): δ -0.30 (q, J_{B-F} = 40.0 Hz). ^{19}F NMR (469.9 MHz, D_2O): δ -137.4 (q, J_{B-F} = 40.0 Hz). HRMS (ESI^-) calcd for $[M-H]^-$: 276.0767, found: 276.0748.

*Preparation of 1, 3-dimethyl-4-maleimide-imidazolium-2-trifluoroborate (**56**)*

A solution of **55** (0.131 g, 0.47 mmol) and sodium acetate (NaOAc) (0.064 g, 0.47 mmol) in acetic anhydride (Ac_2O) (15 mL) was heated to 70 °C for 3 h. After 3 h, the acetic anhydride was removed in vacuum. The crude product was re-dissolved in CH_2Cl_2 (30 mL) and then, the solution was washed with water (3x30 mL). The organic layer was dried with $MgSO_4$. Finally, the solvent was removed in vacuum yielding **56** (0.088 g) as a white powder in a 72 % yield. ^{1}H NMR (499.4 MHz, CD_3CN): δ 3.65 (s, 3H, -C*H*$_3$), 3.91 (s, 3H, -C*H*$_3$), 7.08 (s, 2H, maleimide=C*H*), 7.30 (s, 1H, =C*H*). ^{13}C NMR (125.6 MHz, CD_3CN): δ 32.36 (*C*H_3), 36.70 (*C*H_3), 121.33 (=*C*H), 121.52 (=*C*N(C(O)CH)$_2$), 135.86 (maleimide=*C*H), 168.75 (*C*=O). ^{11}B NMR (128.2 MHz,

CD_3CN): δ 0.29 (q, $J_{B\text{-}F}$ = 35.6 Hz). ^{19}F NMR (375.9 MHz, CD_3CN): δ -138.5 (q, $J_{B\text{-}F}$ = 35.6 Hz). HRMS (ESI^-) calcd for $[M+Na]^-$: 282.0638, found: 282.0650.

*Preparation of (4,5-dicyano-1,3-dimethyl-1H-imidazol-3-ium-2-yl)trifluoroborate (**58**)*

BF_3-OEt_2 (0.55 mL, 4.35 mmol) was added to a suspension of Ag complex **57** (0.5509 g, 1.45 mmol) in CH_2Cl_2 (15 mL) at room temperature. The suspension was stirred for 4 h and then filtered to remove silver iodide by-product. The filtrate was purified by flash chromatography using silica gel as a stationary phase and CH_2Cl_2 as a mobile phase to remove an excess BF_3-OEt_2 and an imidazolium salt impurity. The purified solution was dried in *vacuo* resulting **58** as a white powder (0.1595 g) in a 78 % yield. ^1H NMR (399.5 MHz, CD_3CN): δ 3.99 (s, 6H, -CH_3). ^{13}C NMR (100.45 MHz, CD_3CN): δ 36.84, 106.43, 116.03. ^{11}B NMR (128.2 MHz, CD_3CN): δ -0.20 (q, $J_{B\text{-}F}$ = 31.7 Hz). ^{19}F NMR (375.9 MHz, CD_3CN): δ -138.91 (q, $J_{B\text{-}F}$ = 31.7 Hz). HRMS (ESI^+) calcd for $[M\text{-}F]^+$: 195.0653, found: 195.0748.

*Preparation of (4,5-dicarboxy-1,3-dimethyl-1H-imidazol-3-ium-2-yl)trifluoroborate (**61**)*

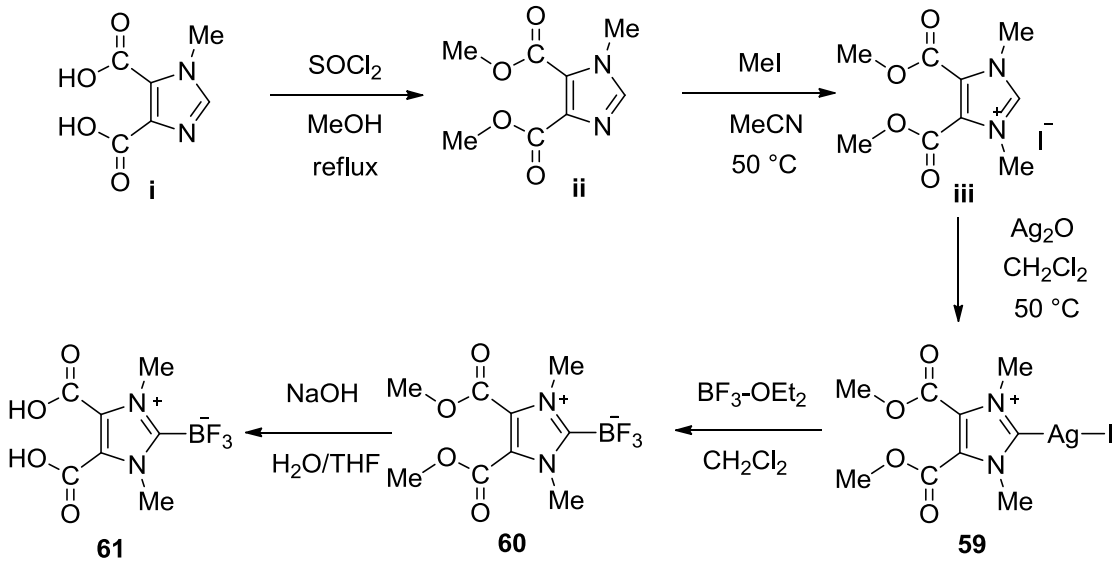

Figure 67. Scheme showing the synthesis of **61**.

$SOCl_2$ (0.40 mL, 5.51 mmol) was added to a solution of **i** (0.3212 g, 1.89 mmol) in methanol (15 mL). The solution mixture was refluxed for 18 h. Upon cooling to 40 °C, solid $NaHCO_3$ was added to raise the pH to 8. The mixture was filtered and the filtrate was evaporated under reduced pressure affording **ii** (0.2920 g) in a 78 % yield. ^{1}H NMR (399.5 MHz, $CDCl_3$): δ 3.83 (s, 3H, -C*H*$_3$), 3.89 (s, 3H, -C*H*$_3$), 3.90 (s, 3H, -C*H*$_3$), 7.47 (s, 1H). Without further purification, **ii** (0.2920 g, 1.47 mmol) was treated with MeI (0.20 mL, 3.21 mmol) in MeCN (15 mL) at 50 °C for 18 h. The solution mixture was concentrated to the volume of 1 mL. Then, Et_2O (15 mL) was added to precipitate **iii** (0.3610 g) in a 72 % yield. ^{1}H NMR (399.5 MHz, CD_3CN): δ 3.94 (s, 6H, -C*H*$_3$), 3.96

(s, 6H, -CH_3), 8.92 (s, 1H). Next, **iii** (0.1239 g, 0.36 mmol) was treated with Ag_2O (0.0420 g, 0.18 mmol) in CH_2Cl_2 (20 mL) at 50 °C for 3 h. The solvent was removed in *vacuo* yielding **59** (0.1401 g) in a 86 %. ^{1}H NMR (399.5 MHz, CD_3CN): δ 3.88 (s, 6H, -CH_3), 3.96 (s, 6H, -CH_3). Then, BF_3-OEt_2 (0.12 mL, 0.97 mmol) was added to a suspension of Ag complex **59** (0.1401 g, 0.31 mmol) in CH_2Cl_2 (20 mL) at room temperature. The suspension was stirred for 4 h and then filtered to remove silver iodide by-product. The filtrate was purified by flash chromatography using silica gel as a stationary phase and CH_2Cl_2 as a mobile phase to remove an excess BF_3-OEt_2 and an imidazolium salt impurity. The purified solution was dried in *vacuo* resulting **60** (0.0541 g) in a 62 % yield. ^{1}H NMR (399.5 MHz, CD_3CN): δ 3.92 (s, 6H, -CH_3), 3.95 (s, 6H, -CH_3). ^{11}B NMR (128.2 MHz, CD_3CN): δ 0.17 (q, $J_{B\text{-}F}$ = 34.3 Hz). ^{19}F NMR (375.9 MHz, CD_3CN): δ -137.5 (q, $J_{B\text{-}F}$ = 34.3 Hz). Finally, 2 mL of 1 M NaOH was added to a solution of **60** (0.00541 g, 0.19 mmol) in 1:1 water/THF mixture (6 mL) at room temperature. The reaction mixture was stirred for 4 h and then neutralized by addition of 2 mL of 1 M HCl. The solvents were removed in vacuum and the resulting powder was re-dissolved in CH_3CN (10 mL). The suspension was filtered through celite to remove NaCl salt. The filtrate was dried by rotary evaporator resulting **61** (0.0432 g) in a 89 %. ^{1}H NMR (399.5 MHz, CD_3CN): δ 4.09 (s, 6H, -CH_3). ^{11}B NMR (128.2 MHz, CD_3CN): δ 0.40 (q, $J_{B\text{-}F}$ = 35.6 Hz). ^{19}F NMR (375.9 MHz, CD_3CN): δ -136.3 (q, $J_{B\text{-}F}$ = 35.6 Hz). HRMS (ESI^-) calcd for $[M\text{-}H]^-$: 251.0450, found: 251.0214.

Crystallographic Measurements

Single crystals of **49** were obtained by slow diffusion of Et_2O into a CH_3CN solution of **49**. Single crystals of **51** and **56** were obtained by slow diffusion of pentane into a THF solution of **51** and **56**, respectively. The crystallographic measurement of **49**, **51**, and **56** were performed using a Bruker APEX-II CCD area detector diffractometer, with graphite-monochromated Mo-K_α radiation (λ = 0.71069 Å). A specimen of suitable size and quality was selected and mounted onto a nylon loop. The semi-empirical method SADABS was applied for absorption correction. The structure was solved by direct methods, and refined by the full-matrix least-square metahod against F^2 with the anisotropic temperature parameters for all non-hydrogen atoms. All H atoms were geometrically placed and refined using the riding model approximations. Data reduction and further calculations were performed using the Bruker SAINT+ and SHELXTL NT program packages. The crystal data are included in Table 12, 13, and 14.

Table 12. Crystal data, data collections, and structure refinements of **49**.

Crystal data	**49**	
Empirical formula	$C_5H_8BF_3N_2$	
Formula weight	163.94	
Crystal size/mm	0.2 x 0.1 x 0.07	
Temperature	110(2) K	
Wavelength	0.71073 Å	
Crystal system	Monoclinic	
Space group	P21/m	
Unit cell dimensions	a = 7.169(2) Å	α = 90.00°
	b = 6.8769(19) Å	β = 105.675(3)°
	c = 7.474(2) Å	γ = 90.00°
Volume	354.77(17) $Å^3$	
Z	2	
Density (calculated)	1.535 g cm^{-3}	
μ	0.148 mm^{-1}	
F(000)	168	
Scan mode	ω, φ	
hkl ranges	-9 → +9	
	-8 → +9	
	-9 → +9	
Reflections collected	4206	
Unique reflections [Rint]	927 [0.0269]	
Reflection used for refinement	927	
Refined parameters	64	
GooF	1.105	
R1,[a] *w*R2[b] (all data)	0.0596, 0.1980	
Largest diff. peak and hole	0.666, -0.771 e.$Å^{-3}$	

[a]$R1 = \Sigma||F_o| - |F_c||/ \Sigma|F_o|$. [b]$wR2 = ([w(F_o^2 - F_c^2)^2]/[\Sigma w(F_o^2)^2])^{1/2}$; $w = 1/[\sigma^2(F_o^2) + (ap)^2 + bp]$; $p = (F_o^2 + 2F_c^2)/3$ with $a = 0.1112$ and $b = 0.47$.

Table 13. Crystal data, data collections, and structure refinements of **51**.

Crystal data	**51**	
Empirical formula	$C_5H_7BF_3N_3O_2$	
Formula weight	208.95	
Crystal size/mm	0.2 x 0.08 x 0.07	
Temperature	110(2)K	
Wavelength	0.71073 Å	
Crystal system	Monoclinic	
Space group	P21/c	
Unit cell dimensions	a = 7.4533(5) Å	α = 90.00°
	b = 9.5695(6) Å	β = 105.0490(10)°
	c = 11.8645(8) Å	γ = 90.00°
Volume	817.21(9) $Å^3$	
Z	4	
Density (calculated)	1.698 g cm^{-3}	
μ	0.170 mm^{-1}	
F(000)	424	
Scan mode	ω, φ	
hkl ranges	-9 → +9	
	-12 → +12	
	-15 → +15	
Reflections collected	10223	
Unique reflections [Rint]	2039 [0.0449]	
Reflection used for refinement	2039	
Refined parameters	57	
GooF	1.066	
R1,[a] *w*R2[b] (all data)	0.0371, 0.1085	
Largest diff. peak and hole	1.214, -0.866 e.$Å^{-3}$	

[a]$R1 = \Sigma||F_o| - |F_c||/ \Sigma|F_o|$. [b]$wR2 = ([w(F_o^2 - F_c^2)^2]/[\Sigma w(F_o^2)^2])^{1/2}$; $w = 1/[\sigma^2(F_o^2) + (ap)^2 + bp]$; $p = (F_o^2 + 2F_c^2)/3$ with $a = 0.0579$ and $b = 0.39$.

Table 14. Crystal data, data collections, and structure refinements of **56**.

Crystal data	**56**	
Empirical formula	$C_9H_9BF_3N_3O_2$	
Formula weight	259.00	
Crystal size/mm	0.33 x 0.30 x 0.07	
Temperature	110(2)K	
Wavelength	0.71073 Å	
Crystal system	Orthorhombic	
Space group	P212121	
Unit cell dimensions	a = 7.5804(12) Å	α = 90.00°
	b = 7.9279(13) Å	β = 90.00°
	c = 18.431(3) Å	γ = 90.00°
Volume	817.21(9) $Å^3$	
Z	4	
Density (calculated)	1.553 g cm^{-3}	
μ	0.142 mm^{-1}	
F(000)	528	
Scan mode	ω, φ	
hkl ranges	-9 → +9	
	-10 → +10	
	0 → +23	
Reflections collected	4997	
Unique reflections [Rint]	2523 [0.0236]	
Reflection used for refinement	2523	
Refined parameters	164	
GooF	1.099	
R1,[a] *w*R2[b] (all data)	0.1079, 0.2763	
Largest diff. peak and hole	0.736, -0.617 e.$Å^{-3}$	

[a]$R1 = \Sigma||F_o| - |F_c||/ \Sigma|F_o|$. [b]$wR2 = ([w(F_o^2 - F_c^2)^2]/[\Sigma w(F_o^2)^2])^{1/2}$; $w = 1/[\sigma^2(F_o^2) + (ap)^2 + bp]$; $p = (F_o^2 + 2F_c^2)/3$ with $a = 0.1000$ and $b = 7.4553$.

^{1}H NMR

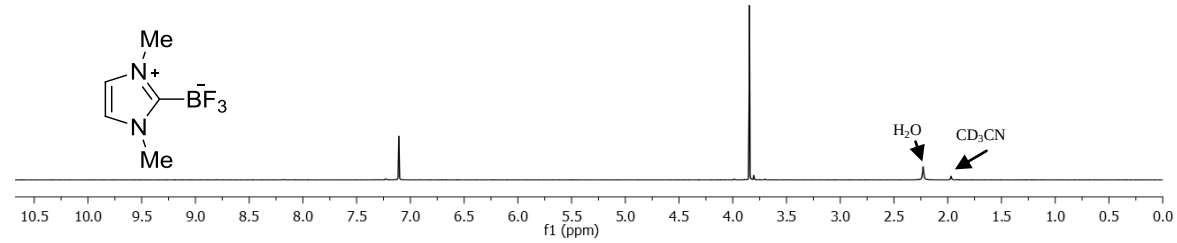

^{13}C NMR

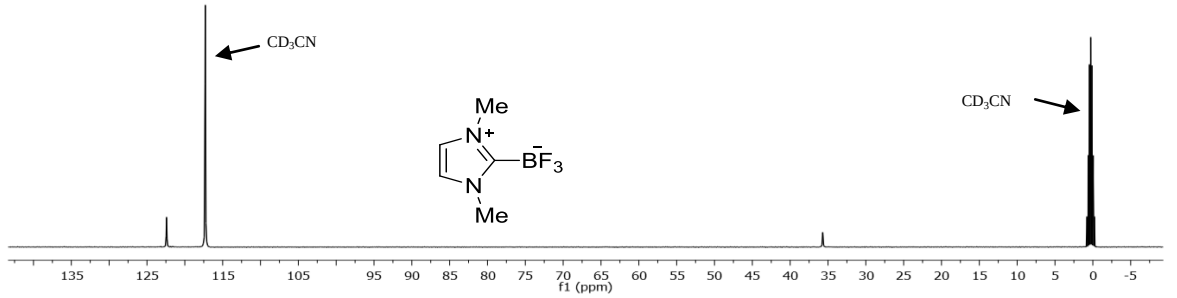

^{11}B NMR

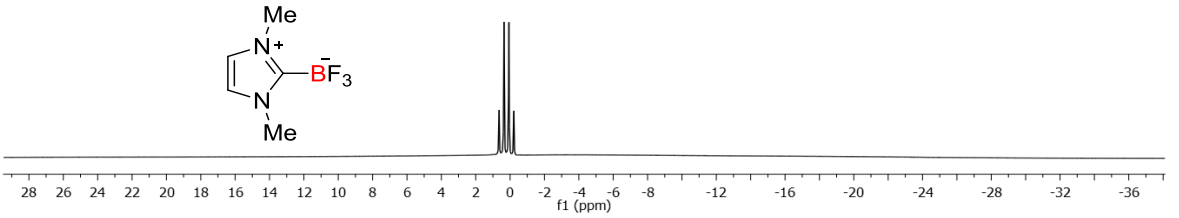

^{19}F NMR

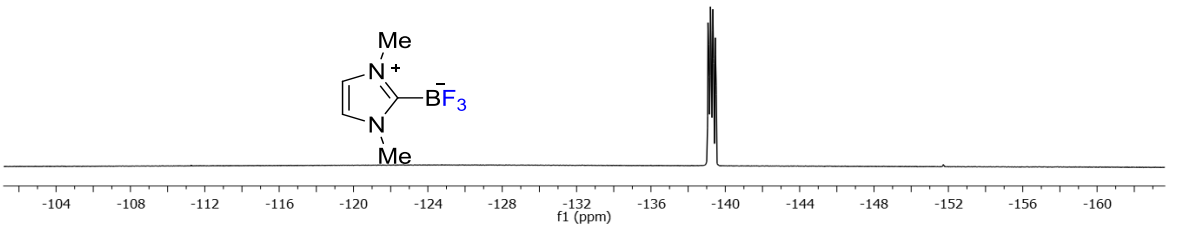

Figure 68. ^{1}H, ^{13}C, ^{11}B, and ^{19}F NMR spectra of **49** in CD_3CN.

^{1}H NMR

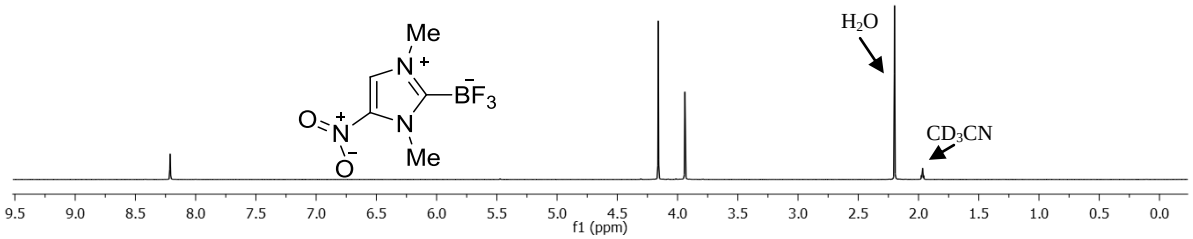

^{13}C NMR

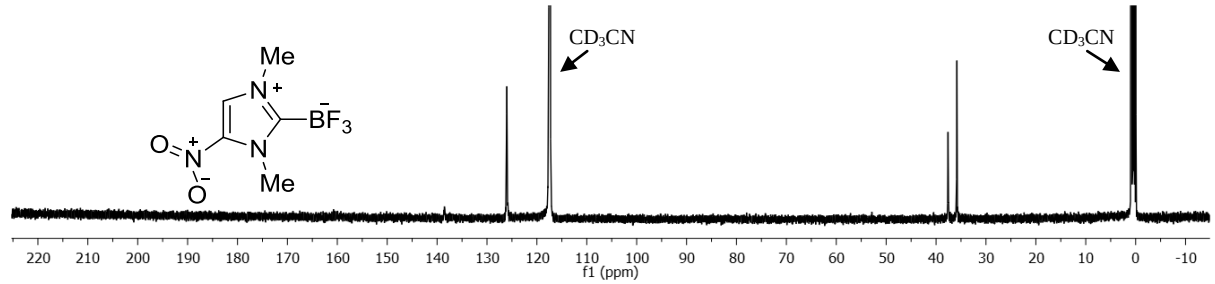

^{11}B NMR

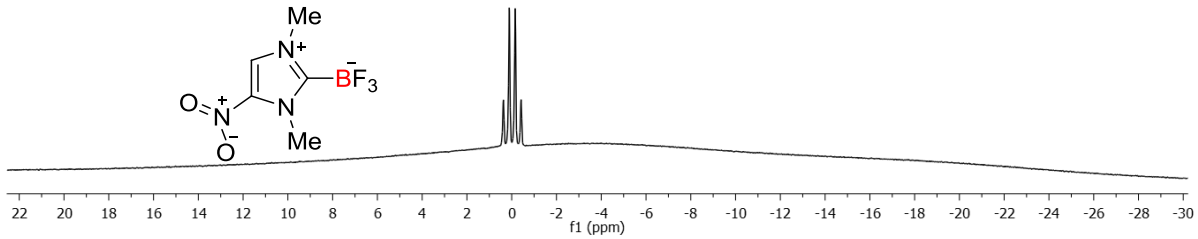

^{19}F NMR

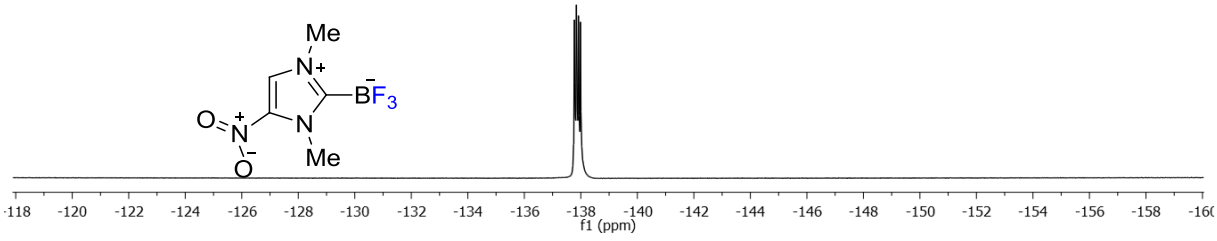

Figure 69. ^{1}H, ^{13}C, ^{11}B, and ^{19}F NMR spectra of **51** in CD_3CN.

^{1}H NMR

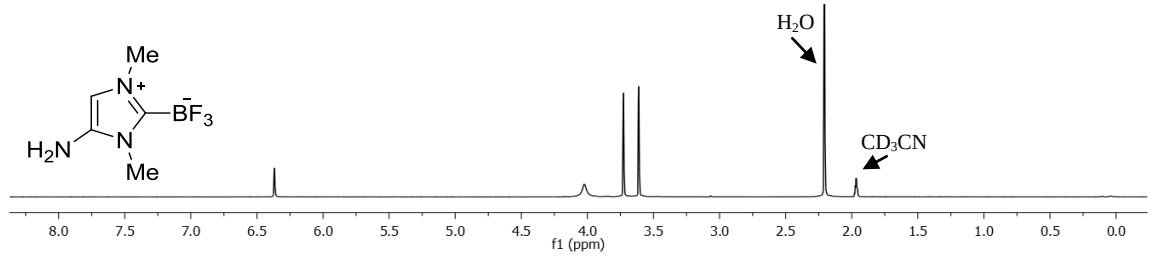

^{13}C NMR

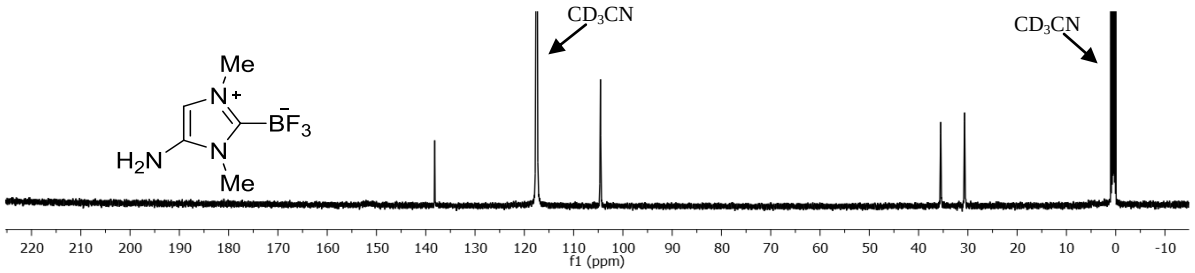

^{11}B NMR

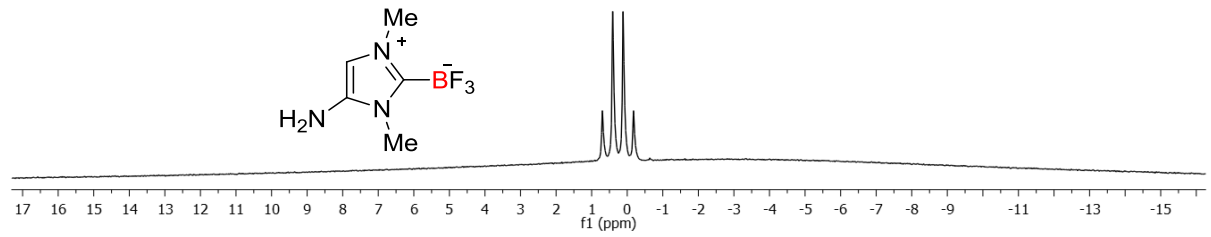

^{19}F NMR

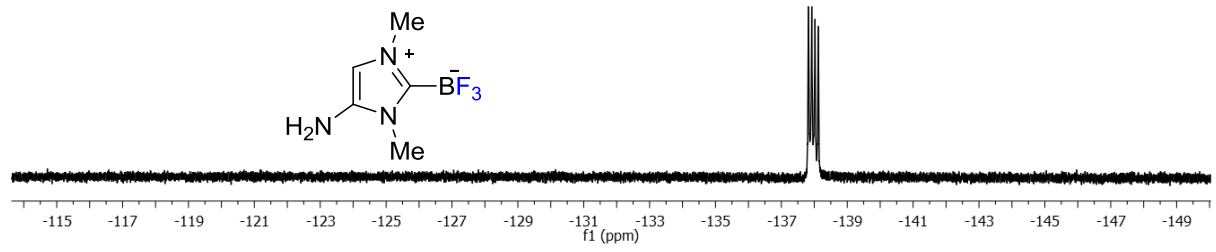

Figure 70. ^{1}H, ^{13}C, ^{11}B, and ^{19}F NMR spectra of **52** in CD_3CN.

^{1}H NMR

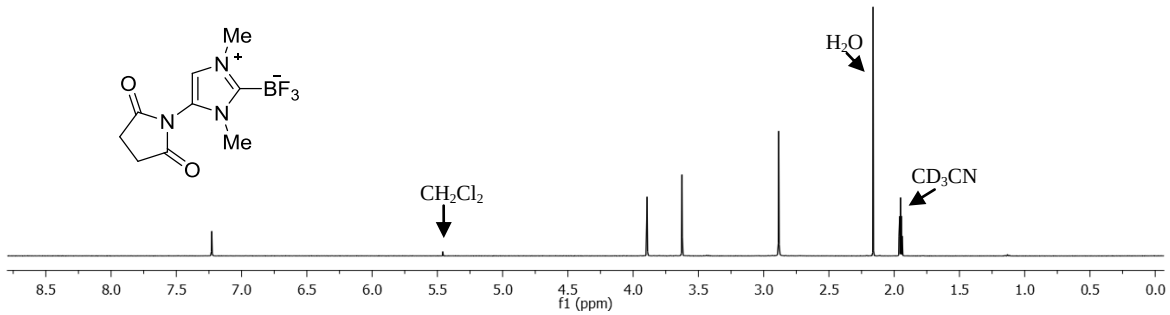

^{13}C NMR

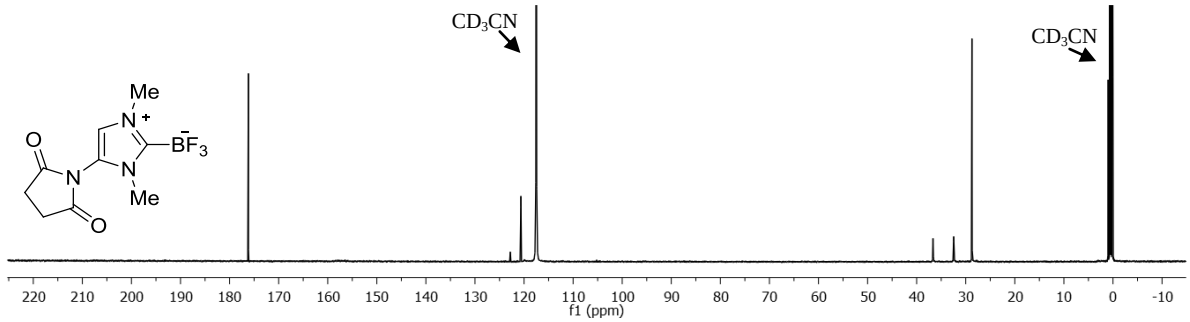

^{11}B NMR

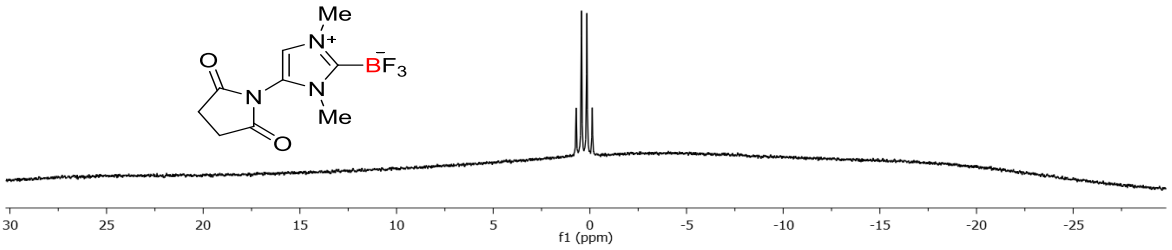

^{19}F NMR

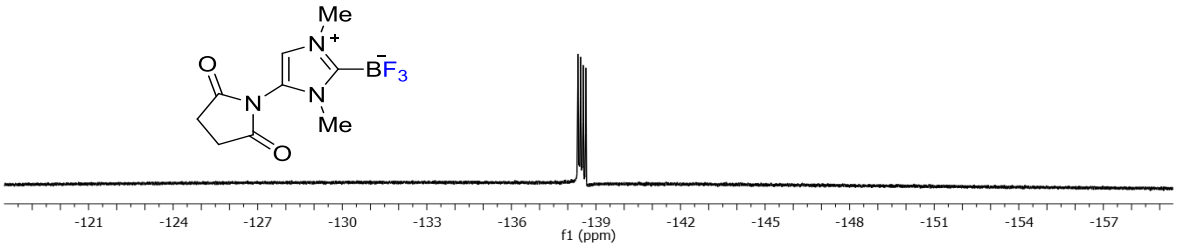

Figure 71. ^{1}H, ^{13}C, ^{11}B, and ^{19}F NMR spectra of **53** in CD_3CN.

^{1}H NMR

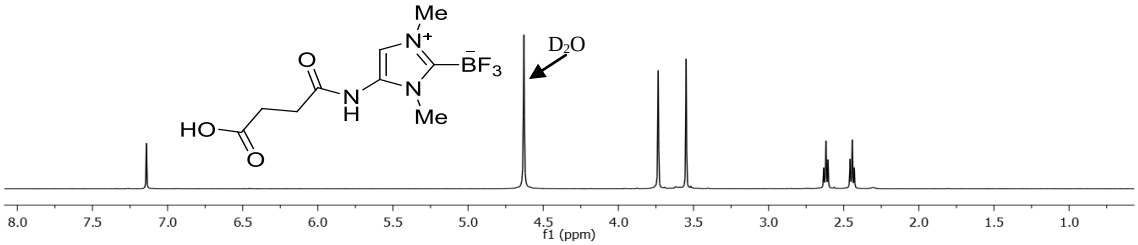

^{13}C NMR

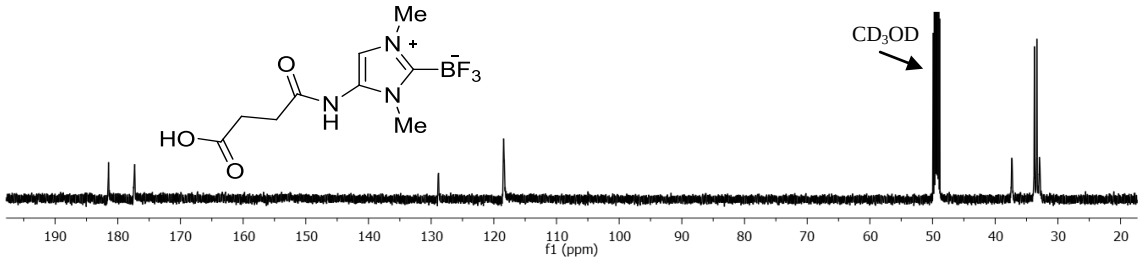

^{11}B NMR

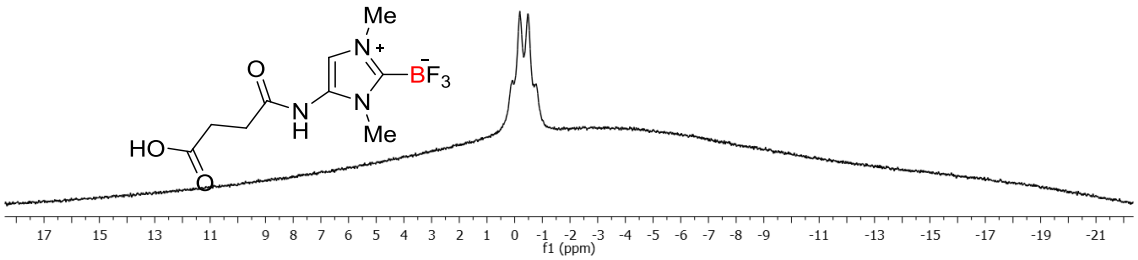

^{19}F NMR

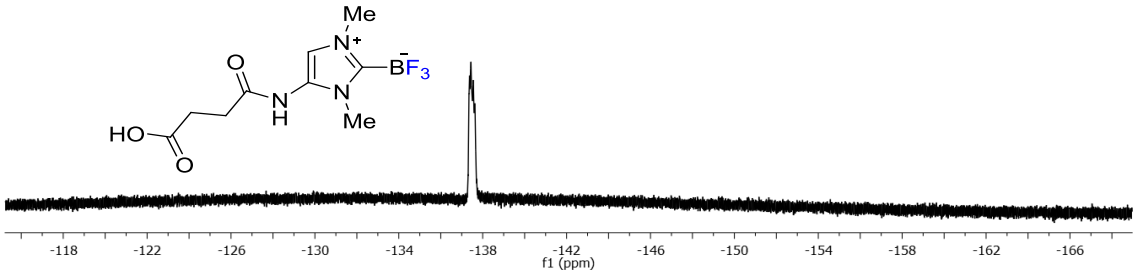

Figure 72. ^{1}H, ^{13}C, ^{11}B, and ^{19}F NMR spectra of **54** in D_2O.

^{1}H NMR

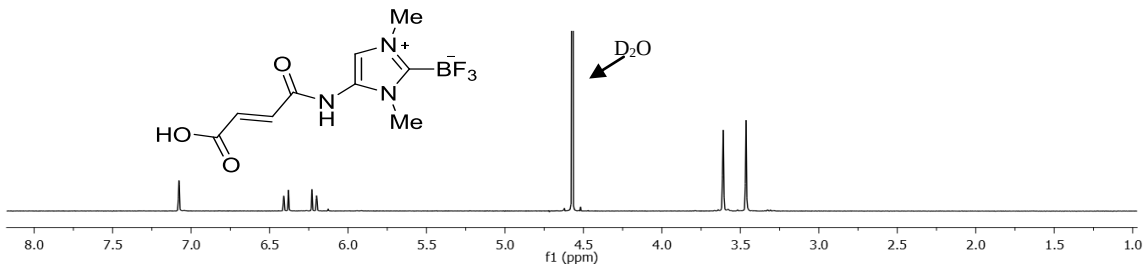

^{13}C NMR

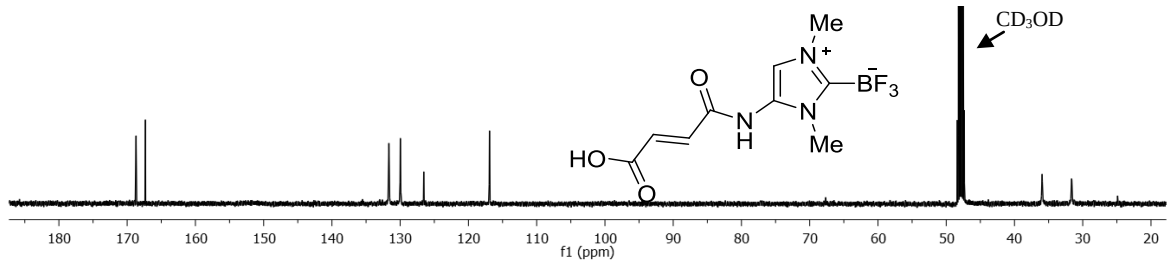

^{11}B NMR

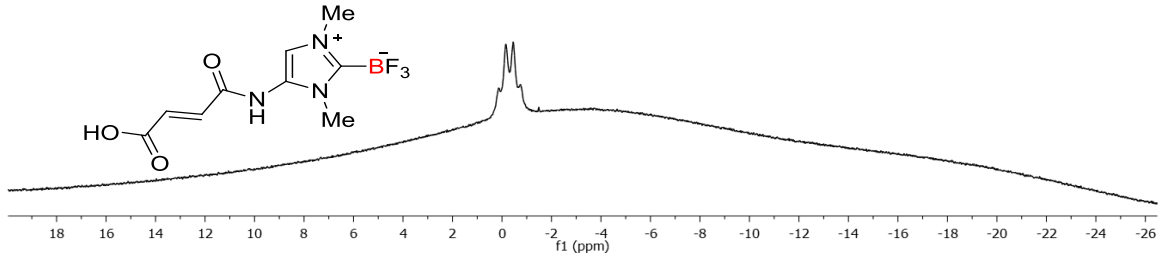

^{19}F NMR

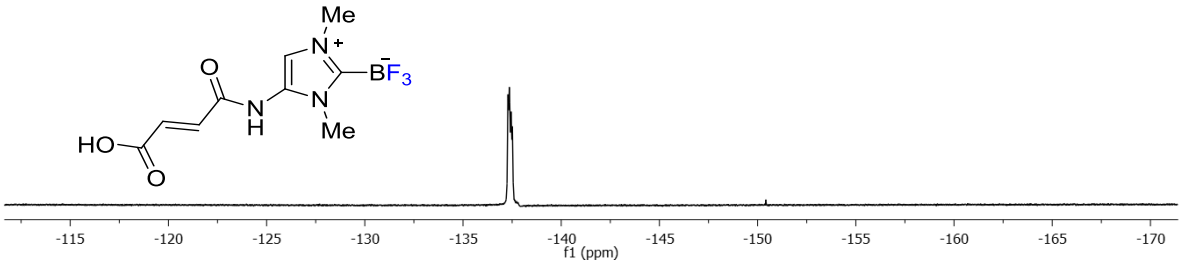

Figure 73. ^{1}H, ^{13}C, ^{11}B, and ^{19}F NMR spectra of **55** in D_2O.

^{1}H NMR

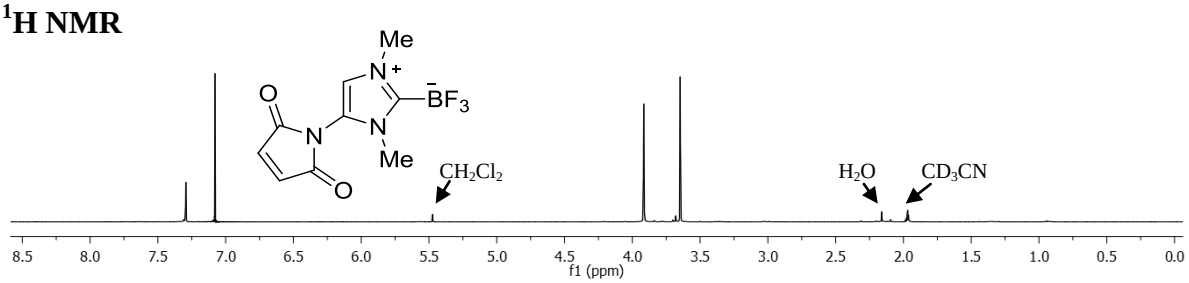

^{13}C NMR

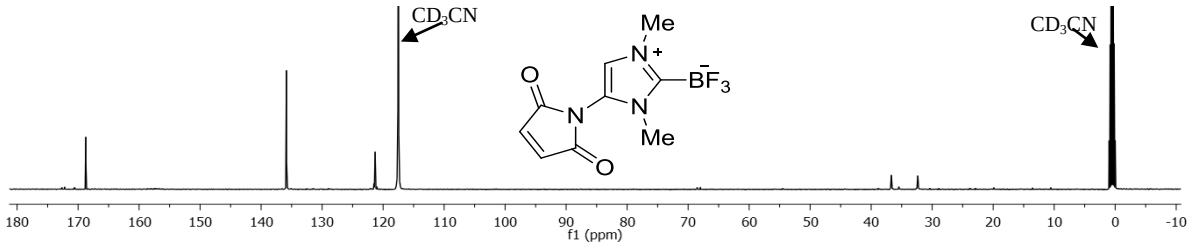

^{11}B NMR

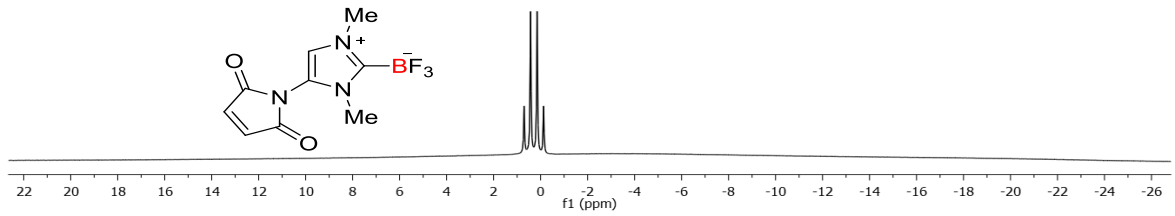

^{19}F NMR

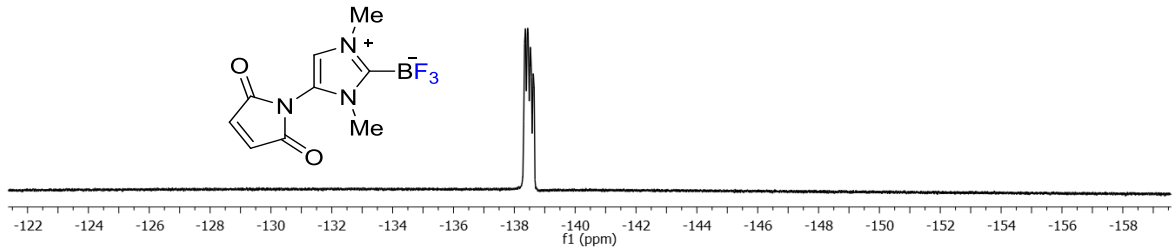

Figure 74. ^{1}H, ^{13}C, ^{11}B, and ^{19}F NMR spectra of **56** in CD_3CN.

^{1}H NMR

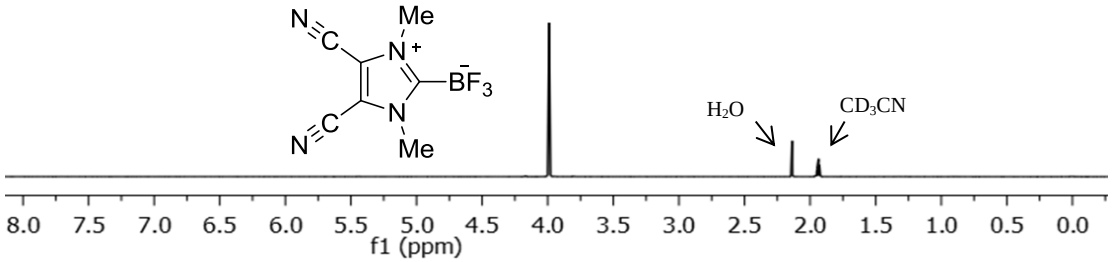

^{13}C NMR

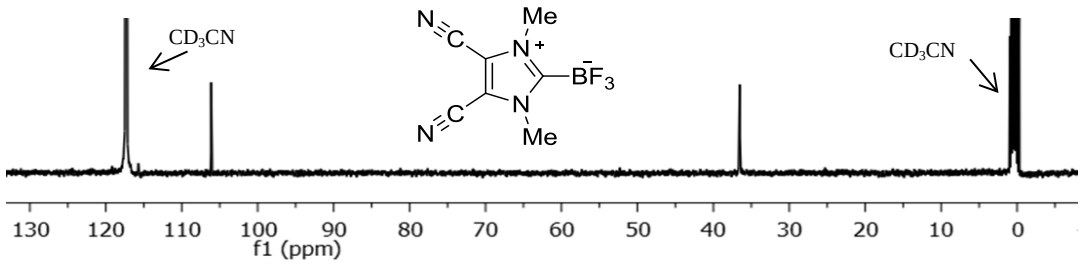

^{11}B NMR

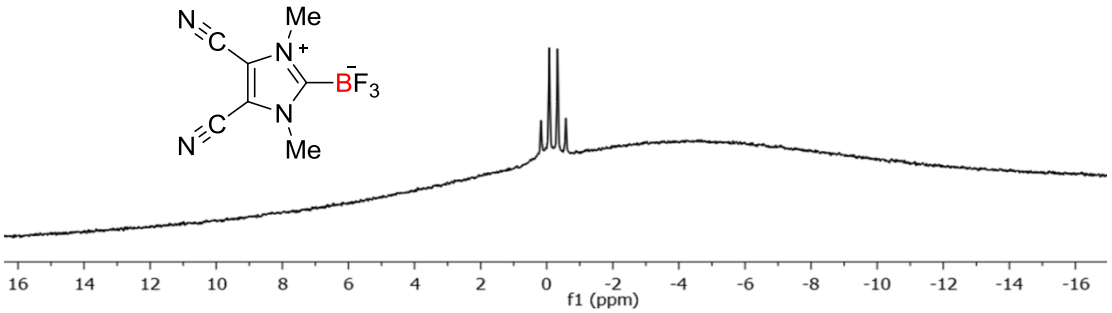

^{19}F NMR

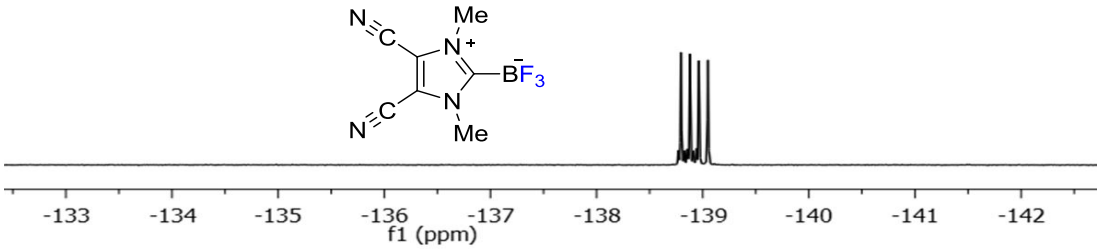

Figure 75. ^{1}H, ^{13}C, ^{11}B, and ^{19}F NMR spectra of **58** in CD_3CN.

Kinetic studies of the hydrolysis reactions

A sample of **49**, **51**, **52**, **54**, **55**, and **56** (5 mg) was dissolved in 0.2 mL CD_3CN and 1.0 mL D_2O phosphate buffer (pH 7.5, 500 mM). The ^{19}F NMR spectra of **49**, **51**, **52**, **54**, **55**, and **56** were collected periodically. The decomposition of aryltrifluoroborate species were monitored by integration of the decreasing aryltrifluoroborate signal in conjunction with the increasing signal corresponding to free F^-. All spectra were processed using the VNMRJ Version 2.2 NMR software. The rate constant, k_{obs}, was calculated using a well-established NMR method reported in the literature.[4] This method is based on the fact that that the concentration in $ArBF_3$ species is proportional to the ^{19}F NMR integration of $ArBF_3$ signal divided by the sum of the integration of $ArBF_3$ signal and the free fluoride signal. For convenience, the value of the $ArBF_3$ integration is arbitrarily set at 100 and the free fluoride integration determined. Based on the ^{19}F NMR results, free F^- NMR signal was only observed in the aqueous solution of **49**, **52**, and **54** after a week. The resulting data is provided in Table **S4**, **S5**, and **S6**.

Table 15. Kinetic data for the hydrolysis of **49**. The values provided for F^- and $ArBF_3$ correspond to the integration of the corresponding NMR signal.

		Data for **49**		
				k_{obs} = 1.2E-6
			exp. Ratio	calc. ratio
Time (min)	[F]	[BF3]	[BF3]/([BF3]+[HF]	[BF3]/([BF3]+[HF]
0	0.00	100	1.0000	1.0000
1141	0.34	100	0.9966	0.9986
2594	0.41	100	0.9959	0.9969
4152	0.48	100	0.9953	0.9950
9776	0.76	100	0.9925	0.9882
11000				0.9867
12000				0.9855
13000				0.9843
14000				0.9831
15000				0.9820

Table 16. Kinetic data for the hydrolysis of **52**. The values provided for F^- and $ArBF_3$ correspond to the integration of the corresponding NMR signal.

		Data for **52**		
				k_{obs} = 1.1E-6
			exp. Ratio	calc. ratio
Time (min)	[F]	[BF3]	[BF3]/([BF3]+[HF]	[BF3]/([BF3]+[HF]
0	0.00	100	1.0000	1.0000
1434	0.20	100	0.9980	0.9984
2884	0.31	100	0.9970	0.9968
4563	0.49	100	0.9952	0.9950
10126	0.91	100	0.9910	0.9889
11000				0.9880
12000				0.9869
13000				0.9858
14000				0.9847
15000				0.9837

Table 17. Kinetic data for the hydrolysis of **54**. The values provided for F^- and $ArBF_3$ correspond to the integration of the corresponding NMR signal.

		Data for **54**		
				k= 4.89E-7
			exp. Ratio	calc. ratio
Time (min)	[F]	[BF3]	[BF3]/([BF3]+[HF]	[BF3]/([BF3]+[HF]
0	0.00	100	1.0000	1.0000
1402	0.09	100	0.9991	0.9993
2851	0.11	100	0.9990	0.9986
4298	0.19	100	0.9981	0.9979
10032	0.53	100	0.9948	0.9951
11000				0.9946
12000				0.9941
13000				0.9937
14000				0.9932
15000				0.9927

Radiochemistry Experiment

All chemicals from commercial were of analytic grade and used without further purification. Analytical reversed-phase HPLC using a Gemini 5μ C18 column (250 x 4.6mm) was performed on a SPD-M30A photodiode array detector (Shimadzu) and model 105S single-channel radiation detector (Carroll & Ramsey Associates). The flow is set to 1mL/min. The mobile phase stayed at 95% solvent A and 5% solvent B from 0-2min and then changed with a gradient from 95% solvent A 5% solvent B to 95% solvent B and 5% solvent A in 20min. Solvent A is 0.1% TFA in water and solvent B is 0.1% TFA in acetonitrile.

Radiochemistry

The radio label reactions were carried out using the following protocol unless specified. **49** or **56** (0.61 μmol) was mixed with $SnCl_4$ (15 eq) in MeCN (10 μL). The resulting solution was then combined with a MeCN solution (30 μL) of [^{18}F]fluoride (40 ± 3mCi). After shaking at room temperature for 10 min, the reaction was quenched by adding 200 μL water. Then the mixture passed through a Sep-Pak cartridge (Sep-Pak Plus tC18) and washed with 3 mL water. The [^{18}F]**49** or [^{18}F]**56** was eluted off the cartridge with 1mL MeCN and an aliquot of the MeCN fraction (30 μCi) was taken for HPLC analysis. After HPLC purification, 0.1N NaOH was added to [^{18}F]**56** solution until the pH reaches 7. The resulting solution was then mixed with an aqueous solution of H-Cys-Phe-OH (200 μg, 0.75μmol). After shaking for 10 min at room temperature, a portion of the reaction mixture (0.01mCi) was loaded onto HPLC for further analysis

and purification. The HPLC containing [^{18}F]**56**/H-Cys-Phe-OH was collected and HPLC eluent was removed using a rotary evaporator. [^{18}F]**56**/H-Cys-Phe-OH was reconstituted in 1x PBS for stability test and small animal study.

In Vitro Stability

[^{18}F]**56**/H-Cys-Phe-OH was incubated in 1x PBS buffer at 37 °C. An aliquot of the solution (10μCi) was taken out and loaded on HPLC at 0.5h, 1h and 2h time point for analysis.

Small animal PET Imaging

Animal procedures were performed according to a protocol approved by the UNC institutional Animal Care and Use Committee. PET scans were performed using a small animal PET/CT scanner (Vista eXplore, GE Healthcare, Inc) with a center resolution of 1.2- and 4.6-mm axial field of view. A CT scan was first acquired for subsequent attenuation correction and anatomic registration. A normal nude mouse was anesthetized using 2% isoflurane and injected with 3.1MBq (86μCi) of [^{18}F]**56**-H-Cys-Phe-OH via tail vein. At 1, 2, and 4h post injection, static emission scans were acquired for 10-20min. Raw PET images were reconstructed using 2D ordered subset expectation maximization (OSEM) algorithms with scatter, random and attenuation correction.

CHAPTER V

TRIAZABOROLOPYRIDINIUMS FOR POSITRON EMISSION TOMOGRAPHY/ FLUORESCENCE DUAL MODALITY IMAGING

5.1 Introduction

Molecular imaging is a fast-growing research field enabling the visualization, characterization, and quantification of biological processes that occur in living subjects. Although a single imaging technique can offer some insight into a disease process, the combination of two or more modalities will eventually provide a diagnosis because each imaging modality has its own limitation(s). Positron Emission Tomography (PET) is one of the powerful techniques that can provide critical *in vivo* information on the distribution of radiolabeled biomolecules in a non-invasive diagnosis; however, this technique gives data with poor resolution. Optical fluorescence imaging is another essential technique that has been used for tumor detection and provides a good spatial resolution data; nonetheless, it is difficult to quantify.[90] Therefore, a system that combines these two imaging modalities could greatly benefit patient diagnosis.

Inspired by the potential synergistic properties of dual modality imaging agents that may be applied to clinical applications, our group has recently developed a radiofluorination protocol for BODIPY dyes.[18] Based on this approach, we found that the incorporation of ^{18}F into the dye could be performed from the corresponding hydroxide derivative in aqueous media at low pH. Subsequently, Weissleder and Mazitschek showed that the ^{18}F-radiolabeling could be processed by allowing the ^{18}F

fluoride anion to react with BODIPY dyes containing either a boron-triflate or boron-DMAP moiety.[19] Although the radioactive fluorescent dyes could be prepared in good radiochemical yields (61 – 67 %), the intermediate of an activated BODIPY dye with a labile hydroxide, triflate, or DMAP bound to a boron atom must be synthesized before radiofluorination (Figure 76). To circumvent the need for an activated dye, our group has investigated a new protocol for radiofluorination of BODIPY dyes by a Lewis acid-assisted isotopic ^{18}F-^{19}F exchange process. We found that $SnCl_4$ can be used to promote ^{18}F-radiolabeling of BODIPY dyes with high radiochemical yield (> 95%) (Figure 76). We also provide evidence that this Lewis acid-assisted approach can be used to prepare BODIPY dyes conjugated with peptides for use as PET/fluorescence cancer imaging probes. The chosen peptide can be connected to the BODIPY dye either before[20] or after[22] ^{18}F-radiofluorination.

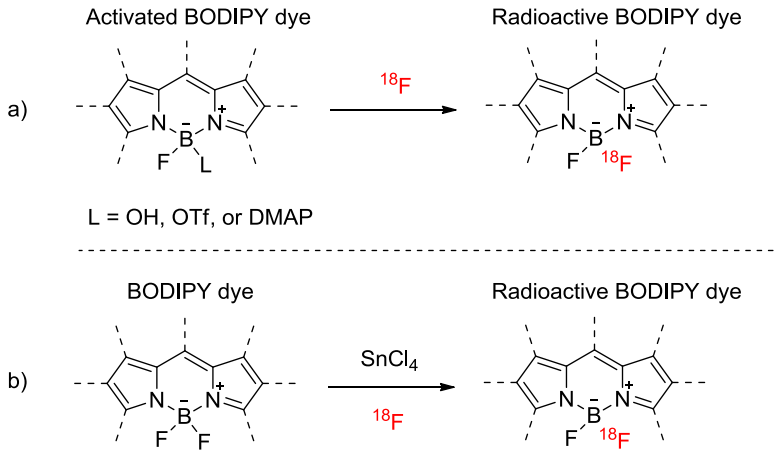

Figure 76. Scheme showing the radiofluorination of a BODIPY dye through a) an activated BODIPY dye, b) a Lewis acid-assisted isotopic ^{18}F-^{19}F exchange.

Although our major interest has focused on the methodological development of the radiofluorination of BODIPY-based PET/fluorescence dual modality imaging agents, we also question whether we can apply our approach to other boron-containing dyes. In 2011, Arterburn and coworker reported a new class of fluorescent dye called triazaborolopyridinium HPY (Figure 77), which can be easily synthesized from hydrazone precursors.[32] These HPY derivatives are ideal for our application as PET/Fluorescence dual modality agents because they are structurally related to BODIPY and share desirable characteristics such as cell permeability. In addition, the authors also demonstrated that the triazaborolopyridinium dyes are appropriate for use in the construction of small molecule probes. With these results in mind, we decided to synthesize novel triazaborolopyridinium derivatives with favorable photophysical properties by varying the hydrazone substituents and investigate their potential as PET/Fluorescence dual modality agents.

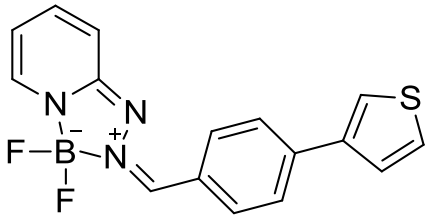

Figure 77. Illustration of the triazaborolopyridinium dye invented by Arterburn's group.

5.2 Synthesis and characterizations

First, we synthesized the hydrazone precursors **62**, **63**, and **64** by the reaction of 2-hydrazinylpyridine with aldehyde precursors (i.e., benzaldehyde for **62**, 4-(dimethylamino) benzaldehyde for **63**, and 4-nitrobenzaldehyde for **64**) in pyridine at 80 °C (Figure 78). The pale yellow powder of **62** and **63** and bright yellow powder of **64** were obtained in high yield (87% for **62**, 91% for **63**, and 75% for **64**). Their ^{1}H NMR spectra show the expected pyridyl and phenyl backbone resonances in the aromatic region (6 – 8 ppm). The NH signal was shifted downfield to 10.76 ppm for **62**, 10.48 ppm for **63**, and 11.30 ppm for **64**. These hydrazone compounds were used without further purification.

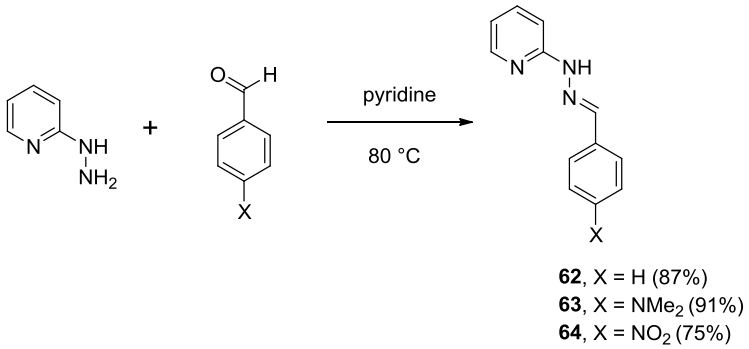

Figure 78. Scheme showing the synthesis of hydrazone precursors with different substituents.

Next, the triazaborolopyridinium dyes **65**, **66**, and **67** were synthesized by the reaction of the hydrazone precursors (**62**, **63**, **64**) with boron trifluoride diethyl etherate (BF_3OEt_2) in the presence of 1,8-diazabicyclo[5.4.0]undec-7-ene base (DBU) at an

elevated temperature (90 °C, Figure 79). After purification *via* silica gel column chromatography, **65** (yellow solid), **66** (orange solid), and **67** (red solid) were obtained in 56, 32, and 63 % yield, respectively. In addition, the nitro group in **67** can be reduced into the amine group by palladium-catalyzed hydrogenation in dichloromethane at room temperature. The amine-derivative dye **68** was obtained as a yellow solid in 72 % yield. These new dyes have been fully characterized. The existence of the BF_2 moiety has been confirmed by the detection of a triplet ^{11}B resonance at 3.43 ppm ($J_{B\text{-}F}$ = 30.51 Hz) for **65**, 3.28 ppm ($J_{B\text{-}F}$ = 30.77 Hz) for **66**, 3.52 ppm ($J_{B\text{-}F}$ = 29.87 Hz) for **67**, and 3.36 ppm ($J_{B\text{-}F}$ = 31.02 Hz) for **68**, as well as a quartet of ^{19}F resonance at -149.0 ppm ($J_{B\text{-}F}$ = 31.58 Hz) for **65**, -148.4 ppm ($J_{B\text{-}F}$ = 31.20 Hz) for **66**, -149.5 ppm ($J_{B\text{-}F}$ = 30.07 Hz) for **67,** and -148.7 ppm ($J_{B\text{-}F}$ = 31.01 Hz) for **68**. The disappearance of the ^1H NMR signal of N-H in **65**, **66**, and **67** indicated the formation of a BF_2 complex with the organic backbone. The appearance of the ^1H NMR signal of NH_2 in **68** confirmed that the nitro group in **67** was successfully reduced.

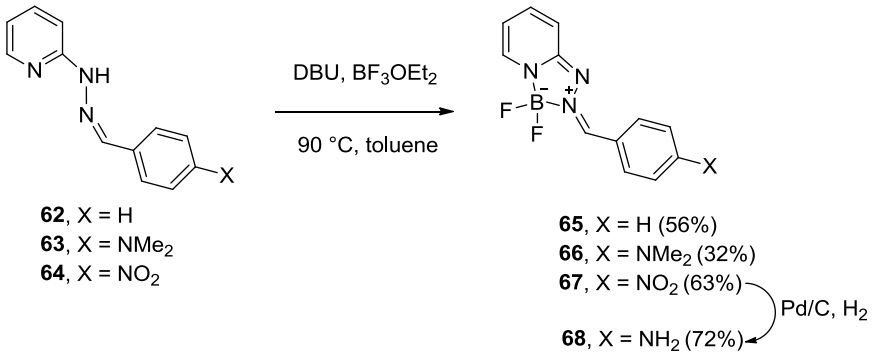

Figure 79. Scheme showing the synthesis of triazaborolopyridinium dyes **65**, **66**, **67**, and **68**.

The photophysical properties of these triazaborolopyridinium dyes have also been investigated. The synthesized HPY dyes exhibit absorption spectra with λ_{max} = 462 nm for **65**, 486 nm for **66**, 504 nm for **67**, and 475 nm for **68**. Further, these dyes exhibit emission spectra with λ_{emi} = 574 nm for **65**, 537 nm for **66**, 652 nm for **67**, and 533 nm for **68**. Compounds **65** and **67** give rise to large stoke shifts (112 nm for **65** and 148 nm for **67**), which facilitate signal detection and improves the resolution by separating the absorption and emission spectra in fluorescent imaging applications.[91] They also display high quantum yields, with Φ_f = 35% for **65** and 45% for **67**. In contrast, compounds **66** and **68** with an amino substituent give an expected low quantum yield (Φ_f = 1.5% for **66** and Φ_f = 2.4% for **68**) because of fluorescence quenching by the lone pair electrons on the amino functional group.

To eliminate fluorescence quenching, compound **66** was methylated with commercially available methyl trifluoromethanesulfonate (MeOTf) in diethyl ether at room temperature. The pale yellow powder was isolated in a 60 % yield. This compound has been fully characterized. The presence of the difluoroborate moiety has been confirmed by the detection of a triplet ^{11}B NMR resonance at 3.73 ppm (J_{B-F} = 23.72 Hz) and a quartet ^{19}F NMR resonance at -145.7 ppm (J_{B-F} = 25.56 Hz). Notably, the ^{1}H NMR spectrum showed two singlet signals at 3.19 and 3.69 ppm, corresponding to a dimethyl amino group and a monomethyl substituent, respectively, suggesting that the dimethyl amino (NMe_2) group was not methylated (Figure 80).

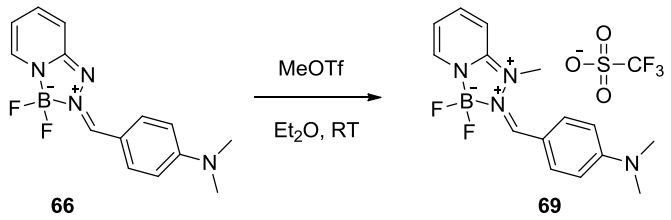

Figure 80. Scheme showing the synthesis of compound **69**.

The structure of this compound, which was analyzed by single crystal X-ray crystallography, revealed that the methyl group attached to the nitrogen atom in the five-membered ring instead of the nitrogen atom in the dimethyl amino moiety (Figure 81). These results are consistent with photophysical properties that this compound is non-fluorescence because of the effect of the remaining lone-pair electrons on the NMe_2 group.

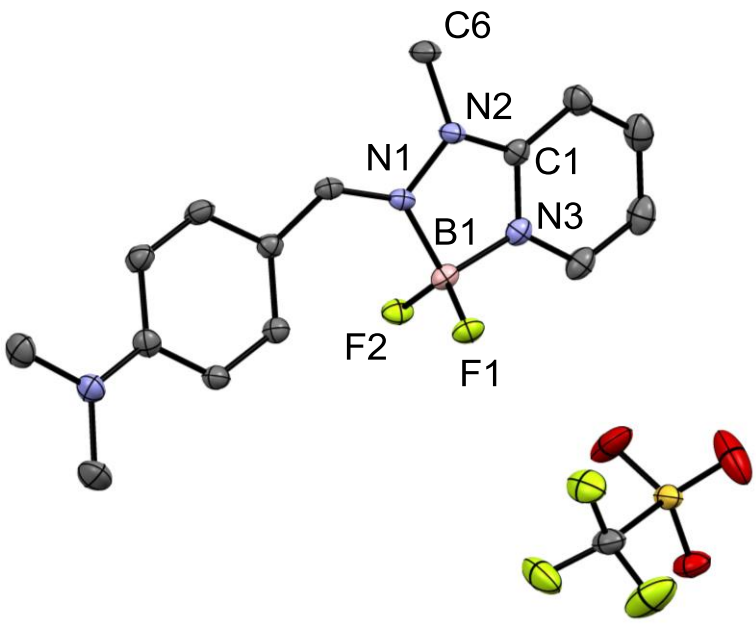

Figure 81. Crystal structure of **69**. Displacement ellipsoids are scaled to the 50% probability level and hydrogen atoms have been omitted for clarity. Selected bond lengths (Å) and angles (deg) for **69**: B1-F1 1.371(3), B1-F2 1.367(3), B1-N1 1.596(3), B1-N3 1.561(3), N1-N2 1.402(2), N2-C1 1.350(3), N3-C1 1.354(3), N2-C6 1.450(3); F1-B1-F2 111.9(2), N1-B1-N3 96.45(17), B1-N1-N2 108.89(17), B1-N3-C1 111.65(18), N1-N2-C1 110.71(18), N2-C1-N3 111.90(19).

Previously, we reported that activated BODIPY dyes with a labile hydroxide group as well as DMAP bound to a boron centre were successfully prepared. Presently, we question whether our new HPY dyes can be activated using the same approaches. To prove our hypothesis, we decided to synthesize the HPY-DMAP adducts *via* the reaction of BF_2-HPY dyes (**65**, **66**, **67,** and **68)** with TMSOTf in CH_3CN followed by the addition of DMAP at room temperature. Unfortunately, only the **5**-DMAP adduct (**70**) was successfully isolated as a red solid in a 57 % yield (Figure 82).

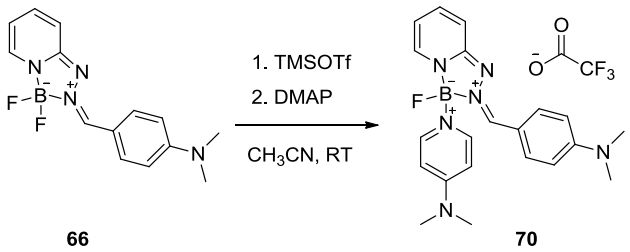

Figure 82. Scheme showing the synthesis of compound **70**.

This boron-DMAP adduct **70** was fully characterized by NMR spectroscopy and single crystal X-ray crystallography. The ^{11}B NMR spectrum presents a doublet signal at 4.12 ppm ($J_{B\text{-}F}$ = 39.35 Hz), indicating that one of the B-F bonds has been activated. The ^{19}F NMR spectrum displays a singlet resonance at -78.12 ppm and a quartet resonance at -161.0 ppm ($J_{B\text{-}F}$ = 40.60 Hz) corresponding to the triflate and BF units, respectively. The short B(1)–N(4) separation of 1.560(3) Å in the crystal structure (Figure 83) suggests a strong coordination of DMAP ligand.

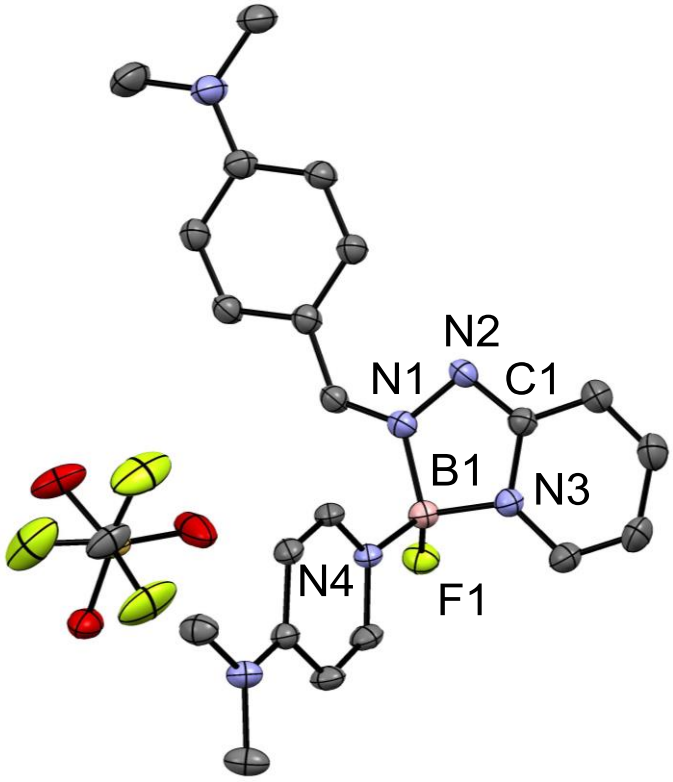

Figure 83. Crystal structure of **70**. Displacement ellipsoids are scaled to the 50% probability level and hydrogen atoms have been omitted for clarity. Selected bond lengths (Å) and angles (deg) for **70**: B1-F1 1.377(3), B1-N4 1.560(3), B1-N1 1.531(3), B1-N3 1.557(3), N1-N2 1.401(3), N2-C1 1.333(3), N3-C1 1.374(3); F1-B1-N4 108.6(2), N1-B1-N3 97.08(19), B1-N1-N2 112.81(19), B1-N3-C1 108.4(2), N1-N2-C1 105.13(19), N2-C1-N3 116.5(2).

As we have already examined that the HPY dye **67** with a nitro substituent gives the highest quantum yield among our newly synthesized HPY dyes, we decided to use this organic backbone (**64**) to synthesize an activated HPY dye with a labile hydroxide group bound to a boron atom. This new derivative was prepared by the reaction of **64** with $PhBCl_2$ in the presence of DBU base at 90 °C in toluene (Figure 84). After column purification, the red powder of **71** was obtained in a 35 % yield. The presence of the B-OH moiety was confirmed by the detection of a broad singlet ^{11}B NMR resonance at 7.22 ppm. The ^{1}H NMR spectrum shows the expected pyridyl and phenyl backbone resonances in the aromatic region (6 – 8 ppm). The photophysical properties of this derivative have also been determined. The compound **71** displays strong absorption maxima at 500 nm and emission maxima at 649 nm and possesses a large stoke shift of 149 nm. In addition, it exhibits a high quantum yield with Φ_f = 50 %, which is greater than the BF_2 analogue (**67**).

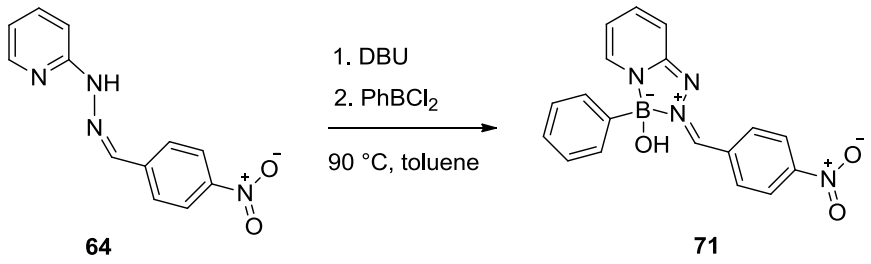

Figure 84. Scheme showing the synthesis of HPY dye **71**.

5.3 Fluorination and aqueous stability of the dyes

In 2008, Gabbai and coworkers reported that the BODIPY-DMAP adduct reacted with fluoride anions to form the corresponding difluoride species.[16] This protocol is significant because it can be used for fluorescent 'turn-on' sensing of fluoride ions. Moreover, it is the first example to demonstrate F^- incorporation into a BODIPY dye. Thus, this approach can be used as a model for the synthesis of PET/Fluorescence dual modality imaging agents. Subsequently, Mazitschek and coworkers investigated the ^{18}F-incorporation reaction of our reported BODIPY-DMAP adduct. They discovered that [^{18}F]-BODIPY can be efficiently prepared at high temperature (100 °C) in DMF. Inspired by these results, we decided to investigate whether our new HPY-DMAP adduct (**70**) could be implemented by similar approach. We were very pleased to find that **70** can indeed be transformed to the corresponding difluoride species (**66**) by the addition of KHF_2 (excess) at 60 °C (Figure 85). As monitored by ^{11}B NMR spectroscopy, 37 % of **70** was transformed to **66** in 20 min (Figure 86). This result is noteworthy because we have shown that the fluorination of an HPY-dye can be achieved in a short reaction time, which is suitable for ^{18}F-incorporation. Finally, **66** was produced in 80 % yield (calculated by integration of ^{11}B NMR signal) at elevated temperature for 5 h.

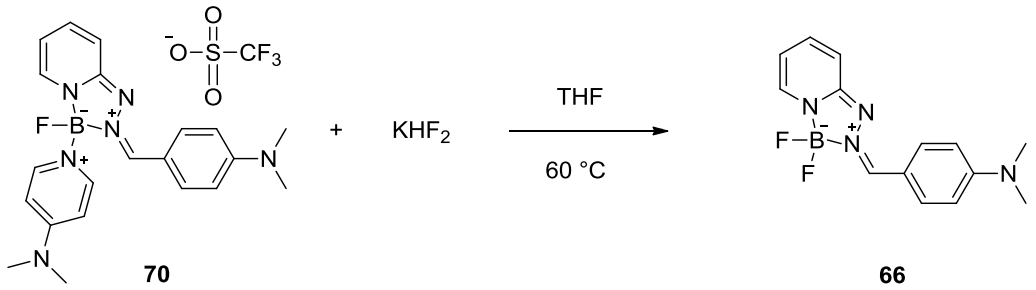

Figure 85. Scheme showing the fluorination of compound **70**.

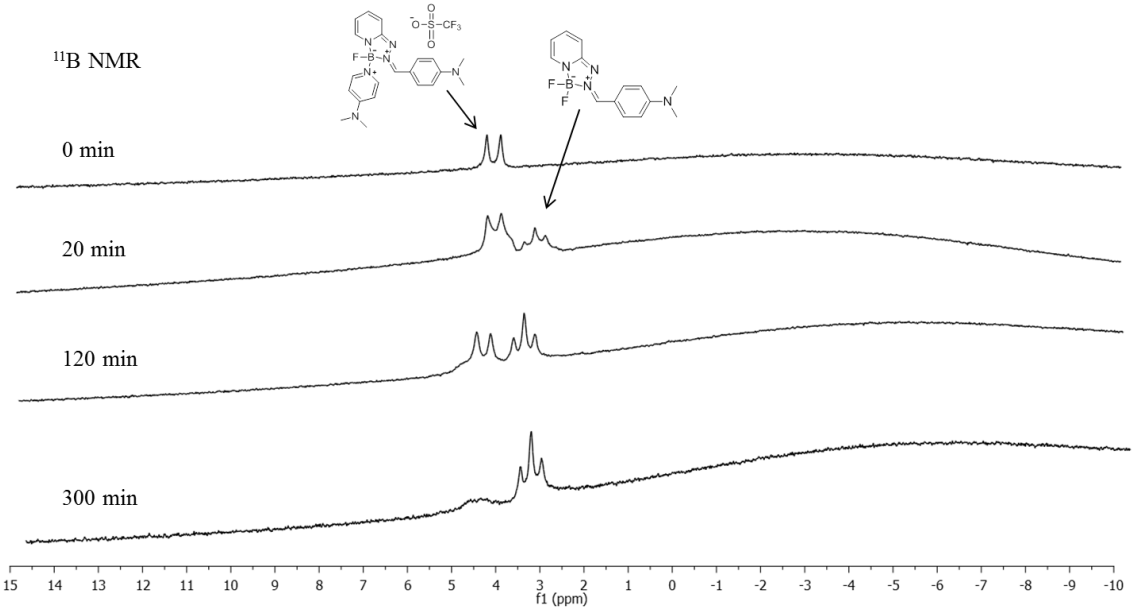

Figure 86. ^{11}B NMR spectra of the fluorination reaction of **70** at different reaction times.

Likewise, Gabbai and coworkers also showed that ^{18}F fluoride anions can be incorporated into the novel ammonium BODIPY-phenylboron hydroxide in aqueous solution.[18] Moreover, they demonstrated that this new [^{18}F]-BODIPY dye is stable *in vivo*. Encouraged by this research, we decided to examine whether our new HPY-

phenylboron hydroxide dye could undergo fluorination to form the corresponding HPY-phenylboron fluoride dye. To achieve this goal, **71** was reacted with an excess of KHF_2 in THF at 60 °C (Figure 87), and the reaction was monitored by ^{19}F NMR spectroscopy. Gratifyingly, the ^{19}F NMR signal of the corresponding HPY-phenylboron fluoride (**72**) was observed at -166 ppm after 20 min. The new HPY-phenylboron fluoride dye was isolated after continuing the reaction overnight to ensure that the fluorination was complete. The photophysical properties of this new dye are typical of HPY dyes. It features a board absorption band centered at 500 nm and an emission band centered at 654 nm with a quantum yield of 55 %. Based on the results of the fluorination of **70** and **71**, we can conclude that these HYP dyes are the new candidates for the design of an alternative PET/Fluorescence dual modality imaging agents.

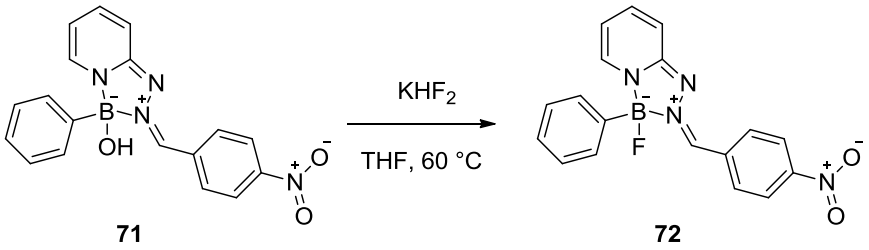

Figure 87. Scheme showing the fluorination of compound **71**.

In addition, we decided to investigate the rate of hydrolysis of our new HPY dyes in aqueous solution. To complete this objective, **65**, **66**, **67**, and **68** were dissolved in 10% w/v triton X-100 in H_2O/ DMSO (7/3 vol) at pH = 7.5 ([phosphate buffer] = 500 mM, [BF_2-dye] = 20 mM with BF_2-dye = HPY dyes). The hydrolysis reactions of the

HPY dyes (**65**, **66**, **67**, and **68**) were monitored periodically by ^{19}F NMR spectroscopy. Based on the kinetic data shown in Figure 88, the first order hydrolysis rate constants (k_{obs}) of the HPY dyes were calculated to be 7.3 x 10^{-4} min^{-1} for **65**, 2.1 x 10^{-4} min^{-1} for **66**, 4.8 x 10^{-4} min^{-1} for **67**, and 3.0 x 10^{-4} min^{-1} for **68**, which are comparatively less stable than our reported *ortho*-phosphonium aryltrifluoroborate[79,80] and *ortho*-ammonium aryltrifluoroborate.[80] However, these HPY dyes are slightly more stable than *ortho*-sulfonium aryltrifluoroborate[80]. Although these results suggest that the HPY dyes are less stable than the reported zwitterionic aryltrifluoroborates and conventional BODIPY dyes, they confirm that subtle structural changes have an impact on the stability of the complexes.

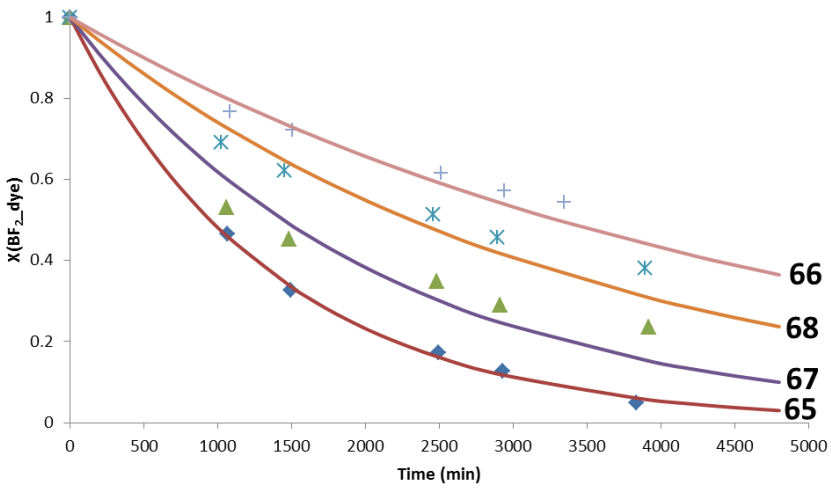

Figure 88. Kinetic plots for the hydrolysis of **65**, **66**, **67**, and **68**. The data were obtained at room temperature in 10% w/v triton X-100 in H_2O/ DMSO (7/3 vol) at pH = 7.5.

5.4 Conclusion

In this study, we have demonstrated that novel triazaborolopyridinium HPY dyes can be easily prepared from hydrazone precursors. The photophysical properties of these dyes are varied based on the nature of the substituent. HPY dyes with an electron-withdrawing nitro group feature high quantum yields and large stoke shifts, which are suitable characteristics for imaging applications. We have also successfully prepared activated HPY dyes, a DMAP-HPY adduct (**70**) and a boron-hydroxide HPY dye (**71**) for the fluorination test. Gratifyingly, the activated dyes **70** and **71** can be fluorinated in a short reaction time, which makes them viable for the ^{18}F-fluorination reaction. Although the HPY dyes have been shown to be potential candidates for application in a PET/Fluorescence dual modality, the low stability of these dyes in aqueous solution might create a major problem for *in vivo* imaging studies because of ^{18}F-defluorination. Therefore, the stability of these dyes must be optimized before the further development of PET imaging applications.

5.5 Experimental

General Consideration

Boron trifluoride diethyl etherate (BF_3OEt_2), dichlorophenylborane ($BPhCl_2$), 4-dimethylaminopyridine (DMAP), methyl trifluoromethanesulfonate (MeOTf), and 10% palladium on carbon (Pd/C) were purchased from Alfar Aesar; 4-(dimethylamino) benzaldehyde and 4-nitrobenzaldehyde were purchased from Sigma Aldrich; 2-hydrazinylpyridine was purchased from Ark Pharm, Inc; 1,8-Diazabicyclo[5.4.0]undec-

7-ene (DBU) was purchased from TCI America; pyridine was purchased from EMD chemicals, Inc; trimethylsilyl trifluoromethanesulfonate (TMSOTf) was purchased from Oakwood Products, Inc. All chemicals were used without further purification except for BF_3OEt_2. BF_3OEt_2 was dried over CaH_2. Solvents were dried by passing through an alumina column (CH_2Cl_2 and toluene), refluxing under N_2 over Na (Et_2O and THF), refluxing under N_2 over CaH_2 (CH_3CN). Electrospray mass spectra were acquired from a MDS Sciex API QStar Pulsar. NMR spectra were recorded on a Varian Unity Inova 400 NMR and an Inova 500B spectrometer at ambient temperature. Chemical shifts are given in ppm, and are referenced to residual ^1H and ^{13}C solvent signals as well as external BF_3-Et_2O (^{11}B NMR and ^{19}F NMR).

*Synthesis of 2-(2-benzylidenehydrazinyl)pyridine (**62**)*

A solution of 2-hydrazinylpyridine (0.4285 g, 3.924 mmol) and benzaldehyde (0.40 mL, 3.920 mmol) in pyridine (20 mL) was stirred at 80 °C for 18 h. Next, the solvent was removed under reduced pressure. The residue was dissolved in ethyl acetate (50 mL) and washed with saturated $NaHCO_3$ solution (50 mL) followed by water (2 x 50 mL). The organic layer was dried over anhydrous $MgSO_4$ and removed in *vacuo* affording **62** as a pale yellow solid (0.6705 g, 87 %). **^{1}H NMR** (399.5 MHz, DMSO -d_6): δ 6.72 (ddd, 1H, J = 7.59, 5.19, and 0.92 Hz), 7.20 (d, 1H, J = 8.79), 7.28 (m, 1H), 7.36 (m, 2H), 7.60 (m, 3H), 7.97 (s, 1H, =C*H*-), 8.05 (ddd, 1H, J = 4.79, 1.76, and 0.72 Hz), 10.76 (s, 1H, N*H*). **^{13}C NMR** (125.6 MHz, DMSO-d_6): δ 106.74, 115.41, 126.37,

128.93, 129.16, 135.83, 138.36, 139.16, 148.22, 157.50. MS (ESI^+) calcd for $[M+H]^+$: 198.1031, found: 198.0995.

*Synthesis of N,N-dimethyl-4-((2-(pyridin-2-yl)hydrazono)methyl)aniline (**63**)*

A solution of 2-hydrazinylpyridine (0.5645 g, 5.173 mmol) and 4-(dimethylamino) benzaldehyde (0.6559 g, 4.396 mmol) in pyridine (20 mL) was stirred at 80 °C for 18 h. Next, the solvent was removed under reduced pressure. The residue was dissolved in ethyl acetate (50 mL) and washed with saturated $NaHCO_3$ solution (50 mL) followed by water (2 x 50 mL). The organic layer was dried over anhydrous $MgSO_4$ and removed in *vacuo* affording **63** as a pale yellow solid (0.9660 g, 91 %). **^{1}H NMR** (399.5 MHz, DMSO-d_6): δ 2.90 (s, 6H, -CH_3), 6.65 (ddd, 1H, pyridinium-C*H*, *J* = 7.19, 4.79, and 1.04 Hz), 6.69 (d, 2H, phenyl-C*H*, *J* = 8.79 Hz), 7.13 (d, 1H, pyridinium-C*H*, *J* = 8.39 Hz), 7.44 (d, 2H, phenyl-C*H*, *J* = 8.79 Hz), 7.55 (ddd, 1H, pyridinium-C*H*, *J* = 8.79, 6.79, and 1.76 Hz), 7.88 (s, 1H, =C*H*-), 8.03 (ddd, 1H, pyridinium-C*H*, *J* = 5.19, 1.84, and 1.24 Hz), 10.48 (s, 1H, N*H*).**^{13}C NMR** (100.5 MHz, DMSO-d_6): δ 40.33, 106.39, 112.45, 114.56, 123.53, 127.58, 138.15, 140.36, 148.14, 151.00, 157.78. MS (ESI^+) calcd for $[M+H]^+$: 241.1453, found: 241.1494.

*Synthesis of 2-(2-(4-nitrobenzylidene)hydrazinyl)pyridine (**64**)*

A solution of 2-hydrazinylpyridine (0.6239 g, 5.718 mmol) and 4-nitrobenzaldehyde (0.8640g, 5.718 mmol) in pyridine (20 mL) was stirred at 80 °C for 18 h. Then, the solvent was removed under reduced pressure. The solid residue was suspended in CH_2Cl_2 (50 mL) and the suspension was filtered. The resulting powder was washed by CH_2Cl_2 (2 x 50 mL) yielding **64** as a yellow solid (1.0347 g, 75 %). **^{1}H NMR** (499.4 MHz, DMSO-d_6): δ 6.83, (dd, 1H, pyridinium-C*H*, *J* = 7.99, 5.99 Hz), 7.32 (d, 1H, pyridinium-C*H*, *J* = 8.49 Hz), 7.68 (dd, 1H, pyridinium-C*H*, *J* = 8.99, 7.49 Hz), 7.89 (d, 2H, phenyl-C*H*, *J* = 8.49 Hz), 8.09 (s, 1H, =C*H*-), 8.15 (d, 1H, pyridinium-C*H*, *J* = 4.64 Hz), 8.22 (d, 2H, phenyl-C*H*, *J* = 8.49 Hz), 11.30 (s, 1H, N*H*). **^{13}C NMR** (100.5 MHz, DMSO-d_6): δ 107.20, 116.40, 124.50, 126.95, 136.45, 138.59, 142.40, 146.94, 148.31, 156.91. MS (ESI^+) calcd for $[M+H]^+$: 243.0882, found: 243.0945.

*Synthesis of 2-benzylidene-3,3-difluoro-2,3-dihydro-[1,2,4,3]triazaborolo[4,5-a]pyridin-2-ium-3-uide (**65**)*

BF_3OEt_2 (0.60 mL, 4.862 mmol) was added dropwise to a solution of **62** (0.2006 g, 1.018 mmol) and 1,8-diazabicycloundec-7-ene (DBU) (0.45 mL, 3.015 mmol) in anhydrous toluene (15 mL) at room temperature. The mixture was heated at 90 °C for 12 h. Then, the reaction mixture was quenched with water (5 mL) and the product was extracted with CH_2Cl_2 (2 x 50 mL). The combined organic layers were washed with water (3 x 50 mL), dried over anhydrous $MgSO_4$, and removed under reduced pressure, respectively. The solid residue was purified by silica gel column chromatography using

CH_2Cl_2 as an eluent. The purified product (0.1383 g) was obtained as **65** in a 56 % yield. **^{1}H NMR** (399.5 MHz, $CDCl_3$): δ 6.35 (dd, 1H, pyridinium-C*H*, *J* = 7.19, 6.79 Hz), 6.79 (d, 1H, pyridinium-C*H*, *J* = 9.19 Hz), 7.38 – 7.47 (m, 5H), 7.52 (d, 1H, pyridinium-C*H*, *J* = 6.39 Hz), 8.34 (m, 2H). **^{13}C NMR** (100.5 MHz, $CDCl_3$): δ 109.21, 112.11, 127.80, 131.06, 131.53, 134.67, 138.65, 140.29. **^{11}B NMR** (128.2 MHz, $CDCl_3$): δ 3.43 (t, $J_{B\text{-}F}$ = 30.51 Hz). **^{19}F NMR** (375.9 MHz, $CDCl_3$): δ -149.0 (q, $J_{B\text{-}F}$ = 31.58 Hz). MS (ESI^+) calcd for $[M+H]^+$: 246.1014, found: 246.0999.

*Synthesis of 2-(4-(dimethylamino)benzylidene)-3,3-difluoro-2,3 dihydro[1,2,4,3] triazaborolo [4,5-a]pyridin-2-ium-3-uide (**66**)*

BF_3OEt_2 (1.00 mL, 8.103 mmol) was added dropwise to a solution of **63** (0.4142 g, 1.726 mmol) and 1,8-diazabicycloundec-7-ene (DBU) (0.77 mL, 5.159 mmol) in anhydrous toluene (15 mL) at room temperature. The mixture was heated at 90 °C for 12 h. Then, the reaction mixture was quenched with water (5 mL) and the product was extracted with CH_2Cl_2 (2 x 50 mL). The combined organic layers were washed with water (3 x 50 mL), dried over anhydrous $MgSO_4$, and removed under reduced pressure, respectively. The solid residue was purified by silica gel column chromatography using CH_2Cl_2 as an eluent. The purified product (0.1590 g) was obtained as **66** in a 32 % yield. **^{1}H NMR** (399.5 MHz, $CDCl_3$): δ 3.02 (s, 6H, -C*H*$_3$), 6.17 (dd, 1H, pyridinium-C*H*, *J* = 7.19, 6.39 Hz), 6.65 (d, 2H, phenyl-C*H*, *J* = 9.19 Hz), 6.66 (dd, 1H, pyridinium-C*H*, *J* = 9.59, 7.19 Hz), 7.24 (ddd, 1H, pyridinium-C*H*, *J* = 9.59, 6.39, and 1.60 Hz), 7.31 (s, 1H, =C*H*-), 7.41 (d, 1H, pyridinium-C*H*, *J* = 6.39 Hz), 8.22 (d, 2H, phenyl-C*H*, *J* = 9.19 Hz).

^{13}C NMR (125.6 MHz, $CDCl_3$): δ 29.72, 40.00, 108.52, 111.29, 113.01, 118.08, 135.13, 135.38, 139.78, 141.54, 152.65, 161.21. **^{11}B NMR** (128.2 MHz, $CDCl_3$): δ 3.28 (t, $J_{B\text{-}F}$ = 30.77 Hz). **^{19}F NMR** (375.9 MHz, $CDCl_3$): δ -148.4 (q, $J_{B\text{-}F}$ = 31.20 Hz). MS (ESI^+) calcd for $[M+H]^+$: 289.1436, found: 289.1351.

*Synthesis of 3,3-difluoro-2-(4-nitrobenzylidene)-2,3-dihydro-[1,2,4,3]triazaborolo[4,5-a]pyridin-2-ium-3-uide (**67**)*

BF_3OEt_2 (1.00 mL, 8.103 mmol) was added dropwise to a suspension of **64** (0.3754 g, 1.550 mmol) and 1,8-diazabicycloundec-7-ene (DBU) (0.70 g, 4.690 mmol) in anhydrous toluene (15 mL) at room temperature. After being stirred at 90 °C for 2 h, all precursors are completely dissolved. The red solution was stirred at elevated temperature for 12 h. Then, the reaction mixture was quenched with water (5 mL) and the product was extracted with CH_2Cl_2 (2 x 50 mL). The combined organic layers were washed with water (3 x 50 mL), dried over anhydrous $MgSO_4$, and removed under reduced pressure, respectively. The solid residue was purified by silica gel column chromatography using CH_2Cl_2 as an eluent. The purified product (0.2855 g) was obtained as **67** in a 63 % yield. **^{1}H NMR** (499.4 MHz, $CDCl_3$): δ 6.53 (dd, 1H, pyridinium-C*H*, *J* = 6.99, 6.49 Hz), 6.91 (d, 1H, pyridinium-C*H*, *J* = 8.99 Hz), 7.41 (s, 1H, =C*H*-), 7.55 (dd, 1H, pyridinium-C*H*, *J* = 8.99, 7.49 Hz), 7.63 (d, 1H, pyridinium-C*H*, *J* = 5.99 Hz), 8.27 (d, 2H, phenyl-C*H*, *J* = 8.49 Hz), 8.52 (d, 2H, phenyl-C*H*, *J* = 8.99 Hz). **^{13}C NMR** (100.5 MHz, $CDCl_3$): δ 111.06, 112.55, 122.81, 123.30, 129.47, 131.65, 133.66, 134.69, 135.21, 141.55. **^{11}B NMR** (128.2 MHz, $CDCl_3$): δ 3.52 (t, $J_{B\text{-}F}$ =

29.87 Hz). **^{19}F NMR** (469.9 MHz, $CDCl_3$): δ -149.5 (q, $J_{B\text{-}F}$ = 30.07 Hz). MS (ESI^+) calcd for $[M+H]^+$: 291.0865, found: 291.0973.

*Synthesis of 2-(4-aminobenzylidene)-3,3-difluoro-2,3-dihydro-[1,2,4,3]triazaborolo[4,5-a] pyridine-2-ium-3-uide (**68**)*

10% palladium on carbon (0.0410 g, 0.0385 mmol Pd) was added to a solution of **67** (0.1118 g, 0.0385 mmol) in CH_2Cl_2 (20 mL). Hydrogen gas was bubbled through the solution for 30 min. The mixture was stirred under hydrogen atmosphere overnight at room temperature. Then, it was filtered over celite and the solvent was removed under vacuum yielding **68** (0.0726 g, 72 %) as a yellow solid. **^{1}H NMR** (399.5 MHz, $CDCl_3$): δ 6.24 (dd, 1H, pyridinium-C*H*, *J* = 7.19, 5.99 Hz), 6.66 (d, 2H, phenyl-C*H*, *J* = 8.79 Hz), 6.73 (d, 1H, pyridinium-C*H*, *J* = 8.79 Hz), 7.30 (ddd, 1H, pyridinium-C*H*, *J* = 9.19, 6.79, and 1.64 Hz), 7.31 (s, br, 1H, =C*H*-), 7.45 (d, 2H, phenyl-C*H*, *J* = 5.99 Hz), 8.17 (d, 2H, phenyl-C*H*, *J* = 8.79 Hz). **^{13}C NMR** (100.5 MHz, $CDCl_3$): δ 108.87, 112.94, 114.27, 135.31, 135.41, 140.16, 141.01, 150.46. **^{11}B NMR** (128.2 MHz, $CDCl_3$): δ 3.36 (t, $J_{B\text{-}F}$ = 31.02 Hz). **^{19}F NMR** (469.9 MHz, $CDCl_3$): δ -148.7 (q, $J_{B\text{-}F}$ = 31.01 Hz). MS (ESI^+) calcd for $[M+H]^+$: 261.1123, found: 261.1173.

*Synthesis of 2-(4-(dimethylamino)benzylidene)-3,3-difluoro-1-methyl-2,3-dihydro-[1,2,4,3] triazaborolo[4,5-a]pyridine-1,2-diium-3-uide 2,2,2-trifluoroacetate (**69**)*

MeOTf (0.036 mL, 0.328 mmol) was added to a solution of **66** (0.0473 g, 0.164 mmol) in Et_2O (5 mL). The reaction mixture was stirred at room temperature. After being stirred overnight, the pale yellow solid precipitated. The solid was collected by filtration affording **69** (0.0411 g) in a 60 % yield. **^{1}H NMR** (399.5 MHz, CD_3CN): δ 3.19 (s, 6H, -CH_3), 3.69 (s, 3H, -CH_3), 6.92 (d, 2H, phenyl-C*H*, *J* = 9.19 Hz), 7.23 (dd, 1H, pyridinium-C*H*, *J* = 7.59, 6.79 Hz), 7.31 (d, 1H, pyridinium-C*H*, *J* = 9.19 Hz), 7.99 (d, 2H, phenyl-C*H*, *J* = 9.19 Hz), 8.18 (d, 1H, pyridinium-C*H*, *J* = 6.39 Hz), 8.20 (ddd, 1H, pyridinium-C*H*, *J* = 9.59, 7.19, and 1.52 Hz), 8.23 (s, br, 1H, =C*H*-). **^{13}C NMR** (100.5 MHz, CD_3CN): δ 33.32, 39.91, 57.29, 108.98, 112.16, 112.75, 117.19, 136.24, 137.15, 146.42, 151.72, 156.06. **^{11}B NMR** (128.2 MHz, CD_3CN): δ 3.73 (t, $J_{B\text{-}F}$ = 23.72 Hz). **^{19}F NMR** (375.9 MHz, CD_3CN): δ -78.41 (trifluoroacetate salt), -145.7 (q, $J_{B\text{-}F}$ = 25.56 Hz). MS (ESI^+) calcd for $[M]^+$: 303.1492, found: 303.1659.

*Synthesis of 2-(4-(dimethylamino)benzylidene)-3-(4-(dimethylamino)pyridin-1-ium-1-yl)-3-fluoro-2,3-dihydro-[1,2,4,3]triazaborolo[4,5-a]pyridin-2-ium-3-uide 2,2,2-trifluoro acetate (**70**)*

Compound **66** (0.0557 g, 0.193 mmol) in CH_3CN (3 mL) was treated with trimethylsilyl trifluoromethanesulfonate (TMSOTf) (0.035 mL, 0.193 mmol) and 4-dimethylaminopyridine (DMAP) (0.0243 g, 0.193 mmol), respectively. The reaction mixture was stirred at room temperature for 10 h. Then, the solution was concentrated in

vacuo to a volume of 1 mL. To the concentrated solution, was added Et_2O (10 mL) which resulted in the precipitation of a red solid. The red solid was washed by Et_2O (3 x 10 mL) yielding **70** (0.0555 g) in a 57 % yield. **^{1}H NMR** (499.4 MHz, $CDCl_3$): δ 3.12 (s, 6H, -C*H*$_3$), 3.24 (s, 6H, -C*H*$_3$), 6.25 (dd, 1H, pyridinium-C*H*, *J* = 7.99, 6.49 Hz), 6.71 (d, 2H, phenyl-C*H*, *J* = 9.49 Hz), 6.80 (d, 2H, phenyl-C*H*, *J* = 9.49 Hz), 6.88 (d, 2H, phenyl-C*H*, *J* = 7.49 Hz), 7.18 (d, 1H, pyridinium-C*H*, *J* = 6.49 Hz), 7.29 (s, 1H, =C*H*-), 7.34 (ddd, 1H, pyridinium-C*H*, *J* = 9.49, 6.99, and 1.05 Hz), 7.90 (d, 2H, phenyl-C*H*, *J* = 6.99 Hz), 8.04 (s, br, 1H, pyridinium-C*H*). **^{13}C NMR** (125.6 MHz, $CDCl_3$): δ 40.03, 40.19, 107.02, 108.26, 109.64, 111.43, 113.39, 117.05, 119.49, 122.05, 134.13, 136.65, 139.12, 140.21, 140.85, 140.89, 145.09, 153.78, 157.21, 160.98. **^{11}B NMR** (128.2 MHz, $CDCl_3$): δ 4.12 (d, $J_{B\text{-}F}$ = 39.35 Hz). **^{19}F NMR** (375.9 MHz, $CDCl_3$): δ -78.12 (trifluoroacetate salt), -161.0 (q, $J_{B\text{-}F}$ = 40.60 Hz). MS (ESI^+) calcd for $[M]^+$: 391.2218, found: 391.2358.

*Synthesis of 3-hydroxy-2-(4-nitrobenzylidene)-3-phenyl-2,3-dihydro-[1,2,4,3]triaza-borolo[4,5-a]pyridin-2-ium-3-uide (**71**)*

$PhBCl_2$ (0.20 mL, 1.544 mmol) was added dropwise to a suspension of **64** (0.1805 g, 0.745 mmol) and 1,8-diazabicycloundec-7-ene (DBU) (0.35 mL, 2.345 mmol) in anhydrous toluene (15 mL) at room temperature. The mixture was heated at 90 °C for 12 h. Then, the reaction mixture was quenched with water (5 mL) and the solvent was removed under reduced pressure. The product was extracted with CH_2Cl_2 (2 x 50 mL). The combined organic layers were washed with water (3 x 50 mL), dried over anhydrous $MgSO_4$, and removed under reduced pressure, respectively. The solid residue was purified by silica gel column chromatography using CH_2Cl_2 as an eluent. The purified product (0.0921g) was obtained as **71** in a 35 % yield. **^{1}H NMR** (399.5 MHz, $CDCl_3$): δ 6.48 (dd, 1H, pyridinium-C*H*, *J* = 7.59, 6.79 Hz), 6.98 (d, 1H, pyridinium-C*H*, *J* = 9.19 Hz), 7.28 (m, 4H), 7.47 (m 3H), 7.52 (ddd, 1H, pyridinium-C*H*, *J* = 9.19, 6.79, and 1.28 Hz), 8.22 (d, 2H, phenyl-C*H*, *J* = 8.79 Hz), 8.45 (d, 2H, phenyl-C*H*, *J* = 9.19 Hz). **^{13}C NMR** (100.5 MHz, $CDCl_3$): δ 112.51, 112.56, 123.67, 128.06, 128.66, 131.94, 132.09, 135.86, 136.11, 137.42, 141.70, 147.88, 161.73. **^{11}B NMR** (128.2 MHz, $CDCl_3$): δ 7.22. MS (ESI^+) calcd for $[M+H]^+$: 347.1315, found: 347.1408.

*Synthesis of 3-fluoro-2-(4-nitrobenzylidene)-3-phenyl-2,3-dihydro-[1,2,4,3]triaza-borolo[4,5-a]pyridin-2-ium-3-uide (**72**)*

A solution of **71** (0.0832 g, 0.240 mmol) in THF (10 mL) was treated with KHF_2 (0.0938 g, 1.202 mmol) and stirred at 60 °C for 12 h. The reaction mixture was then quenched with water (10 mL) and extracted with CH_2Cl_2 (3 x 30 mL). The combined organic layers were dried over anhydrous $MgSO_4$ and removed under reduced pressure. The solid residue was purified by silica gel column chromatography using CH_2Cl_2 as an eluent. The purified product (0.0685 g) was obtained as **72** in a 82 % yield. **^{1}H NMR** (399.5 MHz, $CDCl_3$): δ 6.45 (dd, 1H, pyridinium-C*H*, *J* = 7.19, 6.39 Hz), 6.99 (d, 1H, pyridinium-C*H*, *J* = 8.79 Hz), 7.14 (d, 1H, *J* = 2.24 Hz), 7.28 (m 3H), 7.39 (m 2H), 7.45 (d, 1H, pyridinium-C*H*, *J* = 5.99 Hz), 7.54 (dd, 1H, pyridinium-C*H*, *J* = 9.59, 7.59 Hz), 8.22 (d, 2H, phenyl-C*H*, *J* = 8.79 Hz), 8.46 (d, 2H, phenyl-C*H*, *J* = 9.19 Hz). **^{13}C NMR** (100.5 MHz, $CDCl_3$): δ 111.04, 111.83, 122.69, 126.99, 127.63, 130.44, 130.49, 131.07, 133.77, 135.29, 136.64, 140.89, 146.80, 161.74. **^{11}B NMR** (128.2 MHz, $CDCl_3$): δ 7.66. **^{19}F NMR** (469.9 MHz, $CDCl_3$): δ -166.0. MS (ESI^+) calcd for $[M+H]^+$: 349.1272, found: 349.1349.

^{1}H NMR

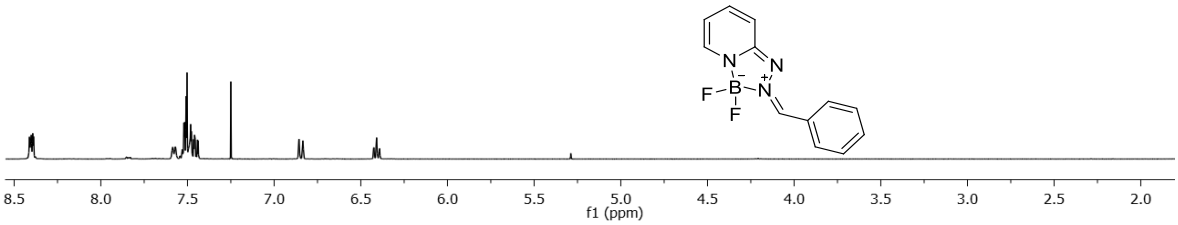

^{13}C NMR

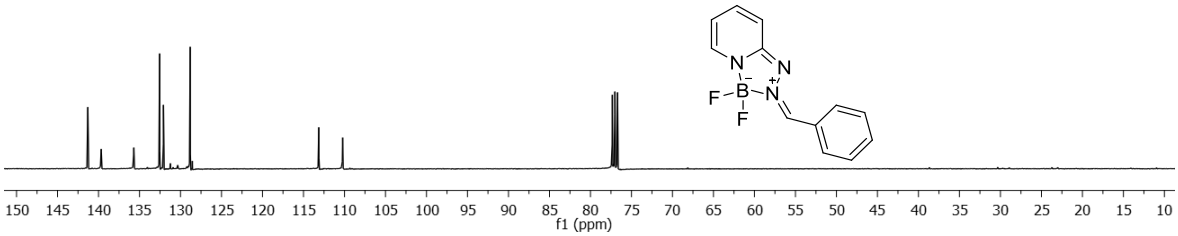

^{11}B NMR

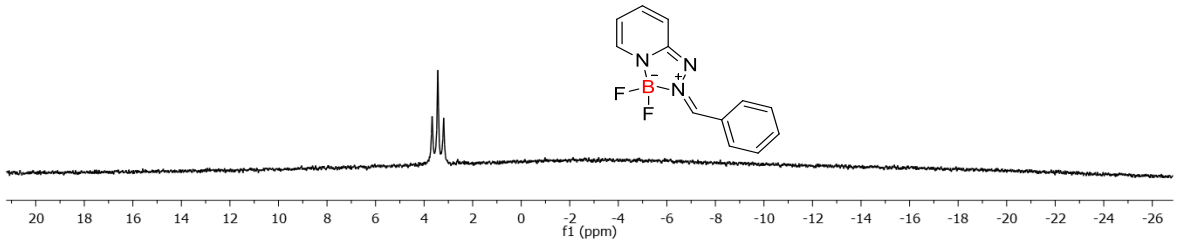

^{19}F NMR

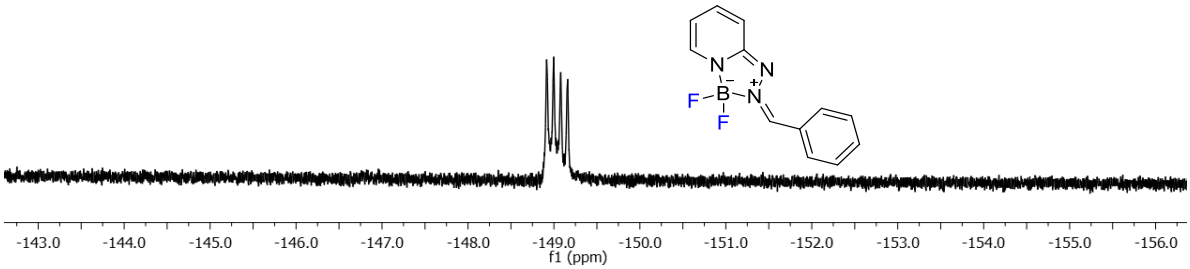

Figure 89. ^{1}H, ^{13}C, ^{11}B, and ^{19}F NMR spectra of **65** in $CDCl_3$.

^{1}H NMR

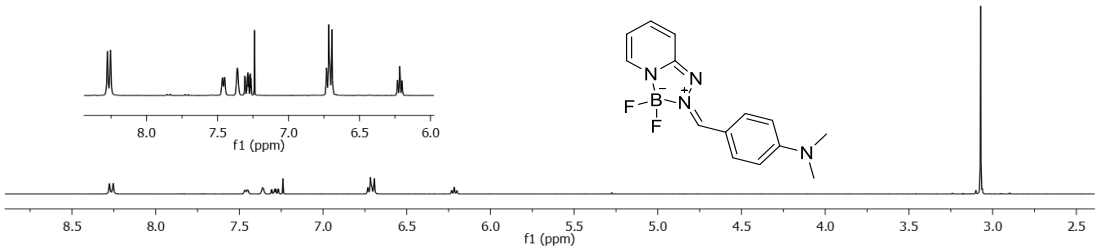

^{13}C NMR

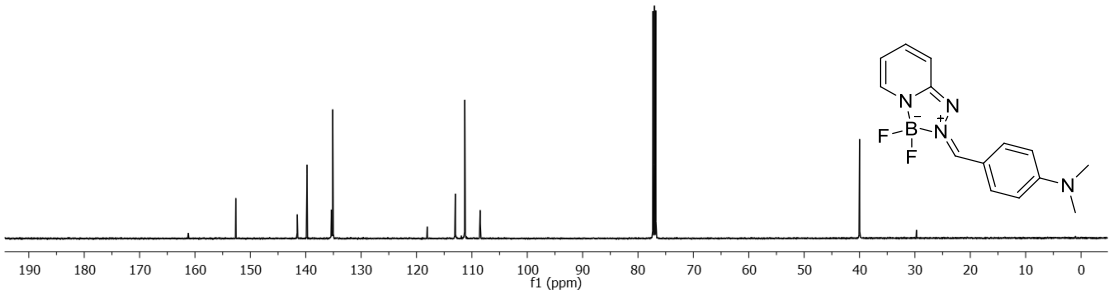

^{11}B NMR

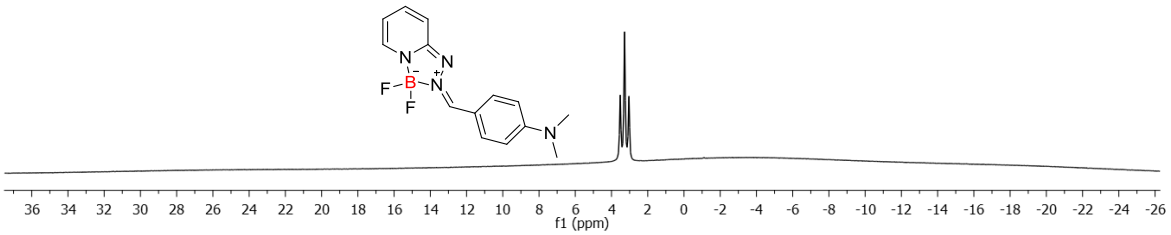

^{19}F NMR

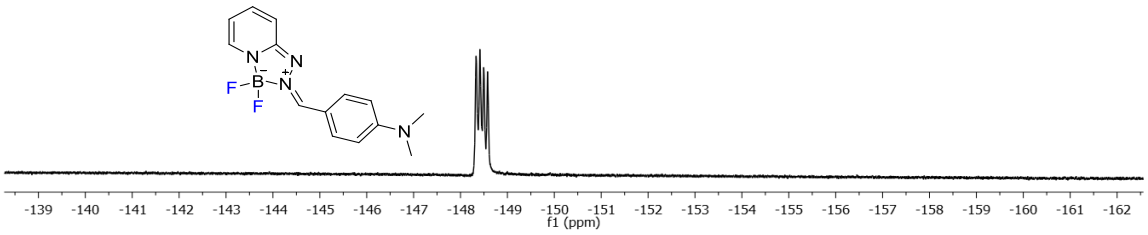

Figure 90. ^{1}H, ^{13}C, ^{11}B, and ^{19}F NMR spectra of **66** in $CDCl_3$.

^{1}H NMR

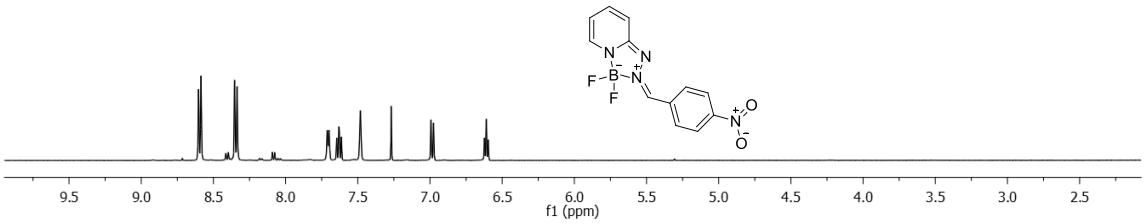

^{13}C NMR

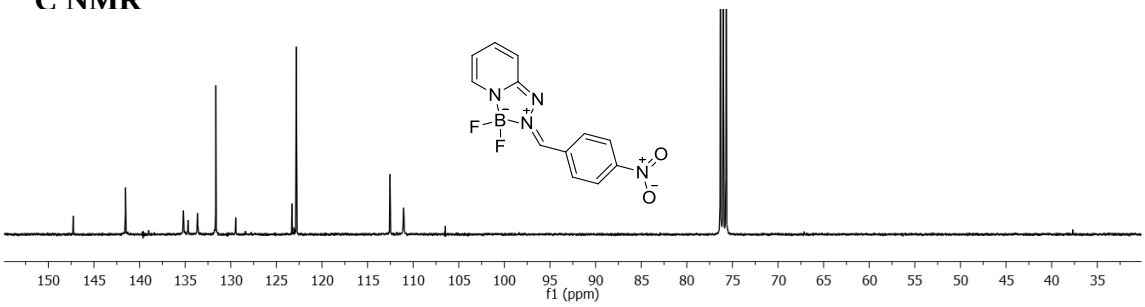

^{11}B NMR

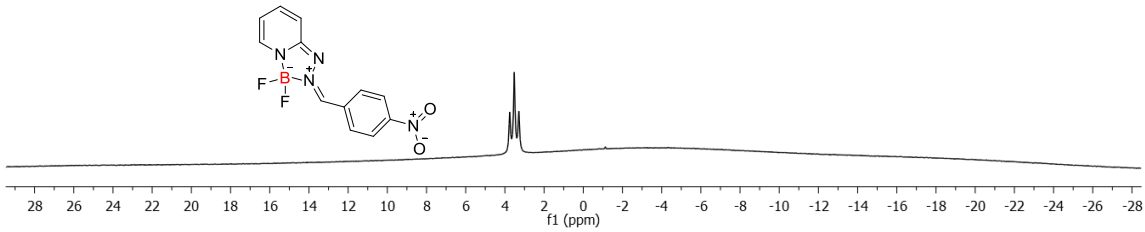

^{19}F NMR

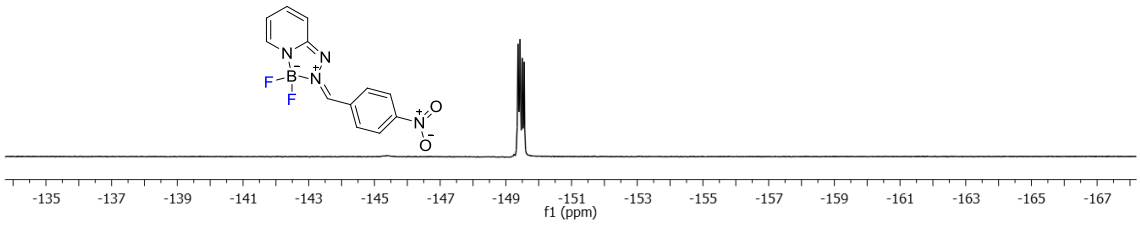

Figure 91. ^{1}H, ^{13}C, ^{11}B, and ^{19}F NMR spectra of **67** in $CDCl_3$.

^{1}H NMR

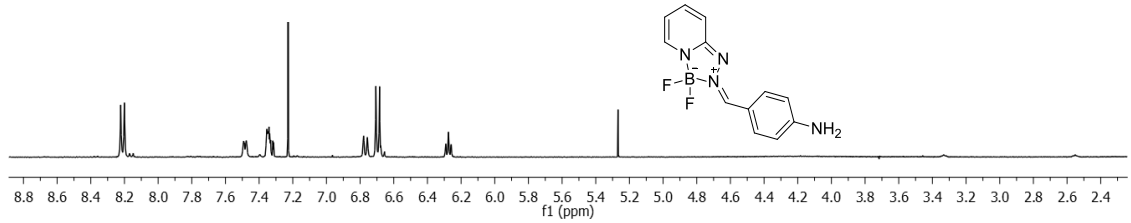

^{13}C NMR

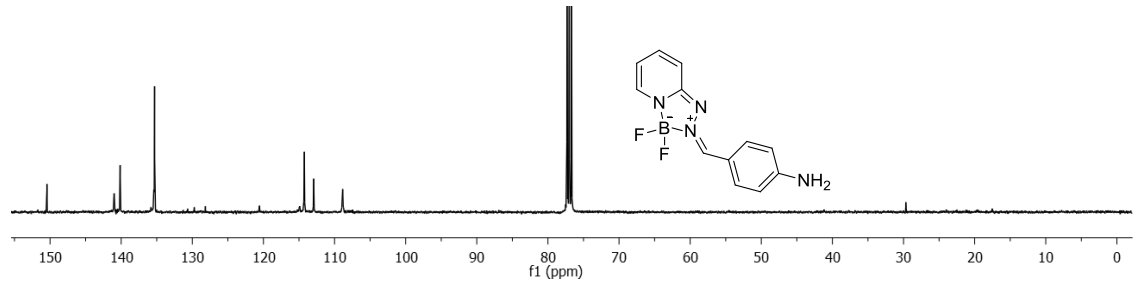

^{11}B NMR

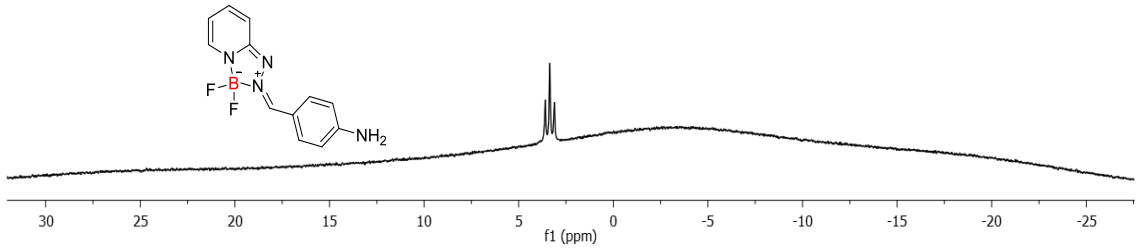

^{19}F NMR

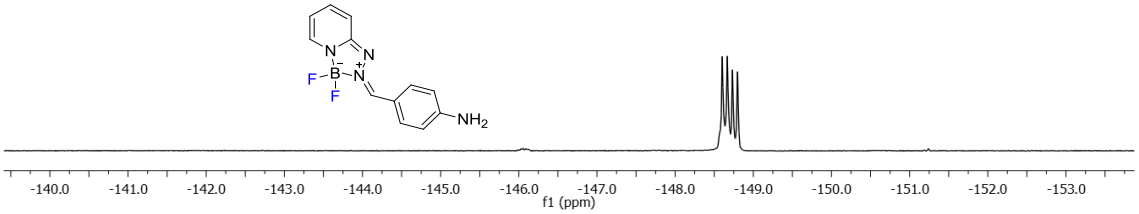

Figure 92. ^{1}H, ^{13}C, ^{11}B, and ^{19}F NMR spectra of **68** in $CDCl_3$.

^{1}H NMR

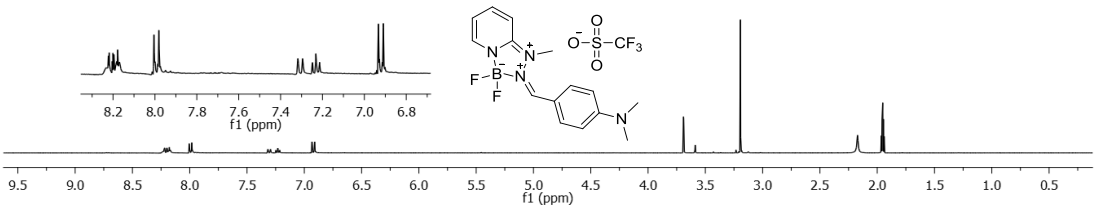

^{13}C NMR

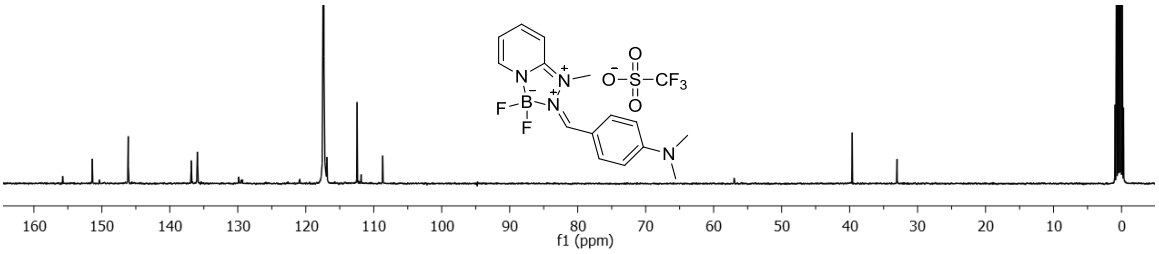

^{11}B NMR

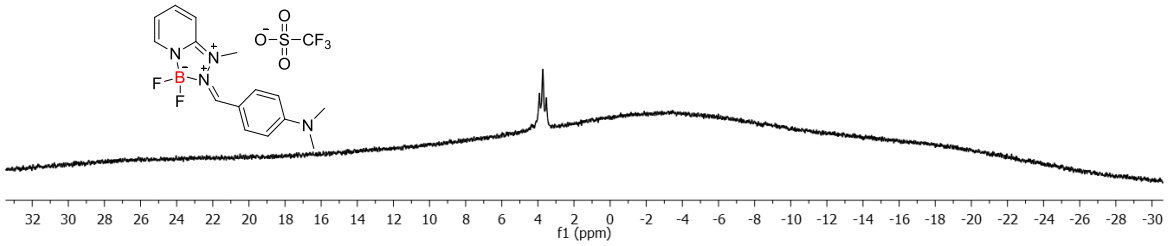

^{19}F NMR

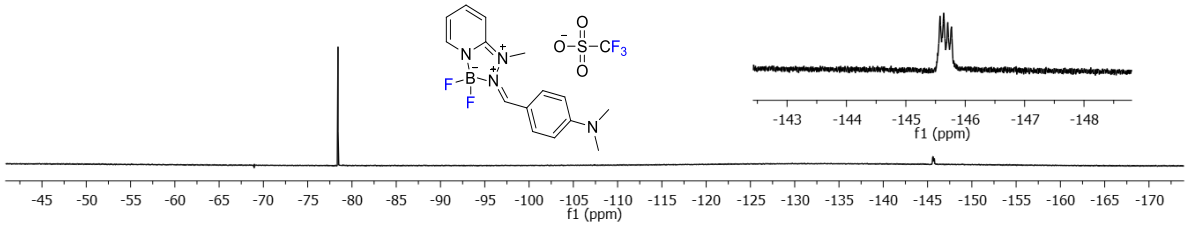

Figure 93. ^{1}H, ^{13}C, ^{11}B, and ^{19}F NMR spectra of **69** in CD_3CN.

^{1}H NMR

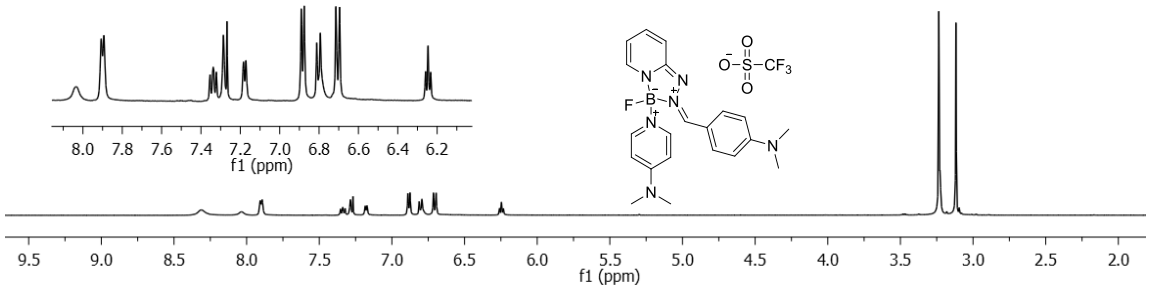

^{13}C NMR

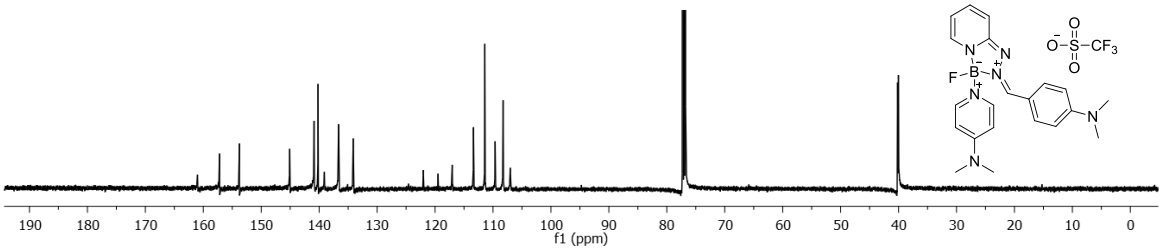

^{11}B NMR

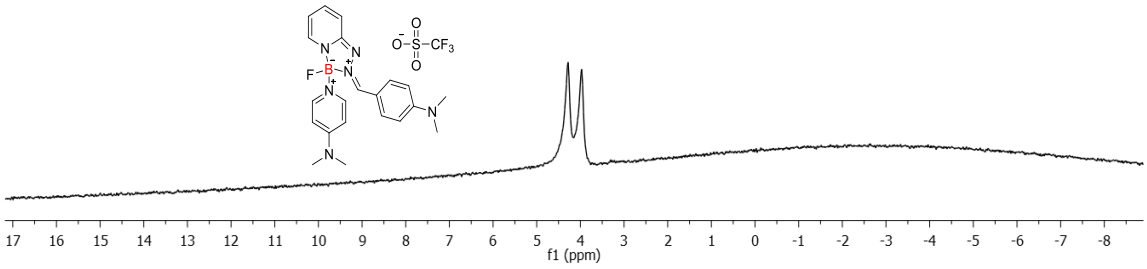

^{19}F NMR

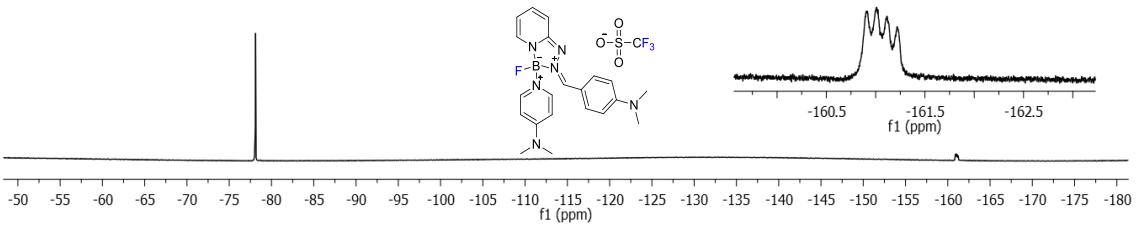

Figure 94. ^{1}H, ^{13}C, ^{11}B, and ^{19}F NMR spectra of **70** in $CDCl_3$.

^{1}H NMR

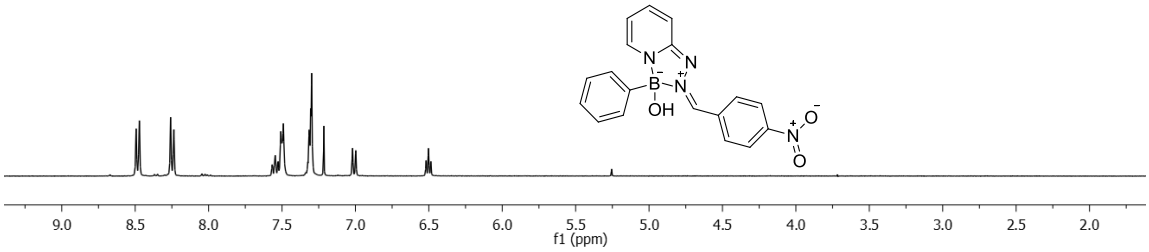

^{13}C NMR

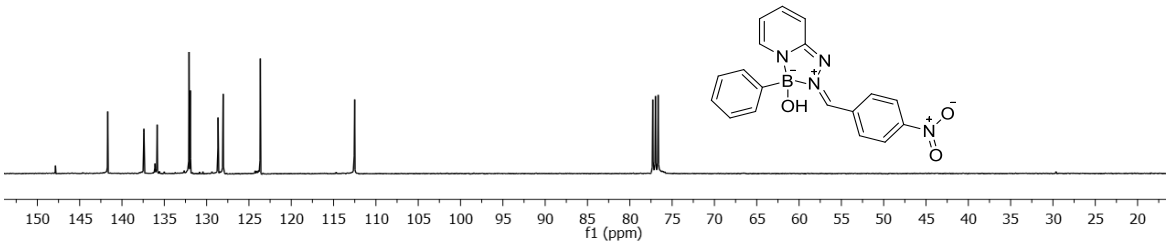

^{11}B NMR

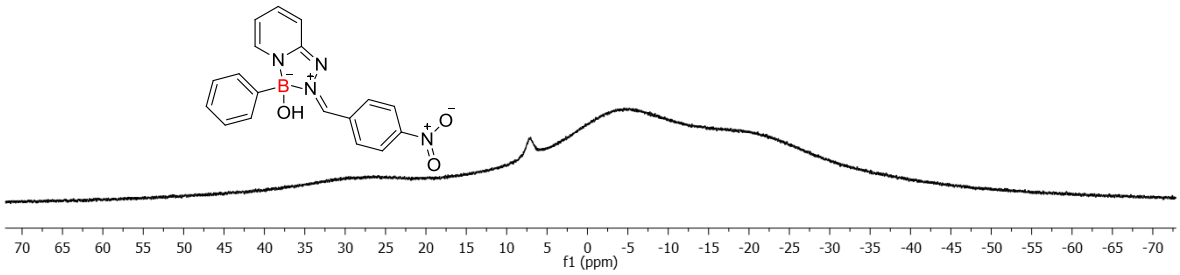

Figure 95. ^{1}H, ^{13}C, and ^{11}B NMR spectra of **71** in $CDCl_3$.

^{1}H NMR

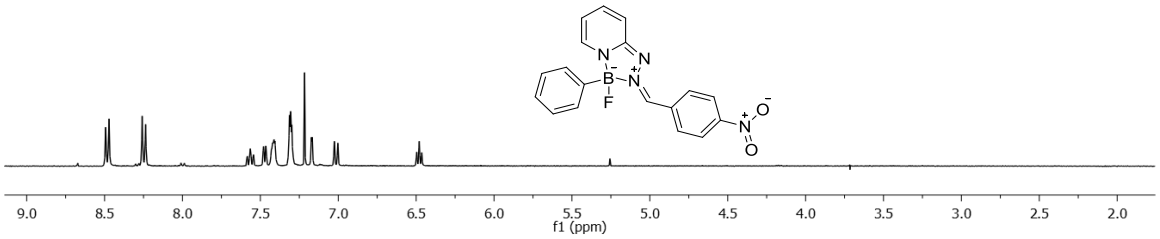

^{13}C NMR

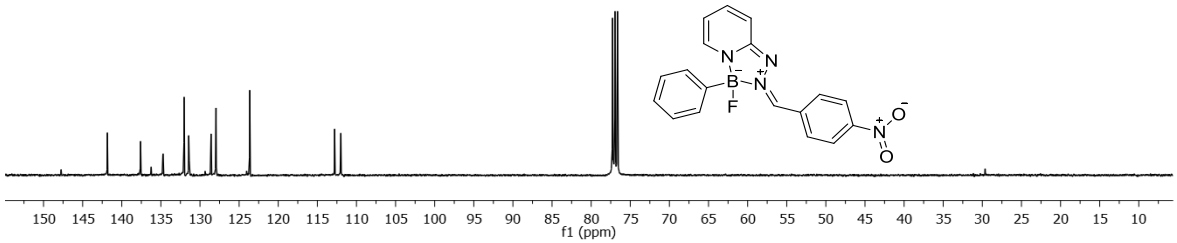

^{11}B NMR

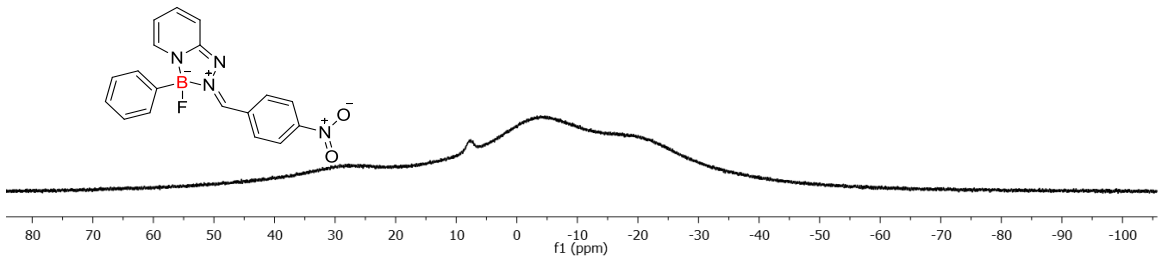

^{19}F NMR

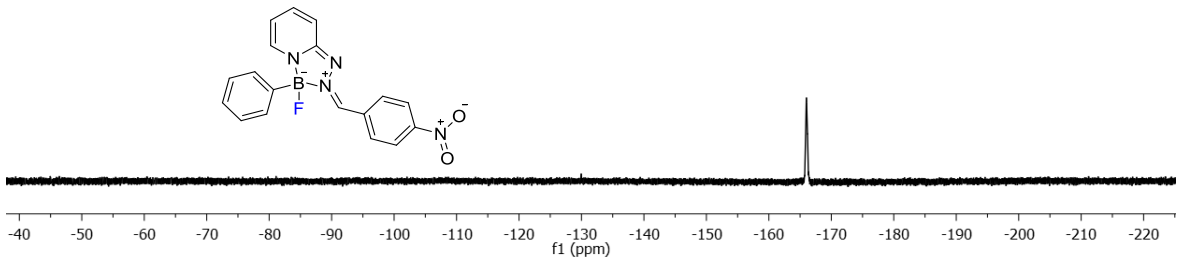

Figure 96. ^{1}H, ^{13}C, ^{11}B, and ^{19}F NMR spectra of **72** in $CDCl_3$.

Crystallographic Measurements

Single crystals of **69** were obtained by slow diffusion of Et_2O into a CH_3CN solution of **69**. Single crystals of **70** were obtained by slow diffusion of Et_2O into a CH_2Cl_2 solution of **70**. The crystallographic measurement of **69** and **70** were performed using a Bruker APEX-II CCD area detector diffractometer, with graphite-monochromated Mo-K_α radiation (λ = 0.71069 Å). A specimen of suitable size and quality was selected and mounted onto a nylon loop. The semi-empirical method SADABS was applied for absorption correction. The structure was solved by direct methods, and refined by the full-matrix least-square method against F^2 with the anisotropic temperature parameters for all non-hydrogen atoms. All H atoms were geometrically placed and refined using the riding model approximations. Data reduction and further calculations were performed using the Bruker SAINT+ and SHELXTL NT program packages. The crystal data are included in Table 18 and 19.

Table 18. Crystal data, data collections, and structure refinements of **69**.

Crystal data	**69**	
Empirical formula	$C_{17}H_{18}BF_5N_4O_2$	
Formula weight	434.07	
Crystal size/mm	0.10 x 0.15 x 0.06	
Temperature	110(2) K	
Wavelength	0.71073 Å	
Crystal system	Triclinic	
Space group	P-1	
Unit cell dimensions	a = 7.778(5) Å	α = 104.721(7)°
	b = 11.445(7) Å	β = 96.536(7)°
	c = 11.847(8) Å	γ = 105.629(7)°
Volume	963.3(11) $Å^3$	
Z	2	
Density (calculated)	1.559 g cm^{-3}	
μ	0.242 mm^{-1}	
F(000)	464.0	
Scan mode	ω, φ	
hkl ranges	-10 → +10	
	-15 → +15	
	-15 → +15	
Reflections collected	12126	
Unique reflections [Rint]	4819 (0.0522)	
Reflection used for refinement	4819	
Refined parameters	271	
GooF	1.597	
R1,[a] *w*R2[b] (all data)	0.0911, 0.1612	
Largest diff. peak and hole	0.92, -0.58 e.$Å^{-3}$	

[a]$R1 = \Sigma||F_o| - |F_c||/ \Sigma|F_o|$. [b]$wR2\ ([w(F_o^2 - F_c^2)^2]/[\Sigma w(F_o^2)^2])^{1/2}$; $w = 1/[\sigma^2(F_o^2) + (ap)^2 + bp]$; $p = (F_o^2 + 2F_c^2)/3$ with $a = 0.0743$ and $b = 0.7221$.

Table 19. Crystal data, data collections, and structure refinements of **70**.

Crystal data	**70**	
Empirical formula	$C_{23}H_{25}BF_4N_6O_2$	
Formula weight	515.15	
Crystal size/mm	0.30 x 0.25 x 0.10	
Temperature	110(2) K	
Wavelength	0.71073 Å	
Crystal system	Triclinic	
Space group	P-1	
Unit cell dimensions	a = 10.532(7) Å	α = 112.408(7)°
	b = 11.026(7) Å	β = 93.202(8)°
	c = 11.582(7) Å	γ = 92.399(8)°
Volume	1238.6(14) $Å^3$	
Z	2	
Density (calculated)	1.449 g cm^{-3}	
μ	0.198 mm^{-1}	
F(000)	560.0	
Scan mode	ω, φ	
hkl ranges	-14 → +14	
	-14 → +14	
	-15 → +15	
Reflections collected	15447	
Unique reflections [Rint]	6119 [0.0332]	
Reflection used for refinement	6119	
Refined parameters	334	
GooF	1.664	
R1,[a] *w*R2[b] (all data)	0.0754, 0.1736	
Largest diff. peak and hole	0.86, -0.43	

[a]$R1 = \Sigma||F_o| - |F_c||/ \Sigma|F_o|$. [b]$wR2 = ([w(F_o^2 - F_c^2)^2]/[\Sigma w(F_o^2)^2])^{1/2}$; $w = 1/[\sigma^2(F_o^2) + (ap)^2 + bp]$; $p = (F_o^2 + 2F_c^2)/3$ with $a = 0.077$ and $b = 1.089$.

Kinetic studies

A sample of **65**, **66**, **67**, and **68** was dissolved in 0.3 mL DMSO-d_6 and 0.7 mL of 10% w/v triton X-100 in D_2O phosphate buffer (pH 7.5, 500 mM) for the stability test. The ^{19}F NMR spectra were collected periodically. The decomposition of BF_2-HPY dyes were monitored by integration of the decreasing BF_2-HPY dye signal in conjunction with the increasing signal corresponding to free F^-. All spectra were processed using the VNMRJ Version 2.2 NMR software. The rate constant, k_{obs}, was calculated using a well-established NMR method reported in the literature.[4] This method is based on the fact that the concentration in BF_2-HPY dye is proportional to the ^{19}F NMR integration of BF_2-HPY dye signal divided by the sum of the integration of BF_2-HPY dye signal and the free fluoride signal. For convenience, the value of the BF_2-HPY dye integration is arbitrarily set at 100 and the free fluoride integration determined. The resulting data is provided in Table 20, 21, and 22.

Table 20. Kinetic data for the hydrolysis of **65** in 10% w/v triton X-100 in H_2O/ DMSO (7/3 vol) at pH = 7.5 ([phosphate buffer] = 500 mM). The values provided for F^- and $ArBF_3$ correspond to the integration of the corresponding NMR signal.

		Data for **65**		k_{obs} = 7.3E-4
Time (min)	$[F^-]$	$[BF_2]$	$[BF_2]/([BF_2]+[F^-]$	$[BF_2]/([BF_2]+[F^-]$
			exp. Ratio	calc. ratio
0	0	100	1.00	1.00
1066	115.28	100	0.46	0.46
1496	205.55	100	0.33	0.34
2495	476.28	100	0.17	0.16
2927	691.42	100	0.13	0.12
3834	1939	100	0.05	0.06
4200				0.05
4500				0.04
4800				0.03

Table 21. Kinetic data for the hydrolysis of **66** in 10% w/v triton X-100 in H_2O/ DMSO (7/3 vol) at pH = 7.5 ([phosphate buffer] = 500 mM). The values provided for F^- and $ArBF_3$ correspond to the integration of the corresponding NMR signal.

		Data for **66**		k_{obs} = 2.1E-4
Time (min)	$[F^-]$	$[BF_2]$	$[BF_2]/([BF_2]+[F^-]$	$[BF_2]/([BF_2]+[F^-]$
			exp	calc
0	0	100	1.00	1.00
1081	30.36	100	0.77	0.80
1509	38.52	100	0.72	0.73
2512	62.3	100	0.62	0.59
2943	75.18	100	0.57	0.54
3346	84.26	100	0.54	0.50
4200				0.41
4500				0.39
4800				0.36

Table 22. Kinetic data for the hydrolysis of **67** in 10% w/v triton X-100 in H_2O/ DMSO (7/3 vol) at pH = 7.5 ([phosphate buffer] = 500 mM). The values provided for F^- and $ArBF_3$ correspond to the integration of the corresponding NMR signal.

		Data for **67**		k_{obs} = 4.8E-4
Time (min)	$[F^-]$	$[BF_2]$	$[BF_2]/([BF_2]+[F^-]$	$[BF_2]/([BF_2]+[F^-]$
			exp	calc
0	0	100	1.00	1.00
1058	88.58	100	0.53	0.60
1482	120.56	100	0.45	0.49
2480	186.78	100	0.35	0.30
2912	245.46	100	0.29	0.25
3915	322.60	100	0.24	0.15
4200				0.13
4500				0.12
4800				0.10

Table 23. Kinetic data for the hydrolysis of **68** in 10% w/v triton X-100 in H_2O/ DMSO (7/3 vol) at pH = 7.5 ([phosphate buffer] = 500 mM). The values provided for F^- and $ArBF_3$ correspond to the integration of the corresponding NMR signal.

		Data for **68**		k_{obs} = 3.0E-4
Time (min)	$[F^-]$	$[BF_2]$	$[BF_2]/([BF_2]+[F^-]$	$[BF_2]/([BF_2]+[F^-]$
			exp	calc
0	0	100	1.00	1.00
1025	44.66	100	0.69	0.74
1452	60.88	100	0.62	0.65
2459	95.02	100	0.51	0.48
2892	118.89	100	0.46	0.42
3894	162.75	100	0.38	0.31
4200				0.28
4500				0.26
4800				0.24

UV-vis and fluorescence measurements

UV-vis spectra were recorded on an Ocean Optics USB4000 spectrometer with an Ocean Optics ISS light source. Steady state emission spectra were collected at room temperature using a PTI QuantaMaster 4 fluorescence spectrophotometer equipped with a Model 810 PMT detector. The spectra were measured in CH_2Cl_2. Quantum yields were measured using fluorescein as a standard in 0.1 M NaOH solution. All absorption and emission spectra were demonstrated in Figure 97-102.

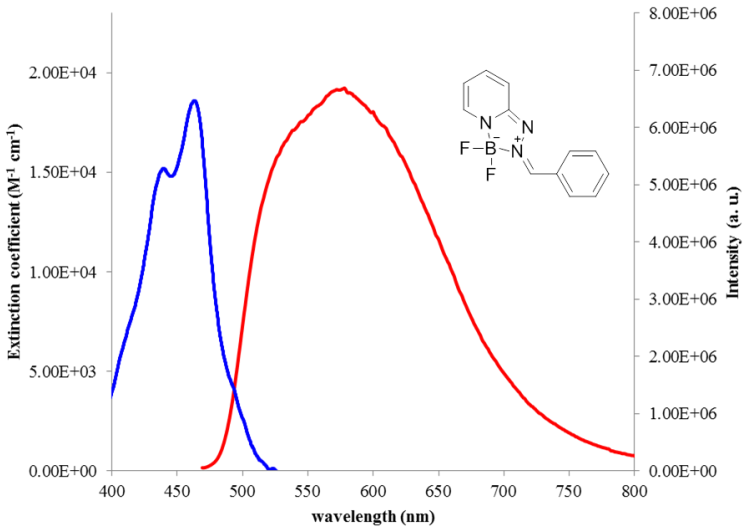

Figure 97. Absorption (blue) and emission (red) spectra of **65** in CH_2Cl_2.

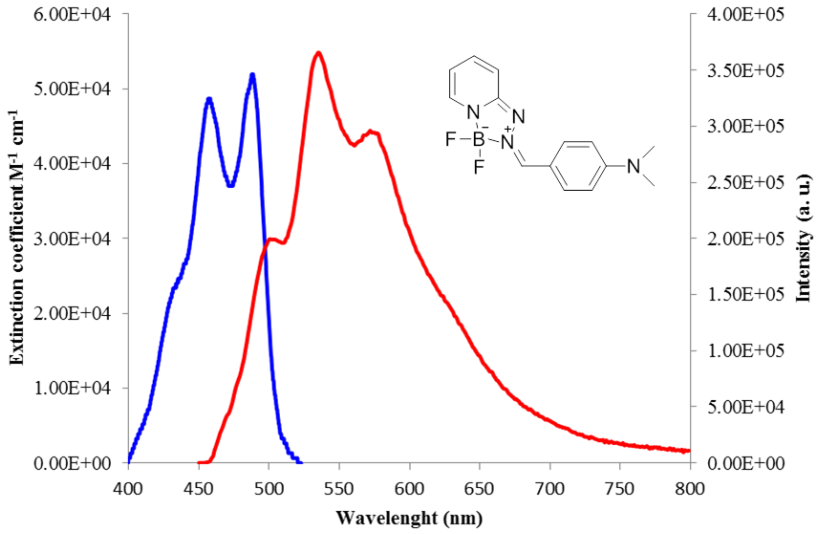

Figure 98. Absorption (blue) and emission (red) spectra of **66** in CH_2Cl_2.

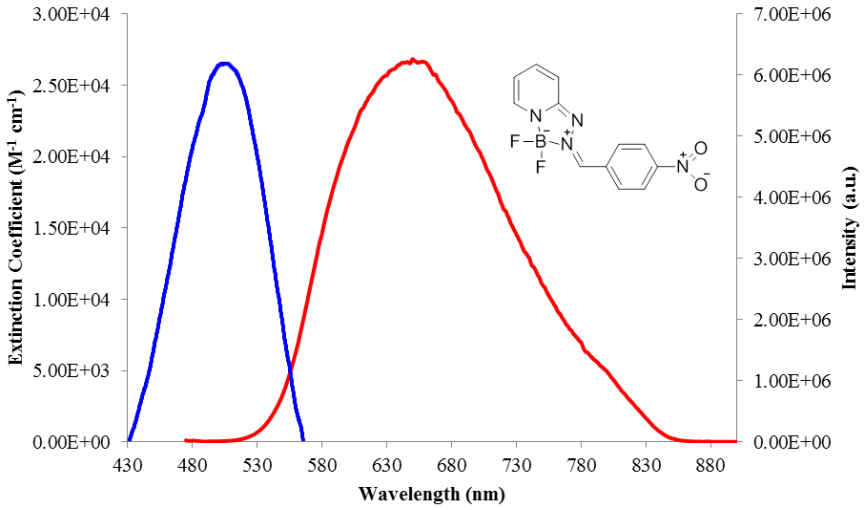

Figure 99. Absorption (blue) and emission (red) spectra of **67** in CH_2Cl_2.

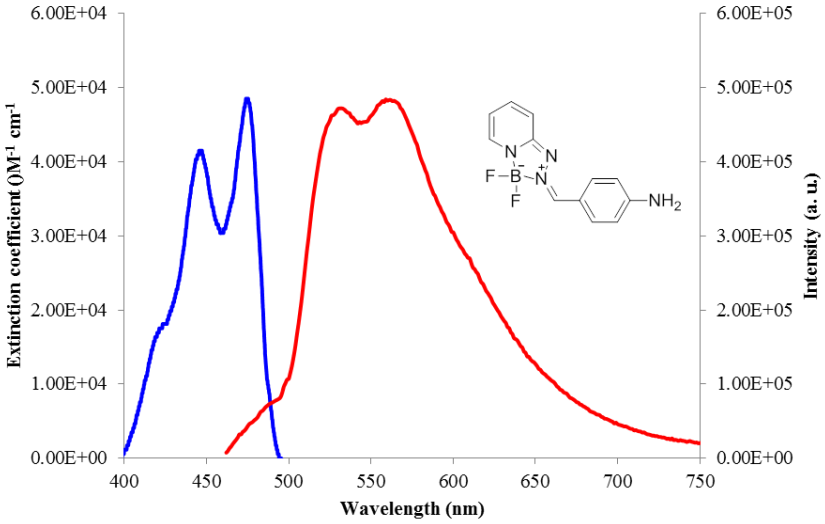

Figure 100. Absorption (blue) and emission (red) spectra of **68** in CH_2Cl_2.

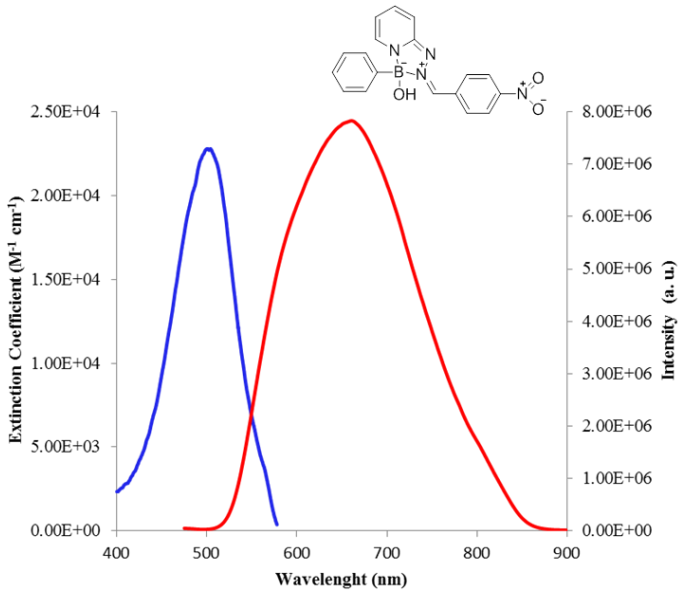

Figure 101. Absorption (blue) and emission (red) spectra of **71** in CH_2Cl_2.

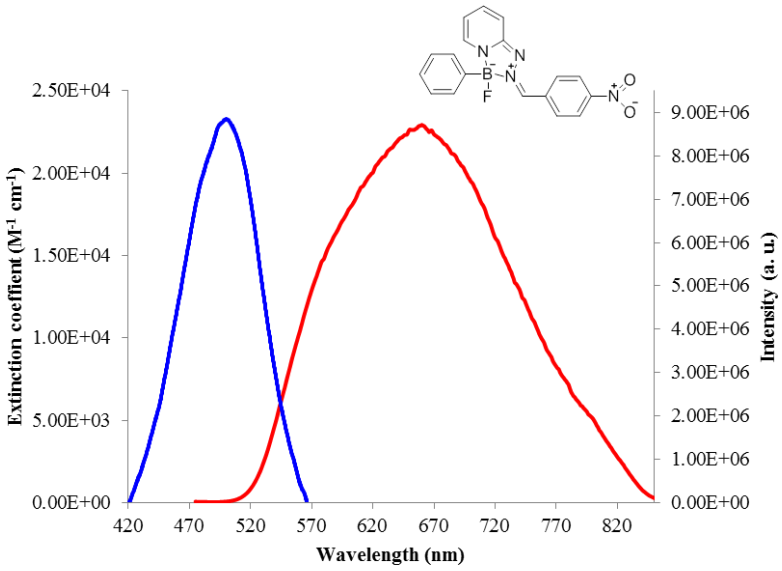

Figure 102. Absorption (blue) and emission (red) spectra of **72** in CH_2Cl_2.

CHAPTER VI

SYNTHESIS, STRUCTURE, AND ISOMERIZATION OF PHOSPHINO-METHYLIUM COMPOUNDS

6.1 Introduction

The discovery of frustrated Lewis pairs (FLPs) and the exploration of their potential for the activation of small molecules have led to the development of metal–free approaches to catalytic reactions.[92-95] One of the first examples of an FLP was the combination of perfluorotriphenylborane and tri-*tert*-butylphosphine, which can activate dihydrogen at room temperature.[96] In addition to intermolecular FLPs, the decoration of a molecular backbone with bulky Lewis acids and Lewis bases in proximity to one another gives rise to intramolecular FLPs, which have found applications in catalysis[97,98] and transition metal complexation.[99-101] Erker and coworkers developed the intramolecular P/B frustrated Lewis pair **I** (Figure 103) for use in heterolytic dihydrogen splitting.[98] They also demonstrated that the resultant borohydride is capable of acting as a reducing agent for organic substrates. These results are noteworthy as they describe useful steps toward the metal-free utilization of dihydrogen in organic syntheses. In addition to catalytic applications, Bourissou and coworkers investigated the use of *ortho*-phenylene phosphino-borane **II**a (Figure 103) as an ambiphilic ligand for the coordination of gold and palladium.[101] This work provided the first evidence of M → B interactions supported by single donor buttresses. Later, they successfully coordinated both Rh and Cu metal centers with the P/B ambiphilic ligands **II**a and **II**b.[99,100] These

studies further substantiated the versatile coordination properties of *ortho*-phenylene phosphino-boranes. Apart from the P/B FLP system, Bourissou and Gabbai synthesized the new *ortho*-phenylene phosphino-stannane derivatives **III**a and **III**b, and studied the intramolecular P-Sn interactions presenting in the compounds. They found the phosphine and stannane groups to be engaged in an intramolecular P→Sn dative interaction. The interaction in **III**b is stronger than that in **III**a because of the intense donicity of the di(*iso*-propyl)phosphine moiety of **III**b.

.

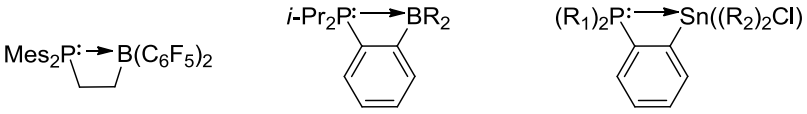

I **II**a (R = Cy) **II**b (R = Ph) **III**a (R_1 = Ph, R_2 = Ph) **III**b (R_1 = *i*-Pr, R_2 = Ph

Figure 103. Illustration of intramolecular frustrated Lewis pair systems.

The utilities of **I**, **II**a and **II**b in catalytic reactions and the interesting interaction in **III**a and **III**b prompted us to investigate whether a carbocation, a strong Lewis acid, and a phosphine, a Lewis base, might be incorporated into the *ortho* positions of the same phenylene backbone to furnish intramolecular FLPs (Figure 104). Gabbai and Wang discovered that a carbocation can be easily generated on a naphthalene backbone through the treatment of 1,8-bis[bis(p-methoxy-phenyl)hydroxymethyl]naphthalene with trifluoroacetic anhydride (TFAA) and fluoroboric acid (HBF_4).[102] With this objective and promising preliminary results in mind, we endeavored to synthesize novel *ortho*-phenylene phosphino-methylium compounds (Figure 104) and to investigate their

properties and reactivities with small molecules.

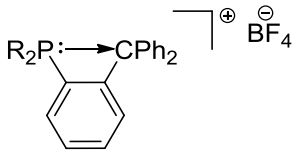

This work
73 (R = Ph)
74 (R = *i*-Pr)

Figure 104. Illustration of the intramolecular P/C^+ frustrated Lewis pairs synthesized in this work.

6.2 Synthesis and characterizations

Inspired by reports from Wang and Gabbai,[102-104] we first prepared the (2-(phosphino)phenyl)diphenylmethanol compounds **a** and **b** by the metalation of (2-bromophenyl)diphenylphosphine or (2-bromophenyl)di-*iso*-propylphosphine with *n*-butyllithium (nBuLi), followed by the addition of benzophenone (Figure 105). The *ortho*-phenylene phosphino-methylium compounds **73** and **74** were then synthesized by the addition of aqueous HBF_4 to suspensions of **a** and **b** in trifluoroacetic anhydride. After precipitation from Et_2O, compounds **73** and **74** were obtained as white powders in 70% and 72% yield, respectively. Surprisingly, compounds **73** and **74** were stable in air. Each was fully characterized by NMR spectroscopy. The presence of the phosphonium moiety was confirmed by the detection of a ^{31}P NMR resonance at 54.4 ppm for **73** and 82.3 ppm for **74**. The low-field ^{31}P NMR signal observed for **74** suggested strong

donation from di-*iso*-propylphosphine to carbon center. The ^{1}H NMR spectra of **73** and **74** showed the expected phenyl backbone resonances in the aromatic region (6 – 8 ppm). The ^{13}C NMR signal of the *C*Ph_2 center appears as a doublet at 74.7 ppm ($^{1}J_{C\text{-}P}$ = 50.01 Hz) for **73** and 70.4 ppm ($^{1}J_{C\text{-}P}$ = 43.5 Hz) for **74.**

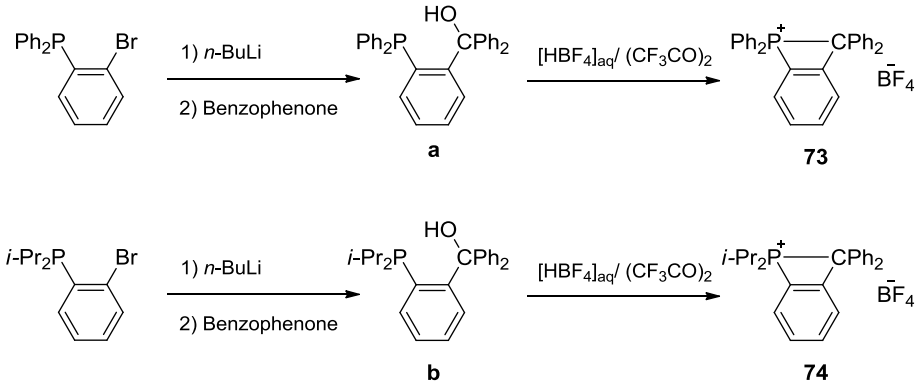

Figure 105. Scheme depicting the synthesis of phosphino-methylium **73** and **74**.

The structures of these compounds, which were confirmed by single-crystal X-ray crystallography, show the formation of strained four-membered rings (Figures 106 and 107). The P(1)-C(1) separations of 1.871(4) Å in **73** and 1.913(2) Å in **74** are slightly longer than typical P-C bonds because of the strain of the four member ring and the bulk of the substituents on the phosphorous and carbon centers. The C(1)-P(1)-C(3) angles of **73** (80.33(18)°) and **74** (74.28(8)°) are smaller than the ideal tetrahedral angle (109.5°), indicating distorted tetrahedral geometries for the P atoms of **73** and **74**.

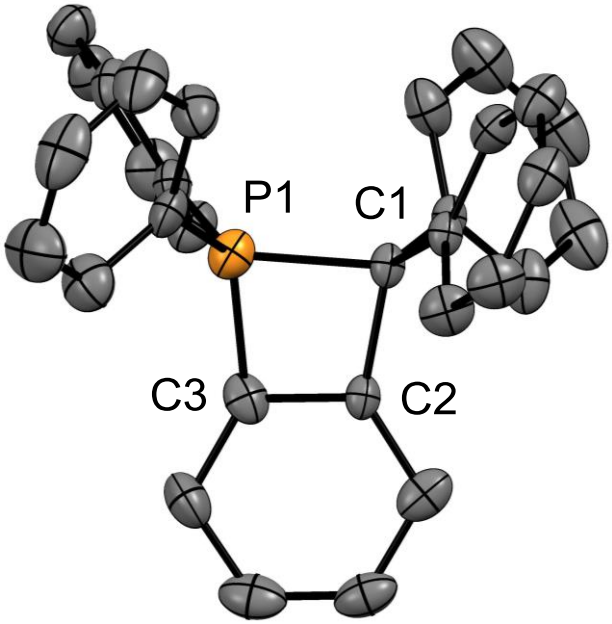

Figure 106. Crystal structure of **73**. Displacement ellipsoids are scaled to the 50% probability level. Tetrafluoroborate counter anion and hydrogen atoms were omitted for clarity. Selected bond lengths (Å) and angles (deg) for **73**: P1-C1 1.871(4), C1-C2 1.597(5), C2-C3 1.401(5), P1-C3 1.735(4); C1-P1-C3 80.33(18), P1-C1-C2 83.4(2), C1-C2-C3 101.7(3), C2-C3-P1 94.6(3).

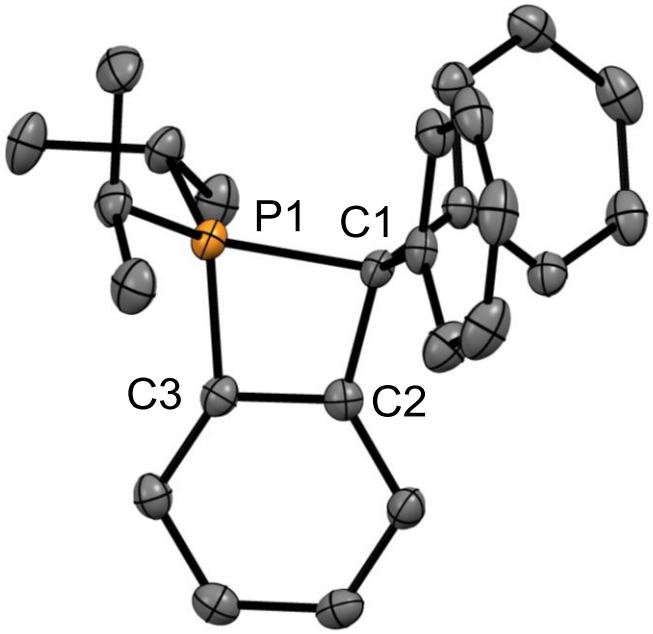

Figure 107. Crystal structure of **74**. Displacement ellipsoids are scaled to the 50% probability level. Tetrafluoroborate counter anion and hydrogen atoms were omitted for clarity. Selected bond lengths (Å) and angles (deg) for **74**: P1-C1 1.9129(18), C1-C2 1.542(2), C2-C3 1.395(3), P1-C3 1.7727(19); C1-P1-C3 74.28(8), P1-C1-C2 83.63(10), C1-C2-C3 104.74(15), C2-C3-P1 93.39(12).

Although the four-membered-ring-containing diphenylphosphino-methylium derivative **73** is air-stable in when stored as a solid, it undergoes an unexpected isomerization when dissolved in polar organic solvent (chloroform and acetonitrile), forming the cyclic diphenylphosphino-methylium derivative **75** (Figure 108). This isomerization was monitored by ^{31}P NMR spectroscopy. The ^{31}P NMR signal shifted from 54.4 ppm to 3.18 ppm over 72 h, suggesting the formation of the new phosphonium salt containing a six-membered ring (**75**). The presence of a methine unit () in **75** was confirmed by detection of a doublet at 5.08 ppm ($^4J_{H\text{-}P}$ = 1.62 Hz) in the ^{1}H NMR spectrum, as well as doublet at 52.9 ppm ($^3J_{C\text{-}P}$ = 9.07 Hz) in the ^{13}C NMR spectrum. Nonetheless, under ambient conditions, the highly strained di-*iso*-propylphosphino-methylium derivative **74** is stable in both the solid and solution phases. To examine whether **74** isomerizes at elevated temperatures, **74** was heated to 80 °C in acetonitrile. Upon heating, the ^{31}P NMR signal of **74** shifted from 82.3 ppm to 17.1 ppm, indicating formation of the isomerized six-membered ring product (**76**). The existence of the methine unit () in **76** was also suggested by the detection of doublet at 5.93 ppm ($^4J_{H\text{-}P}$ = 3.76 Hz) in the ^{1}H NMR spectrum and a doublet at 50.7 ppm ($^3J_{C\text{-}P}$ = 8.58 Hz) in the ^{13}C NMR spectrum.

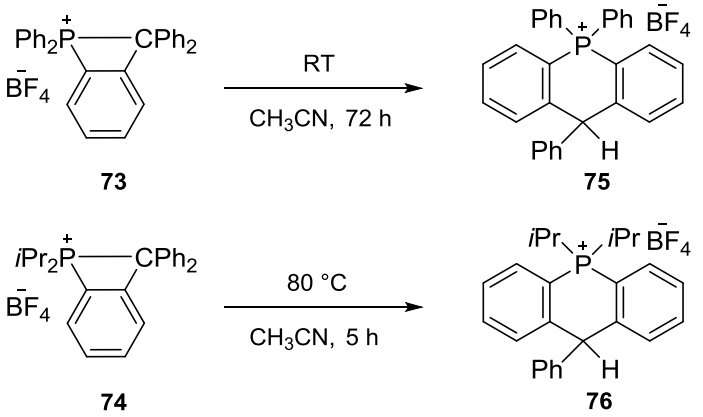

Figure 108. Scheme depicting the isomerization of phosphino-methylium **73** and **74**.

The structure of the isomerized products, confirmed by single crystal X-ray crystallography, confirms formation a six-membered phosphonium ring species (Figure 109 and 110). The P(1)-C(1) distances of 1.7848(18) Å in **75** and 1.773(5) in **76** are shorter than those in the four-membered ring species **73** (1.871(4) Å) and **74** (1.913(2) Å), suggesting the formation of more stable P-C bonds. The C(1)-P(1)-C(5) angles of **75** (109.54(8)°) and **76** (106.65(18)°) are closer to the ideal tetrahedral angle (109.5°), indicating a less strained bonding environment at phosphorus. These structural results indicate that the isomerizations of **73** and **74** are driven by the strain in the four-membered ring species.

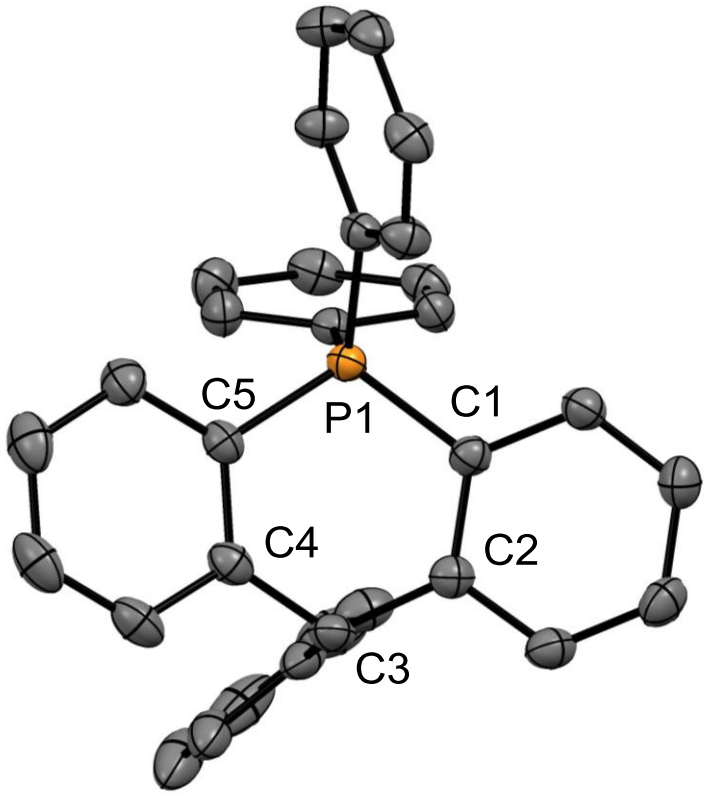

Figure 109. Crystal structure of **75**. Displacement ellipsoids are scaled to the 50% probability level. Tetrafluoroborate counter anion and hydrogen atoms were omitted for clarity. Selected bond lengths (Å) and angles (deg) for **75**: P1-C1 1.7848(18), C1-C2 1.400(2), C2-C3 1.517(2), C3-C4 1.524(2), C4-C5 1.399(2), P1-C5 1.7838; C1-P1-C5 109.54(8), P1-C1-C2 118.56(12), C1-C2-C3 123.38(14), C2-C3-C4 114.87(13), C3-C4-C5 122.25(14), C4-C5-P1 119.09(12).

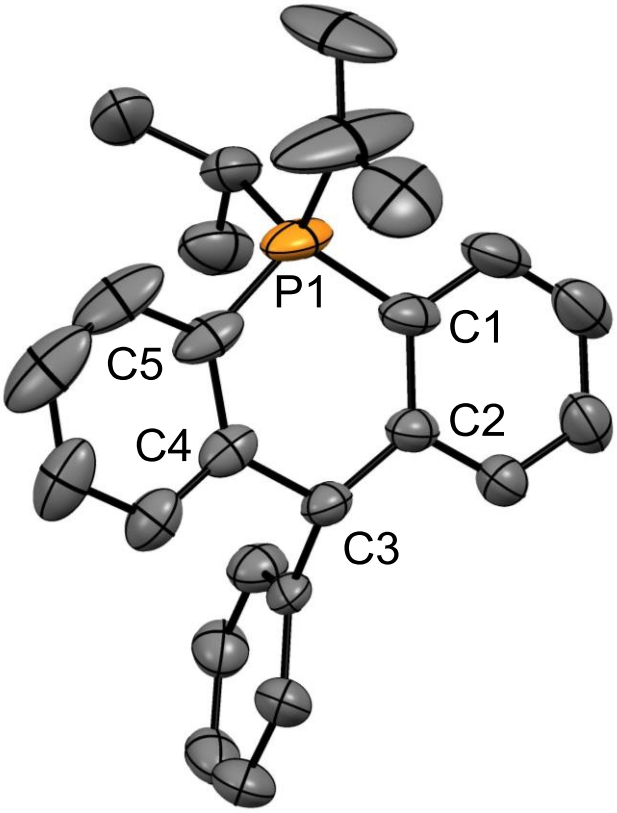

Figure 110. Crystal structure of **76**. Displacement ellipsoids are scaled to the 50% probability level. Tetrafluoroborate counter anion and hydrogen atoms were omitted for clarity. Selected bond lengths (Å) and angles (deg) for **76**: P1-C1 1.773(5), C1-C2 1.405(5), C2-C3 1.513(5), C3-C4 1.529(5), C4-C5 1.406(5), P1-C5 1.779(5); C1-P1-C5 106.65(18), P1-C1-C2 121.8(3), C1-C2-C3 125.5(3), C2-C3-C4 118.8(3), C3-C4-C5 125.1(4), C4-C5-P1 121.8(3).

The four-membered-ring-containing diphenylphosphino-methylium compound (**73**) is easier to isomerize than its di-*iso*-propyl analogue (**74**) due to the weak donicity of the diphenylphosphine moiety. This argument is strengthened by the observation that **73** underwent isomerization upon dissolving in $CDCl_3$ at ambient temperature, whereas **74** showed no reaction. Through periodic monitoring by ^{31}P NMR, we discovered that the room temperature isomerization of **73** could be fit to a first-order rate equation with a rate constant of 0.0011 min^{-1} (Figure 111).

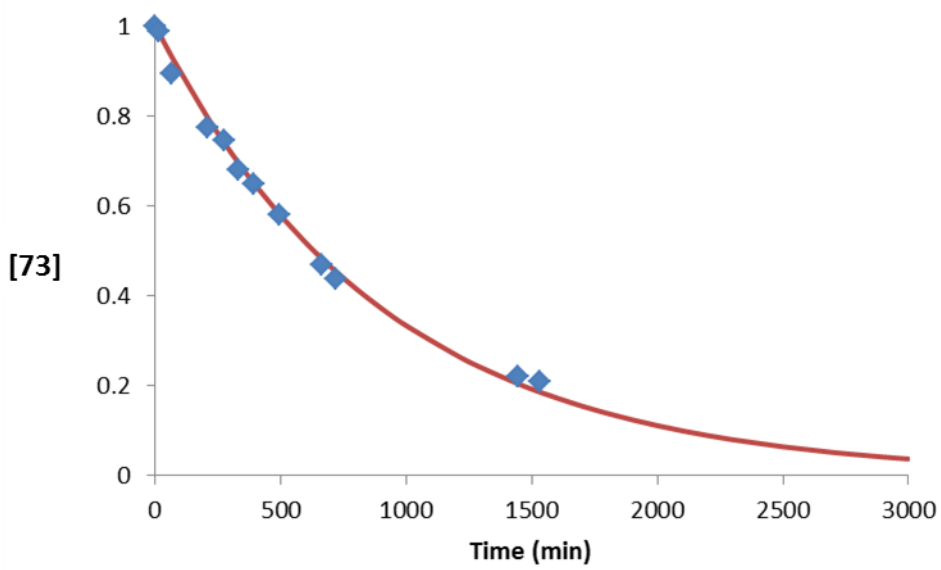

Figure 111. Kinetic plot of the isomerization process of **73**.

Finally, we tested the reactivity of the four-membered-ring-containing phosphino-methylium derivertives **73** and **74** with small molecules, including H_2, CO_2, and N_2O, as well as with late transition metal complexes such as (tht)AuCl and

$Pd(PPh_3)_4$. Unfortunately, neither **73** nor **74** successfully activated the small molecules, nor did they act as ambiphilic ligands with transition metal complexes.

6.3 Conclusion

The phosphine methylium derivatives **73** and **74** have been successfully prepared and fully characterized. These compounds features short intramolecular $P \rightarrow C^+$ bonds indicating that they are not truly frustrated Lewis pairs as originally envisaged. This is especially true for the di-isopropyl derivative **74** which is remarkably inert. Interestingly, **73** undergoes an isomerization reaction when dissolved in organic solvents at room temperature, whereas **74** is stable under the same conditions. The difference observed in the isomerization processes derives from the dissimilarity of the electron donating ability of the phosphine ligand.

6.4 Experimental

General Consideration

(2-bromophenyl) diphenylphosphine[105], and (2-bromophenyl) diisopropyl phosphine[105] were synthesized according to the published procedure. Fluoroboric acid (HBF_4) and n-butyllithium (n-BuLi) were purchased from Alfar Aesar; trifluoroacetic anhydride (TFAA) was purchased from Oakwood product, Inc; benzophenone was purchased from Baker Analyzed. All chemicals were used without further purification. Solvents were dried by passing through an alumina column (CH_2Cl_2) or refluxing under N_2 over Na/K (Et_2O and THF). Electrospray mass spectra were acquired from a MDS

Sciex API QStar Pulsar. NMR spectra were recorded on Inova 300, Inova 400, and an Inova 500B NMR spectrometer at ambient temperature. Chemical shifts are given in ppm, and are referenced to residual ^{1}H and ^{13}C solvent signals as well as external H_3PO_4 (^{31}P NMR) and BF_3-Et_2O (^{11}B NMR and ^{19}F NMR).

*Preparation of 7,7,8,8-tetraphenyl-7-phosphabicyclo[4.2.0]octa-1(6),2,4-trien-7-ium tetrafluoroborate (**73**)*

(2-bromophenyl)diphenylphosphine (0.561 g, 1.65 mmol) was lithiated at 0 °C in diethyl ether (10 mL) using a 2.60 M n-BuLi in hexane (0.62 mL, 1.65 mmol). The solution mixture was stirred at 0 °C for 15 min leading to formation of the lithium salt as white powder. The suspension was allowed to warm up to room temperature. Then, benzophenone (0.300, 1.65 mmol) was added to the suspension of the lithium salt. The solution mixture was stirred overnight. The solvent was removed in *vacuo*. The residue was suspended in CH_2Cl_2 (15 mL) and treated with as saturated NH_4F aqueous solution (10 mL). The mixture was rigorously stirred for 1 h until all white powder dissolved. The organic layer was collected and dried over $MgSO_4$. The mixture was filtered to remove $MgSO_4$ and the solvent was removed under reduced pressure yielding **a** as a white powder (0.483 g, 68% yield). **^{1}H NMR** (299.9 MHz, $CDCl_3$): δ 6.30 (d,1H, $^{3}J_{H\text{-}P}$ = 18.64 Hz), 6.71 (m, 1H), 7.02 – 7.09 (m, 4H), 7.12 – 7.26 (m, 17H), 7.36 (m, 1H). **^{13}C NMR** (100.5 MHz, $CDCl_3$): δ 83.90 (d, $J_{C\text{-}P}$ = 2.88 Hz), 127.14, 127.51, 127.78, 128.29, 128.36, 128.42, 128.61, 128.66, 130.17 (d, $J_{C\text{-}P}$ = 8.81 Hz), 133.31, 133.49, 135.25 (d, $J_{C\text{-}P}$ = 14.02 Hz), 135.68 (d, $J_{C\text{-}P}$ = 5.39 Hz), 138.12 (d, $J_{C\text{-}P}$ = 2.31), 147.18, 154.48 (d,

$J_{C\text{-}P}$ = 23.30 Hz). **^{31}P^{31} NMR** (121.4 MHz, $CDCl_3$): δ -16.00. Mass (ESI^+): calcd for $C_{31}H_{25}OP$ $(M+H)^+$, 445.1721; found 445.1732. **a** was used without further purification. To a suspension of **a** (0.483 g, 1.09 mmol) in trifluoroacetic anhydride (TFAA) (7 mL) was added 48% HBF_4 (0.5 mL, 3.85 mmol). After being stirred for 10 min, all the white powder dissolved and the mixture turned red. The red solution was stirred for 1.5 h and quenched by diethyl ether (20 mL). After addition of diethyl ether, a white powder precipitated. The reaction mixture was filtered yielding **73** as a white solid (0.392 g , 70% yield). **^{1}H NMR** (399.59 MHz, $CDCl_3$): δ 6.98 – 7.01 (m, 4H), 7.16 – 7.22 (m, 5H), 7.36 – 7.49 (m, 8H), 7.61 – 7.66 (m, 2H), 7.71 (d, 1H, $^3J_{H\text{-}H}$ = 7.99 Hz), 8.04 (q, 1H, $^3J_{H\text{-}H}$ = 7.59 Hz), 8.15 (t, 1H, $^3J_{H\text{-}H}$ = 8.39 Hz), 8.41 (dd, 1H, $^3J_{H\text{-}H}$ = 7.99 Hz, $^3J_{H\text{-}P}$ = 11.59 Hz). **^{13}C NMR** (100.5 MHz, $CDCl_3$): δ 74.81 (d, $^1J_{C\text{-}P}$ = 48.24 Hz), 116.85, 117.57, 123.82, 124.60, 127.41, 127.66, 128.83, 128.85, 129.53, 129.60, 130.03, 130.15, 131.99, 133.67, 133.77, 133.83, 134.16, 134.23, 135.31 (d, $J_{C\text{-}P}$ = 5.03 Hz), 138.73 (d, $J_{C\text{-}P}$ = 5.03 Hz), 153.75 ((d, $J_{C\text{-}P}$ = 8.04 Hz),) **^{31}P^{31} NMR** (121.4 MHz,$CDCl_3$): δ 54.43. Anal. Calcd for $C_{31}H_{24}PBF_4$: C, 72.52; H, 4.67. Found: C, 72.30; H, 4.59.

*Preparation of 7,7-diisopropyl-8,8-diphenyl-7-phosphabicyclo[4.2.0]octa-1(6),2,4-trien-7-ium tetrafluoroborate (**74**)*

Ortho-bromo-diisopropylphosphinobenzene (1-Br-2-(P*i*Pr$_2$)C_6H_4) (1.095 g, 4.01 mmol) was lithiated at -78 °C in diethyl ether (15 mL) using a 2.60 M n-BuLi in hexane (1.70 mL, 4.42 mmol). The solution mixture was stirred at -78 °C for 1 h leading to formation of the lithium salt as white powder. Then, benzophenone (0.730, 4.01 mmol)

was added to the suspension of the lithium salt. The solution mixture was allowed to warm to room temperature and stirred overnight. The solvent was removed in *vacuo*. The residue was suspended in CH_2Cl_2 (15 mL) and treated with as saturated NH_4F aqueous solution (10 mL). The mixture was rigorously stirred for 1 h until all white powder dissolved. The dichloromethane layer was separated and dried with $MgSO_4$. The mixture was filtered to remove $MgSO_4$ and the solvent was removed under reduced pressure yielding **b** as a white powder (1.09 g, 72% yield). **^{1}H NMR** (399.5 MHz, CDCl3): δ 1.09 (dd, 6H, isopropyl-C*H*$_3$, $^3J_{H\text{-}P}$ = 19.12 Hz, $^3J_{H\text{-}H}$ = 7.14 Hz), 1.21 (dd, 6H, isopropyl-C*H*$_3$, $^3J_{H\text{-}P}$ = 18.62 Hz, $^3J_{H\text{-}H}$ = 7.14 Hz), 3.10 (m, 2H, isopropyl-C*H*), 7.32 – 7.49 (m, 10H), 7.77 (dd, 1H, $^3J_{H\text{-}P}$ = 7.96 Hz, $^3J_{H\text{-}H}$ = 1.11 Hz) 7.87 (m, 1H), 8.06 (m, 1H), 8.15 (m, 1H). **^{13}C NMR** (100.5 MHz, CDCl3): δ 16.65 (d, $J_{C\text{-}P}$ = 3.04 Hz), 16.99 (d, $J_{C\text{-}P}$ = 3.04 Hz), 26.54 (d, $J_{C\text{-}P}$ = 21.52 Hz), 69.95, 126.03, 127.51, 127.72, 128.16, 128.54, 128.61, 128.95, 129.37 (d, $J_{C\text{-}P}$ = 2.18 Hz), 129.70 (d, $J_{C\text{-}P}$ = 1.75 Hz), 129.87, 129.98, 131.82, 132.78, 132.88, 135.76 (d, $J_{C\text{-}P}$ = 5.41 Hz), 137.55 (d, $J_{C\text{-}P}$ = 2.38 H z), 151.17 (d, $J_{C\text{-}P}$ = 6.28 Hz). **^{31}P{^{1}H} NMR** (161.4 MHz, $CDCl_3$): δ -2.60. Mass (ESI^+): calcd for $C_{25}H_{29}OP$ $(M+H)^+$, 377.2034; found 377.2100. . To a suspension of **b** (0.683 g, 1.82 mmol) in trifluoroacetic anhydride (TFAA) (7 mL) was added 48% HBF_4 (0.5 mL, 3.85 mmol). After being stirred for 10 min, all the white powder dissolved and the mixture turned red. The red solution was stirred for 1.5 h and quenched by diethyl ether (20 mL). After addition of diethyl ether, a white powder precipitated. The mixture was filtered to get **74** as a white powder (0.584 g, 72% yield). **^{1}H NMR** (299.9 MHz, $CDCl_3$): δ 1.11 (dd, 6H, isopropyl-C*H*$_3$, $^3J_{H\text{-}P}$ = 17.99 Hz, $^3J_{H\text{-}H}$ = 7.20 Hz), 1.20 (dd, 6H,

isopropyl-C*H*$_3$, $^3J_{H\text{-}P}$ = 18.89 Hz, $^3J_{H\text{-}H}$ = 7.20 Hz), 3.16 (m, 2H, isopropyl-C*H*), 7.32 – 7.37 (m, 4H), 7.40 – 7.51 (m, 6H), 7.75 (d, 1H, $^3J_{H\text{-}H}$ = 6.00 Hz), 7.87 (m, 1H), 8.05 (t, 1H, $^3J_{H\text{-}H}$ = 6.00 Hz), 8.20 (dd, 1H, $^3J_{H\text{-}H}$ = 7.50 Hz, $^3J_{H\text{-}P}$ = 9.80 Hz). **^{13}C NMR** (75.4 MHz, CD_3CN): δ 16.47 (d, $^2J_{C\text{-}P}$ = 2.94 Hz), 16.64 (d, $^2J_{C\text{-}P}$ = 3.62 Hz), 26.43 (d,$^1J_{C\text{-}P}$ = 21.04 Hz), 70.35 (d, $^1J_{C\text{-}P}$ = 43.51 Hz), 128.71, 128.98, 129.17, 129.26, 129.69, 129.72, 130.11, 131.66, 133.03, 133.18, 136.59 (d, $J_{C\text{-}P}$ = 5.26 Hz), 138.39 (d, $J_{C\text{-}P}$ = 2.74 Hz), 151.65 (d, $J_{C\text{-}P}$ = 7.22 Hz). **^{31}P{^{1}H} NMR** (121.4 MHz, $CDCl_3$): δ 82.28. Anal. Calcd for $CH_{24}PBF_4$: C, 67.30; H, 6.28. Found: C, 66.12; H, 6.27.

*Synthesis of 5,5,10-triphenyl-5,10-dihydroacridophosphin-5-ium tetrafluoroborate (**75**)*

Compound **73** (0.022 g, 0.043 mmol) was dissolved in CD_3CN (5 mL). The solution was stirred at room temperature for 72 h. The solvent was removed in *vacuo* affording **75** as a white powder (0.021) in a 95 % yield. **^{1}H NMR** (299.9 MHz, CD_3CN): δ 5.08 (d, 1H, $^4J_{H\text{-}P}$ = 1.62 Hz), 5.6 – 5.65 (m, 2H), 5.88 – 6.01 (m, 3H), 6.43 – 6.59 (m, 7H), 6.71 – 6.80 (m, 7H), 6.96 – 7.00 (m, 5H). **^{13}C NMR** (75.4 MHz, CD_3CN): δ 52.91 (d, $^3J_{C\text{-}P}$ = 9.07 Hz), 127.84, 128.74, 129.33, 129.81, 129.97, 130.97, 131.14, 131.21, 131.39, 132.61, 132.74, 134.24, 134.39, 135.18, 135.31, 135.70 (d, $J_{C\text{-}P}$ = 3.38 Hz), 135.87, 136.03, 136.23, 136.26, 136.67 (d, $J_{C\text{-}P}$ = 3.38 Hz), 147.91 (d, $J_{C\text{-}P}$ = 6.69 Hz). **^{31}P{^{1}H} NMR** (121.4 MHz,CD_3CN): δ 3.18. Mass (ESI^+): calcd for $[C_{31}H_{24}P]^+$ $(M)^+$, 427.1615; found 427.1368.

*Synthesis of 7,7-diisopropyl-8,8-diphenyl-7-phosphabicyclo[4.2.0]octa-1,3,5-trien-7-ium tetrafluoroborate (**76**)*

Compound **74** (0.018 g, 0.040 mmol) was dissolved in CD_3CN (5 mL). The solution was stirred at 80 °C for 5 h. The solvent was removed in *vacuo* affording **76** as a white powder (0.017) in a 94 % yield. **^{1}H NMR** (299.9 MHz, CD_3CN): δ 1.16 (dd, 6H, isopropyl-C*H*$_3$, $^3J_{H\text{-}P}$ = 18.76 Hz, $^3J_{H\text{-}H}$ = 7.20 Hz), 1.46 (dd, 6H, isopropyl-C*H*$_3$, $^3J_{H\text{-}P}$ = 17.99 Hz, $^3J_{H\text{-}H}$ = 6.94 Hz), 3.21 (m, 1H, isopropyl-C*H*), 3.39 (m, 1H, isopropyl-C*H*), 5.93 (d, 1H, $^4J_{H\text{-}P}$ = 3.76 Hz), 7.14 – 7.20 (m, 2H), 7.28 – 7.42 (m, 4H), 7.46 – 7.56 (m, 3H), 7.64 – 7.72 (m, 2H), 7.75 – 7.82 (m, 2H), 7.94 – 8.03 (m, 2H). **^{13}C NMR** (75.4 MHz, CD_3CN): δ 16.00 (d, $^2J_{C\text{-}P}$ = 2.69 Hz), 16.74 (d, $^2J_{C\text{-}P}$ = 2.17 Hz), 24.98 ($^1J_{C\text{-}P}$ = 45.63 Hz), 26.76 ($^1J_{C\text{-}P}$ = 46.83 Hz), 50.67 ($^3J_{C\text{-}P}$ = 8.58 Hz), 109.69, 110.74, 128.35, 129.36, 129.51, 129.80, 130.23 (d, $J_{C\text{-}P}$ = 3.27 Hz), 132.13, 132.5, 133.67, 133.78, 135.62 (d, $J_{C\text{-}P}$ = 2.32 Hz), 146.19 (d, $J_{C\text{-}P}$ = 1.69 Hz), 147.86 (d, $J_{C\text{-}P}$ = 3.87 Hz) **^{31}P{^{1}H} NMR** (202.2 MHz, CD_3CN): δ 17.13. Mass (ESI^+): calcd for $[C_{25}H_{28}P]^+$ $(M)^+$, 359.1928; found 359.1636.

^{1}H NMR

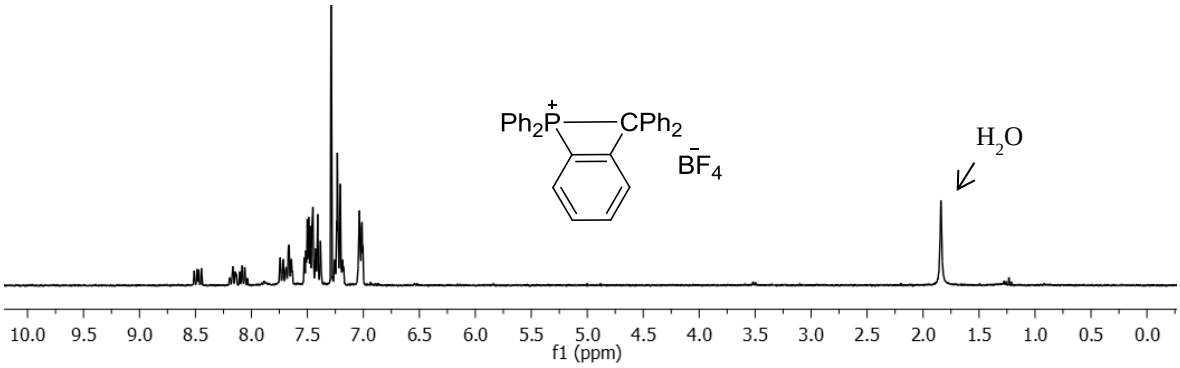

^{13}C NMR

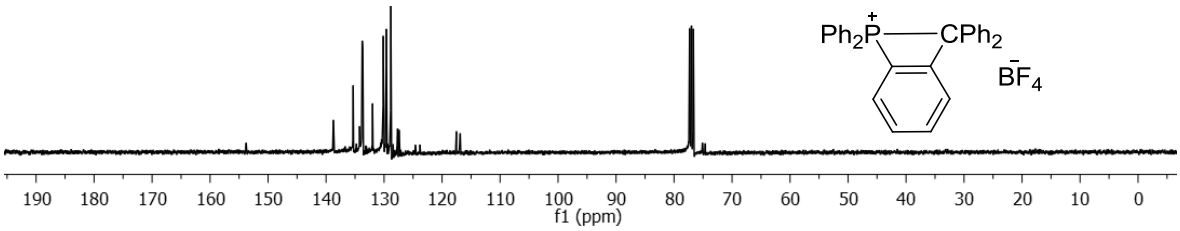

^{31}P NMR

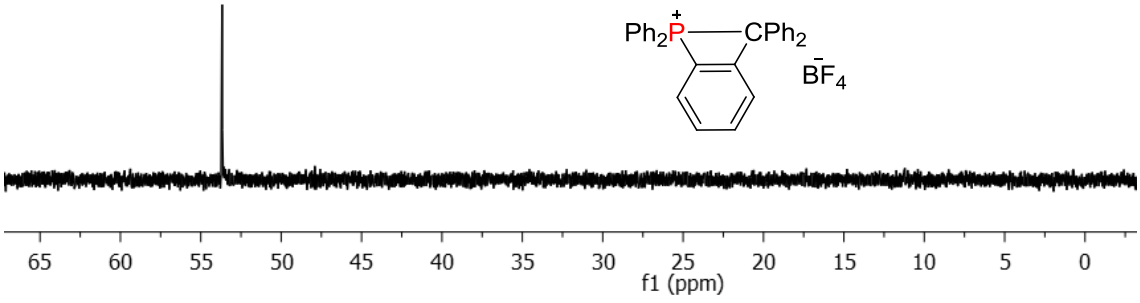

Figure 112. ^{1}H, ^{13}C, and ^{31}P NMR spectra of **73**.

^{1}H NMR

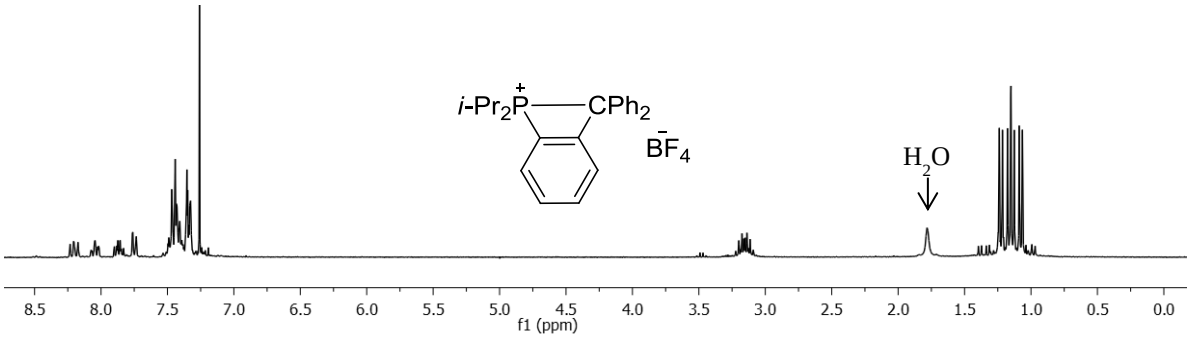

^{13}C NMR

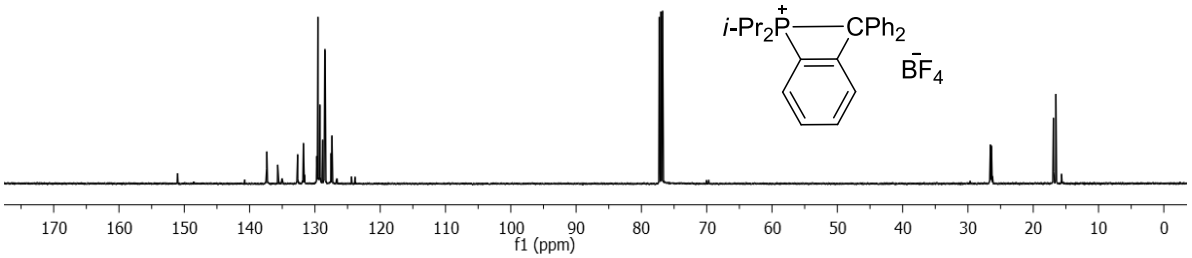

^{31}P NMR

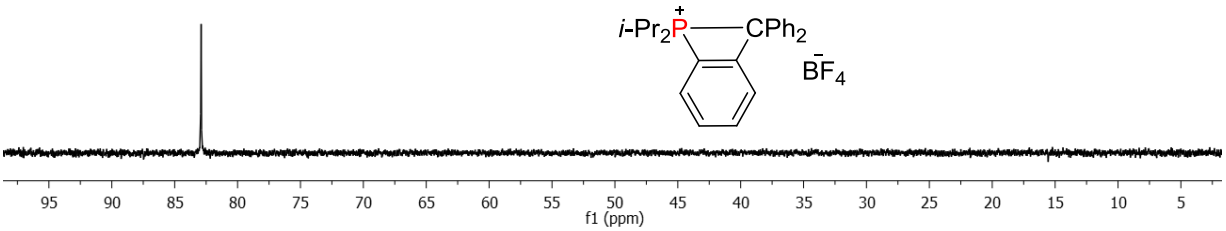

Figure 113. ^{1}H, ^{13}C, and ^{31}P NMR spectra of **74**.

^{1}H NMR

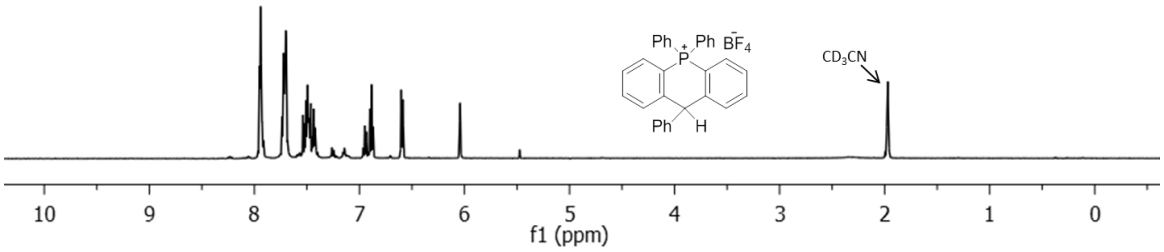

^{13}C NMR

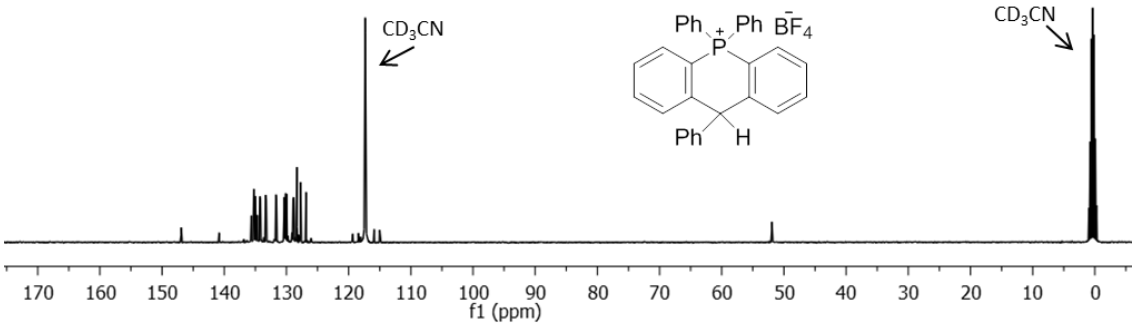

^{31}P NMR

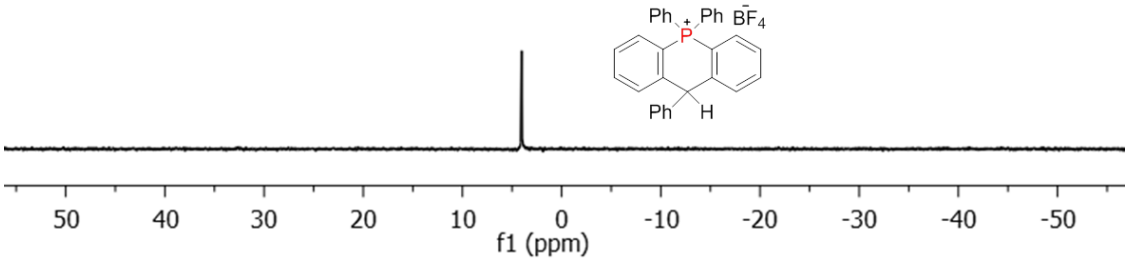

Figure 114. ^{1}H, ^{13}C, and ^{31}P NMR spectra of **75**.

^{1}H NMR

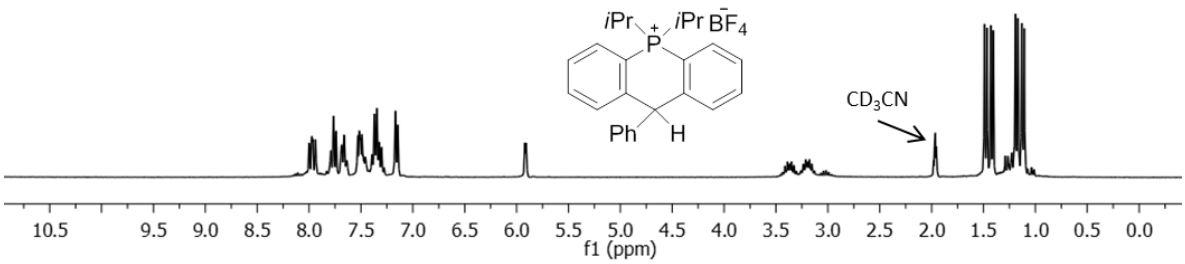

^{13}C NMR

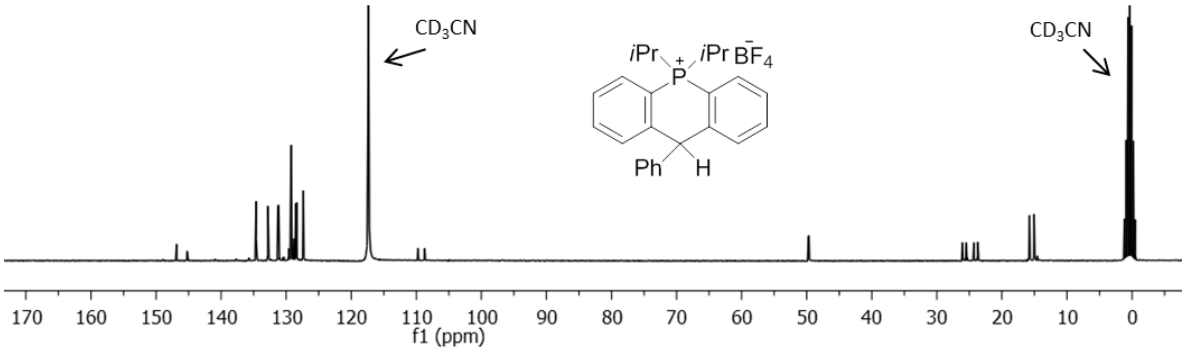

^{31}P NMR

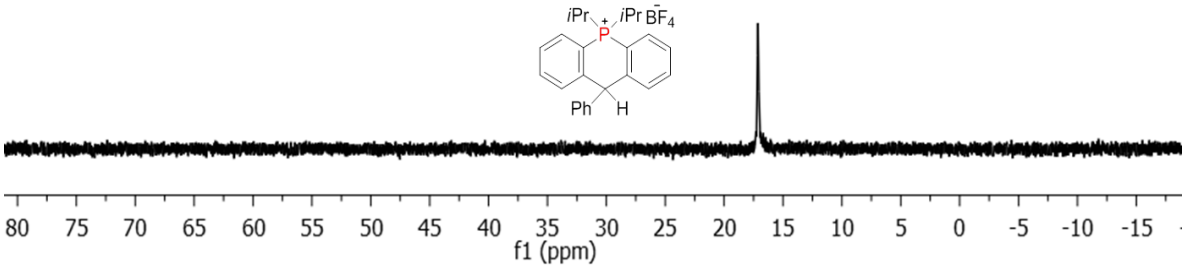

Figure 115. ^{1}H, ^{13}C, and ^{31}P NMR spectra of **76**.

Crystallographic Measurements

Single crystals of **73** and **74** were obtained by slow diffusion of Et_2O into a CH_2Cl_2 solution of **73** and **74**, respectively. In addition, single crystals of **75** and **76** were obtained by slow diffusion of pentane into a CH_2Cl_2 solution of **75** and **76**. The crystallographic measurement of **73**, **74**, **75**, and **76** were performed using a Bruker APEX-II CCD area detector diffractometer, with graphite-monochromated Mo-K_α radiation (λ = 0.71069 Å). A specimen of suitable size and quality was selected and mounted onto a nylon loop. The semi-empirical method SADABS was applied for absorption correction. The structure was solved by direct methods, and refined by the full-matrix least-square method against F^2 with the anisotropic temperature parameters for all non-hydrogen atoms. All H atoms were geometrically placed and refined using the riding model approximations.[4] Data reduction and further calculations were performed using the Bruker SAINT+ and SHELXTL NT program packages. The crystal data are included in Table 24-27.

Table 24. Crystal data, data collections, and structure refinements of **73**.

Crystal data	**73**	
Empirical formula	$C_{31}H_{24}BF_4P$	
Formula weight	514.28	
Crystal size/mm	0.5 x 0.25 x 0.3	
Temperature	110(2) K	
Wavelength	0.71073 Å	
Crystal system	Monoclinic	
Space group	P21	
Unit cell dimensions	a = 8.858(4) Å	α = 90°
	b = 16.639(7) Å	β = 115.031(4)°
	c = 9.682(4) Å	γ = 90°
Volume	1293.0(9) $Å^3$	
Z	2	
Density (calculated)	1.321 g cm^{-3}	
μ	0.154 mm^{-1}	
F(000)	532.0	
Scan mode	ω, φ	
hkl ranges	-10 → +10	
	-20 → +20	
	-11 → +10	
Reflections collected	12767	
Unique reflections [Rint]	5868 [0.035]	
Reflection used for refinement	5868	
Refined parameters	149	
GooF	1.053	
R1,[a] *w*R2[b] (all data)	0.0704, 0.1620	
Largest diff. peak and hole	1.22, -0.45 e.$Å^{-3}$	

[a]$R1 = \Sigma||F_o| - |F_c||/ \Sigma|F_o|$. [b]$wR2 = ([w(F_o^2 - F_c^2)^2]/[\Sigma w(F_o^2)^2])^{1/2}$; $w = 1/[\sigma^2(F_o^2) + (ap)^2 + bp]$; $p = (F_o^2 + 2F_c^2)/3$ with $a = 0.0798$ and $b = 1.0925$.

Table 25. Crystal data, data collections, and structure refinements of **74**.

Crystal data	**74**	
Empirical formula	$C_{25}H_{28}BF_4P$	
Formula weight	446.25	
Crystal size/mm	0.7 x 0.45 x 0.2	
Temperature	110(2) K	
Wavelength	0.71073 Å	
Crystal system	Monoclinic	
Space group	P 21/c	
Unit cell dimensions	a = 8.1220(8) Å	α = 90°
	b = 13.5733(14) Å	β = 91.8340(10)°
	c = 20.319(2) Å	γ = 90°
Volume	2238.9(4) $Å^3$	
Z	4	
Density (calculated)	1.324 g cm^{-3}	
μ	0.166 mm^{-1}	
F(000)	936.0	
Scan mode	ω, φ	
hkl ranges	-10 → +10	
	-18 → +18	
	-27 → +26	
Reflections collected	26228	
Unique reflections [Rint]	5390 [0.0277]	
Reflection used for refinement	5390	
Refined parameters	125	
GooF	1.045	
R1,[a] *w*R2[b] (all data)	0.0624, 0.1618	
Largest diff. peak and hole	1.17, -0.54 e.$Å^{-3}$	

[a]$R1 = \Sigma||F_o| - |F_c||/ \Sigma|F_o|$. [b]$wR2 = ([w(F_o^2 - F_c^2)^2]/[\Sigma w(F_o^2)^2])^{1/2}$; $w = 1/[\sigma^2(F_o^2) + (ap)^2 + bp]$; $p = (F_o^2 + 2F_c^2)/3$ with $a = 0.0911$ and $b = 1.8858$.

Table 26. Crystal data, data collections, and structure refinements of **75**.

Crystal data	**75**	
Empirical formula	$C_{31}H_{24}BF_4P$	
Formula weight	514.28	
Crystal size/mm	0.65 x 0.35 x 0.22	
Temperature	110(2) K	
Wavelength	0.71073 Å	
Crystal system	Monoclinic	
Space group	P 21/n	
Unit cell dimensions	a = 10.748(7) Å	α = 90°
	b = 17.213(11) Å	β = 94.818(8)°
	c = 13.441(9) Å	γ = 90°
Volume	2478(3) $Å^3$	
Z	4	
Density (calculated)	1.378 g cm^{-3}	
μ	0.160 mm^{-1}	
F(000)	1064.0	
Scan mode	ω, φ	
hkl ranges	-14 → +14	
	-22 → +23	
	-17 → +17	
Reflections collected	30020	
Unique reflections [Rint]	6165 [0.0603]	
Reflection used for refinement	6165	
Refined parameters	334	
GooF	1.026	
R1,[a] *w*R2[b] (all data)	0.0640, 0.1069	
Largest diff. peak and hole	0.31, -0.35 e.$Å^{-3}$	

[a]$R1 = \Sigma||F_o| - |F_c||/ \Sigma|F_o|$. [b]$wR2 = ([w(F_o^2 - F_c^2)^2]/[\Sigma w(F_o^2)^2])^{1/2}$; $w = 1/[\sigma^2(F_o^2) + (ap)^2 + bp]$; $p = (F_o^2 + 2F_c^2)/3$ with $a = 0.0414$ and $b = 0.6928$.

Table 27. Crystal data, data collections, and structure refinements of **76**.

Crystal data	**76**	
Empirical formula	$C_{25}H_{28}BF_4P$	
Formula weight	446.25	
Crystal size/mm	0.3 x 0.3 x 0.12	
Temperature	110(2) K	
Wavelength	0.71073 Å	
Crystal system	Monoclinic	
Space group	P 21/c	
Unit cell dimensions	a = 9.807(5) Å	α = 90°
	b = 15.502(11) Å	β = 101.83(6)°
	c = 14.979(7) Å	γ = 90°
Volume	2229(2) $Å^3$	
Z	4	
Density (calculated)	1.330 g cm^{-3}	
μ	0.166 mm^{-1}	
F(000)	936.0	
Scan mode	ω, φ	
hkl ranges	-13 → +12	
	-20 → +20	
	-19 → +20	
Reflections collected	54606	
Unique reflections [Rint]	5760 [0.1069]	
Reflection used for refinement	5760	
Refined parameters	280	
GooF	1.071	
R1,[a] *w*R2[b] (all data)	0.0866, 0.2669	
Largest diff. peak and hole	0.59, -0.65 e.$Å^{-3}$	

[a]$R1 = \Sigma||F_o| - |F_c||/ \Sigma|F_o|$. [b]$wR2\ ([w(F_o^2 - F_c^2)^2]/[\Sigma w(F_o^2)^2])^{1/2}$; $w = 1/[\sigma^2(F_o^2) + (ap)^2 + bp]$; $p = (F_o^2 + 2F_c^2)/3$ with $a = 0.1136$ and $b = 0.5971$.

Kinetic studies

A sample of **73** (10 mg) was dissolved in 0.5 mL CD_3CN in NMR tube. The ^{31}P NMR spectrum of **73** was collected periodically. The isomerization process of the 4-membered ring *ortho*-phenylene phosphine-methylium **73** was monitored by integration of the decreasing ^{31}P NMR signal of **73** in conjunction with the increasing ^{31}P NMR signal of **75** corresponding to the isomerized product. All spectra were processed using the VNMRJ Version 2.2 NMR software. The rate constant was calculated using a well-established NMR method reported in the literature.[4] This method is based on the fact that the concentration of **73** is proportional to the integration of the ^{31}P NMR signal of **73** divided by the sum of the integration of the ^{31}P NMR signal of **73** and **75**. For convenience, the value of the **73** integration is arbitrarily set at 100 and the **75** integration determined. The kinetic data of the isomerization process was shown in Table 28.

Table 28. Kinetic data for the isomerization of **73**.

		Isomerization of **73**		k=0.0011 min^{-1}
Time (min)	[**73**]	[**75**]	[**73**]/([**73**]+[**75**])	[**73**]/([**73**]+[**75**])
			exp	calc
0	100	0	1.00	1.00
15	100	1.22	0.99	0.98
64	100	11.94	0.89	0.93
210	100	29.31	0.77	0.79
272	100	34.26	0.74	0.74
330	100	47.47	0.68	0.70
390	100	54.56	0.65	0.65
492	100	72.77	0.58	0.58
660	100	113.29	0.47	0.48
721	100	129.44	0.44	0.45
1443	100	357.16	0.22	0.20
1530	100	379.05	0.21	0.19
1700				0.15
1900				0.12
2100				0.10
2300				0.08
2500				0.06
2700				0.05
2900				0.04
3000				0.04

CHAPTER VII

SUMMARY

7.1 Zwitterionic arytrifluoroborate for ^{18}F fluoride anion capture

As part of our research in the chemistry of cationic boranes as fluoride anion sensors, we have found that fluoroborate moieties are efficiently stabilized by neighboring onium ions. Capitalizing on this knowledge, the *ortho*-phenylene phosphino-borane derivatives **30**, **35**, **36**, **37** have been synthesized, and kinetic stability experiments have been performed. Based on the amount of $ArBF_3$ in solution as determined by ^{19}F NMR *vs* times, we found that the first order hydrolysis rate constants of **30**, **35**, **36**, and **37** were shown to be 3.4×10^{-6} min^{-1}, 3.9×10^{-5} min^{-1}, 1.5×10^{-5} min^{-1}, and 5.2×10^{-5} min^{-1}, respectively. These kinetic results indicate that the presence of *iso*-propyl substituents decreases the kinetic stability of the complexes. Moreover, comparisons between the hydrolysis rate constants of **30** and **36** as well as **35** and **37** also demonstrate that the pendent carboxylic acid functionality plays a labilizing role in aqueous environment.

The radiolabeled products [^{18}F]**30** and [^{18}F]**35** were prepared by a simple ^{18}F-^{19}F isotopic exchange process in aqueous solution in high yield (>87%). Gratifyingly, [^{18}F]**30** and [^{18}F]**35** are shown to be stable *in vivo* thus illustrating the stabilization of the BF_3 units provided by the neighboring *ortho*-phosphonium group. Encouraged by these results, these zwitterionic fluoroborates are a good candidate for the construction of disease specific ^{18}F PET imaging agents.

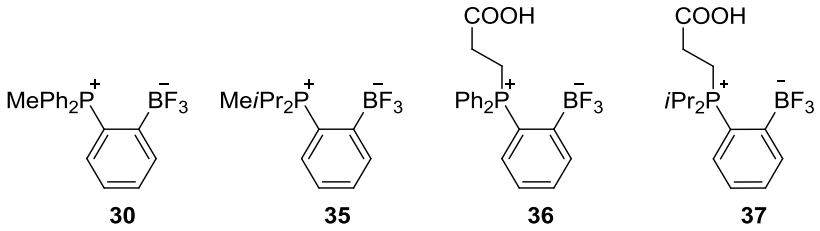

30 **35** **36** **37**

Figure 116. Illustration of zwitterionic aryltrifluoroborate **30**, **35**, **36**, and **37**.

7.2 [^{18}F]-Zwitterionic aryltrifluoroborate/indomethacin conjugates for potential PET probes

Indomethacin is a nonsteroidal anti-inflammatory drug that selectively binds and inhibits cyclooxygenase (COX) enzymes, especially, COX-2 enzyme which is highly upregulated in inflamed tissues as well as tumor tissues. Inspired by these results, the zwitterionic aryltrifluoroborate/indomethacin conjugates **45** and **46** have been synthesized to evaluate their potential as tumor imaging probe. These conjugates were simply radiolabeled by ^{18}F-^{19}F isotopic exchange in aqueous solutions and injected into a tumor bearing murine model. The PET images showed that the [^{18}F]**45** which gave a distinct skeletal signal due to defluorination *in vivo* is the only probe that accumulated into the tumour. These results suggested that the nature of the phosphorus substituents influences both the stability and binding property of the radiotracers.

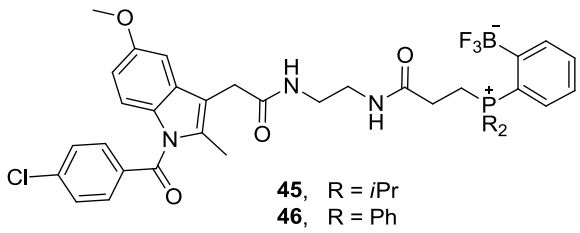

Figure 117. Illustration of zwitterionic aryltrifluoroborate/indomethacin conjugates **45** and **46**.

7.3 [^{18}F]-Carbene-borane adducts as a novel radio-prosthetic group for PET imaging

In addition to phosphonium aryltrifluoroborates, we were drawn by the remarkable stability of a carbene-BF_3 adduct (**34**). This compound can be recrystallized from boiling water suggesting that it is highly resistant to hydrolysis. Encouraged by these properties, novel carbene-BF_3 adducts have been synthesized to use as a potential radio-prosthetic group. Favourably, the [^{18}F]-radiolabeled carbene-borane adducts can be easily constructed by $SnCl_4$ assisted ^{18}F-^{19}F isotopic exchange. The *in vivo* stability of these derivatives was evaluated by injecting the [^{18}F]-carbene-borane (**56**) / H-Cys-Phe-OH peptide conjugate into normal nude mice. The PET-CT images showed that no obvious bone uptake signal at 4 h post-injection indicating that minimal free [^{18}F]-fluoride anions coming off from the radiotracer during the imaging process. Thus, we can conclude that these new [^{18}F]-carbene-borane derivatives have a good B-F stability *in vivo*.

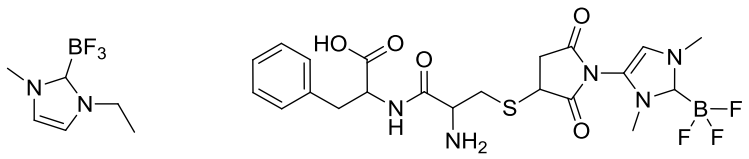

34 **56**/H-Cys-Phe-OH conjugate

Figure 118. Illustration of carbene-borane adducts **34** and **56**/H-Cys-Phe-OH conjugate.

7.4 Triazaborolopyridinium dyes for PET/Fluorescence dual modality imaging agents

Although PET imaging is a powerful technique for medical diagnosis, the spatial resolution provided by this technique is relatively low. Therefore, combining PET imaging with a second imaging technique such as fluorescence gives much higher spatial and temporal resolution. This protocol necessitates the incorporation of a fluorophore into a radiolabeled component. With the goal of developing new boron-based PET/Fluorescence imaging agent, a series of triazaborolopyridinium dyes has been synthesized and studied. We found that the triazaborolopyridinium dye (**71**) with nitro substituent features high quantum yields and large stoke shifts, which are suitable characteristics for imaging applications. **71** can also be easily fluorinated by KHF_2 which is viable for ^{18}F-radiofluorination process.

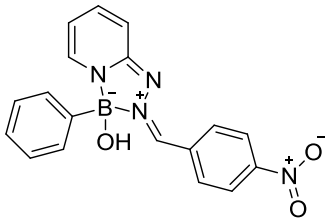

71

Figure 119. Illustration of Triazaborolopyridinium dyes **71**.

7.5 Synthesis, structure, and isomerization of phosphino-methylium compounds

The utilities of intramolecular P/B frustrated Lewis pairs (FLPs) in catalytic reactions and transition metal complexation prompted us to investigate whether a carbocation and a phosphine could be incorporated at the *ortho* positions of the same phenylene backbone to furnish novel intramolecular FLPs. With this in mind, we endeavored to synthesize novel *ortho*-phenylene phosphino-methylium compounds (**73** and **74**) and to investigate their properties. Surprisingly, **73** underwent an isomerization upon dissolving in organic solvent at ambient temperature, whereas **74** showed no reaction. The difference observed in the isomerization processes derives from the dissimilarity of the electron donating ability of the phosphine ligand.

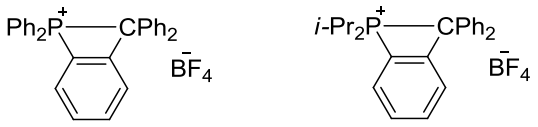

73 **74**

Figure 120. Illustration of phosphino-methylium compounds **73** and **74**.

7.6 Conclusion

This dissertation illustrates how the introduction of cationic moiety impacts the B-F bond stability against hydrolysis and its application for the construction of boron-based radiotracers. Firstly, we demonstrated that the proximal *ortho*-phosphonium group can retard the rate of trifluoroborate hydrolysis. These results lead to the construction of the [^{18}F]*ortho*-phenylene phosphino-boranes and the [^{18}F]*ortho*-phenylene phosphino-borane/ indomethacin conjugates that showed good stability *in vivo*. Exploiting this concept, the new carbene-borane adducts as well as the triazaborolopyridinium dyes were also developed to use as potential probes for PET applications.

REFERENCES

(1) Miller, P. W.; Long, N. J.; Vilar, R.; Gee, A. D. *Angew. Chem. Int. Ed.* **2008**, *47*, 8998-9033.

(2) Li, Z. B.; Conti, P. S. *Adv. Drug Deliver. Rev.* **2010**, *62*, 1031-1051.

(3) Cai, L. S.; Lu, S. Y.; Pike, V. W. *Eur. J. Org. Chem.* **2008**, 2853-2873.

(4) Ting, R.; Harwig, C. W.; Lo, J.; Li, Y.; Adam, M. J.; Ruth, T. J.; Perrin, D. M. *J. Org. Chem.* **2008**, *73*, 4662-4670.

(5) Ting, R.; Lo, J.; Adam, M. J.; Ruth, T. J.; Perrin, D. M. *J. Fluorine Chem.* **2008**, *129*, 349-358.

(6) Harwig, C. W.; Ting, R.; Adam, M. J.; Ruth, T. J.; Perrin, D. M. *Tetrahedron Lett.* **2008**, *49*, 3152-3156.

(7) Ting, R.; Harwig, C.; auf dem Keller, U.; McCormick, S.; Austin, P.; Overall, C. M.; Adam, M. J.; Ruth, T. J.; Perrin, D. M. *J. Am. Chem. Soc.* **2008**, *130*, 12045-12055.

(8) Keller, U. A. D.; Bellac, C. L.; Li, Y.; Lou, Y. M.; Lange, P. F.; Ting, R.; Harwig, C.; Kappelhoff, R.; Dedhar, S.; Adam, M. J.; Ruth, T. J.; Benard, F.; Perrin, D. M.; Overall, C. M. *Cancer Res.* **2010**, *70*, 7562-7569.

(9) Li, Y.; Ting, R.; Harwig, C. W.; Keller, U. A. D.; Bellac, C. L.; Lange, P. F.; Inkster, J. A. H.; Schaffer, P.; Adam, M. J.; Ruth, T. J.; Overall, C. M.; Perrin, D. M. *Medchemcomm* **2011**, *2*, 942-949.

(10) Molander, G. A.; Figueroa, R. *J. Org. Chem.* **2006**, *71*, 6135-6140.

(11) Liu, Z. B.; Li, Y.; Lozada, J.; Schaffer, P.; Adam, M. J.; Ruth, T. J.; Perrin, D. M. *Angew. Chem. Int. Ed.* **2013**, *52*, 2303-2307.

(12) Li, Y.; Guo, J.; Tang, S.; Lang, L.; Chen, X.; Perrin, D. M. *Am. J. Nucl. Med. Mol. Imaging* **2013**, *3*, 44-56.

(13) Li, Y.; Liu, Z.; Harwig, C. W.; Pourghiasian, M.; Lau, J.; Lin, K. S.; Schaffer, P.; Benard, F.; Perrin, D. M. *Am. J. Nucl. Med. Mol. Imaging* **2013**, *3*, 57-70.

(14) Liu, Z.; Hundal-Jabal, N.; Wong, M.; Yapp, D.; Lin, K. S.; Benard, F.; Perrin, D. M. *Medchemcomm* **2014**, *5*, 171-179.

(15) Ting, R.; Aguilera, T. A.; Crisp, J. L.; Hall, D. J.; Eckelman, W. C.; Vera, D. R.; Tsien, R. Y. *Bioconjugate Chem.* **2010**, *21*, 1811-1819.

(16) Hudnall, T. W.; Gabbai, F. P. *Chem. Commun.* **2008**, 4596-4597.

(17) Hudnall, T. W.; Lin, T. P.; Gabbai, F. P. *J. Fluorine Chem.* **2010**, *131*, 1182-1186.

(18) Li, Z. B.; Lin, T. P.; Liu, S. L.; Huang, C. W.; Hudnall, T. W.; Gabbai, F. P.; Conti, P. S. *Chem. Commun.* **2011**, *47*, 9324-9326.

(19) Hendricks, J. A.; Keliher, E. J.; Wan, D.; Hilderbrand, S. A.; Weissleder, R.; Mazitschek, R. *Angew. Chem. Int. Ed.* **2012**, *51*, 6813-6813.

(20) Liu, S. L.; Lin, T. P.; Li, D.; Leamer, L.; Shan, H.; Li, Z. B.; Gabbai, F. P.; Conti, P. S. *Theranostics* **2013**, *3*, 181-189.

(21) Liu, S. L.; Li, D.; Shan, H.; Gabbai, F. P.; Li, Z. B.; Conti, P. S. *Nucl. Med. Biol.* **2014**, *41*, 120-126.

(22) Liu, S. L.; Li, D.; Zhang, Z.; Prakash, G. K. S.; Conti, P. S.; Li, Z. B. *Chem. Commun.* **2014**, *50*, 7371-7373.

(23) Keliher, E. J.; Klubnick, J. A.; Reiner, T.; Mazitschek, R.; Weissleder, R. *Chemmedchem* **2014**, *9*, 1368-1373.

(24) Hudnall, T. W.; Gabbai, F. P. *J. Am. Chem. Soc.* **2007**, *129*, 11978-11986.

(25) Hudnall, T. W.; Kim, Y. M.; Bebbington, M. W. P.; Bourissou, D.; Gabbai, F. P. *J. Am. Chem. Soc.* **2008**, *130*, 10890-10891.

(26) Kim, Y. M.; Hudnall, T. W.; Bouhadir, G.; Bourissou, D.; Gabbai, F. P. *Chem. Commun.* **2009**, 3729-3731.

(27) Wade, C. R.; Gabbai, F. P. *Organometallics* **2011**, *30*, 4479-4481.

(28) Kim, Y.; Zhao, H.; Gabbai, F. P. *Angew. Chem. Int. Ed.* **2009**, *48*, 4957-4960.

(29) Zhao, H. Y.; Gabbai, F. P. *Nat. Chem.* **2010**, *2*, 984-990.

(30) Liu, Z. B.; Pourghiasian, M.; Radtke, M. A.; Lau, J.; Pan, J. H.; Dias, G. M.; Yapp, D.; Lin, K. S.; Benard, F.; Perrin, D. M. *Angew. Chem. Int. Ed.* **2014**, *53*, 11876-11880.

(31) Tian, C.; Nie, W. L.; Borzov, M. V.; Su, P. F. *Organometallics* **2012**, *31*, 1751-1760.

(32) Hapuarachchige, S.; Montano, G.; Ramesh, C.; Rodriguez, D.; Henson, L. H.; Williams, C. C.; Kadavakkollu, S.; Johnson, D. L.; Shuster, C. B.; Arterburn, J. B. *J. Am. Chem. Soc.* **2011**, *133*, 6780-6790.

(33) Dolle, F.; Roeda, D.; Kuhnast, B.; Lasne, M.-C. In *Fluorine and Health*; Tressaud, A., Ed.; Elsevier, Amsterdam: 2008, p 3-65.

(34) Cai, L.; Lu, S.; Pike, V. W. *Eur. J. Org. Chem.* **2008**, 2853-2873.

(35) Ting, R.; Adam, M. J.; Ruth, T. J.; Perrin, D. M. *J. Am. Chem. Soc.* **2005**, *127*, 13094-13095.

(36) Schirrmacher, R.; Bradmoeller, G.; Schirrmacher, E.; Thews, O.; Tillmanns, J.; Siessmeier, T.; Bucholz, H. G.; Bartenstein, P.; Wängler, B.; Niemeyer, C. M.; Jurkschat, K. *Angew. Chem. Int. Ed.* **2006**, *45*, 6047-6050.

(37) Schirrmacher, E.; Wängler, B.; Cypryk, M.; Bradtmöller, G.; Schäfer, M.; Eisenhut, M.; Jurkschat, K.; Schirrmacher, R. *Bioconjugate Chem.* **2007**, *18*, 2085-2089.

(38) McBride, W. J.; Sharkey, R. M.; Karacay, H.; D'Souza, C. A.; Rossi, E. A.; Laverman, P.; Chang, C.-H.; Boerman, O. C.; Goldenberg, D. M. *J. Nucl. Med.* **2009**, *50*, 991-998.

(39) McBride, W. J.; D'Souza, C. A.; Sharkey, R. M.; Karacay, H.; Rossi, E. A.; Chang, C.-H.; Goldenberg, D. M. *Bioconjugate Chem.* **2010**, *21*, 1331-1340.

(40) Ting, R.; Harwig, C. W.; Lo, J.; Li, Y.; Adam, M. J.; Ruth, T. J.; Perrin, D. M. *J. Org. Chem.* **2008**, *73*, 4662-4670.

(41) Ting, R.; Lo, J.; Adam, M. J.; Ruth, T. J.; Perrin, D. M. *J. Fluorine Chem.* **2008**, *129*, 349-358.

(42) Harwig, C. W.; Ting, R.; Adam, M. J.; Ruth, T. J.; Perrin, D. M. *Tetrahedron Lett.* **2008**, *49*, 3152-3156.

(43) Ting, R.; Harwig, C.; auf dem Keller, U.; McCormick, S.; Austin, P.; Overall, C. M.; Adam, M. J.; Ruth, T. J.; Perrin, D. M. *J. Am. Chem. Soc.* **2008**, *130*, 12045-12055.

(44) auf dem Keller, U.; Bellac, C. L.; Li, Y.; Lou, Y.; Lange, P. F.; Ting, R.; Harwig, C.; Kappelhoff, R.; Dedhar, S.; Adam, M. J.; Ruth, T. J.; Bénard, F.; Perrin, D. M.; Overall, C. M. *Cancer Res.* **2010**, *70*, 7562-7569.

(45) Li, Y.; Ting, R.; Harwig, C. W.; auf, d. K. U.; Bellac, C. L.; Lange, P. F.; Inkster, J. A. H.; Schaffer, P.; Adam, M. J.; Ruth, T. J.; Overall, C. M.; Perrin, D. M. *Med. Chem. Comm.* **2011**, *2*, 942-949.

(46) Ting, R.; Aguilera, T. A.; Crisp, J. L.; Hall, D. J.; Eckelman, W. C.; Vera, D. R.; Tsien, R. Y. *Bioconjugate Chem.* **2010**, *21*, 1811-1819.

(47) Li, Z.; Lin, T.-P.; Liu, S.; Huang, C.-W.; Hudnall, T. W.; Gabbaï, F. P.; Conti, P. S. *Chem. Commun.* **2011**, *47*, 9324-9326.

(48) Hendricks, J. A.; Keliher, E. J.; Wan, D.; Hilderbrand, S. A.; Weissleder, R.; Mazitschek, R. *Angew. Chem. Int. Ed.* **2012**, *51*, 4603–4606.

(49) Hendricks, J. A.; Keliher, E. J.; Wan, D.; Hilderbrand, S. A.; Weissleder, R.; Mazitschek, R. *Angew. Chem. Int. Ed.* **2012**, *51*, 6813.

(50) Wade, C. R.; Broomsgrove, A. E. J.; Aldridge, S.; Gabbaï, F. P. *Chem. Rev.* **2010**, *110*, 3958-3984.

(51) Hudnall, T. W.; Kim, Y.-M.; Bebbington, M. W. P.; Bourissou, D.; Gabbaï, F. P. *J. Am. Chem. Soc.* **2008**, *130*, 10890-10891.

(52) Kim, Y.; Kim, M.; Gabbaï, F. P. *Org. Lett.* **2010**, *12*, 600-602.

(53) Zhao, H.; Gabbaï, F. P. *Nat. Chem.* **2010**, *2*, 984-990.

(54) Zhao, H.; Gabbaï, F. P. *Org. Lett.* **2011**, 1444-1446.

(55) Wade, C. R.; Gabbaï, F. P. *Organometallics* **2011**, *30*, 4479-4481.

(56) Wade, C. R.; Zhao, H.; Gabbaï, F. P. *Chem. Commun.* **2010**, 6380-6381.

(57) Moebs-Sanchez, S.; Saffon, N.; Bouhadir, G.; Maron, L.; Bourissou, D. *Dalton Trans.* **2010**, *39*, 4417-4420.

(58) Porcel, S.; Bouhadir, G.; Saffon, N.; Maron, L.; Bourissou, D. *Angew. Chem. Int. Ed.* **2010**, *49*, 6186-6189.

(59) Gott, A. L.; Piers, W. E.; Dutton, J. L.; McDonald, R.; Parvez, M. *Organometallics* **2011**, *30*, 4236-4249.

(60) Hudnall, T. W.; Gabbaï, F. P. *J. Am. Chem. Soc.* **2007**, *129*, 11978-11986.

(61) Wade, C. R.; Gabbai, F. P. *Organometallics.* **2011**, *30*, 4479-4481.

(62) Batsanov, S. S. *Inorg. Mater.* **2001**, *37*, 871-885.

(63) Cordero, B.; Gomez, V.; Platero-Prats, A. E.; Reves, M.; Echeverria, J.; Cremades, E.; Barragan, F.; Alvarez, S. *Dalton Trans.* **2008**, 2832-2838.

(64) Ghorab, M. F.; Winfield, J. M. *J. Fluorine Chem.* **1990**, *49*, 367-383.

(65) Jauregui-Osoro, M.; Sunassee, K.; Weeks, A. J.; Berry, D. J.; Paul, R. L.; Cleij, M.; Banga, J. P.; O'Doherty, M. J.; Marsden, P. K.; Clarke, S. E. M.; Ballinger, J. R.; Szanda, I.; Cheng, S.-Y.; Blower, P. J. *Eur. J. Nucl. Med. Mol. Imaging* **2010**, *37*, 2108-2116.

(66) Moebs-Sanchez, S.; Saffon, N.; Bouhadir, G.; Maron, L.; Bourissou, D. *Dalton Trans.* **2010**, *39*, 4417-4420.

(67) Vane, J. R. *Nature-New Biol* **1971**, *231*, 232-235.

(68) Smith, W. L.; Garavito, R. M.; DeWitt, D. L. *J. Biol. Chem.* **1996**, *271*, 33157-33160.

(69) Gupta, R. A.; DuBois, R. N. *J. Natl. Cancer. I.* **2002**, *94*, 406-407.

(70) Maier, T. J.; Schilling, K.; Schmidt, R.; Geisslinger, G.; Grosch, S. *Biochem. Pharmacol.* **2004**, *67*, 1469-1478.

(71) Rome, L. H.; Lands, W. E. M. *Proc. Natl. Acad. Sci. U.S.A.* **1975**, *72*, 4863-4865.

(72) Kulmacz, R. J.; Lands, W. E. M. *J. Biol. Chem.* **1985**, *260*, 2572-2578.

(73) Kalgutkar, A. S.; Crews, B. C.; Rowlinson, S. W.; Marnett, A. B.; Kozak, K. R.; Remmel, R. P.; Marnett, L. J. *Proc. Natl. Acad. Sci. U.S.A.* **2000**, *97*, 925-930.

(74) Lundholm, K.; Gelin, J.; Hyltander, A.; Lonnroth, C.; Sandstrom, R.; Svaninger, G.; Korner, U.; Gulich, M.; Karrefors, I.; Norli, B.; Hafstrom, L. O.; Kewenter, J.; Olbe, L.; Lundell, L. *Cancer Res.* **1994**, *54*, 5602-5606.

(75) Buchanan, G. R.; Martin, V.; Levine, P. H.; Scoon, K.; Handin, R. I. *Am. J. Clin. Pathol.* **1977**, *68*, 355-359.

(76) Black, W. C.; Bayly, C.; Belley, M.; Chan, C. C.; Charleson, S.; Denis, D.; Gauthier, J. Y.; Gordon, R.; Guay, D.; Kargman, S.; Lau, C. K.; Leblanc, Y.; Mancini, J.; Ouellet, M.; Percival, D.; Roy, P.; Skorey, K.; Tagari, P.; Vickers, P.; Wong, E.; Xu, L.; Prasit, P. *Bioorg. Med. Chem. Lett.* **1996**, *6*, 725-730.

(77) Kalgutkar, A. S.; Marnett, A. B.; Crews, B. C.; Remmel, R. P.; Marnett, L. J. *J. Med. Chem.* **2000**, *43*, 2860-2870.

(78) Uddin, M. J.; Crews, B. C.; Blobaum, A. L.; Kingsley, P. J.; Gorden, D. L.; McIntyre, J. O.; Matrisian, L. M.; Subbaramaiah, K.; Dannenberg, A. J.; Piston, D. W.; Marnett, L. J. *Cancer Res.* **2010**, *70*, 3618-3627.

(79) Li, Z. B.; Chansaenpak, K.; Liu, S. L.; Wade, C. R.; Conti, P. S.; Gabbai, F. P. *Medchemcomm* **2012**, *3*, 1305-1308.

(80) Wade, C. R.; Zhao, H. Y.; Gabbai, F. P. *Chem. Commun.* **2010**, *46*, 6380-6381.

(81) Lennox, A. J. J.; Lloyd-Jones, G. C. *J. Am. Chem. Soc.* **2012**, *134*, 7431-7441.

(82) Jauregui-Osoro, M.; Sunassee, K.; Weeks, A. J.; Berry, D. J.; Paul, R. L.; Cleij, M.; Banga, J.; O'Doherty, M. J.; Marsden, P. K.; Clarke, S. E. M.; Ballinger, J. R.; Szanda, I.; Cheng, S. Y.; Blower, P. J. *Eur. J. Nucl. Med. Mol. Imag.* **2010**, *37*, 2108-2116.

(83) Liu, Z. B.; Radtke, M. A.; Wong, M. Q.; Lin, K. S.; Yapp, D. T.; Perrin, D. M. *Bioconjugate Chem.* **2014**, *25*, 1951-1962.

(84) Schirrmacher, R.; Bradtmoller, G.; Schirrmacher, E.; Thews, O.; Tillmanns, J.; Siessmeier, T.; Buchholz, H. G.; Bartenstein, P.; Waengler, B.; Niemeyer, C. M.; Jurkschat, K. *Angew. Chem. Int. Ed.* **2006**, *45*, 6047-6050.

(85) Schirrmacher, E.; Wangler, B.; Cypryk, M.; Bradtmoller, G.; Schafer, M.; Eisenhut, M.; Jurkschat, K.; Schirrmacher, R. *Bioconjugate Chem.* **2007**, *18*, 2085-2089.

(86) Schroder, T.; Schmitz, K.; Niemeier, N.; Balaban, T. S.; Krug, H. F.; Schepers, U.; Brase, S. *Bioconjugate Chem.* **2007**, *18*, 342-354.

(87) Liu, S.; Lin, T.-P.; Li, D.; Leamer, L.; Shan, H.; Li, Z.; Gabbaï, F. P.; Conti, P. S. *Theranostics* **2013**, *3*, 181-189.

(88) Tommasi, I.; Sorrentino, F. *Tetrahedron Lett.* **2005**, *46*, 2141-2145.

(89) Khramov, D. M.; Lynch, V. M.; Bielawski, C. W. *Organometallics* **2007**, *26*, 6042-6049.

(90) Jennings, L. E.; Long, N. J. *Chem. Commun.* **2009**, 3511-3524.

(91) Zhou, Y.; Xiao, Y.; Chi, S. M.; Qian, X. H. *Org. Lett.* **2008**, *10*, 633-636.

(92) Chen, D. J.; Klankermayer, J. *Chem. Commun.* **2008**, 2130-2131.

(93) Spies, P.; Schwendemann, S.; Lange, S.; Kehr, G.; Frohlich, R.; Erker, G. *Angew. Chem. Int. Edit.* **2008**, *47*, 7543-7546.

(94) Chase, P. A.; Jurca, T.; Stephan, D. W. *Chem. Commun.* **2008**, 1701-1703.

(95) Chase, P. A.; Welch, G. C.; Jurca, T.; Stephan, D. W. *Angew. Chem. Int. Edit.* **2007**, *46*, 8050-8053.

(96) Welch, G. C.; Stephan, D. W. *J. Am. Chem. Soc.* **2007**, *129*, 1880-1881.

(97) Spies, P.; Schwendemann, S.; Lange, S.; Kehr, G.; Frohlich, R.; Erker, G. *Angew. Chem. Int. Ed.* **2008**, *47*, 7543-7546.

(98) Spies, P.; Erker, G.; Kehr, G.; Bergander, K.; Froehlich, R.; Grimme, S.; Stephan, D. W. *Chem. Commun.* **2007**, 5072-5074.

(99) Bontemps, S.; Bouhadir, G.; Apperley, D. C.; Dyer, P. W.; Miqueu, K.; Bourissou, D. *Chem-Asian. J.* **2009**, *4*, 428-435.

(100) Sircoglou, M.; Bontemps, S.; Mercy, M.; Miqueu, K.; Ladeira, S.; Saffon, N.; Maron, L.; Bouhadir, G.; Bourissou, D. *Inorg. Chem.* **2010**, *49*, 3983-3990.

(101) Bontemps, S.; Bouhadir, G.; Miqueu, K.; Bourissou, D. *J. Am. Chem. Soc.* **2006**, *128*, 12056-12057.

(102) Wang, H. D.; Gabbai, F. P. *Angew. Chem. Int. Edit.* **2004**, *43*, 184-187.

(103) Wang, H. D.; Gabbai, F. P. *Org. Lett.* **2005**, *7*, 283-285.

(104) Wang, H. D.; Webster, C. E.; Perez, L. M.; Hall, M. B.; Gabbai, F. P. *J. Am. Chem. Soc.* **2004**, *126*, 8189-8196.

(105) Noel-Duchesneau, L.; Lugan, N.; Lavigne, G.; Labande, A.; Cesar, V. *Organometallics* **2014**, *33*, 5085-5088.